

540
GUH

CENTRAL

MEMBER

Number T 227

Date 2/7/13

Theoretical Studies on the Electronic Structure and Stability of Inorganic Ring Systems, Metallatranes, Carbon Bases and Mechanism of Dinitrogen Reduction

A thesis submitted in partial fulfillment of the requirements for the degree of

Doctor of Philosophy

By

Ankur Kanti Guha

Registration No. 064 of 2010



Department of Chemical Sciences
School of Sciences
Tezpur University
Napaam, Tezpur - 784028
Assam, India

September, 2012

*Dedicated to my
Beloved
Parents and my Younger
Sister*

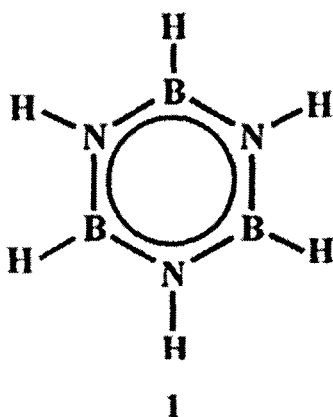
ABSTRACT

The phenomenal advances in software and hardware have enabled the use of computational tools towards solving a wide range of chemical problems. Several instances are there where the computational methodologies facilitated better understanding of the experimental facts which helps in guiding the experimental research. For example, computational methodologies can be easily applied in exploring reaction pathways, structures and energetics of the transition states and intermediates which are otherwise very difficult to study experimentally. Thus, computational chemistry in modern day chemical research has become as indispensable as experimental approaches.

The thesis consists of five chapters, of which the first chapter deals with the brief introduction to theoretical methodologies. This is followed by application of the theoretical methodologies to chemical problems in chapter 2, 3, 4, and 5. A brief overview of the chapters 2-5 is given below.

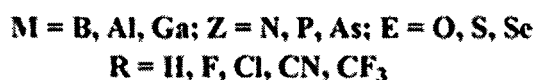
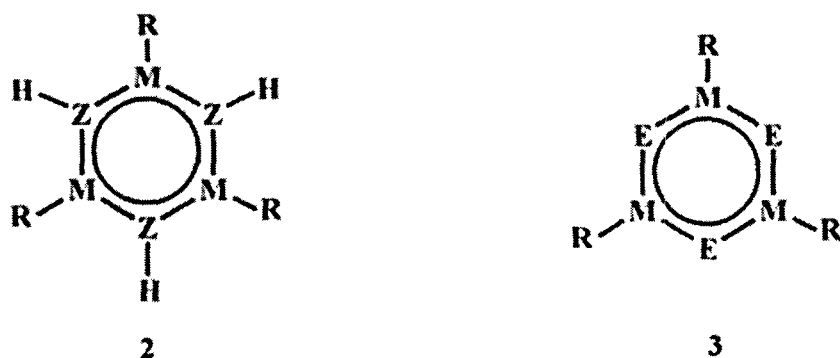
Chapter 2: Aromaticity in Borazine and Its Heavier Analogs

Michael Faraday's isolation of benzene in 1825 paved the way to a vital concept in chemistry – "aromaticity". Numerous organic and inorganic aromatic compounds are now known. One such classic textbook example of an isoelectronic inorganic six- π electron system is borazine (1). Several heavier analogs of borazine have been synthesized. Both gas phase and solution phase electrophilic substitution of borazine have been carried out which suggests its aromatic character.



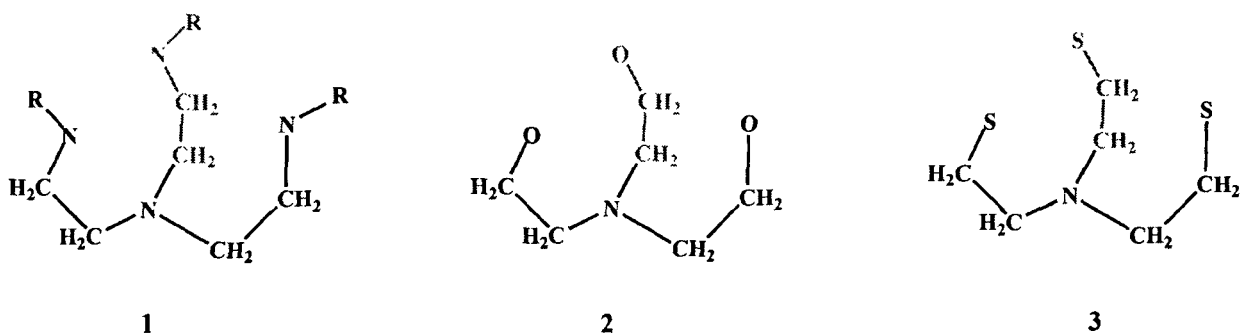
In this chapter, the effect of substituents on the aromaticity of borazine and its heavier analogs (2 and 3) have been studied quantum chemically at B3LYP/6-31+G* level of theory. Topological analysis of these molecules has also been performed within the realm of QTAIM

and ELF. This study reveals that some inorganic rings may be stable even without significant π electron delocalization and provides evidence for the dominant role played by the σ framework.

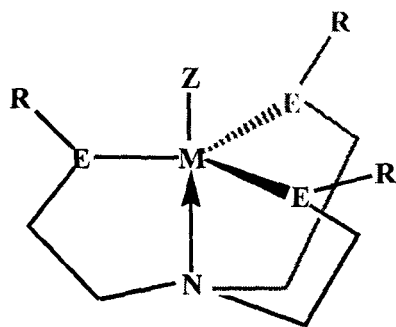


Chapter 3: Nature and Extent of Transannular Interactions in Group 4 and Group 6 Metallatranes

Tripodal ligands such as triamidoamine (1), triethanolatoamine (2) and its sulfur analog (3) have attracted considerable interest over a period of time. They bind to main group and transition metals in tetradentate manner featuring a transannular M...N bond.



In this chapter, the nature and extent of transannular M...N interaction has been studied at B3LYP/LANL2DZ level of theory. The effect of apical (Z) as well as equatorial (E) substituents on the extent of this transannular interaction has been studied for group 4 and 6 metallatranes (4). Topology of this interaction has also been studied using the QTAIM approach and found to possess significant covalent character.



4

Chapter 4: Structure, Stability and Reactivity of Different Carbon Bases

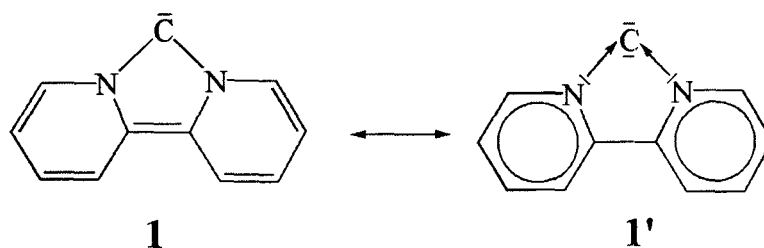
Organic carbon compounds are mostly found in a formal oxidation state of IV. However, carbon compounds in a formal oxidation state of II, (e. g., carbene) which once thought to be a reactive intermediate, are now available in a bottleable form. Very recently, a unique bonding situation in carbon compounds has been proposed which predicts a formal oxidation state of carbon as low as zero.

This chapter has been divided into three parts – (i) the first part of this chapter deals with the study of the reactivity of heterocyclic carbenes which may help in realizing the existence of “hidden” carbon(0) character in them, (ii) in the next part of this chapter, some new cyclic and acyclic carbon(0) compounds stabilized by different coordination modes of heterocyclic carbenes have been proposed, and (iii) the last part of this chapter deals with the reactivity of carbon(II) and carbon(0) bases which may help in distinguishing these two classes of compounds.

(i) Revisiting the Reactivity of Heterocyclic Carbenes

Singlet heterocyclic carbenes are known to have strong σ donating abilities. This has enabled their use in various transition metal catalysis. Owing to the presence of a high energy lone pair, heterocyclic carbenes can show a very high value of first proton affinity. On the other hand, recent prediction of carbon(0) compounds which has two lone pairs may have high values of first and second proton affinities.

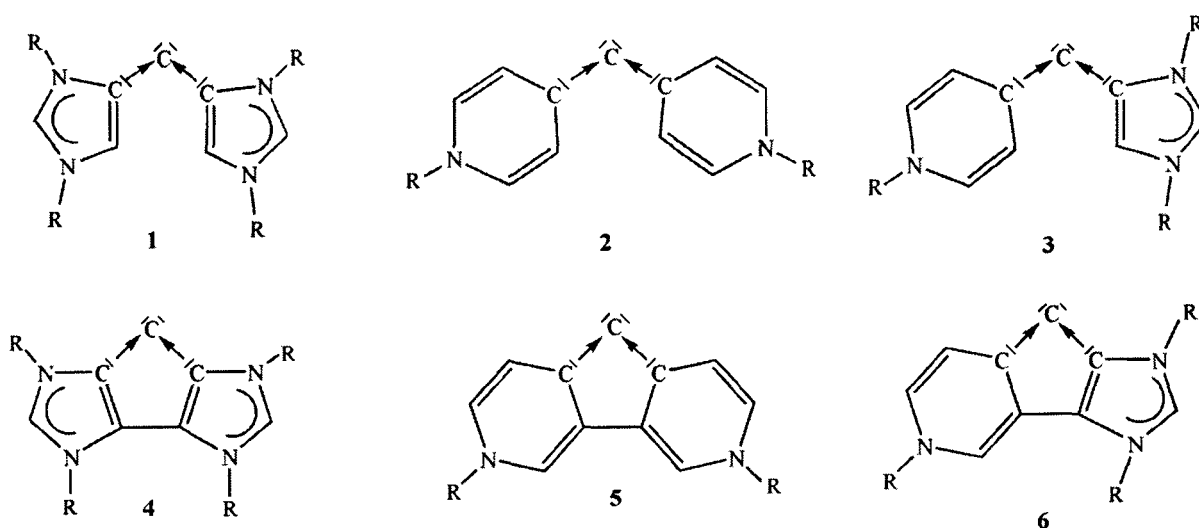
Here, reactivity of an *N*-heterocyclic carbene (**1**) has been studied with an aim to probe the importance of a particular resonance form of **1** which may contain two lone pairs at the central carbon atom (**1'**). This may help in realizing the existence of “hidden” carbon(0) character even in *N*-heterocyclic carbenes.



(ii) Stabilization of Cyclic and Acyclic Carbon(0) Compounds By Differential Coordination of Heterocyclic Carbenes

Heterocyclic carbenes are known to have different coordination modes, e. g., normal, abnormal and remote. Owing to their highly basic nature, these carbenes are expected to stabilize a carbon atom via donor-acceptor interactions resulting in the formation of a carbon(0) compound.

In this part of the chapter, some new cyclic (1-3) and acyclic (4-6) carbon(0) compounds have been proposed. These compounds are predicted to have high thermodynamic stabilities and are predicted to be highly basic. The cyclic compounds (4-6) are unusual in the sense that they contain a five membered ring consisting of only carbon atoms with a central carbon atom in the formal oxidation state of zero.

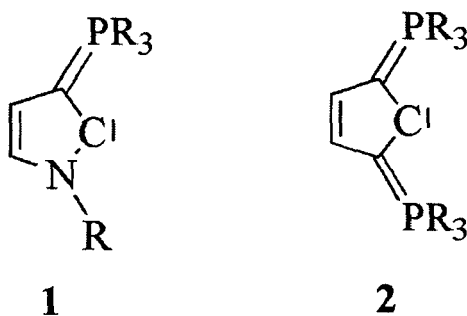


(iii) Reactivity of Different Carbon Bases

Due to the presence of a high energy lone pair orbital, singlet carbenes are highly basic in nature. Consequently, the first proton affinity value obtained for these molecules are also very high. On the other hand, carbon(0) compounds with two lone pair of electrons not only have a very high value of first proton affinity but their second proton affinity is also high. This

reactivity difference has been used as a decisive indicator to distinguish carbenes from carbon(0) compounds.

In this section, emphasize has been given to the π donating ability of ylide stabilized carbenes (1-2). Quantum chemical calculation at BP86/TZVP level of theory showed that ylide stabilized carbenes may have strong σ and π donating abilities and as a result, they showed very high values of first and second proton affinities. This reveals that both carbenes and carbon(0) compounds may show similar reactivity when subjected to electrophilic attack. However, owing to the ambiphilic character of carbenes, they may undergo nucleophilic addition too, which is very difficult to realize for carbon(0) compounds. This reactivity difference has been proposed as a distinguishing feature between these two classes of compounds.



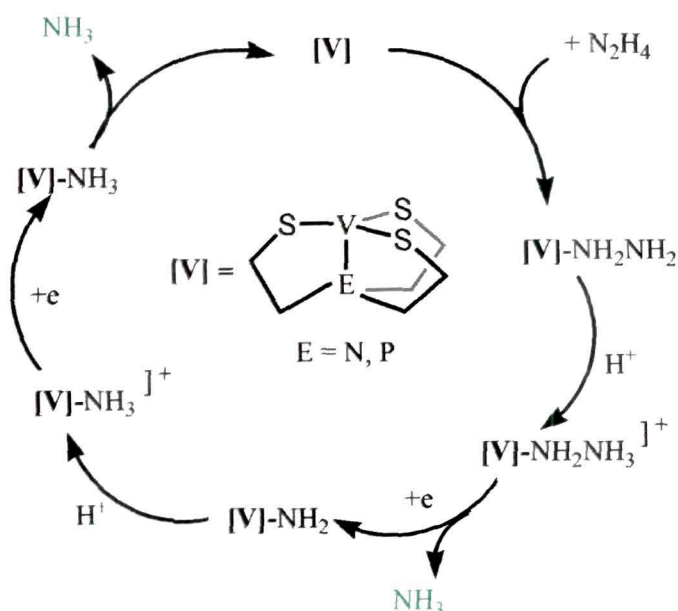
Chapter 5: Mechanistic Study of Dinitrogen Reduction mediated by Tripodal Complexes of Vanadium

Mechanistic detail of dinitrogen reduction is still a fascinating area of research. Reduced forms of dinitrogen are very important for the sustainment of life on earth. Although industrial process of dinitrogen reduction (Haber-Bosch) is available, but it involves high temperature as well as pressure. Therefore, current research is focused towards transition metal catalyzed dinitrogen reduction at ambient condition.

This chapter has also been divided into two parts – (i) the first part of which deals with the mechanistic detail and energy profile for the conversion of hydrazine to ammonia mediated by vanadium(III) thiolate complexes and (ii) the next part of this chapter deals with the complete reduction of dinitrogen to ammonia mediated by vanadium triamidoamine complex.

(i) Mechanistic Details for the Conversion of Hydrazine to Ammonia Mediated by Vanadium(III) Thiolate Complexes

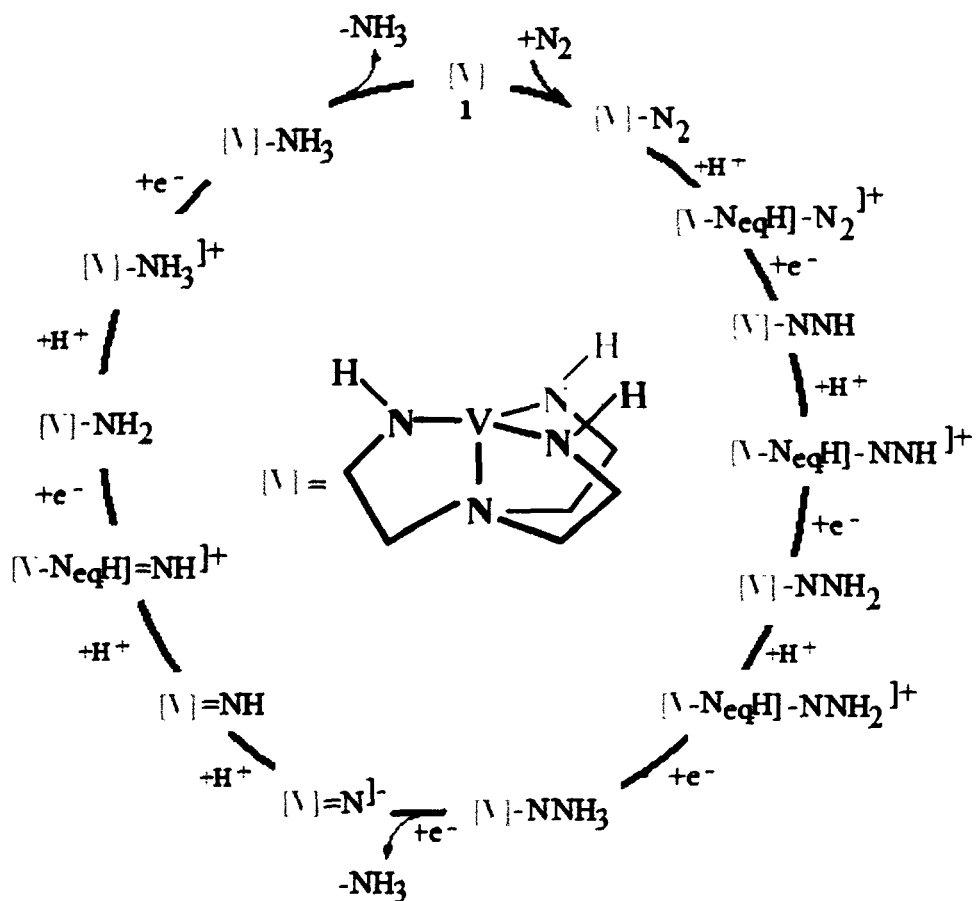
Hydrazine is supposed to be a substrate and an intermediate of nitrogenase, the enzyme responsible for dinitrogen reduction. Like Mo-Fe nitrogenase, V-Fe nitrogenase is now known. Thus, to understand the mode of action of this enzyme, the chemistry of vanadium centre containing three sulfur donor sites which mimic the sulfido environment of the V site in vanadium nitrogenase, is of great importance. In this part of the chapter, a mechanism for the conversion of hydrazine to ammonia mediated by vanadium(III) thiolate complexes [V] has been proposed, and an energetic profile for the same has been calculated at B3LYP/LANL2DZ//TZVP level of theory.



(ii) Mechanistic Study for the Complete Conversion of Dinitrogen to Ammonia Mediated by Vanadium Triamidoamine Complex

Catalytic conversion of dinitrogen to ammonia at a single metal centre has recently been achieved by Schrock and coworkers using a molybdenum triamidoamine complex. They also proposed a probable mechanism for the same which has undergone many theoretical investigations. However, despite having a biological significance, the analogous vanadium triamidoamine complex fails to perform the task. In this part of the chapter, a systematic theoretical study on the thermodynamics of dinitrogen fixation mediated by vanadium triamidoamine has been carried out at PBE1PBE/SDD level of theory. The results were compared to that of molybdenum triamidoamine system for a better understanding of the

intrinsic difficulties associated with the conversion of dinitrogen to ammonia with the vanadium system.



DECLARATION BY THE CANDIDATE

The thesis entitled “*Theoretical Studies on the Electronic Structure and Stability of Inorganic Ring Systems, Metallatranes, Carbon Bases and Mechanism of Dinitrogen Reduction*” is being submitted to Tezpur University in partial fulfillment for the award of the degree of Doctor of Philosophy in Chemical Sciences is a record of bonafide research work accomplished by me under the supervision of *Dr. Ashwini K. Phukan*.

All helps from various sources have been dully acknowledged.

No part of this thesis has been submitted elsewhere for award of any other degree.

Date: 21-09-2012

Place: Tezpur

Ankur Kanti Guha
Ankur Kanti Guha

Department of Chemical Sciences
Tezpur University
Assam, India



Dr. Ashwini K. Phukan
Associate Professor
Department of Chemical
Sciences
Tezpur University
Tezpur 784 028, Assam, INDIA
e-mail : ashwini@tezu.ernet.in
Ph : +91 (3712) 275060
Fax: +91 (3712) 267005

CERTIFICATE OF THE SUPERVISOR

This is to certify that the thesis entitled “*Theoretical Studies on the Electronic Structure and Stability of Inorganic Ring Systems, Metallatranes, Carbon Bases and Mechanism of Dinitrogen Reduction*” submitted to the School of Sciences, Tezpur University in partial fulfillment for the award of the degree of Doctor of Philosophy in the Department of Chemical Sciences is a record of research work carried out by **Mr. Ankur Kanti Guha** under my supervision and guidance.

All help received by him from various sources have been duly acknowledged.

No part of this thesis has been submitted elsewhere for award of any other degree.

Date: 21-09-2012

Place: Tezpur

Dr. Ashwini K. Phukan

Department of Chemical Sciences
School of Sciences
Tezpur University
Assam, India

Acknowledgements

At the outset, I thank God for offering me a luck to fall under the shed of a great person, my supervisor, Dr. Ashwini K, Phukan. I express my deepest sense of gratitude and respect to him. This thesis would have never been possible to accomplish without his inspiring guidance, strong motivation, constant encouragement, untiring help and a brotherly care. I will always remember the discussions that we used to have even during a cup of tea. Thank you very much sir for exposing me to this beautiful world of chemistry.

I gratefully acknowledge Prof. Niranjan Karak, Dr. Ashim J. Thakur and Dr. Panchanan Pujari, Department of Chemical Sciences, Tezpur University, for their suggestions and discussions. I am grateful to all the faculty members and staffs of the Department of Chemical Sciences for their help and support.

I offer my sincere thanks to all my lab mates, Satyajit da and Ujjal for helping me during my work and maintaining a friendly environment in the lab.

My special thanks goes to my well wishers specially, Moumita, Kusum da and Amar.

I am grateful to Prof. Gernot Frenking, Phillips – Universität Marburg, Germany, Prof. Bernard Silvi, Université Pierre et Marie Curie, France and Prof. Carlo Gatti, CNR-ISTM Institute di Scienze e Technologie Moleculari, Italy for their help and suggestions.

I gratefully acknowledge Tezpur University for Institutional Fellowship and Council of Scientific and Industrial Research (CSIR) for Senior Research Fellowship (SRF).

Finally, I thank the authorities of Tezpur University for granting me the permission to carry out my research work.

Last but not the least, I would like to offer my sincere gratitude to my beloved parents and my younger sister Piali for their blessing, love, inspiration and support throughout my studies to fulfill my dreams.

Ankur Kanti Guha

Contents

Abstract	i
Acknowledgements	x
Table of Contents	xi
List of Tables	xv
List of Figures	xx
List of Schemes	xxiv
Abbreviations	xxvi
CHAPTER 1: A Brief Introduction to Computational Chemistry	
[1.0] General Introduction	1
[1.1] Density Functional Theory	3
[1.1.1] The Hohenburg-Kohn Theorem	6
[1.1.2] The Energy Functional	6
[1.1.3] The Local Density Approximation for $E_{xc}[\rho]$	8
[1.1.4] The Generalized Gradient Approximation	9
[1.1.5] Meta-GGA Functionals	10
[1.2] Quantum Theory of Atoms in Molecules (QTAIM)	10
[1.2.1] Localization and Delocalization Indices	12
[1.2.2] The Bond Ellipticity (ε)	12
[1.2.3] Energy Density at the BCP	13
[1.3] The Electron Localization Function (ELF)	14
[1.4] Brief Overview of the Remaining Chapters	16
[1.4.1] Chapter 2: Aromaticity in Borazine and Its Heavier Analogs	16
[1.4.2] Chapter 3: Nature and Extent of Transannular Interactions in Group 4 and Group 6 Metallatranes	17
[1.4.3] Chapter 4: Structure, Stability and Reactivity of Different Carbon Bases	17
[1.4.3.1] Revisiting the Reactivity of Heterocyclic Carbenes	18
[1.4.3.2] Stabilization of Cyclic and Acyclic Carbon(0) Compounds By Differential Coordination of Heterocyclic Carbenes	18
[1.4.3.3] Reactivity of Different Carbon Bases	19
[1.4.4] Chapter 5: Mechanistic Study of Dinitrogen Reduction mediated by Tripodal Complexes of Vanadium	20

[1.4.4.1]	Mechanistic Details for the Conversion of Hydrazine to Ammonia Mediated by Vanadium(III) Thiolate Complexes	20
[1.4.4.2]	Mechanistic Study for the Complete Conversion of Dinitrogen to Ammonia Mediated by Vanadium Triamidoamine Complex	21
[1.5]	Bibliography	22

CHAPTER 2: Aromaticity in Borazine and Its Heavier Analogs

[2.0]	Abstract	24
[2.1]	Introduction	24
[2.2]	Computational Details	27
[2.3]	QTAIM and ELF	27
[2.4]	Results and Discussion	29
[2.4.1]	Molecular Geometry	29
[2.4.1.1]	M ₃ Z ₃ R ₃ systems	29
[2.4.1.2]	M ₃ E ₃ R ₃ systems	34
[2.4.2]	Stabilization Energy and Ring Current	36
[2.4.3]	QTAIM and ELF analysis	42
[2.5]	Conclusions	48
[2.6]	Bibliography	50

CHAPTER 3: Nature and Extent of Transannular Interactions in Group 4 and Group 6

Metallatranes

[3.0]	Abstract	53
[3.1]	Introduction	53
[3.2]	Computational Details	55
[3.3]	Results and Discussion	56
[3.3.1]	Molecular Geometry	56
[3.3.1.1]	Group 4 Metallatranes	56
[3.3.1.2]	Group 6 Metallatranes	63
[3.3.2]	Stabilization Energy	68
[3.3.3]	QTAIM Analysis	70
[3.4]	Conclusions	77
[3.5]	Bibliography	78

Chapter 4: Structure, Stability and Reactivity of Different Carbon Bases

[4.0]	Abstract	81
-------	----------	----

[4.1]	Revisiting the Reactivity of Heterocyclic Carbenes	82
[4.1.1]	Introduction	82
[4.1.2]	Computational Details	85
[4.1.3]	Results and Discussion	85
[4.1.4]	Conclusions	94
[4.2]	Stabilization of Cyclic and Acyclic Carbon(0) Compounds By Differential Coordination of Heterocyclic Carbenes	95
[4.2.1]	Introduction	95
[4.2.2]	Results and Discussion	96
[4.2.2.1]	Molecular Geometry	96
[4.2.2.2]	Molecular Orbital (MO) Analysis	98
[4.2.2.3]	Proton Affinities	100
[4.2.2.4]	Donor-Acceptor Bond Strengths and Thermodynamic Stabilities	102
[4.2.2.5]	Complexation Energies	104
[4.2.3]	Conclusions	107
[4.3]	Reactivity of Different Carbon Bases	108
[4.3.1]	Introduction	108
[4.3.2]	Results and Discussion	110
[4.3.3]	Conclusions	118
[4.4]	Bibliography	119

Chapter 5: Mechanistic Study of Dinitrogen Reduction mediated by Tripodal Complexes of Vanadium

[5.0]	Abstract	122
[5.1]	Mechanistic Details for the Conversion of Hydrazine to Ammonia Mediated by Vanadium(III) Thiolate Complexes	123
[5.1.1]	Introduction	123
[5.1.2]	Computational Details	123
[5.1.3]	Results and Discussion	124
[5.1.4]	Conclusions	127
[5.2]	Mechanistic Study for the Complete Conversion of Dinitrogen to Ammonia Mediated by Vanadium Triamidoamine Complex	129
[5.2.1]	Introduction	129
[5.2.2]	Computational Details	130
[5.2.3]	Results and Discussion	132

[5.2.3.1]	Mechanistic Details of [V] ([V] = (N ₃ N)V)	132
[5.2.3.2]	Comparison between [V] and [Mo] catalyst	139
[5.2.4]	Conclusions	143
[5.3]	Bibliography	145
[5.4]	List of Publications	148
[5.5]	List of School/Workshop/Summer School Attended	150

List of Tables

Chapter	Table	Title	Page No.
2	2.1	List of experimentally known rings with generic formulae $M_3Z_3R_3$ and $M_3E_3R_3$ ($M = B, Al, Ga$; $Z = N, P, As$; $E = O, S, Se$) for which crystal structures are available.	25
	2.2	Calculated bond lengths (\AA) for the planar (Pl) and puckered (Py) geometries, their difference ($\Delta r, \text{\AA}$) and the energy difference between these two geometries (ΔE in kcal/mol) for $R_2M=ZH_2$ and $M_3Z_3R_3$ systems. The Wiberg Bond Index (WBI) values are given within parenthesis.	29
	2.3	Calculated bond lengths (\AA) for $R_2M=EH$ and $M_3E_3R_3$ rings. The Wiberg Bond Index (WBI) values are given within parenthesis.	34
	2.4	Calculated aromatic stabilization energies (ASE in kcal/mol) and nucleus independent chemical shift (NICS) values for $M_3Z_3R_3$ rings.	37
	2.5	Calculated aromatic stabilization energies (ASE in kcal/mol) and nucleus independent chemical shift (NICS) values for $M_3E_3R_3$ rings.	40
	2.6	Summary of QTAIM delocalization index(δ_{AB}), density at AB bond critical point [$\rho(bcp)$] and its laplacian $\nabla^2\rho$ (bcp), total ELF value at the ring bifurcation (ELF_t) and ELF π component ring bifurcation value (ELF_π) for boron heterocyclic rings.	42
	2.7	Summary of QTAIM delocalization index(δ_{AB}), density at AB bond critical point [$\rho(bcp)$] and its laplacian $\nabla^2\rho$ (bcp), total ELF value at the ring bifurcation (ELF_t) and ELF π component ring bifurcation value (ELF_π) for aluminium heterocyclic rings.	44
	2.8	Summary of QTAIM delocalization index(δ_{AB}), density at AB bond critical point [$\rho(bcp)$] and its laplacian $\nabla^2\rho$ (bcp), total ELF value at the ring bifurcation (ELF_t) and ELF π component ring bifurcation value (ELF_π) for gallium heterocyclic rings.	45

	2.9	Summary of the ELF population analysis of the $B_3N_3H_6$, $B_3P_3H_6$, $B_3O_3H_3$, $B_3As_3H_6$, $B_3As_3F_3H_3$ and $Al_3N_3H_6$ molecules. $\Delta\chi$ is the electronegativity difference of centres Z and M, $\bar{N}[V(M, Z)]$ the population of the V(M,Z) basin, σ^2 its variance, $\bar{N}[V(M, Z) Z]$ the contribution of the Z atomic basin to V(M,Z) population, $\langle \text{cov}(M, Z), (M, Z') \rangle$ and $\langle \text{cov}(M, Z), (M', Z) \rangle$ the covariance matrix elements of the populations of the adjacent V(M,Z) basins.	47
3	3.1	List of experimentally known structures of Group 4 and 6 metallatranes ($Z-M[-ER(CH_2)_2-]_3N$) for which crystal structures are available. (Here E is the equatorial substituent and Z is the apical ligand).	54
	3.2	B3LYP/LANL2DZ computed transannular distance (r_{M-Nax}), average metal – equatorial atom (r_{M-E}) and metal – apical (r_{M-Z}) bond distances (Å), pyramidalization angles (in degrees) around metal (θ_M), axial nitrogen (θ_N) and equatorial atom (θ_E), and natural charges at metal (q_M) and axial nitrogen (q_N) for $Z-Ti[-ER(CH_2)_2-]_3N$. The respective Wiberg Bond Index (WBI) values are given within parenthesis.	57
	3.3	B3LYP/LANL2DZ computed transannular distance (r_{M-Nax}), average metal – equatorial atom (r_{M-E}) and metal – apical (r_{M-Z}) bond distances (Å), pyramidalization angles (in degrees) around metal (θ_M), axial nitrogen (θ_N) and equatorial atom (θ_E), and natural charges at metal (q_M) and axial nitrogen (q_N) for $Z-Zr[-ER(CH_2)_2-]_3N$. The respective Wiberg Bond Index (WBI) values are given within parenthesis.	60
	3.4	B3LYP/LANL2DZ computed transannular distance (r_{M-Nax}), average metal – equatorial atom (r_{M-E}) and metal – apical (r_{M-Z}) bond distances (Å), pyramidalization angles (in degrees) around metal (θ_M), axial nitrogen (θ_N) and equatorial atom (θ_E), and natural charges at metal (q_M) and axial nitrogen (q_N) for $Z-Hf[-ER(CH_2)_2-]_3N$. The respective Wiberg Bond Index (WBI) values are given within parenthesis.	62
	3.5	B3LYP/LANL2DZ computed transannular distance (r_{M-Nax}), average metal – equatorial atom (r_{M-E}) and metal – apical (r_{M-Z}) bond distances (Å), pyramidalization angles (in degrees) around metal (θ_M), axial nitrogen (θ_N) and equatorial atom (θ_E), and natural charges at metal (q_M) and axial nitrogen (q_N) for $Z-Cr[-ER(CH_2)_2-]_3N$. The respective Wiberg Bond Index (WBI) values are given within parenthesis.	64

3.6	Relative stability of the different spin states of Group 6 metallatranes at their +3 oxidation state computed at the B3LYP/LANL2DZ level of theory. The values for Cr, Mo and W are given in bold, normal and italics respectively.	65
3.7	B3LYP/LANL2DZ computed transannular distance ($r_{M-N_{ax}}$), average metal – equatorial atom (r_{M-E}) and metal – apical (r_{M-Z}) bond distances (Å), pyramidalization angles (in degrees) around metal (θ_M), axial nitrogen (θ_N) and equatorial atom (θ_E), and natural charges at metal (q_M) and axial nitrogen (q_N) for Z-Mo[-ER(CH ₂) ₂] ₃ N]. The respective Wiberg Bond Index (WBI) values are given within parenthesis.	66
3.8	B3LYP/LANL2DZ computed transannular distance ($r_{M-N_{ax}}$), average metal – equatorial atom (r_{M-E}) and metal – apical (r_{M-Z}) bond distances (Å), pyramidalization angles (in degrees) around metal (θ_M), axial nitrogen (θ_N) and equatorial atom (θ_E), and natural charges at metal (q_M) and axial nitrogen (q_N) for Z-W[-ER(CH ₂) ₂] ₃ N]. The respective Wiberg Bond Index (WBI) values are given within parenthesis.	67
3.9	B3LYP/LANL2DZ computed stabilization energies for Group 4 and 6 metallatranes. Ti and Cr values are given in bold, Zr and Mo values in normal and Hf and W values are in italics.	69
3.10	Topological parameters at the M – N bond critical points of Group 4 metallatranes. Electron density (ρ_b), its laplacian ($\nabla^2 \rho$) and total electronic energy density $H(r)$ are all in a. u.	71
3.11	Topological parameters at the M – N bond critical points of Group 6 metallatranes. Electron density (ρ_b), its laplacian ($\nabla^2 \rho$) and total electronic energy density $H(r)$ are all in a. u.	72
3.12	Delocalization index between M and bridgehead nitrogen atom N [$\delta(M, N)$], magnitude of charge transfer from A to B [$ q(A \rightarrow B) $], magnitude of Ehrenfest forces on the metal atom M [$ F(M) $] and changes in nuclear – electron potential energy for the metal atom [$\Delta V_{ne}(M)$] calculated at B3LYP/6-31+G* level of theory. All the quantities are in atomic units.	74
3.13	Delocalization index between M and bridgehead nitrogen atom N [$\delta(M, N)$], magnitude of charge	75

transfer from A to B [$q(A \rightarrow B)$], magnitude of Ehrenfest forces on the metal atom M [$F(M)$] and changes in nuclear – electron potential energy for the metal atom [$\Delta V_{ne}(M)$] calculated at B3LYP/6-31+G* level of theory. All the quantities are in atomic units.

4.1.1	Energies of the highest occupied π and σ symmetric orbitals (E_π and E_σ in eV) and their occupancies, first (E_{PA-1}) and second (E_{PA-2}) proton affinities in kcalmol ⁻¹ calculated at BP86/TZVP level of theory.	88
4.1.2	Nucleus independent chemical shift (NICS) values of the central five member ring (R_{central}) and the exocyclic six member ring (R_{exo}) calculated at the BP86/6-31+G* level of theory. Values within parenthesis refer to the NICS calculations at BP86/cc-pVTZ level of theory.	89
4.1.3	Calculated bond dissociation energies in kcal mol ⁻¹ (including zero-point vibrational correction) for the dissociation of one molecule of AuCl and Ni(CO) ₂ from E-M and E-(M) ₂ respectively [E = 1, 4, and 7; M = AuCl and Ni(CO) ₂].	91
4.2.1	First (E_{PA-1}) and second (E_{PA-2}) proton affinities in kcal mol ⁻¹ calculated at BP86/TZVP level of theory.	100
4.2.2	Bond dissociation energies D_e (kcal mol ⁻¹) and energies including thermal and vibrational corrections D_o^{298} (kcal mol ⁻¹) calculated using reaction (1) at BP86/TZVP level of theory.	103
4.2.3	Calculated bond dissociation energies in kcal mol ⁻¹ (including zero-point vibrational correction) for the dissociation of one molecule of AuCl from N-AuCl and N-(AuCl) ₂ respectively [N = 1 - 6].	104
4.3.1	Computed natural charge at the central carbon atom (q_C), first and second proton affinities (PA, in kcal mol ⁻¹) and bond dissociation energies (BDE in kcal mol ⁻¹) for the dissociation of one molecule of AuCl from L-AuCl and L-(AuCl) ₂ . All the energies include zero point vibrational correction.	112
5.1.1	Natural charges and vibrational stretching frequencies (cm ⁻¹) calculated at the B3LYP/LANL2DZ level of theory.	124
5.2.1	Comparison with the available X-ray data of [V]-NH ₃ complex	131

5.2.2	Comparison of the energetic with previous reported studies.	131
5.2.3	Charge decomposition (CDA) analysis of [V]-N ₂ and [Mo]-N ₂ complexes calculated at PBE1PBE/SDD level of theory along with NBO occupancies of the two orthogonal π^* orbitals of N \equiv N in their respective complexes. ν_{NN} (cm ⁻¹) is the infrared N ₂ stretching frequencies (without scaling).	132
5.2.4	Energetic (kcal/mol) of the equatorial and terminal protonation of various steps involved in the catalytic reduction of N ₂ to NH ₃ by vanadium triamidoamine complex. For numbering of the molecules, see Figure 5.2.3 of the main text.	137

List of Figures

Chapter	Figure	Title	Page No.
2	2.1	Correlation between changes in bond lengths (Å) and NICS values for few representative $M_3Z_3R_3$ rings, viz., (a) B_3As_3 , (b) Al_3N_3 and (c) Ga_3P_3 .	39
	2.2	Correlation between changes in bond lengths (Å) and NICS values for few representative $M_3E_3R_3$ rings, viz., (a) B_3Se_3 , (b) Al_3O_3 and (c) Ga_3S_3 .	41
	2.3	ELF=0.8 and bifurcation isosurface of ELF_t and ELF_π of $B_3N_3H_6$, $B_3As_3F_3H_3$, $B_3As_3H_6$ and $B_3O_3H_3$ molecules. Color code: magenta=core, light blue = AH bonds, redbrick = lone pairs, green = bonds.	48
3	3.1	Optimized geometry of a titanatrane molecule shown in two different perspectives.	57
	3.2	Variation of $r(M-N)$ (Å) with (a) electron density (ρ , a. u) and (b) laplacian [$\nabla^2\rho$ (bcp), a. u.] at the bond critical point of the transannular Ti-N bonds.	73
	3.3	Contour plots of laplacian, $\nabla^2\rho$ (bcp), in N-Ti-Z plane (obtained with AIMALL program at B3LYP/6-31+G* level of theory) showing the effect of apical, (a) Z = CH ₃ and (b) Z = NH ₃ and equatorial substituents (c) E = O and (d) E = S on the bonding of titanatranes. Regions of charge depletion ($\nabla^2\rho > 0$) are denoted by solid blue lines while regions of charge concentration ($\nabla^2\rho < 0$) are denoted by dashed red lines. Green sphere denotes bond critical points (BCPs) and black solid line denotes bond paths.	73
	3.4	Contour plots of laplacian, $\nabla^2\rho$ (bcp), in N-Cr-Z plane (obtained with AIMALL program at B3LYP/6-31+G* level of theory) showing the effect of apical, (a) Z = CH ₃ and (b) Z = NH ₃ and equatorial substituents (c) E = O and (d) E = S on the bonding of chromatranes. Regions of charge depletion ($\nabla^2\rho > 0$) are denoted by solid blue lines while regions of charge concentration ($\nabla^2\rho < 0$) are denoted by dashed red lines. Green sphere denotes bond critical points (BCPs) and black solid line denotes bond paths.	76

4.1.1	Optimized geometries of 1 , 4 , and 7 at BP86/TZVP level of theory. Bond lengths are in Å and angles are in degrees.	86
4.1.2	Shapes of the HOMO and HOMO-1 of 1 , 4 , and 7 obtained at BP86/TZVP level of theory.	87
4.1.3	Optimized geometries of the first and second protonated species of 1 and 7 . Bond lengths are in Å.	88
4.1.4	Lowest energy structures of E-AuCl , E-(AuCl)₂ , E-Ni(CO)₂ and E{Ni(CO)₂}₂ (E = 1 , 4 , and 7) computed at BP86 level of theory. Bond lengths are in Å and angles are in degrees.	92
4.1.5	Experimentally characterized bridging complexes of NHC.	94
4.2.1	Lowest energy optimized geometries of 1-6 . Bond lengths are in Å and angles are in degrees. q_C represents the natural charge at the central carbon atom.	97
4.2.2	Energies (eV) and shapes of the highest occupied molecular orbitals for 1 – 6 at BP86/TZVP level of theory.	99
4.2.3	Optimized geometries of the first protonated derivatives of the molecules 1 – 6 at BP86/TZVP level of theory. Bond lengths are in Å and angles are in degrees. q_C represents the natural charge at the central carbon atom.	101
4.2.4	Correlation plot between (a) first proton affinity and energy of the σ symmetric lone pair orbital, and (b) second proton affinities and energies of the π symmetric HOMO of the first protonated derivatives of 1 – 6 .	102
4.2.5	Lowest energy optimized geometries of N-AuCl and N-(AuCl)₂ (N = 1 – 6) calculated at BP86/TZVP level of theory. Bond lengths are in Å and angles are in degrees.	105
4.3.1	Important frontier molecular orbitals of 1-6 . Energies are in eV. R = Me.	111
4.3.2	Optimized geometries of the first and second protonated species of 1-6 . The optimized geometry of the second protonated species of 2 is not shown as optimization leads to a broken geometry.	113

4.3.3	Correlation plot between the energy of the σ symmetric lone pair orbital and first proton affinity.	114
4.3.4	Correlation plot between the energy of the lone pair orbital of the first protonated species and second proton affinity.	114
4.3.5	Optimized geometries of mono and diaurated complexes of 1-6 . Bond lengths are in Å.	115
4.3.6	Optimized geometries of the adducts 11 and 12 .	117
5.1.1	Catalytic cycle and energy profile (in kcal/mol) for the reduction of hydrazine to ammonia mediated by vanadium (III) thiolate [VPS3] complex computed at the B3LYP/LANL2DZ//B3LYP/TZVP level of theory.	125
5.1.2	Catalytic cycle and energy profile (in kcal/mol) for the reduction of hydrazine to ammonia mediated by vanadium (III) thiolate [VNS3] complex computed at the B3LYP/LANL2DZ//B3LYP/TZVP level of theory.	128
5.2.1	Three possible pathways of dinitrogen addition, protonation and reduction of [V] ([V] = (N ₃ N)V) to yield [V]-N=NH. Energies are in kcal/mol.	133
5.2.2	Two possibilities (ligand derived amido and terminal) for the initial protonation of [V]-N ₂ (R = H). Energies are in kcal/mol.	134
5.2.3	Catalytic cycle (top right) and free energy profile for the reduction of N ₂ to ammonia mediated by [V] ([V] = (N ₃ N)V) systems. Energies correspond to standard free energies of formation (ΔG^0) and are in kcal/mol. Energies shown are not to scale.	135
5.2.4	Possible intermediate and transition state for the conversion of 3 to 4 . Energies correspond to standard free energies of formation (ΔG^0) and are in kcal/mol.	136
5.2.5	Possible intermediate and transition state for the conversion of 7 to 8 . Energies correspond to standard free energies of formation (ΔG^0) and are in kcal/mol.	138
5.2.6	$\sigma^*_{N\sigma-N\beta}$ orbitals of (a) [V]-N-NH ₃ (8) (Energy = 4.1 eV) and (b) [Mo]-N-NH ₃ ¹⁺ (Energy = 1.7 eV).	140
5.2.7	Different possibilities of initial NH ₃ /N ₂ exchange. Energies are in kcal/mol.	141

5.2.8

Optimized geometries of the (a) $[\text{V}](\text{NH}_3)(\text{N}_2)$ and (b) $[\text{Mo}](\text{NH}_3)(\text{N}_2)$ complex. The spheres represent the van der Waals' spheres of the atoms. Hydrogen atoms are omitted for clarity.

142

List of Schemes

Chapter	Scheme	Title	Page No.
1	1.0	Interplay between experiment and theory, taken from reference 1.	1
2	2.1	Schematic representation of borazine and its heavier analogs with different substituents at the group 13 elements.	27
3	3.1	Schematic representation of group 4 and group 6 metallatranes with different equatorial (E) and apical (Z) substituents.	55
4	4.1.1	Schematic representation of Arduengo carbene 1 and carbodiphosphorane 2 . Resonance form 2b which represents the C(0) character of 2 are also shown.	82
	4.1.2	Carbodicarbene, C(NHC) ₂ (4) and its resonance form 4b indicating its C(0) character.	83
	4.1.3	Possible resonance forms of <i>N</i> -heterocyclic carbene and silylene showing its divalent element (II) character 1a , 5a and divalent element (0) character 1b , 5b .	84
	4.1.4	Possible resonance forms of 2, 2'-bipyridyl carbene 7 showing carbene (7a) and carbene (7b) character.	85
	4.2.1	Schematic representation of acyclic carbodicarbenes (1 – 3) with both the L groups as abnormal carbene (1), remote carbene (2) and one of the L groups is abnormal and the other one is remote carbene (3) and their cyclic derivatives 4 – 6 .	96
	4.3.1	<i>N</i> -heterocyclic carbene 1 , cyclic(alkyl)(amino)carbene 2 , (amino)-(ylide) carbene 3 , carbocyclic carbene stabilized by two ylides 4 , carbodiphosphorane 5 and carbodicarbene 6 . R = Me.	108
	4.3.2	Nucleophilic addition reaction of electrophilic carbene. ⁴⁰	117
	4.3.3	Theoretically calculated nucleophilic addition reactions of 2 and 5 yielding 11 and 12 respectively.	117

5	5.2.1	Model vanadium and molybdenum complexes of triamidoamine ligand.	130
---	-------	--	-----

Abbreviations used in this thesis

<i>a</i> -NHC	Abnormal <i>N</i> -heterocyclic carbene
ASE	Aromatic stabilization energy
AYC	(Amino)-(ylide) carbene
BCP	Bond critical point
CAAC	Cyclic(alkyl)(amino)carbene
CC	Coupled Cluster
CDA	Charge decomposition analysis
CDP	Carbodiphosphorane
CI	Configuration interaction
CCP	Cage critical point
DFT	Density Functional Theory
ECP	Effective core potential
ELF	Electron Localization Function
EPR	Electron paramagnetic resonance
ENDOR	Electron nuclear double resonance
GIAO	Gauge independent atomic orbital
GGA	Generalized gradient approximation
HF	Hartree-Fock
HIPT	Hexa- <i>iso</i> -propyl terphenyl
LDA	Local density approximation
MP	Møller-Plesset
MRCI	Multireference configuration interaction
MCSCF	Multiconfigurational self consistent field
NBO	Natural bond orbital
NHC	<i>N</i> -heterocyclic carbene
NICS	Nucleus independent chemical shift
OMCVD	Organometallic chemical vapour deposition
QTAIM	Quantum theory of atoms in molecules
<i>r</i> -NHC	Remote <i>N</i> -heterocyclic carbene
TEA	Triethoxyamine
WBI	Wiberg bond index

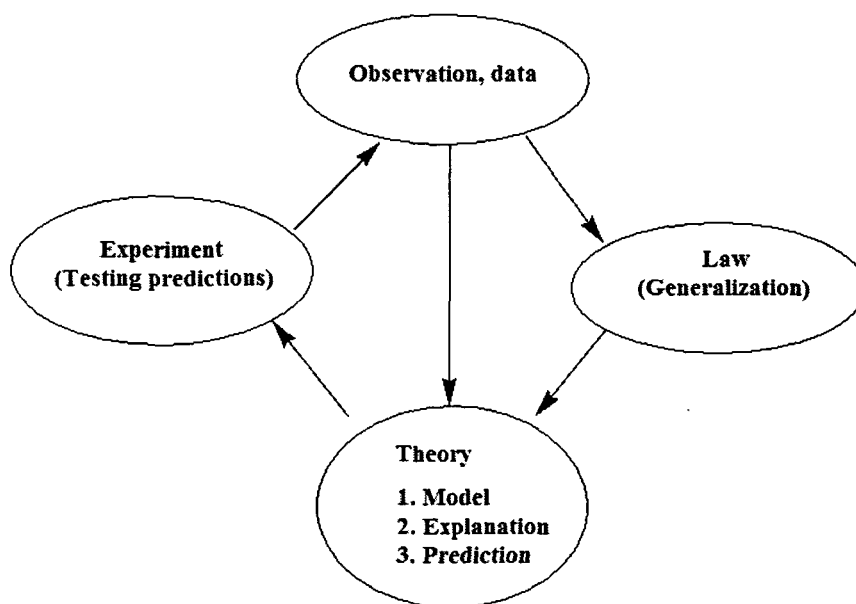


CHAPTER - 1

**Brief Introduction To Computational
Chemistry**

[1.0] General Introduction

Chemistry is the science of matter, its composition, structure and properties. Chemistry is concerned with atoms and their interactions with other atoms, and particularly with the properties of chemical bonds.¹ Although chemistry is primarily an experimental science, however, presently, parallel to the experiments, computational techniques guided by modern quantum mechanics have become indispensable tools not only in chemistry but also in allied areas such as biology, medicine and material chemistry. Thus, viewed from the historical point of view, observations and accumulation of data from an experiment lead to the generalization (law) which results in the evolution of a new theory which, in turn, suggests predictions that can be tested by designing new experiments, and the whole process starts all over again (Scheme 1.0).¹ The intense interplay between theory and experiment has led to the enhancement of creativity, stimulation, teamwork which results in increase in ones overall competence in tackling a given problem.



Scheme 1.0. Interplay between experiment and theory, taken from reference 1.

The phenomenal advances in software and hardware have enabled the use of computational tools towards solving a wide range of chemical problems. Several instances are there where the computational methodologies facilitated better understanding of the experimental facts which helps in guiding the experimental research. For example, computational methodologies can be easily applied in exploring reaction pathways, structures and energetics of the transition states and intermediates which are otherwise very difficult to

study experimentally. Thus, a successful marriage between theory and experiment is necessary in modern day science as far as a better understanding of chemistry is concerned.

Although the mathematical basis for solving the quantum mechanical equations of chemical systems was clearly established nearly 86 years ago,² analytical solutions were only possible for two particle system. This was a fundamental lacuna which restricted the possibility of studying multiparticle systems. Since then, attempts were made in various directions for solving the quantum mechanical equations approximately. Stimulated by the tremendous advancement of modern day computers, a large number of theoretical methodologies with varying degree of sophistication have emerged.³⁻⁹

The crucial role of the application of theoretical methodologies in solving chemical problems has been recognized in recent years, which is reflected in the award of the 1998 Noble prize for chemistry to Professors John. A. Pople and Walter Kohn.⁹ Professor Pople popularized the usage of quantum chemistry in solving chemical problems through the development of Gaussian program package.¹⁰ This single software package enables one to use accurate quantum methodologies in solving various chemical problems like structure, stability, reactivity, magnetic properties and so on. Noteworthy to mention that this Gaussian package has been used throughout this thesis in studying different chemical problems.

Several computational methodologies are now available to deal with chemical problems. The Hartree-Fock (HF) formalism, where the wavefunction is described as single Slater determinant and optimized using a self consistent field iterative procedure, suffers from electron correlation. Various procedures have evolved throughout the years towards inclusion of electron correlation, which ultimately lead to the development of several post-HF methods like configuration interaction (CI), multireference CI (MRCI), multiconfigurational self consistent field (MCSCF), coupled cluster (CC), Møller-Plesset (MP) perturbation methods, etc. Although a full CI calculation with an adequate quality basis set represents the most intense computational treatment, it is too expensive to be used for systems with moderate size. The MP perturbation and CC which are capable of incorporating dynamic electron correlation have shown to yield reliable molecular structure and energies for systems which are not multireference in nature.

On the other hand, density functional theory (DFT) which also include electron correlation is computationally less expensive. While DFT based methods were much popular to solid state physicist, application of such methods for chemical problems was much limited. The X- α method,¹¹ a semi empirical variant of DFT was not particularly attractive as it showed poor performance in computing geometries, activation energies and reaction energies

compared to molecular orbital based methods. Another impediment of DFT based method was the limited availability of software packages. The breakthrough proposal of Kohn-Sham (KS) formalism, which use the one electron orbitals (K-S orbitals) similar to the SCF molecular orbitals provided easy access with much improved accuracy in studying chemical problems.¹² Kohn and Hohenberg provided the proof that ground state energy and the electron density are directly related, although the exact form of the functional relating these two is not known.¹³

Over the years, many functional for the exchange and correlation energy were proposed to deal with chemical problems. The DFT based methods were implemented in the Gaussian suite of programs by Pople and coworkers.¹⁰ The KS based DFT methods may be categorized as pure and hybrid methods. In pure DFT methods, functionals both exchange and correlation parts of the energy functional are approximated, whereas in case of hybrid DFT methods, functionals are approximated only for the correlation part while the exchange functional are derived from the exact exchange obtained from the HF method. The computational efficiency of DFT based methods coupled with its reliable adequacy has made them attractive choice. The present thesis deals with chemical problems employing DFT theory as implemented in Gaussian suite of program. A brief account of the theory is provided below.

[1.1] Density Functional Theory

The ground state energy of a collection of atoms may be computed by solving the Schrödinger's equation – the time independent and non relativistic form of which is given by,²

$$\hat{H}\Psi(\mathbf{r}_1, \mathbf{r}_2, \dots, \mathbf{r}_N) = E\Psi(\mathbf{r}_1, \mathbf{r}_2, \dots, \mathbf{r}_N) \quad (1)$$

The Hamiltonian operator, \hat{H} , is the summation of kinetic energy, the interaction with the external potential (V_{ext}) and the electron-electron interaction (V_{ee}), i. e.,

$$\hat{H} = -\frac{1}{2} \sum_i^N \nabla_i^2 + \hat{V}_{ee} + \sum_{i<j}^N \frac{1}{|\mathbf{r}_i - \mathbf{r}_j|} \quad (2)$$

In general, the external potential of interest is simply the interactions of electrons with the atomic nuclei;

$$\hat{V}_{ext} = - \sum_{\alpha}^{Nat} \frac{Z_{\alpha}}{|\mathbf{r}_i - \mathbf{R}_{\alpha}|} \quad (3)$$

where \mathbf{r}_i and \mathbf{R}_α are the coordinate of electron i and nucleus α respectively, and Z_α is the charge on the nucleus. For simplification, the spin part is omitted here and from further discussions on DFT. Equation 1 is solved for a set of ψ with the antisymmetric constraint. The lowest eigenvalue, E_0 , is the ground state energy and the probability density of finding an electron with any particular set of coordinates $\{\mathbf{r}_i\}$ is $|\psi_0|^2$. The average value of a state for a particular ψ is the expectation value of H , i. e.,

$$E[\psi] = \int \psi^* \hat{H} \psi \, d\mathbf{r} \equiv \langle \psi | \hat{H} | \psi \rangle \quad (4)$$

The notation $E[\psi]$ indicates that energy is a *functional* of the wavefunction. The variational theorem states that the energy so obtained is higher than that of the ground state (E_0) unless ψ corresponds to ψ_0 .

$$E[\psi] \geq E_0 \quad (5)$$

The ground state wavefunction and the energy may be evaluated by looking for all possible wavefunctions and finding the one that minimizes the total energy. One such procedure is Hartree-Fock theory where the total wavefunction is assumed to be the antisymmetric product of functions (φ_i) each of which is dependent on the coordinates of one electron, i. e.,

$$\psi_{HF} = \frac{1}{\sqrt{N!}} \det[\varphi_1 \varphi_2 \varphi_3 \dots \varphi_N] \quad (6)$$

where ‘det’ indicates a matrix determinant. Substitution of ψ into Schrödinger equation results in Hartree-Fock expression for energy;

$$\begin{aligned} E_{HF} = & \int \varphi_i^*(\mathbf{r}) \left(-\frac{1}{2} \sum_i^N \nabla_i^2 + V_{ext} \right) \varphi_i(\mathbf{r}) \, d\mathbf{r} \\ & + \frac{1}{2} \sum_{i,j}^N \int \frac{\varphi_i^*(\mathbf{r}_1) \varphi_i(\mathbf{r}_1) \varphi_j^*(\mathbf{r}_2) \varphi_j(\mathbf{r}_2)}{|\mathbf{r}_i - \mathbf{r}_j|} \, d\mathbf{r}_1 d\mathbf{r}_2 \\ & - \frac{1}{2} \sum_{i,j}^N \int \frac{\varphi_i^*(\mathbf{r}_1) \varphi_j(\mathbf{r}_1) \varphi_i(\mathbf{r}_2) \varphi_j^*(\mathbf{r}_2)}{|\mathbf{r}_i - \mathbf{r}_j|} \, d\mathbf{r}_1 d\mathbf{r}_2 \quad (7) \end{aligned}$$

The second term in eqn. 7 is the classical coulomb energy and the third term is the exchange energy written in terms of the orbitals. Applying variation theorem to the energy expression within the constraint that orbitals are orthonormal yields the ground state energy and lead to the Hartree-Fock equations,

$$\left[-\frac{1}{2} \nabla^2 + V_{ext}(\mathbf{r}) + \int \frac{\rho(\mathbf{r}')}{|\mathbf{r} - \mathbf{r}'|} \, d\mathbf{r}' \right] \varphi_i(\mathbf{r}) + \int V_X(\mathbf{r}, \mathbf{r}') \varphi_i(\mathbf{r}') \, d\mathbf{r}' = \varepsilon_i \varphi_i(\mathbf{r}) \quad (8)$$

where V_X is the non-local exchange potential and is such that

$$\int V_X(\mathbf{r}, \mathbf{r}') \varphi_i(\mathbf{r}') d\mathbf{r}' = - \sum_j^N \int \frac{\varphi_j(\mathbf{r}) \varphi_j^*(\mathbf{r}')}{|\mathbf{r} - \mathbf{r}'|} \varphi_i(\mathbf{r}') d\mathbf{r}' \quad (9)$$

Thus, the Hartree-Fock equations describe non-interacting electrons under the influence of a mean potential field consisting of the classical coulomb potential and a non-local exchange potential. From this point onwards, better approximation (correlated methods) for ψ and E_0 are readily obtained. However, the cost of such computation is very high. Many correlated methods are now available such as MP2, MP3, MP4, CISD, CCSD and CCSD(T) which formally scales with the number of electrons raised to the power of 5,6,7,6,6 and 7 respectively. In most cases, the accuracy of CCSD(T) calculations are sufficient enough for determination of chemical properties. However, the accuracy of such calculations comes at very high cost thereby limiting their use in real systems. Thus, it appears that solution of Schrödinger's equations for realistic system is very cumbersome. This gave rise to the development of a new theory called the density functional theory.

The Hamiltonian operator (eqn. 2) involves the coordinates of one and two electrons only. For the computation of total energy, knowledge of two-particle probability density, i. e., probability of finding an electron at \mathbf{r}_1 and another at \mathbf{r}_2 is sufficient. This implies that the total energy can be computed without the proper knowledge of $3N$ dimensional wave function.

The second order density matrix, a quantity of great use in analyzing the energy expression, is given by,

$$P_2(\mathbf{r}'_1, \mathbf{r}'_2; \mathbf{r}_1, \mathbf{r}_2) = \frac{N(N-1)}{2} \int \psi^*(\mathbf{r}'_1, \mathbf{r}'_2, \dots, \mathbf{r}'_N) \psi(\mathbf{r}_1, \mathbf{r}_2, \dots, \mathbf{r}_N) d\mathbf{r}_3 d\mathbf{r}_4 \dots d\mathbf{r}_N \quad (10)$$

The diagonal elements of P_2 , referred to as two-particle density matrix or pair density, are given by,

$$P_2(\mathbf{r}_1, \mathbf{r}_2) = P_2(\mathbf{r}_1, \mathbf{r}_2; \mathbf{r}_1, \mathbf{r}_2)$$

This is the required two electron probability function which determines all two particle operators. The first order density matrix, P_1 , may be defined in a similar way and can be written in terms of P_2 as,

$$P_1(\mathbf{r}'_1; \mathbf{r}_1) = \frac{2}{N-1} \int P_2(\mathbf{r}'_1, \mathbf{r}'_2; \mathbf{r}_1, \mathbf{r}_2) d\mathbf{r}_2 \quad (11)$$

Knowing P_1 and P_2 , the total energy can be determined exactly,

$$E = \int \left[\left(-\frac{1}{2} \nabla_1^2 - \sum_{\alpha}^{Nat} \frac{Z_{\alpha}}{|\mathbf{r}_1 - \mathbf{R}_{\alpha}|} \right) P_1(\mathbf{r}'_1, \mathbf{r}_1) \right]_{\mathbf{r}_1 = \mathbf{r}'_1} d\mathbf{r}_1 + \int \frac{1}{|\mathbf{r}_1 - \mathbf{r}_2|} P_2(\mathbf{r}_1, \mathbf{r}_2) d\mathbf{r}_1, d\mathbf{r}_2 \quad (12)$$

The diagonal elements of the first and second order density matrices completely determine the total energy. This vastly simplifies the task. The solution of full Schrödinger equation for ψ is not required – it is sufficient to determine P_1 and P_2 – and the problem in $3N$ coordinates space has been reduced to a problem in a 6 dimensional space.

Direct minimization of $E(P_1, P_2)$ suffers from specific problems as the density matrices should be constructed from an antisymmetric ψ . This is non trivial and currently an unsolved problem.¹⁴ Thus, it appears that eqn. 12 does not lead immediately to a reliable method for computing the total energy without calculating the many body wavefunction. However, the fact that boosts the density functional theory is the diagonal elements of the first order density matrix, i. e., the charge density, can completely determine the ground state energy.

[1.1.1] The Hohenburg-Kohn Theorems

In 1964, Hohenburg and Kohn provided two theorems¹³ which simplified the task in hand. The first theorem may be stated as:

The electron density determines the external potential (to within an additive constant).

As the external potential is used to specify the Hamiltonian operator (eqn. 2), thus, in principle, the Hamiltonian operator can be uniquely determined by the charge density and all the wavefunction of all the states can be computed. The second theorem establishes a variational theorem for a system of N electrons:

For any positive definite trial density, ρ_t , such that $\int \rho_t(\mathbf{r}) d\mathbf{r} = N$, then $E[\rho_t] \geq E_0$.

The two theorems lead to the fundamental statement of density functional theory:

$$\delta[E[\rho] - \mu(\int \rho(\mathbf{r})d\mathbf{r} - N)] = 0 \quad (13)$$

where μ is the chemical potential or the Lagrange multiplier of the constraint that the density contains the correct number of electrons. Thus, it appears that there is a *universal* functional $E[\rho]$ (i. e., it is independent of the external potential) which, if we know its form, can be inserted into the above equation and minimized to obtain the exact ground state density and energy.

[1.1.2] The Energy Functional

The energy functional contains three terms – the kinetic energy, the interaction with external potential and the electron-electron interaction;

$$E[\rho] = T[\rho] + V_{\text{ext}}[\rho] + V_{\text{ee}}[\rho]$$

The interaction with external potential is given by,

$$V_{ext}[\rho] = \int \hat{V}_{ext} \rho(\mathbf{r}) d\mathbf{r}$$

The kinetic and electron-electron functionals are not known. Direct minimization of the energy would be possible if good approximation to these functionals could be found. This possibility is a matter of recent research.¹⁵

Kohn and Sham proposed the following for approximating the kinetic and electron-electron functionals.¹² They introduced a system of N non-interacting electrons to be described by a single determinant wave function in N “orbitals” ϕ_i . In this system, the kinetic energy and electron density are known exactly from the orbitals,

$$T_s[\rho] = -\frac{1}{2} \sum_i^N \langle \phi_i | \nabla^2 | \phi_i \rangle$$

The true ground state density can be expressed in terms of ϕ_i as,

$$\rho(r) = \sum_i^N |\phi_i|^2 \quad (14)$$

The construction of density from a set of orbitals ensures that it is legal and can be constructed from an asymmetric wavefunction.

If one considers that classical Coulomb interaction or the Hartree energy represents a significant component of electron-electron interaction, then the second term in eqn. 7 written in terms of density will be,

$$V_H[\rho] = \frac{1}{2} \int \frac{\rho(\mathbf{r}_1)\rho(\mathbf{r}_2)}{|\mathbf{r}_1 - \mathbf{r}_2|} d\mathbf{r}_1 d\mathbf{r}_2$$

The energy functional can be rearranged as,

$$E[\rho] = T_s[\rho] + V_{ext}[\rho] + V_H[\rho] + E_{xc}[\rho] \quad (15)$$

where $E_{xc}[\rho]$ is the *exchange-correlation functional* which can be expressed as,

$$E_{xc}[\rho] = (T[\rho] - T_s[\rho]) + (V_{ee}[\rho] - V_H[\rho])$$

E_{xc} is simply the sum of error in using a non-interacting kinetic energy and the error in treating the electron-electron interaction classically. Writing the functional (eqn. 15) explicitly in terms of the density obtained from non-interacting orbitals (eqn. 14) and applying the variational theorem (eqn. 13), one finds that the orbitals which minimize the energy satisfy the following set of equation,

$$\left[-\frac{1}{2} \nabla^2 + V_{ext}(\mathbf{r}) + \int \frac{\rho(\mathbf{r}')}{|\mathbf{r} - \mathbf{r}'|} d\mathbf{r}' + V_{xc}(\mathbf{r}) \right] \phi_i(\mathbf{r}) = \varepsilon_i \phi_i(\mathbf{r}) \quad (16)$$

where the local multiplicative potential is the functional derivative of exchange correlation energy with respect to the density,

$$V_{xc}(\mathbf{r}) = \frac{\delta E_{xc}[\rho]}{\delta \rho} \quad (17)$$

This set of non-linear equations (the Kohn-Sham) describes the behavior of non-interacting electrons under the influence of an effective local potential. Thus, for the exact functional and exact local potential, the orbitals yield the exact ground state density and energy via eqn. 14 and 15 respectively. These Kohn-Sham equations are similar to the Hartree-Fock equations (eqn. 8) where the non-local exchange potential has been replaced by the local exchange-correlation potential, V_{xc} . However, the exact functional and its associated potential are not known. But, in principle, it is possible to solve the Schrödinger equations for a particular system and determine the energy functional and its associated potential. This of course needs greater effort. Nevertheless, the ability to determine the universal functional in a number of systems allows excellent approximations to the functional to be made. The approximations are discussed below in brief.

For calculations in which energy is the quantity of primary interest, DFT provides excellent and highly accurate alternative to the costly wavefunction based methods. However, the utility of this theory (DFT) is dependent on the approximation used for $E_{xc}[\rho]$.

[1.1.3] The Local Density Approximation for $E_{xc}[\rho]$

The generation of approximations for E_{xc} has initiated a rapidly expanding field of research. Different functional are now available which are more or less appropriate for any particular study. The early model that led to a practical utility of density functional theory was that of homogeneous electron gas for which exact results could be obtained. In this model, the electrons are subjected to a constant external potential and hence, the charge density is constant. The system can be specified by a single number – the value of the constant electron density, $\rho=N/V$.

The homogeneous electron gas was studied by Thomas and Fermi in 1920's¹⁶ considering the plane wave orbitals of the system. If the electron-electron interaction is approximated by classical Hartree potential (i. e., neglecting exchange and correlation effects), then the total energy functional can be readily obtained.¹⁶ Under these conditions, the kinetic and exchange energy (eqn. 7) can be expressed in terms of *local* functions of density. Application of the kinetic and exchange energy densities of the non-interacting homogeneous electron gas leads to following eqns,

$$T[\rho] = 2.87 \int \rho^{\frac{5}{3}}(\mathbf{r})d\mathbf{r} ; \text{ and, } E_x[\rho] = 0.74 \int \rho^{\frac{4}{3}}(\mathbf{r})d\mathbf{r} \quad (18)$$

The local exchange correlation energy per electron may be approximated as,

$$E_{xc}[\rho] \approx \int \rho(r)\varepsilon_{xc}(\rho(r))dr \quad (19)$$

where $\varepsilon_{xc}(\rho)$ is the local charge density which by choice is approximated to be the exchange and correlation energy density of the homogeneous electron gas of density ρ . This is the *local density approximation* (LDA). Within LDA, $\varepsilon_{xc}(\rho)$ can be separated into exchange and correlation contributions,

$$\varepsilon_{xc} = \varepsilon_x(\rho) + \varepsilon_c(\rho) \quad (20)$$

The Dirac form¹⁷ of ε_x can be written as,

$$\varepsilon_x(\rho) = -C\rho^{1/3} \quad (21)$$

where C is a constant introduced rather than that determined for a homogeneous electron gas. The functional form of the correlation energy density $\varepsilon_c(\rho)$ is unknown and can be obtained by numerical Monte Carlo calculations on homogeneous electron gas which yield exact results.¹⁸

LDA has been a fruitful approximation by the fact that it reduces the energy functional to a simple local function of the density. It provides reliable results of many properties such as structure, vibrational frequencies etc. However, in computing energy difference between rather different structures, energy barriers in diffusion or chemical reactions, LDA has proven to be not so reliable. Thus, the modification of the approximation is required and as such is now available.

One of the obvious extensions of the LDA is to recognize that the exchange contribution to the energy is dominant over the correlation energy for many systems. Thus, computation of the non-local exchange potential exactly as in Hartree Fock theory (eqn 7) and approximating the correlation potential within the LDA would yield a functional of the form,

$$E_{xc} \approx E_{Fock} + E_c^{LDA} \quad (22)$$

[1.1.4] The Generalized Gradient Approximation

The LDA can be considered as the zeroth order approximation to the semi-classical expansion of the density matrix in terms of the density and its derivative. A natural strategy is to adopt the gradient expansion approximation (GEA) in which the first order gradient terms in the expansion is included.

In the generalized gradient approximation (GGA), a functional form is implemented which ensures the normalization condition and leads to an energy functional that depends on

both density and its gradient. However, the analytic properties of the exchange correlation hole within LDA are retained. The typical form for a GGA functional is,

$$E_{xc} \approx \int \rho(\mathbf{r}) \varepsilon_{xc}(\rho, \nabla \rho) d\mathbf{r} \quad (23)$$

[1.1.5] Meta-GGA Functionals

Recently, functionals that depend on the Laplacian of the spin density or of the local kinetic energy density have been developed.¹⁹ Such functionals are referred to as meta-GGA functionals.

The typical form of such a functional is,

$$E_{xc} \approx \int \rho(\mathbf{r}) \varepsilon_{xc}(\rho, |\nabla \rho|, \nabla^2 \rho, \tau) d\mathbf{r} \quad (24)$$

where the kinetic energy density is,

$$\tau = \frac{1}{2} \sum_i |\nabla \varphi_i|^2 \quad (25)$$

Significant advances in approximations for $E_{xc}[\rho]$ have made DFT a practical, efficient and unbiased tool for computing various properties of molecules.

The three dimensional electron density distribution in a molecule is a primary quantity of interest as it can be used to calculate many observable properties of a molecule.²⁰ The recognition that electron density plays a crucial role in explaining and understanding the experimental observations of chemistry led Richard Bader to devise a topological theory called “*Atoms in Molecules*”.²¹ In recent literatures, this theory is often called the quantum theory of atoms in molecules (QTAIM) due to its rigorous basis in quantum mechanics.²² A brief account of the theory is given below.

[1.2] Quantum Theory of Atoms in Molecules (QTAIM)

QTAIM is rigorous and very powerful. It provides a thread of physical insight to chemistry. Many physical observables can be directly obtained using this theory which enables it to be applied to a wide range of problems from solid state physics to inorganic chemistry and drug design. The theory can provide various topological parameters; however the inclusion of all is not possible here. A brief discussion of the parameters which have been extensively used in this thesis are given below.

The theory is based on the physics of an open system. A proper open system is a region of space bounded by a surface $S(\mathbf{r})$ through which there is no flux in the gradient vector field of the electron density ρ , as expressed by the following equation,

$$\nabla\rho(\mathbf{r}) \cdot \mathbf{n}(\mathbf{r}) = 0 \quad \forall \mathbf{r} \in S(\mathbf{r}) \quad (26)$$

Eqn. 26 serves as the boundary condition for the definition of an open system within the principle of stationary action. The atoms in chemistry is recognized as an open system as their characteristic properties are additive and can be transferred from one system to another. For the cases where atomic and group properties are essentially additive and transferrable, these properties defined in this manner help in predicting the experimentally determined contributions to volume, polarizability and magnetic susceptibility.²³

The approach of two atoms results in the formation of critical points (CP) in the density. It is a point in space at which the first derivatives of the electron density vanish, i. e.,

$$\nabla\rho(r) = i \frac{d\rho}{dx} + j \frac{d\rho}{dy} + k \frac{d\rho}{dz} = \begin{cases} = \vec{0} & \text{(At CPs and at } \infty) \\ \text{Generally } \neq \vec{0} & \text{(At all other points)} \end{cases} \quad (27)$$

where the zero vector implies that each individual derivative in the gradient operator, ∇ , is zero and not just their summation.

A bond path is a line of maximum electron density connecting the two bonded atoms whose minimum lies in the bond critical point (bcp). A bond critical point is identified as three non-zero curvature of electron density (ρ_b), two of which are negative and is classified as (3, -1) critical point in ρ . The positive curvature λ_3 lies along the bond path and the two negative curvature λ_1 and λ_2 lie perpendicular to it. The laplacian of the electron density at the bond critical point [$\nabla^2\rho(bcp)$] is the summation of these three curvatures (or eigenvalues of the Hessian) as shown below:

$$\nabla^2\rho(\mathbf{r}) = \nabla \cdot \nabla\rho(\mathbf{r}) = \frac{d^2\rho(\mathbf{r})}{dx^2} + \frac{d^2\rho(\mathbf{r})}{dy^2} + \frac{d^2\rho(\mathbf{r})}{dz^2} = \lambda_1 + \lambda_2 + \lambda_3 \quad (28)$$

The compression of electron density perpendicular to the bond path results in negative values of λ_1 and λ_2 , and its expansion along the bond path results in positive eigenvalue λ_3 . Bader pointed out that these two competing processes decide the sign of the laplacian at the bond critical point. The sum of the negative values is greater than the positive one resulting in negative sign of the laplacian at the bond critical point (bcp) for homopolar covalent bonds. However, for closed shell bonding interactions (ionic, hydrogen bonding, etc.), Pauli's exclusion principle requires removal of electron density from the interatomic surface²⁴ resulting in positive value of the laplacian and low electron density at the bond critical point.

Each critical points are classified on the basis of their *rank* (ω) and *signature* (σ) and represented as (ω, σ). The rank is the number of non-zero curvatures of ρ at the critical point

while signature is algebraic sum of the signs of the curvatures. Thus, different critical points are categorized as: (a) (3, -3) – nuclear critical point (NCP), (b) (3, -1) – bond critical point (BCP), (c) (3, +1) – ring critical point (RCP) and (d) (3, -3) – cage critical point (CCP).

The number and type of critical points observed for a system must follow a strict topological relationship:

$$n_{\text{NCP}} - n_{\text{BCP}} + n_{\text{RCP}} - n_{\text{CCP}} = 1 \text{ or } 0 \quad (29)$$

The set $\{n_{\text{NCP}}, n_{\text{BCP}}, n_{\text{RCP}}, n_{\text{CCP}}\}$ for a given system is known as ‘characteristic set’. For finite systems such as molecules, the above expression is equal to one and is known as Poincaré – Hopf relationship,²¹ while for infinite periodic lattices, the expression equals zero and is known as Morse equation.²⁵

[1.2.1] Localization and Delocalization Indices

The delocalization index $\delta(A,B)$ for a closed shell system is defined²⁶ as the magnitude of the exchange of electrons in the basin of atom A with those in the basin of atom B, i. e.,

$$\delta(A, B) = 2|F^\alpha(A, B)| + 2|F^\beta(A, B)| \quad (30)$$

where the Fermi correlation is defined as

$$F^\sigma(A, B) = - \sum_i \sum_j S_{ij}(A)S_{ji}(B) \quad (31)$$

where $S_{ij}(\Omega) = S_{ji}(\Omega)$ is the overlap integral of two spin orbitals over a region Ω and σ represents spin (α or β).

Similarly, the localization index $[\lambda(A)]$ may be defined as

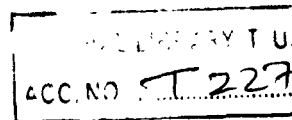
$$\lambda(A, A) = |F^\alpha(A, A)| + |F^\beta(A, A)| \quad (32)$$

For ionic systems, the limit of total localization approaches quite closely ($\geq 95\%$) to the actual number of electrons, $N^\sigma(A)$. However, one usually obtains $|F^\sigma(A, A)| < N^\sigma(A)$ indicating that the electrons in region A always exchange, i. e., they are delocalized. Thus, the total number of electrons is the sum of localization indices and half of all the delocalization indices and is given by,

$$N(A) = \lambda(A) + \frac{1}{2} \sum_{B \neq A} \delta(A, B) \quad (33)$$

[1.2.2] The Bond Ellipticity (ϵ)

It is a measure of the extent to which density is accumulated in a given plane containing the bond path and is defined as,



$$\varepsilon = \frac{\lambda_1}{\lambda_2} - 1 \quad (\text{where } |\lambda_1| \geq |\lambda_2|) \quad (34)$$

For cylindrically symmetric bonds such as C-C and C \equiv C, $\lambda_1 = \lambda_2$ and $\varepsilon = 0$. For double bonds, ε reaches maximum. Thus, ε is a measure of the π -character of a bond. For an aromatic bond, ε is ca. 0.23 while it is ca. 0.45 for a formal double bond in ethylene.²⁷

[1.2.3] Energy Density at the BCP

The knowledge of energy densities (potential, kinetic and total) at the BCP is useful to summarize the mechanics of a bonding interaction.

The relationship between kinetic energy density, potential energy density and laplacian of electron density for a stationary state in terms of local statement of virial theorem is,^{21, 28}

$$\left(\frac{\hbar^2}{4m}\right) \nabla^2 \rho(r) = 2G(r) + V(r) \quad (35)$$

where $G(r)$ is the gradient kinetic energy density and is always greater than zero, and $V(r)$ is the gradient potential energy density and is always less than zero. Thus, interactions for which $\nabla^2 \rho < 0$, the virial theorem when applied at BCP implies that such interactions are dominated by a local reduction of potential energy. On the other hand, interactions for which $\nabla^2 \rho > 0$ are dominated by a local excess in kinetic energy.

Cremer and Kraka²⁹ proposed to evaluate total energy density, $H(r) = G(r) + V(r)$ at BCP to take into account both kinetic and potential energy densities on equal footings. A value of $H(r) < 0$ at BCP indicates the presence of significant covalent character and accounts for the lowering of potential energy of electrons at BCPs. The magnitude of $H(r)$ reflects the "covalence" of interaction.

The use of QTAIM is many folds and is very successful in predicting many experimental properties. The theory has benefitted from the parallel advancement of accurate X-ray crystallography. Nowadays, crystallographers routinely rely on QTAIM to uncover chemical information contained in experimental electron-density maps. This has brought crystallography and chemical bonding theory closer than ever before.

Another topological descriptor is the electron localization function (ELF) introduced by Becke and Edgecombe³⁰ from the leading term in the Taylor series expansion of the spherically averaged *same-spin* conditional pair probability.³¹ A brief review of the theory is given below.

[1.3] The Electron Localization Function (ELF)

The ELF presents a different approach to the analysis of chemical bonding. Like QTAIM, ELF also deals with the topology of a function to analyze the molecular space. However, unlike QTAIM, it does not deal with the electron density itself but the conditional probability of the same spin pairs. ELF divides the molecular space in such a way that each basin provides chemical insights such as bonding regions, lone pairs or core basins.

The basins of ELF attractors are closely related to Gillespie's electronic domains and recover the ideas of Lewis. There are two type of basins: on the one hand are the core basins denoted $C(A)$ encompassing the nucleus of atom A , and on the other hand are the valence basins labelled $V(A, B, \dots)$. The valence shell of an atom, say A , in a molecule is therefore the union of the valence basins having a boundary with $C(A)$. A valence basin may belong to several atomic valence shells. The synaptic order is defined as the number of such valence shells to which a valence basin participates. There are therefore monosynaptic basins $V(A)$ corresponding to lone pair, disynaptic basins $V(A, B)$ corresponding to two centre bonds and higher polysynaptic basins for polycentric bonds.

The conditional probability has advantages over the pair density as it contains all the relevant information about the motion of pairs of electrons, while it does not contain irrelevant information concerning the position of the reference electron. The conditional probability, i. e., the probability density of electron **2** near \mathbf{r}_2 when electron **1** is at \mathbf{r}_1 , is given by,

$$P(\vec{r}_1, \vec{r}_2) = \frac{\gamma^{(2)}(\vec{r}_1, \vec{r}_2)}{\rho(\vec{r}_1)} \quad (36)$$

where $\gamma^{(2)}(\vec{r}_1, \vec{r}_2)$ and $\rho(\vec{r}_1)$ are the pair density and density respectively. Since, the conditional pair contains all the necessary information about the correlation of electrons, Becke and Edgecombe chose the spherical average of the conditional probability for same spin electrons:

$$\begin{aligned} \langle e^{\vec{s} \cdot \vec{\nabla}} P^{\sigma\sigma}(\vec{r}, \vec{r} + \vec{s}) \rangle &= \frac{1}{4\pi} \left(\int_{-1}^1 \int_0^{2\pi} e^{s\nabla\theta} d\theta d\phi \right) P^{\sigma\sigma}(\vec{r}, \vec{r} + \vec{s})|_{\vec{s}=\vec{0}} \\ &= \frac{\sinh(s\nabla)}{s\nabla} P^{\sigma\sigma}(\vec{r}, \vec{r} + \vec{s})|_{\vec{s}=\vec{0}} \end{aligned} \quad (37)$$

and expanded it by series of Taylor around the position of the reference electron³²

$$\begin{aligned} \langle e^{\vec{s} \cdot \vec{\nabla}} P^{\sigma\sigma}(\vec{r}, \vec{r} + \vec{s}) \rangle &= \left(1 + \frac{1}{6} s^2 \nabla_s^2 + \dots \right) P^{\sigma\sigma}(\vec{r}, \vec{r} + \vec{s})|_{\vec{s}=\vec{0}} \\ &\approx \frac{1}{6} s^2 \nabla_s^2 P^{\sigma\sigma}(\vec{r}, \vec{r} + \vec{s})|_{\vec{s}=\vec{0}} \end{aligned} \quad (38)$$

The right hand side of eqn. 38 holds as according to Pauli's principle, the same spin pair density at the coalescence point is zero, $\gamma^{\sigma\sigma}(\mathbf{r}, \mathbf{r}) = 0$. Hence, the leading term in the Taylor expansion of the spherically averaged conditional pair becomes proportional to:

$$D_\sigma = \frac{1}{2} \nabla_s^2 P^{\sigma\sigma}(\vec{r}, \vec{r} + \vec{s})|_{\vec{s}=\vec{0}} \quad (39)$$

Becke and Edgecombe used a relative ratio of D_σ with respect to the same quantity for homogeneous electron gas, D_σ^0 for a monodeterminantal wave function (which yields pair density straightforwardly from density),³³

$$D(\vec{r}) = \frac{D_\sigma}{D_\sigma^0} = \frac{\langle e^{\vec{s} \cdot \vec{\nabla}} P^{\sigma\sigma}(\vec{r}, \vec{r} + \vec{s}) \rangle / (\frac{s^2}{3})}{3/5(6\pi^2)^{2/3}[\rho^\sigma(\vec{r})]^{5/3}} \Big|_{\vec{s}=\vec{0}} = \frac{\nabla_s^2 \gamma^{(2)\sigma\sigma}(\vec{r}, \vec{r} + \vec{s})|_{\vec{s}=\vec{0}}}{C_F [2\rho^\sigma(\vec{r})]^{8/3}} \quad (40)$$

where C_F is the Fermi constant.

The probability of finding an electron of spin σ simultaneously when there is already another electron with same spin nearby is lower when the former is localized. Thus, the ratio $D(\vec{r})$ (eqn. 40) accounts for electron localization. The higher the ratio, lower is the localization. To range the electron localization within the interval $[0, 1]$, Becke and Edgecombe³² defined ELF as,

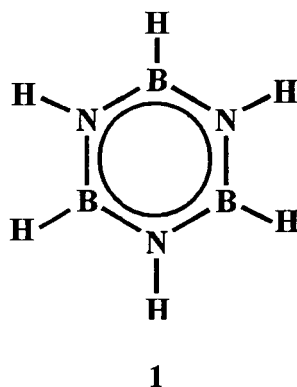
$$ELF = \eta = \frac{1}{1 + D(\vec{r})^2} = \frac{1}{1 + (D_\sigma/D_\sigma^0)^2} \quad (41)$$

With $ELF = 1$ corresponds to complete localization, 0 corresponds to delocalized system, while $ELF = 0.5$ corresponds to value for homogeneous electron gas.

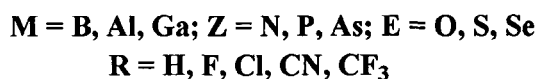
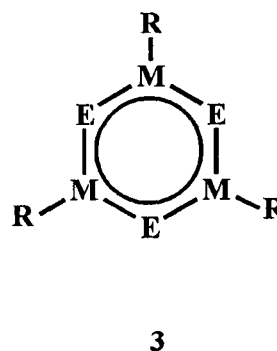
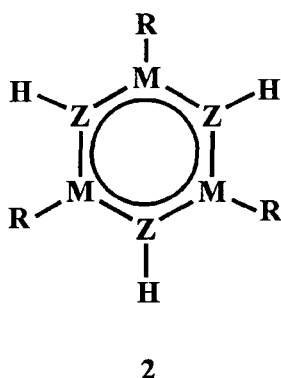
[1.4] Brief Overview of the Remaining Chapters

[1.4.1] Chapter 2: Aromaticity in Borazine and Its Heavier Analogs

Michael Faraday's isolation of benzene in 1825 paved the way to a vital concept in chemistry – “aromaticity”.³⁴ Numerous organic and inorganic aromatic compounds are now known. One such classic textbook example of an isoelectronic inorganic six- π electron system is borazine (1).³⁵ Several heavier analogs of borazine have been synthesized. Both gas phase³⁶ and solution phase³⁷ electrophilic substitution of borazine have been carried out which suggests its aromatic character.

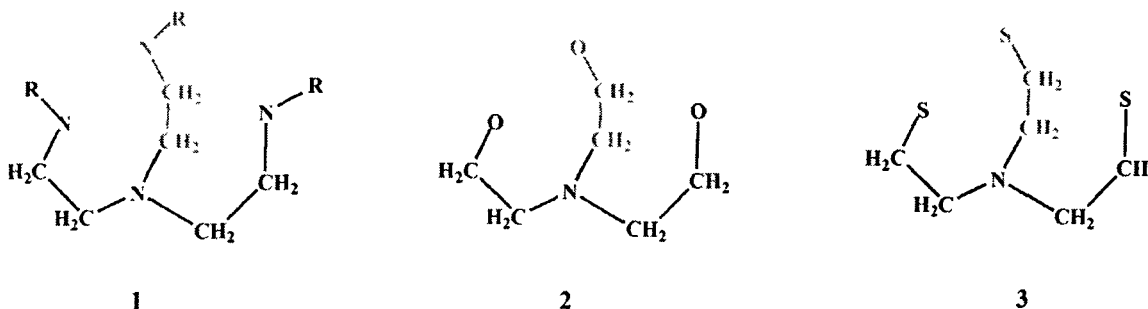


In this chapter, the effect of substituents on the aromaticity of borazine and its heavier analogs (2 and 3) have been studied quantum chemically at B3LYP/6-31+G* level of theory. Topological analysis of these molecules has also been performed within the realm of QTAIM and ELF. This study reveals that some inorganic rings may be stable even without significant π electron delocalization and provides evidence for the dominant role played by the σ framework.

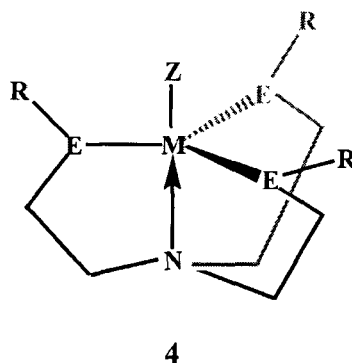


[1.4.2] Chapter 3: Nature and Extent of Transannular Interactions in Group 4 and Group 6 Metallatranes

Tripodal ligands such as triamidoamine (1), triethanolatoamine (2) and its sulfur analog (3) have attracted considerable interest over a period of time. They bind to main group and transition metals in tetradentate manner featuring a transannular M N bond.



In this chapter, the nature and extent of transannular M N interaction has been studied at B3LYP/LANL2DZ level of theory. The effect of apical (Z) as well as equatorial (E) substituents on the extent of this transannular interaction has been studied for group 4 and 6 metallatranes (4). Topology of this interaction has also been studied using the QTAIM approach and found to possess significant covalent character.



[1.4.3] Chapter 4: Structure, Stability and Reactivity of Different Carbon Bases

Organic carbon compounds are mostly found in a formal oxidation state of IV. However, carbon compounds in a formal oxidation state of II, (e. g., carbene) which once thought to be a reactive intermediate, are now available in a bottleable form. Very recently, a unique bonding situation in carbon compounds has been proposed which predicts a formal oxidation state of carbon as low as zero.

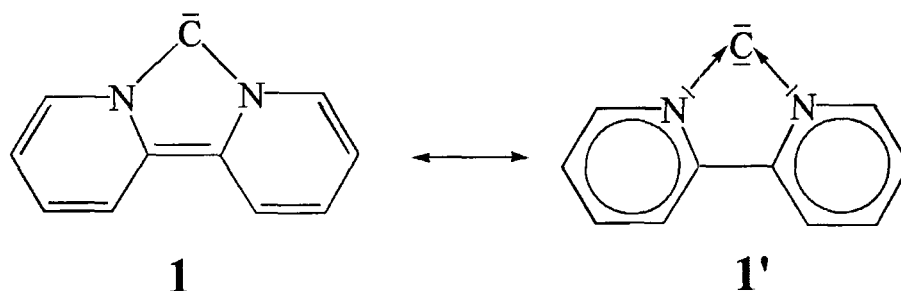
The first part of this chapter deals with the study of the reactivity of heterocyclic carbenes which may help in realizing the existence of “hidden” carbon(0) character in them. The next part of this chapter deals with the reactivity of carbon(II) and carbon(0) bases which

may help in distinguishing these two classes of compounds. In the last part of this chapter, some new cyclic and acyclic carbon(0) compounds stabilized by different coordination modes of heterocyclic carbenes have been proposed.

[1.4.3.1] Revisiting the Reactivity of Heterocyclic Carbenes

Singlet heterocyclic carbenes are known to have strong σ donating abilities. This has enabled their use in various transition metal catalysis. Owing to the presence of a high energy lone pair, heterocyclic carbenes can show a very high value of first proton affinity. On the other hand, recent prediction of carbon(0) compounds which has two lone pairs may have high values of first and second proton affinities.

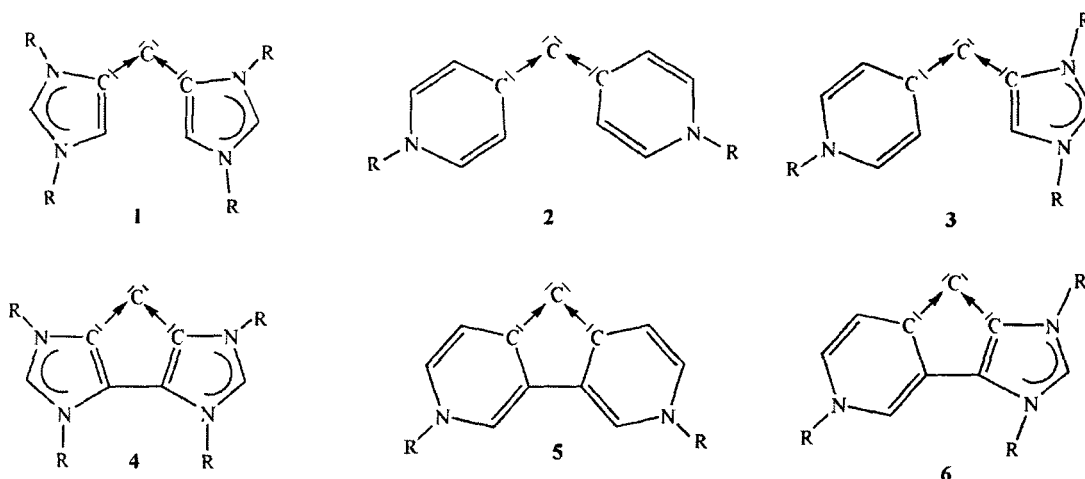
Here, reactivity of an *N*-heterocyclic carbene (**1**) have been studied with an aim to probe the importance of a particular resonance form of **1** which may contain two lone pairs at the central carbon atom (**1'**). This may help in realizing the existence of “hidden” carbon(0) character even in *N*-heterocyclic carbenes.



[1.4.3.2] Stabilization of Cyclic and Acyclic Carbon(0) Compounds By Differential Coordination of Heterocyclic Carbenes

Heterocyclic carbenes are known to have different coordination modes, e. g., normal, abnormal and remote. These carbenes owing to their highly basic nature are expected to stabilize a carbon atom via donor-acceptor interactions resulting in the formation of a carbon(0) compound.

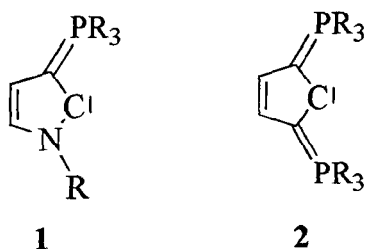
In this part of the chapter, some new cyclic (**1-3**) and acyclic (**4-6**) carbon(0) compounds have been proposed. These compounds are predicted to have high thermodynamic stabilities and are predicted to be highly basic. The cyclic compounds (**4-6**) are unusual in the sense that they contain a five membered ring consisting of only carbon atoms with a central carbon atom in the formal oxidation state of zero.



[1.4.3.3] Reactivity of Different Carbon Bases

Due to the presence of a high energy lone pair orbital, singlet carbenes are highly basic in nature. Consequently, the first proton affinity value obtained for these molecules are also very high. On the other hand, carbon(0) compounds with two lone pair of electrons not only have a very high value of first proton affinity but their second proton affinity is also high. This reactivity difference has been used as a decisive indicator to distinguish carbenes from carbon(0) compounds.

In this section, emphasize has been given to the π donating ability of ylide stabilized carbenes (1-2). Quantum chemical calculation at BP86/TZVP level of theory showed that ylide stabilized carbenes may have strong σ and π donating abilities and as a result, they showed very high values of first and second proton affinities. This reveals that both carbenes and carbon(0) compounds may show similar reactivity when subjected to electrophilic attack. However, owing to the ambiphilic character of carbenes, they may undergo nucleophilic addition too, which is very difficult to realize for carbon(0) compounds. This reactivity difference has been proposed as a distinguishing feature between these two classes of compounds.



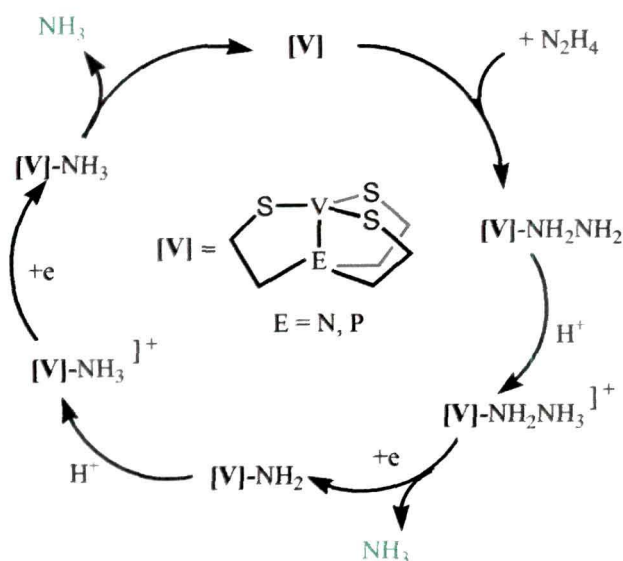
[1.4.4] Chapter 5: Mechanistic Study of Dinitrogen Reduction mediated by Tripodal Complexes of Vanadium

Mechanistic detail of dinitrogen reduction is still a fascinating area of research. Reduced forms of dinitrogen are very important for the sustainment of life on earth. Although industrial process of dinitrogen reduction (Haber-Bosch) is available, but it involves high temperature as well as pressure. Therefore, current research is focused towards transition metal catalyzed dinitrogen reduction at ambient condition.

In the first part of this chapter, mechanistic detail and energy profile for the conversion of hydrazine to ammonia mediated by vanadium(III) thiolate complexes have been studied at B3LYP/LANL2DZ//TZVP level of theory. The next part of this chapter deals with the complete reduction of dinitrogen to ammonia mediated by vanadium triamidoamine complex.

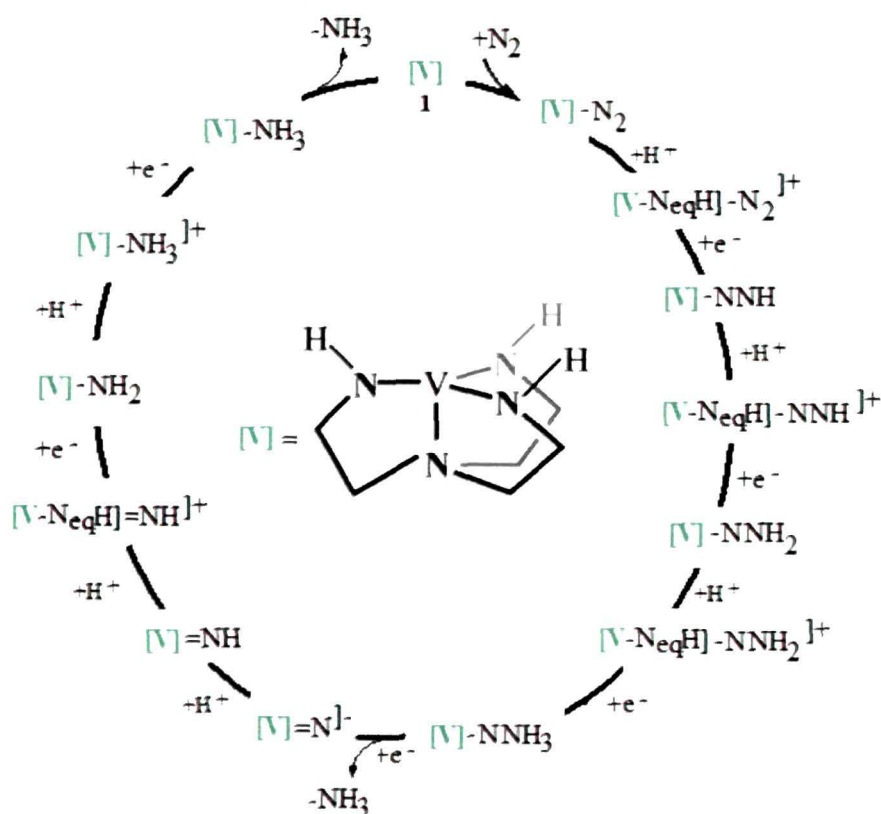
[1.4.4.1] Mechanistic Details for the Conversion of Hydrazine to Ammonia Mediated by Vanadium(III) Thiolate Complexes

Hydrazine is supposed to be a substrate and an intermediate of nitrogenase, the enzyme responsible for dinitrogen reduction. Like Mo-Fe nitrogenase, V-Fe nitrogenase is now known. Thus, to understand the mode of action of this enzyme, the chemistry of vanadium centre containing three sulfur donor sites and mimicking the sulfido environment of the V site in vanadium nitrogenase, is of great importance. In this part of the chapter, a mechanism for the conversion of hydrazine to ammonia mediated by vanadium(III) thiolate complexes [V] has been proposed and an energetic profile for the same has been calculated at B3LYP/LANL2DZ//TZVP level of theory.



[1.4.4.2] Mechanistic Study for the Complete Conversion of Dinitrogen to Ammonia Mediated by Vanadium Triamidoamine Complex

Catalytic conversion of dinitrogen to ammonia at a single metal centre has recently been achieved by Schrock and coworkers using a molybdenum triamidoamine complex.³⁸ They also proposed a probable mechanism for the same which has undergone many theoretical investigations. However, despite having a biological significance, the analogous vanadium triamidoamine complex fails to perform the task. In this part of the chapter, a systematic theoretical study on the thermodynamics of dinitrogen fixation mediated by vanadium triamidoamine has been carried out at PBE1PBE/SDD level of theory. The results were compared to that of molybdenum triamidoamine system for a better understanding of the intrinsic difficulties associated with the conversion of dinitrogen to ammonia with the vanadium system.



[1.5] Bibliography

1. John B. Russell, General Chemistry, McGraw-Hill International Book Company, 1980.
2. Schrödinger, E. "An Undulatory Theory of the Mechanics of Atoms and Molecules" *Physical Review*. **28** (6), 1049-1070, 1926.
3. Schleyer, P. v. R., et. al., Encyclopedia of Computational Chemistry, Ed.; John-Wiley, New York, 1999.
4. Szabo, A., & Ostlund, N. S. Modern Quantum Chemistry: Introduction to Advanced Electronic Structure Theory; McGraw-Hill; New York, 1989.
5. Pople, J. A. et. al., Ab Initio Molecular Orbital Theory; Wiley: New York, 1986.
6. Jensen, F. Introduction to Computational Chemistry; Wiley: Chichester, 1999.
7. Simons, J. *J. Phys. Chem.* **95** (3), 1017-1029, 1991.
8. Foresman, J. B., & Frisch, A. Exploring Chemistry with Electronic Structure Methods; Gaussian. Inc.: Pittsburgh, 1993, 1995-96.
9. (a) Pople, J. A. *Angew. Chem. Int. Ed.* **38** (13-14), 1894-1902, 1999. (b) Kohn, W., *Rev. Mod. Phys.* **71** (5), 1253, 1999.
10. Pople, J. A. et. al., *Gaussian 03*, revision D.02, Gaussian, Inc.: Pittsburgh, PA, 2004.
11. Slater, J. C. *Phys. Rev.* **81** (3), 385-390, 1951.
12. Kohn, W., & Sham, L. J. *Phys. Rev. A* **140** (4A), 1133-1138, 1965.
13. Hohenberg, P., & Kohn, W. *Phys. Rev.* **136** (3B), B864-B871, 1964.
14. (a) Coleman, J. Calculation of the first- and second-order density matrices, in, The Force Concept in Chemistry, Ed. Deb, B. M. (Van Nostrand Reinhold, New York, 1981). (b) Erdahl, R., & Smith Jr., V. H. Eds. *Density matrices and Density Functionals*, (Reidel, Dordrecht 1987).
15. Foley, M., & Madden, P. A. *Phys. Rev. B* **53** (16), 10589-10598, 1996.
16. (a) Fermi, E. *Z. Phys.* **48**, 73-79, 1928. (b) Thomas, L. H. *Proc. Camb. Phil. Soc.* **23** (5), 542-548, 1927.
17. Dirac, P. A. M. *Proc. Camb. Phil. Soc.* **26** (3), 376-385, 1930.
18. Ceperley, D. M., & Alder, B. J. *Phys. Rev. Lett.* **45** (7), 566-569, 1980.
19. (a) Tschinke, V., & Ziegler, T. *Can. J. Chem.* **67**, 460-472, 1989. (b) Neumann, R., & Handy, N. C. *Chem. Phys. Lett.* **266** (1-2), 16-22, 1997. (c) Perdew, J. P. et. al., *Phys. Rev. Lett.* **82** (12), 2544-2547, 1999.
20. Löwdin, P. -O. *Adv. Chem. Phys.* **2**, 207-322, 1959.

21. Bader, R. F. W. *Atoms in Molecules: A Quantum Theory*, Oxford University Press, Oxford, 1990.
22. (a) Bader, R.F.W. The quantum mechanical basis of conceptual chemistry. *Monatsh. Chem.* **136**, 819–854, 2005. (b) Bader, R.F.W., in: Schleyer, P.v.-R. (Ed.); *Encyclopedia of Computational Chemistry*; John Wiley and Sons: Chichester, UK, 1998, pp 64–86. (c) Popelier., P.L.A. *Atoms in Molecules: An Introduction*; Prentice Hall: London, 2000.
23. Bader, R. F. W. et. al., *Angew. Chem., Int. Ed. Engl.* **33** (6), 620-631, 1994.
24. (a) Bader, R. F. W. *J. Phys. Chem. A.* **102** (37), 7314-7323, 1998. (b) Bader, R. F. W. *Chem. Rev.* **91** (5), 893-928, 1991.
25. Coppens, P. *X-ray Charge Densities and Chemical Bonding*, Oxford University Press, Inc.: New York, 1997.
26. Bader, R. F. W. et. al., *J. Phys. Chem. A* **103** (2), 304-314, 1999.
27. Matta, C. F., & Boyd, R. J. *The Quantum Theory of Atoms in Molecules: From Solid State to DNA and Drug Design*, WILEY-VCH Verlag GmbH & Co. KGaA, Weinheim, 2007.
28. (a) Bader, R. F. W. *Phys. Rev. B* **49** (19), 13348-13356, 1994. (b) Bader, R. F. W., & Nguyen-Dang, T. T. *Adv. Quantum Chem.* **14**, 63-124, 1981.
29. Cremer, D., & Kraka, E. *Angew. Chem. Int. Ed. Engl.* **23** (8), 627-628, 1984.
30. Becke, A. D., & Edgecombe, K. E. *J. Chem. Phys.* **92** (9), 5397-5403, 1990.
31. (a) Bochicchio, R. C. et. al., *J. Phys. Chem. A* **104** (40), 9130-9135, 2000. (b) Boyd, R. J., & Wang, L. C. *J. Comp. Chem.* **10**, 367-371, 1989. (c). Chesnut, D. B., & Bartolotti, L. *J. Chemical Physics*, **257** (2-3), 175-181, 2000.
32. Becke, A. D. *Int. J. Quantum Chem.* **23**, 1915-1922, 1983.
33. Löwdin, P. O. *Phys. Rev.* **97**, 1474-1489, 1955.
34. Faraday, M. *Philos. Trans. R. Soc. London* **115**, 440-466, 1825.
35. Huheey, J. E. et. al., *Inorganic Chemistry: Principles of Structure and Reactivity*, Fourth Edition, Pearson Education (Singapore) Pte. Ltd., 2004.
36. Chiavarino, B. et. al., *J. Am. Chem. Soc.* **121** (11), 2619-2620, 1999.
37. Timoshkin, A. Y. et. al., *Inorg. Chem.* **50** (18), 9039-9044, 2011.
38. (a) Yandulov, D. V., & Schrock, R. R. *J. Am. Chem. Soc.* **124** (22), 6252-6253, 2002. (b) Yandulov, D. V., & Schrock, R. R. *Science* **301**, 76-78, 2003. (c) Yandulov, D. V., & Schrock, R. R. *Inorg. Chem.* **44** (4), 1103-1117, 2005. (d) Schrock, R. R. et. al., *Inorg. Chem.* **42** (3), 796-813, 2003. (e) Schrock, R. R. et. al., *J. Am. Chem. Soc.* **126** (19), 6150-6163, 2004. (f) Schrock, R. R. *Angew. Chem. Int. Ed.* **47** (30), 5512-5522, 2008.



CHAPTER - 2

**Structure, Stability and Aromaticity of
Inorganic Ring Systems**

[2.0] ABSTRACT

A combined DFT, AIM and ELF study has been carried out on borazine and its heavier analogs containing both the pnictogens and chalcogens as the ring constituent. The effect of substituents on the extent of aromaticity of these rings has also been assessed. Compared to the pnictogen substituted rings, chalcogen substituted rings are found to be less aromatic. Except for a few systems, the computed aromatic stabilization energies (ASE) do not correlate with the NICS values. For these ring systems, NICS and bond length equalization are found to be better indicators of aromaticity than ASE. It is found that bulky electronegative substituents at the group 13 elements dramatically increase the stability and aromaticity of these molecules. AIM and ELF analysis predicts that boron and gallium based heterocycles are moderately aromatic while the aluminium analogs are significantly less aromatic.

[2.1] Introduction

Michael Faraday's isolation of benzene in 1825 leads the way to a vital concept in chemistry—"aromaticity".¹ Numerous organic and inorganic aromatic compounds have been synthesized and characterized thereafter. One such classic textbook example of an isoelectronic inorganic six-p electron system having a six membered ring is borazine.² Its physical properties like bond length equalization, planarity of the ring shows great resemblance with benzene. Hence, it is justified to coin borazine as "inorganic benzene". However, the chemical properties of borazine are distinctly different from benzene. Several polar addition reactions are possible with borazine but very difficult with benzene. The substantial electronegativity difference between boron and nitrogen makes the B–N bond highly polar which results in less cyclic delocalization. Hence, it is expected that more electronegative substituents on the boron atom will help in withdrawing more electron density from the nitrogen atom thereby resulting in more delocalization. As a result, B-trisubstituted derivatives (with electronegative substituents on B atom) are supposed to be more aromatic than borazine. Aromaticity in borazine and its heavier analogues is still a matter of debate.³ Despite the fact that borazine does not undergo electrophilic aromatic substitution under normal conditions, Chiavarino et al. have successfully carried out electrophilic aromatic substitution of borazine in the gas phase.⁴ Very recently, electrophilic aromatic substitution of borazine in solution phase has also been achieved.⁵ This reactivity pattern can be taken as an indication of aromaticity in borazine.

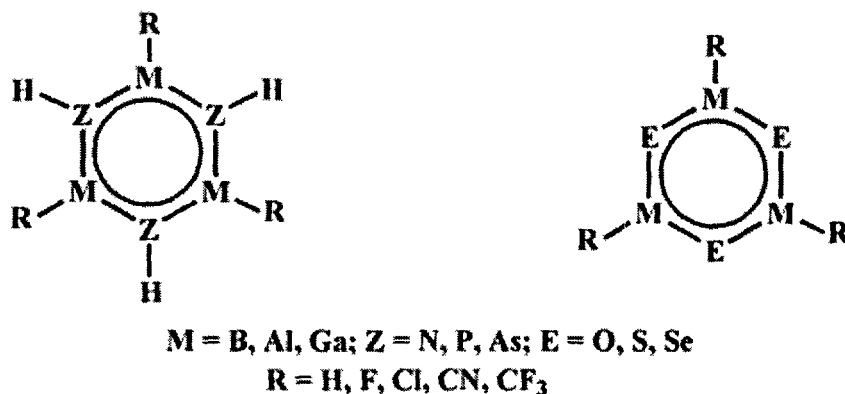
Apart from the isolation of borazine in Alfred Stock's laboratory,^{6g} several analogous rings are isolated by various groups, most notably by Power's group in which the tricoordinate boron atom is replaced by aluminium and gallium (Table 2.1).⁶⁻⁹ However, there are still some heavier congeners of borazine which are yet to be realized experimentally even though several sixmembered rings with tetra-coordinated metal atoms are known.⁹ Also, many clusters are synthesized with these six membered rings as building blocks.^{7f} Usually, aromatic compounds are highly stable due to extensive cyclic electron delocalization. But, the experimentally known borazine type inorganic ring compounds have a varying degree of calculated aromatic stabilization energies (ASE). For example, the ASE of boraphosphazene is more than that of borazine which in turn is half as aromatic as benzene. On the other hand, the ASE of alumazene is very low.¹⁰ Such a discrepancy between the stability and calculated ASE of these molecules prompted us to undertake a comprehensive study aimed at checking the importance of delocalization in stabilizing polar ring systems.

Table 2.1. List of experimentally known rings with generic formulae $M_3Z_3R_3$ and $M_3E_3R_3$ ($M = B, Al, Ga$; $Z = N, P, As$; $E = O, S, Se$) for which crystal structures are available.

Molecules	Reference
$H_3B_3N_3H_3$	6g, 6h
$Cl_3B_3N_3H_3$	8c
$(N_3)_3B_3N_3H_3$	8a
$(Mes)_3B_3P_3R_3$ [$R = Ph, Cy, Mes, ^iBu$]	6a
$(Ph)_3B_3P_3(Mes)_3$	6a
$(Mes)_3B_3P_3(C_6H_{11})_3$	6b
$Et_3B_3O_3$	7a
$Ph_3B_3O_3$	7a
$(SH)_3B_3S_3$	8f
$Me_3Al_3N_3(2,6-i-Pr_2C_6H_3)_3$	6a
$(Mes)_3Al_3P_3(Ph)_3.4Et_2O$	9a
$(Mes)_3Al_3As_3(Ph)_3.5Et_2O$	9a
$(2,4,6-Ph_3C_6H_2)_3Ga_3P_3(cyclo-C_6H_{11})_3$	6d

The concept of aromaticity has been reviewed recently.¹¹ Theoretical evaluation of aromaticity in inorganic analogues of benzene has been a major area of current research.^{3a-c}

In an effort to estimate the aromaticity of $X_3Y_3H_6$ ($XY = BN, BP$ and AlN) systems, Fink and Richards have carried out *ab initio* calculations on these systems.^{10d} Their result based on homodesmotic reactions reveal that the relative stability of BP is more than BN which in turn is more stable than AlN systems. However, all these rings possess much less stabilization energies than that of benzene. Gordon and Matsunaga have studied the prismane geometry of these inorganic rings and compared their structure and energetics with those of the planar, boat and chair conformations.^{3d} Jemmis et al. have carried out an in-depth study on a series of unsubstituted borazine and its heavier analogues.^{3c} Their study based on magnetic susceptibility exaltation (MSE) and nucleus independent chemical shift (NICS) values revealed that $B_3P_3H_6$ ring is more aromatic than $B_3N_3H_6$ although they possess nearly equal aromatic stabilization energies. There also exists experimental evidence on the strong influence of substituents on borazine. Beachley et al. have experimentally examined the 1H nmr, ^{11}B nmr, infrared and mass spectral properties of some substituted borazines. Their experiments proved the existence of π -electron delocalization in the borazine ring.¹² However, very little theoretical work has been done on the effect of substituents on borazine.¹⁰ Pietro and coworkers have studied the effect of substitution on borazine using natural bond orbital (NBO) wave function. Their results indicated similar *para* π -electron density changes in similar benzene and borazine derivatives which indicates a significant delocalization of the p-electron density.^{10b} Zhu and co-workers have studied the effect of substituents on the molecular geometry and aromaticity of B-trisubstituted borazine.^{10a} They found that meta-directing deactivating substituents such as nitro and cyano groups enhance the aromaticity of the substituted borazine derivatives while *ortho-para* directing and deactivating substituents such as fluorine and *ortho-para* directing and activating substituents such as the hydroxyl group and the amino group decreases the aromaticity of the same. Thus, most of these studies were confined to borazine. Here, an attempt has been made to study the effect of substituents on the aromaticity and stability of heavier analogues of borazine containing both pnictogens and chalcogens as the ring constituent (Scheme 2.1).



Scheme 2.1. Schematic representation of borazine and its heavier analogs with different substituents at the group 13 elements.

[2.2] Computational Details

All the structures were fully optimized using B3LYP/6-31+G* levels of theory.¹³ Frequency calculations were performed using the same level of theory to identify the ground state of the molecule. The bonding pattern of all the compounds was analyzed by natural bond orbital analysis (NBO).¹⁴ The strength of individual bonds have been ascertained from their values of Wiberg Bond Indices (WBI) available within the NBO routine. For computing nucleus independent chemical shift (NICS) values, the gauge independent atomic orbital (GIAO) scheme is used by placing a ghost atom (Bq) at the geometric centre of the ring, 1Å and 2Å above the plane of the ring.¹⁵ They are denoted as NICS (0), NICS (1) and NICS (2) respectively. For the computation of NICS and aromatic stabilization energies (ASE), only the planar structures were considered. All the calculations were performed using the Gaussian 03 suite of programs.¹⁶

[2.3] QTAIM and ELF

The Quantum Theory of Atoms in Molecules (QTAIM)¹⁷ and Becke-Edgecombe electron localization function (ELF),¹⁸ both aim to make a partition of the molecular space into adjacent non-overlapping regions with the help of the gradient dynamical system theory. The QTAIM analyzes the electron density and provides a partition into atomic basins whereas the electron localization function basins are closely related to chemical entities such as core shells, lone pairs and bonds. ELF has been initially conceived as a local measure of the Fermi hole curvature around a reference point within the Hartree-Fock approximation.¹⁸ Another interpretation, in terms of the local excess of kinetic energy due to the Pauli

principle, extended its calculation to Kohn-Sham orbitals.¹⁹ More recently, it was shown that the ELF kernel can be rigorously derived by considering the number of same spin pairs contained in a sample around the reference point.^{20,21}

The basins of ELF attractors are closely related to Gillespie's electronic domains and recover the ideas of Lewis. There are two type of basins: on the one hand are the core basins denoted $C(A)$ encompassing the nucleus of atom A and on the other hand are the valence basins labelled $V(A, B, \dots)$. The valence shell of an atom, say A , in a molecule is therefore the union of the valence basins having a boundary with $C(A)$. A valence basin may belong to several atomic valence shells. The synaptic order²² is defined as the number of such valence shells to which a valence basin participates. There are therefore monosynaptic basins $V(A)$ corresponding to lone pair, disynaptic basins $V(A, B)$ corresponding to two centre bonds and higher polysynaptic basins for polycentric bonds.

Both the AIM and ELF methods enable a qualitative analysis of the bonding and delocalization through the calculation of the basin populations and the corresponding covariance matrix elements (eqn (2.1) and (2.2)).²³

$$\bar{N}(\Omega_A) = \int_{\Omega_A} \rho(r) dr \quad (2.1)$$

$$\langle \text{cov}(\Omega_A, \Omega_A) \rangle = \iint_{\Omega_A} \Pi(r, r') dr dr' - \bar{N}(\Omega_A)(\bar{N}(\Omega_A) - 1) \quad (2.2)$$

$$\langle \text{cov}(\Omega_A, \Omega_B) \rangle = \int_{\Omega_A} \int_{\Omega_B} \Pi(r, r') dr dr' - \bar{N}(\Omega_A)\bar{N}(\Omega_B)$$

Here $\rho(r)$ and $\Pi(r, r')$ denote the one particle and two particle density distributions respectively. In the QTAIM framework, the delocalization index δ_{AB} (eq 2.3)²⁴ is used

$$\delta_{AB} = -2\langle \text{cov}(\Omega_A, \Omega_B) \rangle \quad (2.3)$$

rather than the covariance matrix elements themselves. The covariance matrix provides a measure of the quantum mechanical uncertainties of the electron distribution and support a phenomenological interpretation in terms of weighted mesomeric structures.²⁵ It is possible to combine the QTAIM and ELF analyses by evaluating the contributions of each atomic basin to the population of an ELF basin.²⁶ Santos *et al.*²⁷ have proposed to compute the contribution of the σ and π orbitals to the total ELF thereby enabling to build an aromaticity scale based on the ELF_σ and ELF_π values at certain saddle points. The QTAIM and ELF analyses have been carried out with the TopMod package.^{28,29} The ELF isosurfaces have been visualized with the Amira 3.0 software.³⁰

[2.4] Results and Discussion

[2.4.1] Molecular Geometry

[2.4.1.1] $M_3Z_3R_3$ systems: Geometry optimization of the rings result in two different type of rings—planar for $Z = N$, and puckered for $Z = P$ and As . Out of the puckered rings, some adopt chair conformations while others adopt boat conformations depending on the substituents at the metal, M . In order to appreciate the effect of puckering on molecular geometry, we have also included the planar rings for discussion even though they are not minima in the potential energy surface. The calculated bond lengths (r_{M-Z}), the changes in bond lengths (Δr) and the energy difference (E_p) between the planar and puckered form of these molecules are given in Table 2.2.

Table 2.2. Calculated bond lengths (\AA) for the planar (Pl) and puckered (Py) geometries, their difference (Δr , \AA) and the energy difference between these two geometries (ΔE in kcal/mol) for $R_2M=ZH_2$ and $M_3Z_3R_3$ systems. The Wiberg Bond Index (WBI) values are given within parenthesis.

Bond M – Z	R	$R_2M = ZH_2$					$M_3Z_3R_3$				
		r_{M-Z} (Pl)	r_{M-Z} (Py)	Δr	r_{M-Z} (expt.)	ΔE	r_{M-Z} (Pl)	r_{M-Z} (Py)	Δr	r_{M-Z} (expt.)	ΔE
B – N	H	1 386					1 433				
		(1 247)					(1 005)				
	F	1 399					1 430				
		(1 063)					(0 940)				
	Cl	1 392			1 402 ^{8e}		1 428			1 429 ^{8h}	
		(1 154)					(0 962)				
CN	1 387					1 429					
	(1 283)					(1 005)					
CF ₃	1 375					1 425					
	(1 311)					(1 004)					
B – P	H	1 796	1 872	0 07		4 7	1 842	1 862	0 02		0 3
		(1 635)	(1 345)				(1 349)	(1 303)			
	F	1 841	1 930	0 08		16 5	1 868	1 909	0 04		11 6
		(1 281)	(1 099)				(1 293)	(1 139)			
	Cl	1 823	1 918	0 09	1 859 ^{8h}	13 0	1 855	1 885	0 03	1 837 ^{8h}	6 2
		(1 445)	(1 177)				(1 286)	(1 176)			
CN	1 802	1 866	0 06		6 3	1 845	1 874	0 03		1 4	
	(1 587)	(1 294)				(1 322)	(1 254)				
CF ₃	1 783	1 862	0 07		4 2	1 838	1 857	0 02		0 3	
	(1 684)	(1 390)				(1 352)	(1 308)				
B – As	H	1 865	1 973	0 11		8 9	1 914	1 966	0 05		3 2
		(1 584)	(1 266)				(1 358)	(1 229)			
	F	1 904	2 021	0 12		23 0	1 937	2 007	0 07		18 9
		(1 288)	(1 076)				(1 245)	(1 130)			
	Cl	1 887	2 008	0 12	2 085 ^{9f}	18 2	1 931	1 988	0 06		11 5
		(1 457)	(1 138)				(1 286)	(1 139)			
CN	1 863	1 971	0 12		9 4	1 921	1 980	0 06		5 5	
	(1 599)	(1 232)				(1 321)	(1 174)				
CF ₃	1 846	1 952	0 12		7 3	1 913	1 951	0 04		1 7	
	(1 704)	(1 367)				(1 355)	(1 238)				

Al-N	H	1 789 (0 688)				1 806 (0 575)				
	F	1 764 (0 606)				1 793 (0 545)			1 780 ^{6a}	
	Cl	1 767 (0 668)				1 794 (0 566)				
	CN	1 762 (0 732)				1 793 (0 586)				
	CF ₃	1 765 (0 705)				1 795 (0 570)				
Al-P	H	2 238 (1 075)	2 339 (0 906)	0 10	9 1	2 270 (0 926)	2 300 (0 907)	0 03		8 5
	F	2 209 (0 912)	2 317 (0 891)	0 11	15 9	2 257 (0 864)	2 305 (0 862)	0 05		16 6
	Cl	2 214 (1 030)	2 322 (0 934)	0 11	14 7	2 258 (0 905)	2 303 (0 874)	0 05	2 328 ^{8a}	15 0
	CN	2 205 (1 145)	2 311 (0 974)	0 11	11 9	2 254 (0 946)	2 293 (0 927)	0 04		12 2
	CF ₃	2 209 (1 115)	2 318 (0 927)	0 11	11 4	2 257 (0 924)	2 295 (0 896)	0 04		12 3
Al-As	H	2 229 (1 125)	2 429 (0 908)	0 20	14 2	2 332 (0 968)	2 420 (0 888)	0 09		18 1
	F	2 259 (0 945)	2 401 (0 907)	0 14	22 1	2 314 (0 896)	2 405 (0 875)	0 09		26 7
	Cl	2 264 (1 067)	2 402 (0 942)	0 14	20 1	2 319 (0 940)	2 405 (0 899)	0 09	2 430 ^{9a}	24 4
	CN	2 251 (1 196)	2 387 (0 979)	0 14	16 1	2 315 (0 901)	2 401 (0 921)	0 09		19 9
	CF ₃	2 253 (1 162)	2 391 (0 936)	0 14	16 0		2 392 (0 906)			
Ga-N	H	1 835 (0 800)				1 848 (0 671)				
	F	1 805 (0 724)	1 817 (0 731)	0 01	0 2	1 836 (0 638)				
	Cl	1 813 (0 765)	1 819 (0 764)	0 01	0 2	1 837 (0 651)				
	CN	1 807 (0 855)				1 836 (0 683)				
	CF ₃	1 814 (0 812)				1 840 (0 664)				
Ga-P	H	2 196 (1 181)	2 290 (0 959)	0 09	10 2	2 234 (0 999)	2 284 (0 948)	0 05		11 2
	F	2 179 (1 028)	2 286 (0 953)	0 11	21 2	2 225 (0 936)	2 303 (0 884)	0 08		28 4
	Cl	2 185 (1 100)	2 291 (0 952)	0 11	18 8	2 225 (0 962)	2 300 (0 899)	0 08	2 300 ^{6d}	24 8
	CN	2 178 (1 236)	2 285 (1 012)	0 11	14 2	2 221 (1 016)	2 291 (0 915)	0 07		19 7
	CF ₃		2 292 (0 954)			2 224 (0 990)	2 294 (0 917)	0 07		18 8
Ga-As	H	2 269 (1 218)	2 385 (0 951)	0 12	15 2	2 304 (0 992)	2 384 (0 903)	0 08		21 5
	F	2 242 (1 053)	2 375 (0 956)	0 13	28 1	2 286 (0 965)	2 389 (0 899)	0 10		40 6
	Cl	2 252 (1 129)	2 382 (0 948)	0 13	25 5	2 292 (0 988)	2 397 (0 908)	0 11		38 2
	CN	2 239 (1 276)	2 374 (1 006)	0 14	20 1	2 283 (1 049)	2 393 (0 925)	0 11		32 4
	CF ₃		2 368 (0 955)				2 383 (0 917)			

All the optimized B-N rings are planar with equal B-N bond lengths. The B-N bond lengths do not vary appreciably as a result of substitution at B (Table 2.2). The shortest B-N bond is computed for CF₃ (1.425 Å) and the longest for H (1.433 Å). However, all the computed B-N distances are in close agreement with the experimentally observed one (1.429 Å).^{6h} A slight increase in bond length is observed in the B-N ring systems compared to the reference amino borane molecules R₂B=NH₂. The shortest B-N bond length in these substituted amino borane molecules is observed for R = CF₃ (1.375 Å) and the longest for R = F (1.399 Å).

The minimum energy structures of B - P rings are puckered resulting from pyramidalization of P atoms. They found to adopt chair conformations with H, CN and CF₃ and boat conformation with F and Cl as substituents. The puckering energy (E_p), i.e., the energy difference between the planar and puckered geometry, is highest for F (11.6 kcal/mol) and lowest for CF₃ (0.3 kcal/mol). It implies that with more bulky ligands, the B - P rings will attain planarity. This result is in good agreement with experimentally observed B - P rings which are found to be planar with bulky substituents on B and P.^{6a, b} All the planar and puckered B - P rings have different B - P bond lengths as the substituents are changed from H to CF₃. For all the substituents, the B - P bond strength decreases as one goes from the planar to the non-planar geometry. This is true for both phosphino borane as well as the ring structures. It is to be noted that pyramidalization of the P atom reduces the B - P π -bonding and thus, the B - P distances are longer in the puckered geometry than in the planar geometry. However, in spite of the pyramidalization of the P atoms, the B - P bond still retains some degree of double bond character albeit less than the planar form as evident from the Wiberg Bond Index (WBI) values (Table 2.2). The shortest and longest B - P distance is found for R = CF₃ and F respectively in both the planar and puckered geometries (Table 2.2). It is interesting to note that the highly electronegative F atom weakens the B - P bond. This anomaly is due to the strong σ -electron withdrawing ability of F atom which results in strengthening of σ bond and weakening of the π bond between B and P atoms. As a result, B - P bond weakens and becomes elongated. It is also observed that the B - P distances vary appreciably ($\Delta r \approx 0.08 \text{ \AA}$) in going from the planar form to the pyramidalized phosphino borane geometry. However, the variation in B - P distances is not very significant ($\Delta r \approx 0.02 \text{ \AA}$) for the ring structure. The computed B - P bond lengths are in good agreement with the experimentally observed values.^{6b}

Like B - P rings, all the optimized B - As rings are found to be puckered and they also show conformational variation. While chair conformation is the most stable geometry for H and CN, the preferred conformation for F, Cl and CF₃ is the boat form. The lowest value of puckering energy is found for CF₃ (1.7 kcal/mol, Table 2.2), a clear endorsement of the importance of bulky substituents in stabilizing planar rings. Although six-membered B - As rings are not known experimentally, a four membered planar ring with B₂As₂ core have been synthesized.^{9f} The B - As bond lengths of arsino boranes and ring structures elongates as one moves from the planar to the pyramidalized geometry (Table 2.2). The strongest B - As bond is obtained with R = CF₃ for both the molecules in the two different geometries. It is found that the variation of bond lengths in the planar and pyramidalized ethylene analogues (≈ 0.1 Å) is almost uniform. Similar trend was found for planar and puckered rings (≈ 0.04 Å).

Al - N rings are found to be planar with equal bond lengths. Compared to B - N bonds, Al - N bonds are much weaker as indicated by low value of WBI which arises from large electronegativity difference between Al and N. Interestingly, except with H, there is no significant variation in Al - N bond length for other substituents. This is true for both the ring and amino alane geometry (Table 2.2). The computed Al - N bond lengths of Al - N rings are in excellent agreement with the experimentally observed one (Table 2.2).^{6a}

All the optimized Al - P rings are found to adopt boat conformation which is in tune with the experimental observation.^{9a} Compared to B - P rings, the distortion is higher for Al - P rings which results in larger values of puckering energy (Table 2.2). The larger pyramidalization at P for Al - P rings may be necessitated by the increase in ring strain caused by the larger Al atoms. Similar to B - P rings, the Al - P bond length increases as one moves from planar to pyramidalized geometry. The geometrical variation observed for the ring structure is also reflected in the phosphino alane molecules. Compared to B - P compounds, the delocalization of phosphorous lone pair into the vacant Al 3p orbital is less pronounced due to the large electronegativity difference between aluminium ($\chi_{Al} = 1.61$) and phosphorous ($\chi_P = 2.19$). The Al - P bond length varies uniformly in going from the planar phosphino alane or ring structure to the pyramidalized one. The variation is significant ($\Delta r = 0.1$ Å) for the former while it is less pronounced ($\Delta r = 0.04$ Å) for the alumaphosphazenes. The computed Al - P bond lengths are in good agreement with the experimental value (Table 2.2). Out of all the substituents, substitution with fluorine results in highest value of puckering energy (16.6 kcal/mol). It may be noted that no planar structure is obtained with CF₃ as the substituent for the phosphino alane geometry.

Like Al - P rings, Al - As rings are also puckered in their optimized form and they adopt both chair and boat conformations depending on the substituents which is in agreement with the experimental results where a nonplanar boat conformation was observed with mesityl group on aluminium and phenyl group on phosphorus.^{9a} While the boat conformation is the stable form for the rings with R = H, F, Cl and CN, a deformed chair conformation is found to be the stable form for the ring with R = CF₃. The changes in Al - As bond lengths in going from the planar to the pyramidalized form are uniform for both arsino alane and Al - As ring compounds. However, the variation is significant for both the compounds. For the arsino alane geometry, the variation is 0.14Å, while for the ring structure it is 0.09Å (Table 2.2). It is interesting to note that all the substituents very well reproduces the experimental value of Al - As bond length. Both the structures are not minima in the planar form with one imaginary frequency which point towards the pyramidalization of the As atoms. However, with R = CF₃, geometry optimization of the planar structure straight away leads to the chair form without any imaginary frequency. The higher value of puckering energy for Al - As rings can be traced to the higher inversion barrier for As than P.^{3c} As observed for Al - P rings, here also the lone pair is largely localized on As atoms which can be related to the large electronegativity difference between Al ($\chi_{Al} = 1.61$) and As ($\chi_{As} = 2.18$).

To date, no Ga-N ring with tricoordinate gallium atom is known experimentally. Of the computed structures, R = H computes the largest Ga - N bond length. The bond lengths do not change appreciably for other substituents. Unlike amino boranes and amino alanes, the ground state geometry of amino gallanes are found to have a puckered structure with R = F and Cl resulting from pyramidalization of the nitrogen atoms. However, the structures with other substituents are planar. All the Ga - N bonds have single bond character as seen from the low value of Wiberg Bond Index.

In tune with the experimental results,^{6d} all the optimized Ga - P rings found to adopt deformed boat conformation. The calculated Ga - P bond lengths are in excellent agreement with the experimental values. As expected, there is substantial lengthening of all the Ga - P bonds in going from the planar to the nonplanar geometry. Due to the high degree of pyramidalization at phosphorous, delocalization of the lone pairs of electron on phosphorous to gallium is not possible in these compounds, and thus, all the Ga - P bonds have single bond character as manifested by WBI values which is close to 1.0. The shortest bond was found for R = H whereas other substituents have similar bond lengths. We could not get a planar

structure for the phosphino gallane molecule with R = CF₃ as geometry optimization leads to a puckered structure with no imaginary frequency.

To the best of our knowledge, so far no six-membered Ga - As ring is known with tricoordinate gallium. As found for Ga₃P₃ rings, here also the Ga - As bond lengthens considerably in going from the planar to the puckered geometry. Conformational variation is also observed for these Ga - As rings. While boat conformation is found to be the most stable form with R = H and Cl, a deformed boat and a deformed chair conformation is found with R = F and CF₃ respectively. However, Ga - As ring with R = CN adopts neither a boat nor a chair form but adopts a deformed geometry. The large pyramidalization at arsenic results in single bond character of the Ga - As bonds for both the arsino gallanes and Ga₃As₃ rings. Optimization of the molecules with R = CF₃ directly leads to a puckered geometry. R = H and F computes the lowest and highest values of puckering energy (Table 2.2).

[2.4.1.2] M₃E₃R₃ systems: All the calculated geometric parameters are given in Table 2.3. Unlike the M₃Z₃R₃ systems, here both the ring and ethylene type molecules are planar.

Table 2.3. Calculated bond lengths (Å) for R₂M=EH and M₃E₃R₃ rings. The Wiberg Bond Index (WBI) values are given within parenthesis.

M-E Bond	R	R ₂ M=EH	M ₃ E ₃ R ₃	
		r _{M-E}	r _{M-E}	r _{M-E} (expt.)
B - O	H	1.357 (1.051)	1.378 (0.872)	
	F	1.351 (0.954)	1.374 (0.843)	
	Cl	1.347 (1.003)	1.374 (0.850)	1.379 ^{7a}
	CN	1.344 (1.093)	1.374 (0.882)	
	CF ₃	1.333 (1.113)	1.371 (0.879)	
B - S	H	1.784 (1.435)	1.810 (1.258)	
	F	1.811 (1.208)	1.822 (1.177)	
	Cl	1.803 (1.327)	1.818 (1.214)	1.814 ^{8f}
	CN	1.784 (1.446)	1.813 (1.250)	
	CF ₃	1.763 (1.527)	1.805 (1.272)	
B - Se	H	1.906 (1.472)	1.929 (1.293)	
	F	1.937 (1.218)	1.944 (1.201)	
	Cl	1.926 (1.341)	1.934 (1.242)	
	CN	1.902 (1.471)	1.928 (1.277)	
	CF ₃	1.875 (1.571)	1.919 (1.285)	
Al - O	H	1.723 (0.546)	1.724 (0.480)	
	F	1.695 (0.525)	1.712 (0.466)	
	Cl	1.701 (0.565)	1.714 (0.485)	
	CN	1.692 (0.591)	1.713 (0.495)	

	CF ₃	1.695 (0.565)	1.715 (0.479)
Al - S	H	2.201 (0.909)	2.194 (0.834)
	F	2.169 (0.859)	2.179 (0.817)
	Cl	2.176 (0.931)	2.183 (0.841)
	CN	2.165 (0.995)	2.179 (0.867)
Al - Se	CF ₃	2.170 (0.956)	2.181 (0.845)
	H	2.312 (0.988)	2.308 (0.908)
	F	2.279 (0.922)	2.291 (0.882)
	Cl	2.287 (0.995)	2.299 (0.909)
Ga - O	CN	2.272 (1.073)	2.293 (0.941)
	CF ₃	2.273 (1.034)	2.296 (0.921)
	H	1.816 (0.632)	1.808 (0.547)
	F	1.783 (0.632)	1.798 (0.552)
Ga - S	Cl	1.790 (0.647)	1.796 (0.549)
	CN	1.784 (0.690)	1.794 (0.570)
	CF ₃	1.792 (0.641)	1.798 (0.544)
	H	2.194 (0.976)	2.199 (0.883)
Ga - Se	F	2.168 (0.952)	2.188 (0.874)
	Cl	2.177 (0.978)	2.189 (0.883)
	CN	2.172 (1.059)	2.189 (0.918)
	CF ₃	2.176 (1.006)	2.191 (0.886)
Ga - Se	H	2.304 (1.046)	2.309 (0.953)
	F	2.275 (1.005)	2.293 (0.928)
	Cl	2.287 (1.037)	2.298 (0.938)
	CN	2.276 (1.132)	2.295 (0.980)
	CF ₃	2.268 (1.092)	2.293 (0.956)

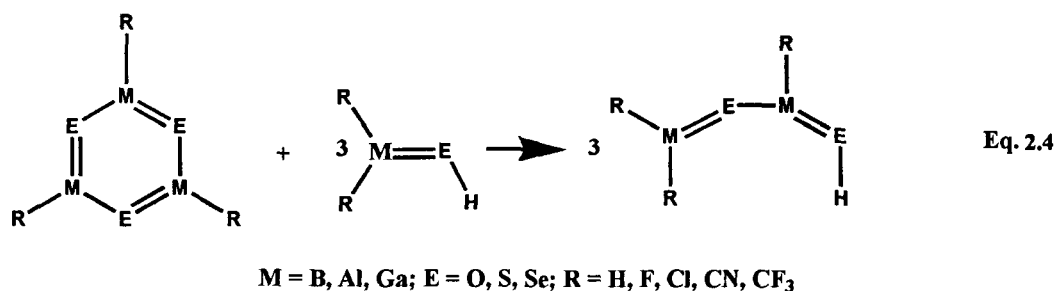
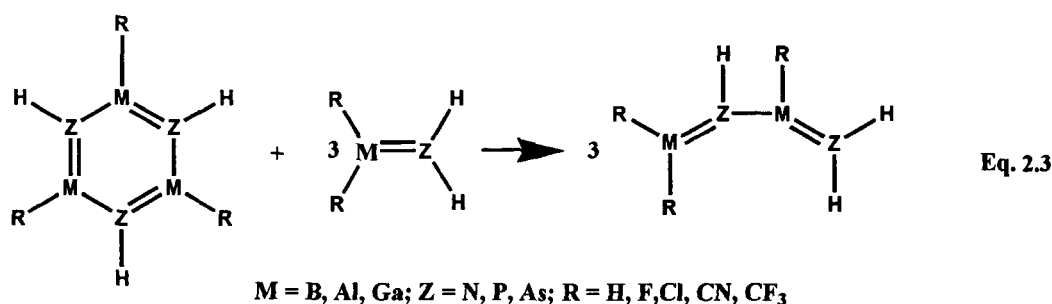
For the B - O systems, H and CF₃ compute the longest and shortest B - O bond respectively. The B - O bond length changes appreciably in the ethylene type geometry for different R groups. However, the changes are not so significant in the ring geometry. The computed B - O bond lengths of the B₃O₃ rings are in excellent agreement with the experimentally reported values (Table 2.3).^{7a} All the B - O bonds of B₃O₃ rings have single bond character as evident from the low values of the Wiberg Bond Indexes (WBI). Both B - S and B - Se bonds show similar variation in bond distances in both the ethylene type and ring geometries. Also, unlike B - O bonds, these bonds have significant double bond character as evident from the high WBI values. This difference can be explained by looking at the electronegativity of the constituent atoms, viz, B, O, S and Se. Due to the higher electronegativity of oxygen, B-O bonds are polar. However, the electronegativity of sulfur ($\chi_S = 2.58$) and selenium ($\chi_{Se} = 2.55$) are closer to that of boron ($\chi_B = 2.04$) and thus, these bonds are covalent in nature.

All the Al_3E_3 rings show similar variation in Al - E bond lengths for all the substituents. For all the molecules, R = H computes the longest bond lengths. The Al - E bonds are much weaker (smaller WBI values) than B - E bonds due to large electronegativity difference between Al and the E atoms, viz, O, S and Se. There is no example of experimentally observed Al - E six-membered rings where Al atoms are tricoordinated. However, some examples of six-membered Al - E rings are found in literature where Al atoms are tetracoordinated.^{9b, c}

In the case of Ga-E compounds, the shortest Ga-E bond (higher value of WBI) is found for R = CN. This is true for both ethylene type and ring geometry. As observed for Al_3E_3 rings here also the variation in Ga-E bond lengths is similar for all the compounds.

[2.4.2] Stabilization Energy and Ring Current

We have used two homodesmotic equations, eqn. 2.3 and eqn. 2.4 to compute the stabilization energies of $M_3Z_3R_3$ and $M_3E_3R_3$ systems respectively. The extent of ring current or cyclic delocalization of electrons in these rings are evaluated from their respective NICS values.



For the B - N rings, CF_3 and F compute the highest and lowest stabilization energies respectively (Table 4). The stabilization energy is almost equal for R = H and Cl, and it is slightly lesser than that with R = CN (Table 2.4). But NICS (0) tells a different story. It is found that the NICS value at the geometric centre of the ring is highest for R = F. On the other hand, NICS at 1Å and 2Å above the ring has the lowest value for this ring. This is

Table 2.4. Calculated aromatic stabilization energies (ASE in kcal/mol) and nucleus independent chemical shift (NICS) values for $M_3Z_3R_3$ rings.

Bond M-Z	R	ASE	NICS (0)	NICS (1)	NICS (2)
B - N	H	10.6	-1.9	-2.7	-1.5
	F	2.2	-4.4	-2.1	-0.9
	Cl	10.5	-3.0	-2.2	-1.1
	CN	12.5	-3.3	-3.3	-1.7
	CF ₃	20.6	-3.3	-3.3	-1.7
B - P	H	13.5	-8.3	-6.9	-3.9
	F	2.2	-9.2	-5.6	-2.5
	Cl	6.4	-8.3	-5.9	-2.9
	CN	8.4	-9.8	-7.7	-4.1
	CF ₃	-6.3	-10.3	-8.0	-4.1
B - As	H	10.0	-8.2	-7.4	-4.3
	F	-1.8	-9.1	-6.2	-2.7
	Cl	1.5	-8.2	-6.3	-3.1
	CN	2.8	-9.6	-8.0	-4.4
	CF ₃	-5.7	-10.2	-8.5	-4.5
Al - N	H	1.4	-2.1	-0.6	-0.1
	F	-3.0	-3.9	-1.3	-0.2
	Cl	-1.0	-3.5	-1.3	-0.3
	CN	-0.1	-3.4	-1.4	-0.4
	CF ₃	0.3	-3.1	-1.2	-0.3
Al - P	H	4.1	-4.8	-3.2	-1.5
	F	-2.0	-6.1	-3.7	-1.4
	Cl	-0.6	-6.0	-3.7	-1.5
	CN	0.9	-6.0	-4.0	-1.8
	CF ₃	-16.2	-5.8	-3.8	-1.6
Al - As	H	1.7	-5.5	-3.9	-1.8
	F	-7.5	-6.2	-3.9	-1.4
	Cl	-4.0	-6.2	-4.0	-1.7
	CN	-1.1	-6.5	-4.4	-1.8
	CF ₃	-7.2			
Ga - N	H	1.6	-1.4	-1.2	-0.6
	F	-7.8	-4.1	-2.0	-0.4
	Cl	-3.1	-3.2	-1.8	-0.5
	CN	-2.2	-3.1	-1.9	-0.7
	CF ₃	-1.5	-2.7	-1.6	-0.5
Ga - P	H	3.8	-5.2	-3.8	-1.7
	F	-4.0	-6.7	-4.1	-1.2
	Cl	-2.8	-6.4	-4.1	-1.5
	CN	1.9	-6.6	-2.0	-4.6
	CF ₃	-24.8	-6.4	-1.8	-4.4
Ga - As	H	3.2	-6.2	-4.7	-2.1
	F	-8.8	-6.9	-4.4	-1.4
	Cl	-6.1	-6.9	-4.7	-1.8
	CN	-1.4	-7.1	-4.8	-2.1
	CF ₃	-7.3			

due to the fact that F has a strong σ -electron withdrawing ability which results in strengthening of the B - N σ -bond. It is evident from Table 2.4 that replacement of the H atom on boron by other group significantly enhances the ring current.

In the planar B - P rings, highest stabilization is computed for the ring with R = H which is higher than its B - N counterpart. Some discrepancies are found between stabilization energy and ring currents. Planar B - P ring with R = CF₃ has the shortest B - P distance and hence it should have the highest stabilization energy. But this ring is found to have the lowest value of stabilization energy. This is due to the fact that in computing stabilization energy for the planar rings, we have considered only the planar geometries of all the molecules in eqn. 2.3, but it is found that the B - P analogue of *cis*-butadiene is puckered with no imaginary frequency in its optimized form. But, NICS values suggest that this ring should be the most aromatic. With R = F, same lowering of stabilization energy is found as in the case of B - N rings. But, NICS at the molecular plane indicates increase in ring current due to strong σ -delocalization.

Among the B - As rings, highest stabilization energy is computed for the ring with R = H. NICS values for these rings are found to be higher than B - N rings due to the small electro negativity difference between B and As atoms. In all the fluoro and chloro substituted B-Z rings, considerable delocalization of the lone pair on F and Cl to the π^* orbital of the ring was found. From second order perturbation theory analysis of the NBO basis, significant interaction energy arising out of such donor-acceptor interaction was obtained which accounts for the extra stability of these rings. This interaction energy is found to be more for the fluoro substituted rings than with chloro substituted ones. For most of the B - Z rings, good correlation was found between the M - Z bond distance and NICS (1) values (Figure 2.1).

Al - N rings are found to possess very low stabilization energies. The NICS (0) values are similar to that of B - N rings. Al - P ring with H is found to have the highest stabilization energy. Similar to B - P and B - As rings, Al - P ring with R=CF₃ is found to have very low stabilization energies and this anomaly arises from the pyramidalization of the phosphorus and arsenic atoms in the ground state geometry of the *cis*-butadiene type molecules used in eqn 2.3. Compared to B - P and B - As rings, the cyclic electron delocalization is much smaller in Al - P and Al - As rings due to large electronegativity difference between the constituent atoms. This is evident from the lower values of NICS (0) and NICS (1) for these rings. NICS values for the Al - As ring with R = CF₃ could not be computed as the ring adopts a puckered geometry in its ground state with no imaginary

frequency. As found for the B-Z rings, significant delocalization of the lone pairs on Cl and F were obtained for these Al-Z rings as well. The computed interaction energy is found to be more for the chloro substituted rings than with fluoro substituted ones.

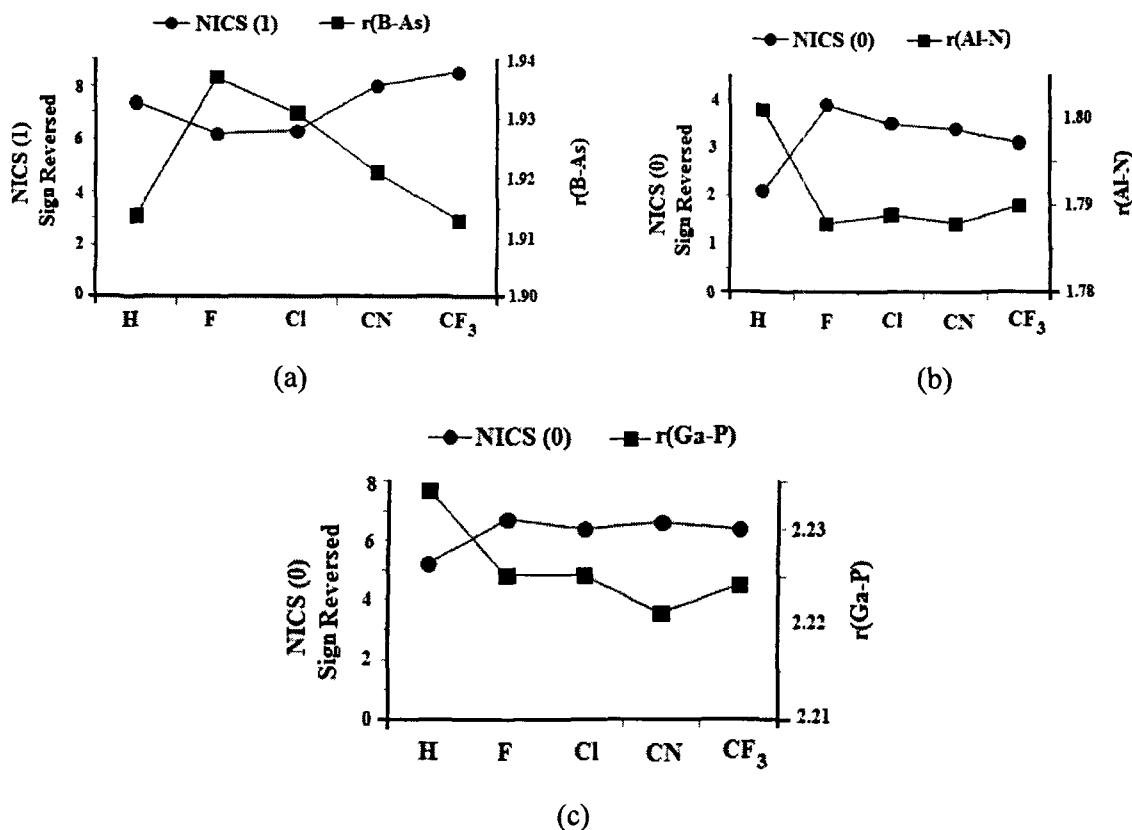


Figure 2.1. Correlation between changes in bond lengths (Å) and NICS values for few representative M₃Z₃R₃ rings, viz., (a) B₃As₃, (b) Al₃N₃ and (c) Ga₃P₃.

Except for R = H, all the Ga-Z rings have negative stabilization energies. Compared to the Ga - N rings, Ga - P and Ga - As rings are more aromatic as evident from the higher NICS (0) and NICS (1) values for these rings. This is expected because delocalization is more prominent in Ga - P and Ga - As rings due to less polarity of these bonds than Ga - N bond. In all the Ga-Z rings, similar stabilizing interaction energies are obtained for fluoro and chloro substituted rings with the chloro derivative possessing more interaction energies than the fluoro one. For most of the Al - Z and Ga - Z rings, NICS (0) values correlates well with the M - Z bond distance (Figure 2.1).

Owing to the more polar nature of the B - O bond than the B - S and B - Se bonds, B₃S₃ and B₃Se₃ rings are more stable and aromatic than the B₃O₃ rings (Table 2.5). For

Table 2.5. Calculated aromatic stabilization energies (ASE in kcal/mol) and nucleus independent chemical shift (NICS) values for M₃E₃R₃ rings.

Bond M-E	R	ASE	NICS (0)	NICS (1)	NICS (2)
B - O	H	05	-03	-19	-18
	F	-02	-29	-19	-09
	Cl	40	-15	-17	-10
	CN	73	-16	-24	-14
	CF ₃	20	-13	-24	-13
B - S	H	90	-13	-31	-25
	F	64	-40	-33	-16
	Cl	144	-28	-31	-19
	CN	155	-28	-39	-26
	CF ₃	201	-32	-42	-27
B - Se	H	47	-09	-27	-24
	F	17	-35	-28	-14
	Cl	89	-25	-27	-18
	CN	61	-26	-36	-26
	CF ₃	57	-31	-40	-28
Al - O	H	-104	-28	-11	-02
	F	-163	-41	-15	-04
	Cl	-154	-37	-15	-05
	CN	-153	-37	-17	-06
	CF ₃	-179	-35	-14	-04
Al - S	H	17	-27	-19	-10
	F	05	-46	-30	-13
	Cl	28	-43	-29	-14
	CN	49	-37	-26	-13
	CF ₃	53	-34	-23	-11
Al - Se	H	-12	-18	-18	-06
	F	-39	-39	-21	-08
	Cl	-30	-37	-23	-10
	CN	-07	-30	-19	-09
	CF ₃	-12	-27	-17	-08
Ga - O	H	05	-18	-10	-02
	F	-102	-41	-20	-04
	Cl	-49	-33	-17	-05
	CN	-23	-28	-15	-04
	CF ₃	-60	-23	-12	-03
Ga - S	H	01	-11	-10	-06
	F	-61	-42	-25	-08
	Cl	-06	-35	-22	-09
	CN	16	-30	-22	-10
	CF ₃	38	-25	-18	-08
Ga - Se	H	09	-10	-09	-06
	F	-81	-38	-23	-07
	Cl	-17	-33	-22	-09
	CN	00	-29	-21	-10
	CF ₃	36	-25	-18	-09

B_3O_3 rings, maximum stabilization is found with $R = CN$. For B_3S_3 rings, significant stabilization is found with $R = Cl, CN$ and CF_3 . Also, these rings are more aromatic than those with $R = H$ and F which is evident from the NICS (1) values (Table 2.5). The stabilization energies of B_3Se_3 are much smaller than that of B_3S_3 rings. However, their NICS values are comparable with those given for B_3S_3 structures. Excluding few exceptions, all the B - E bond lengths nicely correlate with the computed NICS (1) values (Figure 2.2).

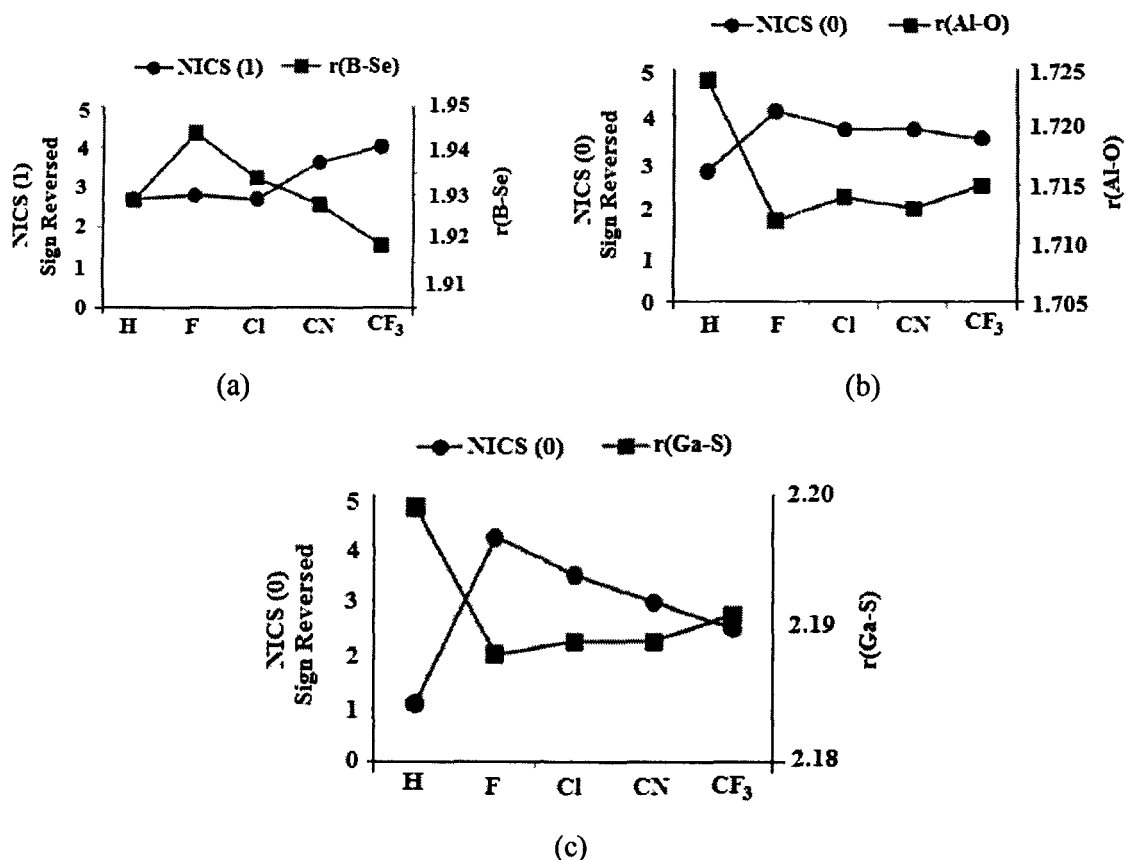


Figure 2.2. Correlation between changes in bond lengths (Å) and NICS values for few representative $M_3E_3R_3$ rings, viz., (a) B_3Se_3 , (b) Al_3O_3 and (c) Ga_3S_3 .

Among the Al - E rings, Al_3O_3 rings have very low stabilization energies. Al_3Se_3 rings also have low ASE but that of Al_3S_3 compounds are not negligible. $R = F$ computes the highest NICS (0) values for all the compounds. All the Al_3E_3 rings are moderately aromatic. The NICS (0) values correlates well with the changes in Al - E bond lengths of respective rings (Figure 2.2).

Similar to Al_3E_3 rings, Ga_3E_3 rings also have low ASE. For these systems, NICS (0) correlates with the changes in Ga-E bond lengths (Figure 2.2) and $R = F$ computes the highest NICS (0) values.

[2.4.3] QTAIM and ELF analysis

A survey of the literature^{25, 31} show that there is no satisfactory topological indicator for measuring the aromaticity of heterocycles. However, for the heterocycles of our interest, one can consider – (a) QTAIM delocalization index δ_{AB} ²⁴ where A and B are the heteroatoms, (b) the electron density ρ and its laplacian $\nabla^2\rho$ at the AB bond critical point (bcp), (c) the total ELF value at the ring bifurcation and (d) the π – ELF component ring bifurcation value for the planar rings. The values for benzene, the reference compound for aromaticity, are the following: $\delta_{AB} = 1.4$, $\rho(bcp) = 0.31$, $\nabla^2\rho(bcp) = -0.85$, $ELF_{tot} = 0.67$, $ELF_{\pi} = 0.90$.

Table 2.6 contains the numerical data of AIM and ELF analysis for $B_3Z_3R_3$ and $B_3E_3R_3$ ring systems. The QTAIM delocalization index δ_{AB} values indicate that for boron

Table 2.6. Summary of QTAIM delocalization index(δ_{AB}), density at AB bond critical point [$\rho(bcp)$] and its laplacian $\nabla^2\rho(bcp)$, total ELF value at the ring bifurcation (ELF_t) and ELF π component ring bifurcation value (ELF_{π}) for boron heterocyclic rings.

Rings	δ_{AB}	$\rho(bcp)$	$\nabla^2\rho(bcp)$	ELF_t	ELF_{π}
$B_3N_3H_6$	0.52	0.20	0.56	0.33	0.78
$B_3N_3HF_3$	0.46	0.20	0.49	0.35	0.56
$B_3N_3HCl_3$	0.51	0.20	0.52	0.34	
$B_3N_3H_3(CN)_3$	0.43	0.20	0.57	0.32	0.75
$B_3N_3H_3(CF_3)_3$	0.51	0.20	0.56	0.34	
$B_3P_3H_6$ (planar)	0.85	0.15	-0.28	0.52	0.87
$B_3P_3H_6$ (puckered)	0.89	0.15	-0.35	0.58	
$B_3P_3H_3F_3$ (planar)	0.88	0.15	-0.37	0.52	
$B_3P_3H_3F_3$ (puckered)	0.95	0.15	-0.31		
$B_3P_3H_3Cl_3$ (planar)	0.90	0.15	-0.36	0.51	0.76
$B_3P_3H_3Cl_3$ (puckered)	0.99	0.15	-0.31	0.53	
$B_3P_3H_3(CN)_3$ (planar)	0.86	0.15	-0.32	0.52	
$B_3P_3H_3(CN)_3$ (puckered)	0.96	0.15	-0.33	0.59	
$B_3P_3H_3(CF_3)_3$ (planar)	0.87	0.15	-0.31	0.52	0.88
$B_3P_3H_3(CF_3)_3$ (puckered)	0.93	0.15	-0.36	0.58	
$B_3As_3H_6$ (planar)	1.06	0.14	-0.27	0.55	
$B_3As_3H_6$ (puckered)	1.05	0.13	-0.21	0.64	
$B_3As_3H_3F_3$ (planar)	1.02	0.14	-0.24	0.56	
$B_3As_3H_3F_3$ (puckered)	0.99	0.13	-0.20		

$B_3As_3H_3Cl_3$ (planar)	1.06	0.14	-0.23	0.54	0.76
$B_3As_3H_3Cl_3$ (puckered)	1.02	0.13	-0.18		
$B_3As_3H_3(CN)_3$ (planar)	1.04	0.14	-0.25	0.55	
$B_3As_3H_3(CN)_3$ (puckered)	1.00	0.13	-0.19	0.63	
$B_3As_3H_3(CF_3)_3$ (planar)	1.07	0.14	-0.26	0.55	0.87
$B_3As_3H_3(CF_3)_3$ (puckered)	1.06	0.14	-0.20	0.58	
$B_3O_3H_3$	0.47	0.20	0.94	0.29	0.69
$B_3O_3F_3$	0.42	0.20	0.90	0.30	0.45
$B_3O_3Cl_3$	0.45	0.20	0.93	0.30	0.52
$B_3O_3(CN)_3$	0.44	0.20	0.93	0.30	0.60
$B_3O_3(CF_3)_3$	0.45	0.20	0.97	0.29	
$B_3S_3H_3$	0.75	0.15	-0.20	0.51	
$B_3S_3F_3$	0.69	0.15	-0.29	0.47	0.52
$B_3S_3Cl_3$	0.75	0.15	-0.26	0.47	
$B_3S_3(CN)_3$	0.73	0.15	-0.24	0.49	
$B_3S_3(CF_3)_3$	0.74	0.16	-0.22	0.49	
$B_3Se_3(CN)_3$	0.93	0.14	-0.32	0.55	
$B_3Se_3(CF_3)_3$	0.91	0.15	-0.33	0.54	

heterocyclic rings, the delocalization follows the order $B - As > B - P \approx B - Se > B - S > B - N > B - O$. Except for the polar $B - N$ and $B - O$ rings, negative values of the laplacian $\nabla^2\rho$ (bcp) and high values of δ_{AB} are computed for all the other boron rings – indicating the presence of cyclic electron delocalization as well as covalent nature of the constituent bonds. The total ELF (ELF_t) value at the ring bifurcation and the ELF π component ring bifurcation value (ELF_π) also reflects the same trend. According to Poater and co-workers, aromatic compounds have a ELF_π value greater than 0.70, whereas for antiaromatic compounds they are in the range of 0.11 – 0.35.²⁵ It is evident from Table 6 that planar $B - P$ and $B - As$ rings as well as the borazine ring are aromatic as revealed by the ELF_π value greater than 0.70. However, the ELF_π values for other rings are greater than 0.35 and thus, they are not antiaromatic.

All the δ_{AB} values for aluminium heterocyclic rings are less than 0.6 (Table 2.7). Electron density at the AB bond critical point $\rho(bcp)$ are very small and the laplacian $\nabla^2\rho$ (bcp) are small and positive. Also, no significant delocalization is observed from the ELF analysis. Thus, both the indicators fail to characterize any aromatic character in aluminium

based rings. However, like boron rings, a similar trend in delocalization is also observed for the aluminium heterocyclic rings as seen from the delocalization index values δ_{AB} (Table 2.7). Gallium heterocyclic rings have a larger value of δ_{AB} (Table 2.8) compared to aluminium heterocycles, although they are still less than 1.0. The $\rho(bcp)$ values are small and its laplacian $\nabla^2\rho$ (bcp) is very small and positive. Like aluminium, gallium also computes negligible values of ELF_t and ELF_π . Thus, while the values of δ_{AB} indicate some amount of aromaticity in gallium heterocycles, ELF analysis fails to exhibit any aromatic character.

Table 2.7. Summary of QTAIM delocalization index(δ_{AB}), density at AB bond critical point [$\rho(bcp)$] and its laplacian $\nabla^2\rho$ (bcp), total ELF value at the ring bifurcation (ELF_t) and ELF_π component ring bifurcation value (ELF_π) for aluminium heterocyclic rings.

Rings	δ_{AB}	$\rho(bcp)$	$\nabla^2\rho$ (bcp)	ELF_t	ELF_π
$Al_3N_3H_6$	0.42	0.09	0.61	0.13	0.01
$Al_3N_3H_3F_3$	0.40	0.09	0.64	0.06	
$Al_3N_3H_3(CN)_3$	0.41	0.09	0.64		
$Al_3N_3H_3Cl_3$	0.42	0.09	0.63	0.13	
$Al_3N_3H_3(CF_3)_3$	0.43	0.09	0.63		0.02
$Al_3P_3H_6$ (planar)	0.51	0.06	0.16	0.30	
$Al_3P_3H_6$ (puckered)	0.52	0.06	0.14		
$Al_3P_3H_3F_3$ (planar)	0.49	0.07	0.16	0.32	0.02
$Al_3P_3H_3F_3$ (puckered)	0.53	0.07	0.11		
$Al_3P_3H_3Cl_3$ (planar)	0.51	0.07	0.16	0.30	0.02
$Al_3P_3H_3Cl_3$ (puckered)	0.54	0.07	0.11	0.29	
$Al_3P_3H_3(CN)_3$ (planar)	0.52	0.07	0.17	0.32	
$Al_3P_3H_3(CN)_3$ (puckered)	0.54	0.07	0.13		
$Al_3P_3H_3(CF_3)_3$ (planar)	0.53	0.07	0.16	0.32	
$Al_3P_3H_3(CF_3)_3$ (puckered)	0.55	0.07	0.12		
$Al_3As_3H_6$ (planar)	0.54	0.06	0.14	0.34	0.02
$Al_3As_3H_6$ (puckered)	0.55	0.06	0.08	0.34	
$Al_3As_3H_3F_3$ (planar)	0.51	0.07	0.14	0.36	0.02
$Al_3As_3H_3F_3$ (puckered)	0.55	0.06	0.09		0.00
$Al_3As_3H_3Cl_3$ (planar)	0.54	0.06	0.14	0.34	
$Al_3As_3H_3Cl_3$ (puckered)	0.57	0.06	0.09	0.90	
$Al_3As_3H_3(CN)_3$ (planar)	0.54	0.07	0.14		

$\text{Al}_3\text{As}_3\text{H}_3(\text{CN})_3$ (puckered)	0.56	0.06	0.09	0.06	
$\text{Al}_3\text{As}_3\text{H}_3(\text{CF}_3)_3$ (puckered)	0.57	0.06	0.09		
$\text{Al}_3\text{O}_3\text{H}_3$	0.38	0.09	0.83		0.01
$\text{Al}_3\text{O}_3\text{F}_3$	0.36	0.10	0.86		0.01
$\text{Al}_3\text{O}_3\text{Cl}_3$	0.38	0.10	0.86		0.01
$\text{Al}_3\text{O}_3(\text{CN})_3$	0.37	0.10	0.86		0.01
$\text{Al}_3\text{O}_3(\text{CF}_3)_3$	0.38	0.10	0.85		0.08
$\text{Al}_3\text{S}_3\text{H}_3$	0.50	0.07	0.23	0.27	0.01
$\text{Al}_3\text{S}_3\text{F}_3$	0.49	0.07	0.23	0.28	0.01
$\text{Al}_3\text{S}_3\text{Cl}_3$	0.51	0.07	0.23	0.27	0.01
$\text{Al}_3\text{S}_3(\text{CN})_3$	0.51	0.07	0.23	0.28	0.18
$\text{Al}_3\text{S}_3(\text{CF}_3)_3$	0.52	0.07	0.23	0.27	
$\text{Al}_3\text{Se}_3\text{H}_3$	0.53	0.06	0.17	0.29	0.01
$\text{Al}_3\text{Se}_3\text{F}_3$	0.52	0.07	0.17	0.29	0.01
$\text{Al}_3\text{Se}_3\text{Cl}_3$	0.54	0.07	0.17	0.29	0.01
$\text{Al}_3\text{Se}_3(\text{CN})_3$	0.55	0.07	0.18	0.30	0.19
$\text{Al}_3\text{Se}_3(\text{CF}_3)_3$	0.55	0.07	0.17	0.29	

Table 2.8. Summary of QTAIM delocalization index(δ_{AB}), density at AB bond critical point [$\rho(\text{bc}p)$] and its laplacian $\nabla^2\rho$ (bc p), total ELF value at the ring bifurcation (ELF_t) and ELF π component ring bifurcation value (ELF_π) for gallium heterocyclic rings.

Rings	δ_{AB}	$\rho(\text{bc}p)$	$\nabla^2\rho$ (bc p)	ELF_t	ELF_π
$\text{Ga}_3\text{N}_3\text{H}_6$	0.81	0.12	0.56		
$\text{Ga}_3\text{N}_3\text{H}_3\text{F}_3$	0.81	0.12	0.56	0.15	
$\text{Ga}_3\text{N}_3\text{H}_3\text{Cl}_3$	0.81	0.12	0.56	0.15	0.01
$\text{Ga}_3\text{N}_3\text{H}_3(\text{CN})_3$	0.81	0.12	0.57	0.16	0.00
$\text{Ga}_3\text{N}_3\text{H}_3(\text{CF}_3)_3$	0.82	0.12	0.57		
$\text{Ga}_3\text{P}_3\text{H}_6$ (planar)	0.93	0.09	0.07		0.00
$\text{Ga}_3\text{P}_3\text{H}_6$ (puckered)	0.91	0.09	0.05		
$\text{Ga}_3\text{P}_3\text{H}_3\text{F}_3$ (planar)	0.92	0.09	0.06		
$\text{Ga}_3\text{P}_3\text{H}_3\text{F}_3$ (puckered)	0.89	0.09	0.03		
$\text{Ga}_3\text{P}_3\text{H}_3\text{Cl}_3$ (planar)	0.92	0.09	0.06		0.00
$\text{Ga}_3\text{P}_3\text{H}_3\text{Cl}_3$ (puckered)	0.89	0.09	0.03	0.26	
$\text{Ga}_3\text{P}_3\text{H}_3(\text{CN})_3$ (planar)	0.93	0.09	0.06		

$\text{Ga}_3\text{P}_3\text{H}_3(\text{CN})_3$ (puckered)	0.88	0.08	0.02		
$\text{Ga}_3\text{P}_3\text{H}_3(\text{CF}_3)_3$ (planar)	0.93	0.09	0.07		0.00
$\text{Ga}_3\text{P}_3\text{H}_3(\text{CF}_3)_3$ (puckered)	0.89	0.09	0.03		
$\text{Ga}_3\text{As}_3\text{H}_6$ (planar)	0.94	0.08	0.05		
$\text{Ga}_3\text{As}_3\text{H}_6$ (puckered)	0.90	0.08	0.01		
$\text{Ga}_3\text{As}_3\text{H}_3\text{F}_3$ (planar)	0.93	0.09	0.04		0.01
$\text{Ga}_3\text{As}_3\text{H}_3\text{F}_3$ (puckered)	0.89	0.08	0.00		
$\text{Ga}_3\text{As}_3\text{H}_3\text{Cl}_3$ (planar)	0.94	0.09	0.04		
$\text{Ga}_3\text{As}_3\text{H}_3\text{Cl}_3$ (puckered)	0.89	0.08	0.00		
$\text{Ga}_3\text{As}_3\text{H}_3(\text{CN})_3$ (planar)	0.95	0.09	0.04		0.01
$\text{Ga}_3\text{As}_3\text{H}_3(\text{CN})_3$ (puckered)	0.89	0.08	0.00		
$\text{Ga}_3\text{As}_3\text{H}_3(\text{CF}_3)_3$ (puckered)	0.90	0.08	0.00		
$\text{Ga}_3\text{O}_3\text{H}_3$	0.73	0.12	0.73	0.12	
$\text{Ga}_3\text{O}_3\text{F}_3$	0.75	0.12	0.75		
$\text{Ga}_3\text{O}_3\text{Cl}_3$	0.73	0.12	0.75	0.13	0.00
$\text{Ga}_3\text{O}_3(\text{CN})_3$	0.73	0.12	0.76	0.13	
$\text{Ga}_3\text{O}_3(\text{CF}_3)_3$	0.73	0.12	0.75	0.12	
$\text{Ga}_3\text{S}_3\text{H}_3$	0.91	0.09	0.15		0.00
$\text{Ga}_3\text{S}_3\text{F}_3$	0.92	0.09	0.14	0.20	
$\text{Ga}_3\text{S}_3\text{Cl}_3$	0.91	0.09	0.14		0.01
$\text{Ga}_3\text{S}_3(\text{CN})_3$	0.92	0.09	0.14		0.00
$\text{Ga}_3\text{S}_3(\text{CF}_3)_3$	0.92	0.09	0.15		0.00
$\text{Ga}_3\text{Se}_3\text{H}_3$	0.94	0.08	0.09		0.01
$\text{Ga}_3\text{Se}_3\text{F}_3$	0.94	0.09	0.08	0.21	0.00
$\text{Ga}_3\text{Se}_3\text{Cl}_3$	0.94	0.09	0.08	0.22	0.01
$\text{Ga}_3\text{Se}_3(\text{CN})_3$	0.95	0.09	0.08	0.23	0.01
$\text{Ga}_3\text{Se}_3(\text{CF}_3)_3$	0.96	0.09	0.08		

In order to understand the different trends a detailed ELF analysis has been carried out on few representative systems. Table 2.9 reports the quantitative population analysis of these systems whereas Figure 2.3 displays the $\eta = 0.8$ and the bifurcation isosurfaces of few selected molecules. The largest $V(\text{M},\text{Z})$ populations are found for $\text{B}_3\text{N}_3\text{H}_6$ and $\text{Al}_3\text{N}_3\text{H}_6$, because as expected, the nitrogen lone pairs are merged into the M-Z bonds. As a consequence, the contribution of the N atom to $V(\text{M},\text{Z})$ is very large (c.a. 94%). The covariance matrix elements of adjacent $V(\text{M},\text{Z})$ basin have very asymmetric values: their

absolute values are small when N is the common atom and large when it is the group XIII element. Phosphorus and arsenic derivatives have lone pair basins and therefore, the $V(M,Z)$ population is lower than for the former molecules, the polarizations of the bonds are smaller and the covariance matrix elements are much more symmetrical. The lone pairs on the P and As atoms can be interpreted by invoking the “hybridization defect” of period III and IV elements. The presence of these lone pairs explains the puckering of the molecules involving P and as atoms. The puckering do not noticeably change the properties of the $V(M,Z)$ basins. Finally, substituting H by a more electronegative group slightly lowers the $V(M,Z)$ population.

Table 2.9. Summary of the ELF population analysis of the $B_3N_3H_6$, $B_3P_3H_6$, $B_3O_3H_3$, $B_3As_3H_6$, $B_3As_3F_3H_3$ and $Al_3N_3H_6$ molecules. $\Delta\chi$ is the electronegativity difference of centres Z and M, $\bar{N}[V(M,Z)]$ the population of the $V(M,Z)$ basin, σ^2 its variance, $\bar{N}[V(M,Z)|Z]$ the contribution of the Z atomic basin to $V(M,Z)$ population, $\langle cov(M,Z), (M, Z') \rangle$ and $\langle cov(M,Z), (M', Z) \rangle$ the covariance matrix elements of the populations of the adjacent $V(M,Z)$ basins.

Molecule	$\Delta\chi$	$\bar{N}[V(M,Z)]$	$\bar{N}[V(M,Z) Z]$	σ^2	$\langle cov(M,Z), (M, Z') \rangle$	$\langle cov(M,Z), (M', Z) \rangle$
$B_3N_3H_6$	1.06	2.90	2.72	1.33	-0.11	-0.51
$B_3P_3H_6$	0.05	2.30	1.78	1.12	-0.16	-0.14
$B_3O_3H_3$	1.49	2.19	2.02	1.16	-0.07	-0.28
$B_3As_3H_6$	0.19	2.30	1.50	1.26	-0.14	-0.12
$B_3As_3F_3H_3$ (planar)	0.19	2.27	1.39	1.23	-0.14	-0.12
$B_3As_3F_3H_3$ (puckered)	0.19	2.27	1.37	1.22	-0.14	-0.12
$Al_3N_3H_6$	1.60	3.0	2.82	1.35	-0.06	-0.63

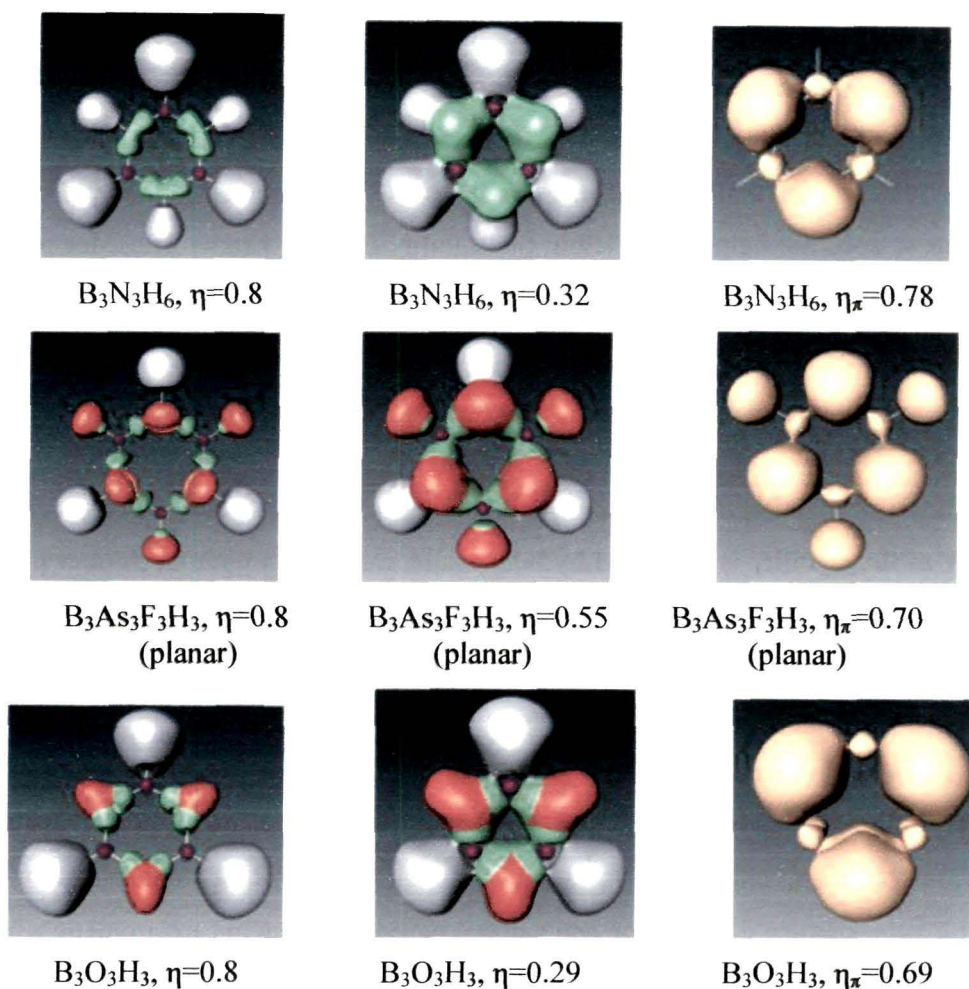


Figure 2.3. ELF=0.8 and bifurcation isosurface of ELF_t and ELF_π of $B_3N_3H_6$, $B_3As_3F_3H_3$, $B_3As_3H_6$ and $B_3O_3H_3$ molecules. Color code: magenta=core, light blue = AH bonds, redbrick = lone pairs, green = bonds.

[2.5] Conclusions

The effect of substituents on the aromaticity and stability of borazine and its analogs were studied by using density functional theory. AIM and ELF calculations were further carried out to gain insight into the bonding and aromaticity of these heterocycles. Based on NICS values, the BP and BAs rings were found to be more aromatic than borazine. Similar trend was found for the Al, and Ga substituted rings. Compared to the pnictogen substituted rings, chalcogen substituted rings are found to be less aromatic which arise from the large electronegativity difference between the constituent atoms of the respective rings. For majority of the rings, the variation in NICS nicely correlates with the changes in the respective M – Z or M – E bond lengths. As the bond length decreases, NICS increases and vice versa. However, except for few systems, the computed aromatic stabilization energies

(ASE) do not correlate with the NICS values. This discrepancy originates from the use of reference molecules in the calculation of ASE while computation of NICS do not need any reference molecule. In spite of the low ASE of alumazene, this compound is stable enough to be characterized experimentally. While the concept of ASE works well for non polar systems like benzene, it does not help in predicting the stability of polar rings. Thus, for polar ring systems, NICS and bond length equalization is a better indicator of aromaticity. While the delocalization of lone pairs of electrons on the pnictogen or chalcogen atom to the empty p orbital of the group 13 element (B, Al and Ga) enhances the stability of these inorganic rings, the lack of it does not necessarily mean that these molecules are not stable. In other words, cyclic delocalization of π electrons in these kinds of polar systems is not a prerequisite for stability as the stability is governed by both σ and π electrons with the former playing a dominant role.³² Our calculations show that it should be possible to synthesize the hitherto unknown six membered rings such as B_3As_3 and Ga_3As_3 by taking bulky electronegative substituents such as CF_3 , C_6F_5 or 1,3,5 trifluoromethyl benzene at the group 13 element and invite experimental verification.

The results obtained from AIM and ELF analysis agrees reasonably well with those obtained from geometric and magnetic parameters. The QTAIM based delocalization index δ_{AB} and ELF values indicate that boron and gallium based ring systems are aromatic while the aluminium based ones are not aromatic.

[2.6] Bibliography

1. Faraday, M. *Philos. Trans. R. Soc. London* **115**, 440-466, 1825.
2. Huheey, J. E. et. al., *Inorganic Chemistry: Principles of Structure and Reactivity*, Fourth Edition, Pearson Education (Singapore) Pte. Ltd., 2004.
3. (a) Schleyer, P. v. R. et. al., *J. Am. Chem. Soc.* **119** (51), 12669 – 12670, 1997. (b) Jemmis, E. D. et. al., *Inorg. Chem.* **40** (14), 3615 – 3618, 2001. (c) Jemmis, E. D., & Kiran, B. *Inorg. Chem.* **37** (9), 2110 – 2116, 1998. (d) Matsunaga, N., & Gordon, M. *J. Am. Chem. Soc.* **116** (25), 11407 – 11419, 1994 and references there in.
4. Chiavarino, B. et. al., *J. Am. Chem. Soc.* **121** (11), 2619-2620, 1999.
5. Timoshkin, A. Y. et. al., *Inorg. Chem.* **50** (18), 9039-9044, 2011.
6. (a) Power, P. P. *J. Organomet. Chem.* **400**, 49 – 69, 1990. (b) Dias, H. v. R., & Power, P. P. *Angew. Chem. Int. Ed. Engl.* **26** (12), 1270 – 1271, 1987. (c) Dias, H. v. R., & Power, P. P. *J. Am. Chem. Soc.* **111** (1), 144 – 148, 1989. (d) Power, P. P. et. al., *Angew. Chem. Int. Ed. Engl.* **30** (6), 691 – 693, 1991. (e) Waggoner, K. M., & Power, P. P. *J. Am. Chem. Soc.* **113** (9), 3385 – 3393, 1991. (f) Kouvetakis, J. et. al., *Inorg. Chem.* **39** (17), 3805 – 3809, 2000. (g) Stock, A., & Pohland, E. *Chem. Ber.* **59** (9), 2215 – 2223, 1926. (h) Boese, R., Maulitz, A. H., & Stellberg, P. *Chem. Ber.* **127** (10), 1887 – 1889, 1994.
7. (a) Boese, R. et. al., *Angew. Chem. Int. Ed. Engl.* **26** (3), 245 – 247, 1987. (b) Chang, C. H. et. al., *Inorg. Chem.* **8** (8), 1689 – 1693, 1969. (c) Kolder, A., & Porter, R. F. *Inorg. Chem.* **10** (4), 775 – 785, 1971. (d) Tossell, J. A., & Lazzeretti, P. *J. Phys. Chem.* **94** (5), 1723 – 1724, 1990. (e) Noth, H., & Schuchardt, U. *J. Organomet. Chem.* **134**, 297 – 303, 1977. (f) Diercks, H., & Krebs, B. *Angew. Chem. Int. Ed. Engl.* **16** (5), 313, 1977.
8. (a) Paine, R. T., et. al., *Inorg. Chem.* **38** (16), 3738 – 3743, 1999. (b) Haasnoot, J. G., et. al., *Acta Crystallogr. Sect B* **28** (7), 2070 -2073, 1972. (c) Coursen, D. L., & Hoard, J. L. *J. Am. Chem. Soc.* **74** (7), 1742 – 1750, 1952. (d) Atwood, D. A., et. al., *Organometallics* **12** (1), 24 – 29, 1993. (e) Cowley, A. H., et. al., *Organometallics* **10** (5), 1635 – 1637, 1991. (f) Schwarz, W., et. al., *Acta Crystallogr. Sect B* **29** (9), 2029 – 2031, 1973. (g) Braunschweig, H., et. al., *J. Organomet. Chem.* **619**, 305 – 312, 2001. (h) Feng, X., Olmstead, M. M., & Power, P. P. *Inorg. Chem.* **25** (26), 4615 – 4616, 1986.
9. (a) Wehmschulte, R. J., & Power, P. P. *J. Am. Chem. Soc.* **118** (4), 791 – 797, 1996. (b) Mason, M. R. et. al., *J. Am. Chem. Soc.* **115** (12), 4971 – 4984, 1993. (c) Taghiof, M. et. al., *Organometallics* **14** (6), 2903 – 2917, 1995. (d) Nogai, S. D., & Schmidbaur, H. *Dalton Trans.* **12** (12), 2488 – 2495, 2003. (e) Schmidbaur, H. et. al., *Naturforsch. B: Chem. Sci.* **56**, 711 – 718, 2001. (f) Power, P. P., et. al., *J. Am. Chem. Soc.* **115** (8), 3221 – 3226, 1993.

10. (a) Zhu, L. et. al., *Theochem* **728** (1-3), 197 – 202, 2005. (b) Nelson, J. T., & Pietro, W. J. *Inorg. Chem.* **28** (3), 544 – 548, 1989. (c) Timoshkin, A. Y., & Frenking, G. *Inorg. Chem.* **42** (1), 60 – 69, 2003. (d) Fink, W. H., & Richards, J. C. *J. Am. Chem. Soc.* **113** (9), 3393 – 3398, 1991. (e) Igor, N., & Branca, K. *Chemical Physics Letters* **440** (1-3), 70 – 72, 2007. (f) Engelberts, J. J. et. al., *Inorg. Chem.* **44** (15), 5266 – 5272, 2005.
11. (a) Nyulász, L. *Chem. Rev.* **101** (5), 1229 – 1246, 2001. (b) Proft, F. D., & Geerlings, P. *Chem. Rev.* **101** (5), 1451 – 1464, 2001. (c) Shaik, S. et. al., *Chem. Rev.* **101** (5), 1501 – 1540, 2001.
12. Beachley, O. T. & Durkin, T. R. *Inorg. Chem.* **13** (7), 1768 – 1770, 1974.
13. B3LYP is Becke's three-parameter hybrid method using the LYP correlation functional (a) Becke, A. D. *J. Chem. Phys.* **98** (7), 5648 – 5652, 1993. (b) Lee, C. et. al., *Phys. Rev. B.* **37** (2), 785 – 789, 1988. (c) Vosko, S. H. et. al., *Can. J. Phys.* **58** (8), 1200 – 1211, 1980.
14. (a) Glendening, E. D. et. al., *NBO Program 3.1*: Madison, W. T. 1988. (b) Reed, A. et. al., *Chem. Rev.* **88** (6), 899 – 926, 1988.
15. Schleyer, P. v. R. et. al., *J. Am. Chem. Soc.* **118** (26), 6317 – 6318, 1996.
16. Pople, J. A. et. al., Gaussian 03, Revision D.01, Gaussian, Inc., Wallingford CT, 2004.
17. Bader, R. F. W. *Atoms in Molecules: A Quantum Theory*. Oxford Univ. Press, Oxford, 1990.
18. (a) Silvi, B., & Savin, A. *Nature* **371** (6499), 683–686, 1994. (b) Becke, A. D., & Edgecombe, K. E. *J. Chem. Phys.* **92** (9), 5397–5403, 1990.
19. Savin, A. et. al., *Angew. Chem. Int. Ed. Engl.* **30** (4), 409, 1991.
20. Silvi, B. *J. Phys. Chem. A* **107** (17), 3081–3085, 2003.
21. Kohout, M. et. al., *Theor. Chem. Acc.* **112**, 453–459, 2004.
22. Silvi, B. *J. Mol. Struct.* **614** (1-3), 3–10, 2002.
23. Silvi, B. *Phys. Chem. Chem. Phys.* **6** (2), 256–260, 2004.
24. Fradera, X., Austen, M. A., & Bader, R. F. W. *J. Phys. Chem. A* **103** (2), 304–314, 1998.
25. Silvi, B. et. al., *Chem. Rev.* **105** (10), 3911–3947, 2005.
26. Raub, S., & Jansen, G. *Theor. Chem. Acc.* **106**, 223–232, 2001.
27. Santos, J. C. et. al., *J. Chem. Phys.* **120** (4), 1670–1673, 2004.
28. Silvi, B. et. al., *Comput. in Chem.* **23** (6), 597–604, 1999.
29. Silvi, B. et. al., *J. Chem. Phys.* **125** (2), 024301, 2006.

30. *Amira 3.0*. TGS, Template Graphics Software, Inc., San Diego, USA, 2002.
31. (a) Islas, R. et. al., *Struct. Chem.* **18** (6), 833 – 839, 2007. (b) Feixas, F. et. al., *J. Comput. Chem.* **29** (10), 1543 – 1554, 2008.
32. (a) Shaik, S. S., & Hiberty, P. C. *J. Am. Chem. Soc.* **107** (11), 3089 – 3095, 1985. (b) Shaik, S. S. et. al., *J. Am. Chem. Soc.* **109** (2), 363 – 374, 1987. (c) Jug, K., & Köster, A. M. *J. Am. Chem. Soc.* 1990, **112** (19), 6772 – 6777.



CHAPTER - 3

**Transannular Interaction in Group 4 and
Group 6 Metallatranes**

[3.0] ABSTRACT

Density functional calculations coupled with Quantum Theory of Atoms in Molecules analysis were carried out on Group 4 and 6 metallatranes with special emphasis on the nature of transannular M–N bond present in these molecules. Substituents at both the apical and equatorial positions are found to influence the extent of transannular interaction. The degree of pyramidalization around the metal and the bridgehead nitrogen atom play a key role in strengthening or weakening the M–N bond. The stability of these molecules are found to depend to a large extent on the strength of M–N bonds with significant contribution coming in from metal-equatorial and metal-apical bonds. Group 6 metallatranes are found to have stronger transannular bonds and hence higher stabilization energies than their Group 4 counterparts. AIM analysis reveals the presence of considerable amount of covalent character in the M–N bonds which increase from Group 4 to Group 6.

[3.1] Introduction

Triamidoamine $[(RNCH_2CH_2)_3N]^{3-}$ ($R = SiR'_3$, $R' = \text{aryl, alkyl}$), triethanolatoamine $[(OCH_2CH_2)_3N]^{3-}$ and its sulphur analogs have attracted considerable interest over a period of time.¹ They bind to main group and transition metals in tetradentate manner to create a sterically protected, 3-fold-symmetric pocket around the metal atom^{1a,d} having either a trigonal monopyramidal or bipyramidal geometry. The molecules so formed are popularly known as metallatranes featuring a transannular M–N bond. These metallatranes are widely used as catalysts for olefin polymerization and organometallic chemical vapour deposition (OMCVD) of thin films.² Among the transition metal atranes, those formed by Group 4 and Group 6 elements are extensively reported in the literature.²⁻⁸

Titanatranes of the general formula $Cp^*Ti(TEA)$ [TEA is triethoxyamine, $N(CH_2CH_2O)_3^{3-}$] have shown promising catalytic efficiency for the syndiotactic polymerization of styrene.^{2c} The presence of transannular interaction coupled with ancillary ligand Cp^* at the apical position leads to the higher catalytic activity of the complex. Zirconatranes are found to be an efficient catalyst for the dehydrocoupling of primary phosphines with silanes and germanes to form P–Si and P–Ge bonds.^{2b} Nitrides of Group 4 metallatranes are used as a substitute for gold in decorative coatings.⁹ Group 6 metallatranes have various catalytic applications. Silica-supported Cr^{IV} species have shown promising catalytic activity in polymerization of α -olefins.¹⁰ Schmid et al have shown theoretically that Cr (IV) model compounds $[Cr^{IV}(NR_2)_2R']$ ($R = H, Me, SiH_3$; $R' = Me, Et$) are efficient catalysts for ethylene polymerization.¹¹ Molybdenum and tungsten complexes of these

triamidoamine ligands are relatively rigid and possess trigonal mono and bipyramidal geometry with unusual reactivity. This unusual reactivity of molybdenum and tungsten complexes initiates the activation of dinitrogen¹² and form stable complexes with metal-pnictogen triple bonds.³

The chemistry of these metallatranes are largely governed by the extent of transannular M N interaction as well as the nature of substituents at the equatorial (E) and apical (Z) positions. The experimentally characterized metallatranes show varying degree of M N interaction (Table 3.1). However, these transannular distances are much shorter than the sum of the van der Waals radii of the respective metal and the bridgehead nitrogen atom.

Table 3.1. List of experimentally known structures of Group 4 and 6 metallatranes (Z-M[-ER(CH₂)₂]₃N) for which crystal structures are available. (Here E is the equatorial substituent and Z is the apical ligand).

Metal	E	Z	Ranges of r _{M-Nax} (Å)	References
Ti	NR, O	Cl, NR' ₂ , OR', OAr ^a	2.006 - 2.451	2, 4
Zr	NR	Cl, NR' ₂ , CH ₃ , PPhPh, CH ₂ Ph	2.393 - 2.548	2b, 5
Hf	NSi(CH ₃) ₃	N(CH ₃) ₂	2.488	4b
Cr	NR, NAr ^b	H, F, Cl, Br, CN, NO, CO, CH ₃ ,	2.393-2.548	6
Mo	NR, NAr ^c , NAr ^b , S	Cl, NH ₃ , NNR', NR', N ₂ , C ₂ H ₅ , CD ₃ , Cyclo- C ₆ H ₁₁ , CN, PPhPh, OR', NO	2.171-2.422	3a, 7
W	NR, NAr ^b	Cl, N ₂ , NNR, Cyclo- C ₄ H ₇ , CO, OR'	2.174-2.395	3b, 8

R = H, CH₃, C₂H₅, i-Pr, CH₂(^tBu), C₆F₅, Si(CH₃)₃, (CH₃)₃C₆H₂, (^tBu)₂C₆H₃, (CF₃)₂C₆H₃, Si(CH₃)₂(^tBu),

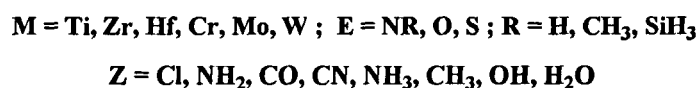
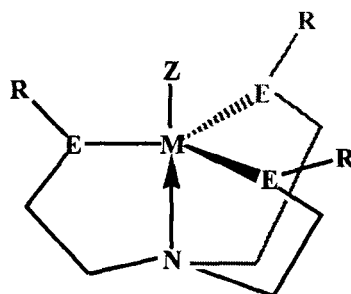
R' = CH₃, SO₂CF₃, (^tBu)₂C₆H₃, (CH₂Ph)(CHPPh), (CH₃)₂C₆H₃, Si(CH₃)₃, SiPh₃, Si(i-Pr)₃

^aAr = (^tBu)₂C₆H₂CPh₂, (^tBu)₂C₆H₂C(Ph)(^tBu)₂OHC₆H₂, (iPr)₂C₆H₃, ^bAr = (i-Pr)₃C₆H₂)₂C₆H₃

^cAr = (^tBu₃C₆H₂)₂C₆H₃

Large numbers of metallatranes involving both main group metals¹³ as well as transition metals (Table 3.1) are reported till date. While the literature is enriched with

theoretical studies of main group atranes,¹⁴ such studies related to transition metal atranes are very few.¹⁵ Gordon and coworkers have carried out *ab initio* calculations on the molecular structure of a series of azatitanatranes. Their studies reveal that the transannular Ti...N interaction is stronger than those found for analogous azasilatranes.^{15a} Filippou's group has reported the first structurally characterized trigonal monopyramidal chromium (II) complexes with triamidoamine ligands and rationalised the structural changes theoretically.^{15b} Thus, it is worthwhile to carry out a systematic study on the structural trends of these metallatranes. We present here a comprehensive study on the effect of substituents at the metal and equatorial atom on the structure and stability of Group 4 and 6 metallatranes. A variety of substituents were employed at the metal so that the effect of both σ – donor as well as π – donor/acceptor ligands can be studied (Scheme 3.1). Also, the range of substituents is considerably larger than that of experimentally known compounds. Our main emphasis will be on the nature of transannular M...N interaction as a function of E and Z. Besides this transannular M...N interaction, any other factors which may enhance the stability of these molecules are also explored. In all our discussions, we will use the prefix aza, azamethyl, azasilyl, oxa and thia to indicate metallatranes with NH, NCH₃, NSiH₃, O and S as the equatorial substituents.



Scheme 3.1. Schematic representation of group 4 and group 6 metallatranes with different equatorial (E) and apical (Z) substituents.

[3.2] Computational Details

All the structures were fully optimized with gradient-corrected density functional theory (DFT) using the Becke's three-parameter hybrid functional (B3LYP) with nonlocal correlation functional of Lee, Yang, and Parr.¹⁶ We employed the LANL2DZ basis set with

the effective core potentials (ECP) of Hay and Wadt.¹⁷ Frequency calculations were performed at the same level of theory and using the same basis set to ascertain the nature of the stationary points. All the structures were verified as a minimum by confirming that their respective hessian (matrix of analytically determined second order energy derivative) is all positive. The bonding nature of all the compounds were analyzed by natural bond orbital analysis (NBO).¹⁸ The strengths of individual bonds were ascertained from their values of Wiberg Bond Indices (WBI) available within the NBO routine. All the computations were performed using Gaussian 03 suite of program.¹⁹ The oxidation states and thus, the d – electron count at the central metal atom changes with variation in the nature of apical ligands (Z). For neutral Z groups, the d – electron count at the metal atom is 1 and 3 for the Group 4 and 6 metals respectively, whereas for anionic Z groups, the d – electron count decreases by one unit to 0 and 2 respectively. For the Group 6 metals in +3 oxidation state, both the spin states (high and low) were considered. In order to understand the nature of bonding in these molecules in greater detail, the topological properties of the resultant electron density, ρ , obtained from the wave functions of all the optimized structures were analyzed with the quantum theory of atoms in molecules (QTAIM).²⁰ The QTAIM analyses were carried out with the programs AIMPAC²¹ and AIMALL²² whereas the wave functions were generated with Gaussian03 at the same level of theory as was used for geometry optimization.¹⁹ However, to produce the contour plots of the laplacian with AIMALL, the corresponding wave functions were generated by running single point calculations at B3LYP/6-31+G* level of theory.

[3.3] Results and Discussion

[3.3.1] Molecular Geometry: The molecular structure of metallatranes consists of three five membered envelope shaped rings with the transannular M...N bond being common to all the rings. The optimized geometries of these molecules adopt pseudo trigonal bipyramidal geometry around the metal atom (Figure 3.1) with the metal and the bridgehead nitrogen atoms being pyramidalized outwardly and inwardly respectively.

[3.3.1.1] Group 4 Metallatranes

The key structural parameters of titanatranes are given in Table 3.2. Comparison of the X – ray bond lengths of titanatranes with our computed ones reveal that there is a close agreement between experiment and theory. For example, the computed Ti...N, Ti - N and Ti – Cl bond distances of 2.253Å, 1.933Å and 2.342Å with Cl and NCH₃ as the respective apical

and equatorial substituents are in close agreement with corresponding experimental values of 2.229Å, 1.919Å and 2.332Å.^{4a} On an average, the calculated transannular Ti...N distances are found to be 12.4% longer than the sum of the covalent radii (2.07Å) for Ti and N. Similar results were obtained by the group of Gordon for azatitanatranes.^{15a} Irrespective of the nature of the substituents at the equatorial position, the shortest transannular bonds are computed for the σ – donating apical ligands, viz, CO, NH₃ and H₂O. This can be explained by looking at

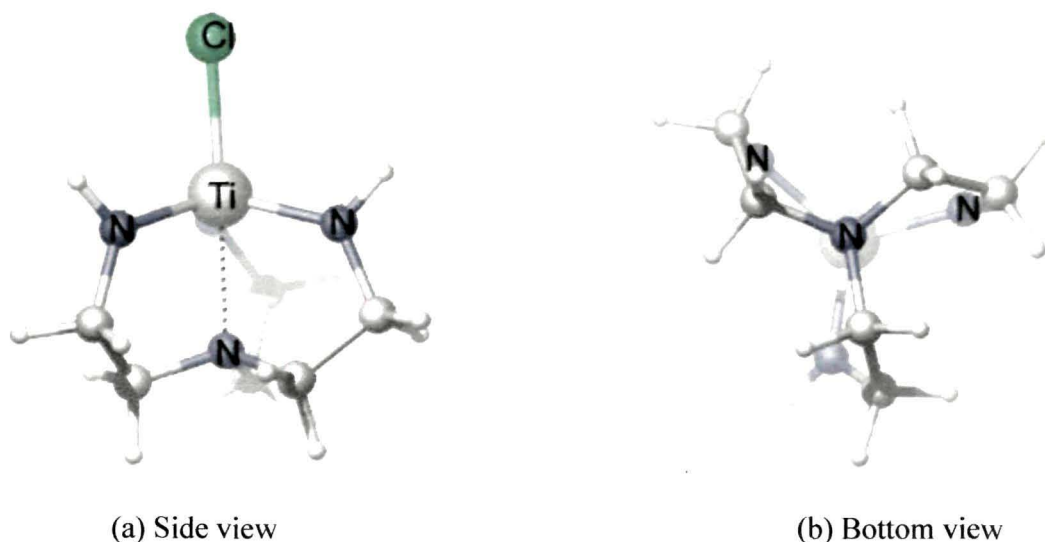


Figure 3.1. Optimized geometry of a titanatrane molecule shown in two different perspectives.

Table 3.2: B3LYP/LANL2DZ computed transannular distance ($r_{M-N_{ax}}$), average metal – equatorial atom (r_{M-E}) and metal – apical (r_{M-Z}) bond distances (Å), pyramidalization angles (in degrees) around metal (θ_M), axial nitrogen (θ_N) and equatorial atom (θ_E), and natural charges at metal (q_M) and axial nitrogen (q_N) for Z-Ti[-ER(CH₂)₂]₃N]. The respective Wiberg Bond Index (WBI) values are given within parenthesis.

Z	Geometric Parameters	E=NH	NCH ₃	NSiH ₃	O	S
Cl	r_{M-N}	2.329 (0.264)	2.253 (0.291)	2.326 (0.261)	2.539 (0.182)	2.354 (0.268)
	$\theta_M / \theta_N / \theta_E$	15.4 / 22.7 / 0.2	14.6 / 22.3 / 0.3	10.4 / 22.4 / 0.1	22.9 / 16.2	4.8 / 31.0
	r_{M-E}	1.919 (0.928)	1.933 (0.874)	1.927 (0.885)	1.810 (0.906)	2.344 (1.082)
	r_{M-Z}	2.312 (1.013)	2.342 (0.956)	2.331 (0.973)	2.285 (1.011)	2.235 (1.251)
	q_M / q_N	1.200 / -0.555	1.207 / -0.542	1.252 / -0.564	1.425 / -0.570	0.328 / -0.575
NH ₂	r_{M-N}	2.415 (0.192)	2.392 (0.198)	2.366 (0.209)	2.563 (0.138)	2.386 (0.218)
	$\theta_M / \theta_N / \theta_E$	15.9 / 20.0 / 4.6	14.3 / 19.8 / 0.4	11.3 / 20.3 / 0.4	22.0 / 15.0	4.9 / 29.6
	r_{M-E}	1.927 (0.883)	1.942 (0.851)	1.942 (0.836)	1.836 (0.835)	2.360 (1.034)
	r_{M-Z}	1.910 (1.010)	1.918 (0.988)	1.913 (0.993)	1.890 (1.030)	1.864 (1.193)
	q_M / q_N	1.376 / -0.576	1.372 / -0.574	1.410 / -0.579	1.603 / -0.585	0.609 / -0.594

CO	$\Gamma_{M...N}$	2 290 (0 230)	2 278 (0 227)	2 265 (0 235)	2 348 (0 213)	2 240 (0 272)
	$\theta_M / \theta_N / \theta_E$	9 5 / 21 3 / 0 1	8 6 / 20 4 / 4 6	7 0 / 20 7 / 1 0	12 4 / 19 9	1 2 / 29 4
	Γ_{M-E}	1 934 (0 853)	1 947 (0 819)	1 959 (0 786)	1 854 (0 782)	2 376 (0 944)
	Γ_{M-Z}	2 109 (0 729)	2 110 (0 736)	2 125 (0 707)	2 126 (0 681)	2 175 (0 602)
	q_M / q_N	1 080 / -0 579	1 055 / -0 577	1 107 / -0 581	1 303 / -0 587	-0 243 / -0 292
CN	$\Gamma_{M...N}$	2 354 (0 216)	2 353 (0 213)	2 357 (0 203)	2 571 (0 141)	2 359 (0 216)
	$\theta_M / \theta_N / \theta_E$	14 8 / 21 6 / 0 2	14 3 / 21 3 / 3 6	10 2 / 20 6 / 0 1	23 7 / 14 9	4 9 / 30 1
	Γ_{M-E}	1 901 (0 952)	1 914 (0 935)	1 913 (0 913)	1 810 (0 925)	2 325 (1 123)
	Γ_{M-Z}	2 124 (0 666)	2 142 (0 651)	2 127 (0 663)	2 087 (0 712)	2 062 (0 757)
	q_M / q_N	1 321 / -0 575	1 280 / -0 572	1 333 / -0 585	1 540 / -0 583	0 500 / -0 600
NH ₃	$\Gamma_{M...N}$	2 271 (0 249)	2 261 (0 252)	2 260 (0 254)	2 292 (0 230)	2 258 (0 282)
	$\theta_M / \theta_N / \theta_E$	7 1 / 20 2 / 1 9	6 7 / 19 5 / 2 7	6 2 / 20 6 / 0 1	8 0 / 19 3	1 3 / 28 1
	Γ_{M-E}	1 977 (0 732)	1 987 (0 696)	2 000 (0 660)	1 903 (0 667)	2 398 (0 913)
	Γ_{M-Z}	2 269 (0 284)	2 281 (0 275)	2 261 (0 291)	2 230 (0 292)	2 217 (0 345)
	q_M / q_N	1 284 / -0 576	1 288 / -0 574	1 368 / -0 578	1 457 / -0 590	0 645 / -0 586
CH ₃	$\Gamma_{M...N}$	2 450 (0 159)	2 438 (0 161)	2 441 (0 156)	2 684 (0 087)	2 436 (0 183)
	$\theta_M / \theta_N / \theta_E$	17 0 / 18 6 / 0 3	16 4 / 18 1 / 0 4	12 8 / 18 2 / 0 1	8 0 / 19 3	6 2 / 28 2
	Γ_{M-E}	1 918 (0 899)	1 932 (0 869)	1 934 (0 852)	1 818 (0 873)	2 351 (1 059)
	Γ_{M-Z}	2 100 (0 783)	2 115 (0 758)	2 111 (0 774)	2 073 (0 848)	2 044 (0 890)
	q_M / q_N	1 412 / -0 580	1 405 / -0 576	1 454 / -0 586	1 606 / -0 586	0 631 / -0 599
OH	$\Gamma_{M...N}$	2 356 (0 233)	2 288 (0 252)	2 329 (0 241)	2 535 (0 169)	2 364 (0 249)
	$\theta_M / \theta_N / \theta_E$	16 2 / 22 3 / 0 4	14 0 / 22 1 / 0 3	11 2 / 22 3 / 0 3	21 6 / 16 4	6 0 / 30 7
	Γ_{M-E}	1 931 (0 858)	1 950 (0 822)	1 947 (0 820)	1 837 (0 830)	2 507 (0 898)
	Γ_{M-Z}	1 793 (1 022)	1 800 (1 001)	1 794 (1 015)	1 783 (0 985)	1 750 (1 198)
	q_M / q_N	1 429 / -0 570	1 400 / -0 562	1 459 / -0 577	1 660 / -0 583	0 680 / -0 592
H ₂ O	$\Gamma_{M...N}$	2 268 (0 256)	2 254 (0 259)	2 231 (0 267)	2 291 (0 235)	2 262 (0 291)
	$\theta_M / \theta_N / \theta_E$	7 3 / 20 6 / 2 6	6 7 / 20 1 / 0 1	5 6 / 20 8 / 0 3	8 0 / 19 6	1 6 / 29 1
	Γ_{M-E}	1 973 (0 734)	1 983 (0 696)	2 003 (0 651)	1 904 (0 661)	2 399 (0 910)
	Γ_{M-Z}	2 153 (0 272)	2 159 (0 267)	2 125 (0 301)	2 112 (0 284)	2 094 (0 337)
	q_M / q_N	1 307 / -0 576	1 305 / -0 574	1 387 / -0 580	1 493 / -0 593	0 680 / -0 592

the values of the pyramidalization angle at the metal (θ_M) and bridgehead nitrogen atom (θ_N) (Table 3.2). While θ_N do not vary appreciably with the changes either in the apical or equatorial substituents, θ_M decreases for these σ – donating ligands. In general, a decrease in θ_M and increase in θ_N makes it ideal for a strong transannular interaction. Thus, the replacement of the apical ligands by CO, NH₃ and H₂O results in shortening of the Ti N bond. Corresponding to the increase or decrease of Ti N distance, the Ti – Z distances decrease or increase accordingly. This is also reflected in the WBI values of respective bonds (Table 3.2). For example, in the case of Cl and OH as the apical substituents, the Ti N distance of azasilyltitanatrane is more than that of azamethyltitanatrane even though the value of θ_M is more for the later than the former. This lengthening of the Ti N bond can be explained by the apparent strengthening of the Ti – Cl and Ti – O bonds. However, this correlation was not observed for CO as in this case, back donation from the filled metal

orbital to the π^* orbital of CO results in strengthening of the Ti – CO bond. In the case of azatitanatranes, substitution of the hydrogen atoms attached to the equatorial nitrogen atoms by CH_3 and SiH_3 groups results in considerable decrease in the value of θ_M which results in shortening of the Ti – N bond. This is because the bulky methyl and silyl group orbitals force the metal atom to move towards the equatorial plane defined by the three nitrogen atoms. Out of all the apical and equatorial substituents, $Z = \text{CH}_3$ and $E = \text{O}$ computes the longest Ti – N distance. Our results are in contrast to those reported by Gordon and coworkers for the parent azatitanatrane geometry by taking CH_3 and NH_2 as the apical substituents. They found a longer Ti – N bond for NH_2 than CH_3 . This difference may arise from the non inclusion of electron correlation in their study. The Ti – N bonds of oxatitanatranes are much more longer than others. Interestingly, replacement of the oxygen atom by the heavier sulphur atom dramatically changes the structure. It results in slight deformation of the cage structure even though the trigonal bipyramidal geometry around the metal atom is retained to a large extent. The most significant changes took place at the metal and bridgehead nitrogen atom. The bigger sulphur atom forces the metal atom to lie almost in the plane defined by the three sulphur atoms. Also, the pyramidalization at the bridgehead nitrogen atom increase by $10^\circ - 15^\circ$. These geometrical changes at the metal and bridgehead nitrogen atom result in enhancement of the transannular interaction. NBO analysis reveals that the occupancy of the lone pair at the bridgehead nitrogen atom increases or decreases with respect to decrease or increase in Ti – N distance. The Ti – N bond strength decreases marginally from $E = \text{NH}$ to NSiH_3 . For the parent azatitanatranes, the shortest and longest Ti – N bond was computed with CN and NH_3 respectively as the apical substituents.

The computed minimum energy structures of zirconatranes are also in very good agreement with experimentally observed ones (Table 3.3).^{5a} The average calculated transannular Zr – N distance is 11% longer than the sum of covalent radii (2.23Å) for Zr and N. As in the case with titanatranes, similar variation in transannular distances with changes in the apical ligands are observed here, i. e., the transannular Zr – N distances are found to be shorter with σ – donating apical ligands. This is again due to the comparatively smaller pyramidalization angle around the metal atom for these ligands. However, the transannular Zr – N bonds are slightly weaker than the transannular Ti – N bonds as revealed by the smaller values of the Wiberg Bond Indices (WBI) of the respective bonds. This can be explained by considering the hardness or softness of the participating atoms. The smaller, hard titanium atom will bind more effectively to the hard nitrogen atom than the larger and soft zirconium

Table 3.3. B3LYP/LANL2DZ computed transannular distance ($r_{M-N_{ax}}$), average metal – equatorial atom (r_{M-E}) and metal – apical (r_{M-Z}) bond distances (Å), pyramidalization angles (in degrees) around metal (θ_M), axial nitrogen (θ_N) and equatorial atom (θ_E), and natural charges at metal (q_M) and axial nitrogen (q_N) for Z-Zr[-ER(CH₂)₂]₃N]. The respective Wiberg Bond Index (WBI) values are given within parenthesis.

Z		E=NH	NCH ₃	NSiH ₃	O	S
Cl	$r_{M \cdots N}$	2 473 (0 196)	2 416 (0 208)	2 461 (0 193)	2 602 (0 152)	2 514 (0 205)
	$\theta_M / \theta_N / \theta_E$	24 0 / 23 5 / 0 2	23 4 / 23 1 / 0 2	18 7 / 23 4 / 0 3	29 3 / 20 0	12 0 / 31 2
	r_{M-E}	2 074 (0 740)	2 087 (0 710)	2 092 (0 687)	1 978 (0 692)	2 507 (1 007)
	r_{M-Z}	2 487 (0 895)	2 517 (0 859)	2 491 (0 917)	2 472 (0 852)	2 412 (1 112)
	q_M / q_N	1 928 / -0 615	1 903 / -0 609	1 956 / -0 625	2 124 / -0 617	1 033 / -0 629
NH ₂	$r_{M \cdots N}$	2 533 (0 145)	2 462 (0 161)	2 506 (0 151)	2 626 (0 114)	2 541 (0 165)
	$\theta_M / \theta_N / \theta_E$	23 9 / 21 6 / 0 1	23 0 / 22 0 / 0 4	19 6 / 21 6 / 0 1	28 9 / 18 6	10 8 / 27 8
	r_{M-E}	2 095 (0 697)	2 109 (0 663)	2 113 (0 639)	2 004 (0 639)	2 531 (0 940)
	r_{M-Z}	2 088 (0 779)	2 102 (0 746)	2 080 (0 802)	2 069 (0 779)	2 032 (0 958)
	q_M / q_N	2 131 / -0 621	2 125 / -0 615	2 170 / -0 627	2 312 / -0 622	1 339 / -0 635
CO	$r_{M \cdots N}$	2 466 (0 168)	2 452 (0 165)	2 448 (0 165)	2 536 (0 144)	2 440 (0 196)
	$\theta_M / \theta_N / \theta_E$	20 6 / 22 7 / 0 2	19 5 / 21 8 / 0 7	17 2 / 22 6 / 0 1	25 3 / 21 0	7 4 / 30 2
	r_{M-E}	2 089 (0 721)	2 102 (0 689)	2 107 (0 659)	2 001 (0 654)	2 520 (0 944)
	r_{M-Z}	2 279 (0 704)	2 279 (0 722)	2 278 (0 725)	2 261 (0 695)	2 276 (0 699)
	q_M / q_N	1 796 / -0 626	1 773 / -0 625	1 799 / -0 632	1 979 / -0 628	0 157 / -0 318
CN	$r_{M \cdots N}$	2 498 (0 160)	2 490 (0 158)	2 504 (0 150)	2 620 (0 121)	2 545 (0 162)
	$\theta_M / \theta_N / \theta_E$	24 0 / 22 9 / 0 2	23 5 / 22 5 / 1 7	19 3 / 22 6 / 0 1	30 0 / 19 3	12 8 / 30 7
	r_{M-E}	2 069 (0 758)	2 075 (0 711)	2 083 (0 706)	1 973 (0 707)	2 498 (1 033)
	r_{M-Z}	2 303 (0 581)	2 317 (0 583)	2 298 (0 601)	2 271 (0 594)	2 235 (0 682)
	q_M / q_N	2 048 / -0 624	2 006 / -0 621	2 059 / -0 633	2 228 / -0 623	1 203 / -0 638
NH ₃	$r_{M \cdots N}$	2 463 (0 186)	2 438 (0 189)	2 408 (0 196)	2 553 (0 145)	2 390 (0 234)
	$\theta_M / \theta_N / \theta_E$	20 2 / 22 5 / 1 3	18 7 / 21 4 / 1 9	14 7 / 21 9 / 0 1	24 1 / 19 5	4 8 / 29 2
	r_{M-E}	2 113 (0 659)	2 125 (0 614)	2 150 (0 550)	2 034 (0 583)	2 550 (0 850)
	r_{M-Z}	2 394 (0 270)	2 410 (0 256)	2 454 (0 225)	2 392 (0 247)	2 409 (0 269)
	q_M / q_N	1 659 / -0 624	1 670 / -0 622	1 776 / -0 624	1 805 / -0 627	1 046 / -0 631
CH ₃	$r_{M \cdots N}$	2 569 (0 131)	2 529 (0 141)	2 563 (0 131)	2 698 (0 092)	2 602 (0 152)
	$\theta_M / \theta_N / \theta_E$	25 7 / 20 6 / 0 2	25 1 / 20 9 / 1 0	20 9 / 20 3 / 0 2	31 6 / 16 2	12 8 / 28 9
	r_{M-E}	2 085 (0 715)	2 094 (0 681)	2 102 (0 655)	1 989 (0 666)	2 519 (0 976)
	r_{M-Z}	2 285 (0 628)	2 298 (0 604)	2 278 (0 635)	2 260 (0 664)	2 212 (0 764)
	q_M / q_N	2 154 / -0 615	2 150 / -0 612	2 197 / -0 620	2 306 / -0 614	1 334 / -0 625
OH	$r_{M \cdots N}$	2 488 (0 163)	2 456 (0 170)	2 458 (0 166)	2 591 (0 131)	2 506 (0 179)
	$\theta_M / \theta_N / \theta_E$	23 7 / 23 4 / 0 4	22 1 / 23 6 / 3 5	18 3 / 23 1 / 0 2	27 8 / 20 2	10 6 / 30 9
	r_{M-E}	2 097 (0 684)	2 106 (0 653)	2 117 (0 628)	2 006 (0 632)	2 533 (0 927)
	r_{M-Z}	1 969 (0 765)	1 978 (0 747)	1 959 (0 785)	1 957 (0 732)	1 919 (0 927)
	q_M / q_N	2 179 / -0 626	2 172 / -0 625	2 220 / -0 635	2 360 / -0 629	1 421 / -0 644
H ₂ O	$r_{M \cdots N}$	2 467 (0 185)	2 429 (0 192)	2 406 (0 195)	2 575 (0 134)	2 412 (0 225)
	$\theta_M / \theta_N / \theta_E$	22 5 / 23 0 / 1 3	21 0 / 23 0 / 2 0	15 1 / 22 2 / 0 5	24 3 / 18 8	6 1 / 30 2
	r_{M-E}	2 096 (0 677)	2 112 (0 633)	2 147 (0 556)	2 036 (0 575)	2 547 (0 853)
	r_{M-Z}	2 260 (0 285)	2 272 (0 275)	2 306 (0 242)	2 258 (0 243)	2 292 (0 261)
	q_M / q_N	1 693 / -0 625	1 702 / -0 625	1 783 / -0 628	1 844 / -0 629	1 080 / -0 633

atom. Also, the pyramidalization around zirconium is much larger than for titanium. By virtue of its size, the larger zirconium atom cannot lie in the plane defined by the three equatorial atoms. The observed trend in θ_M for azazirconatranes is also similar to that observed for azatitanatranes, i. e., θ_M decreases as the equatorial groups are changed from NH to NSiH₃ although no such significant variation is obtained for θ_N . However, θ_N increases by about 10° - 12° as the equatorial atoms are changed from O to S. Oxa and azamethyl zirconatranes compute the largest and shortest transannular distances for most of the apical ligands except σ donating ones for which the shortest transannular Zr - N distances are found with the thia derivative (with a minor discrepancy shown by Z = H₂O for which the shortest transannular Zr - N distance is computed for E = NSiH₃). Thiazirconatranes show similar deformation of the cage structure as observed for thiatitanatranes. The Zr - E bond strengths decreases as the equatorial substituents are changed from NH to NSiH₃ and increases from O to S. The relative strengths of the metal - equatorial bonds are governed by the hard - hard or hard - soft interaction. Irrespective of the nature of the apical substituents, all Zr - E bonds are weaker than those for titanium.

Like titanatranes and zirconatranes, excellent agreement is observed between theoretical result and the experimentally characterized azahafnatrane (Table 3.4).^{4b} The calculated average transannular Hf - N distances are found to be 9% longer than the sum of the covalent radii (2.24 Å) for Hf and N. The transannular interaction of hafnatranes are computed to be the weakest among Group 4 metallatranes as revealed by the low values of WBI of the respective bonds. However, the weakening of transannular Hf - N bond compared to Zr - N bond is less in comparison to that between Zr - N and Ti - N bond. This is due to the fact that the size and electronegativity of Ti is significantly different from that of Zr whereas both these parameters are comparable for Zr and Hf. Structural variations in hafnatranes are slightly different from those observed for titanatranes and zirconatranes, such as shorter transannular distances are not computed with σ - donating ligands at the apical position for all the equatorial substituents. However, the variation in pyramidalization around the metal atom follows the same trend as was observed for titanatranes and zirconatranes. Among the azahafnatranes, θ_M decreases as the equatorial substituents are changed from NH to NSiH₃. Barring few exceptions, the shortest and longest transannular Hf - N distance is computed NCH₃ and oxygen as the equatorial substituents. In general, the strength of M - E bonds decreases as one moves from titanatranes to hafnatranes and this correlates with the

Table 3.4. B3LYP/LANL2DZ computed transannular distance (r_{M-Nax}), average metal – equatorial atom (r_{M-E}) and metal – apical (r_{M-Z}) bond distances (Å), pyramidalization angles (in degrees) around metal (θ_M), axial nitrogen (θ_N) and equatorial atom (θ_E), and natural charges at metal (q_M) and axial nitrogen (q_N) for Z-Hf[-ER(CH₂)₂]₃N]. The respective Wiberg Bond Index (WBI) values are given within parenthesis.

Z		E=NH	NCH ₃	NSiH ₃	O	S
Cl	$r_{M...N}$	2 422 (0 186)	2 367 (0 194)	2 408 (0 183)	2 567 (0 142)	2 453 (0 196)
	$\theta_M / \theta_N / \theta_E$	20 7 / 24 0 / 0 2	19 8 / 23 6 / 0 3	16 2 / 22 6 / 0 1	27 1 / 20 1	9 4 / 31 6
	r_{M-E}	2 050 (0 666)	2 064 (0 629)	2 068 (0 614)	1 950 (0 641)	2 487 (0 956)
	r_{M-Z}	2 455 (0 891)	2 479 (0 871)	2 458 (0 915)	2 444 (0 833)	2 384 (1 103)
	q_M / q_N	2 106 / -0 638	2 096 / -0 634	2 127 / -0 647	2 260 / -0 631	1 216 / -0 656
NH ₂	$r_{M...N}$	2 484 (0 140)	2 415 (0 152)	2 452 (0 145)	2 589 (0 109)	2 490 (0 158)
	$\theta_M / \theta_N / \theta_E$	21 2 / 22 3 / 0 1	20 1 / 22 2 / 0 5	17 2 / 21 9 / 0 4	26 6 / 18 9	8 9 / 30 2
	r_{M-E}	2 069 (0 632)	2 083 (0 594)	2 087 (0 575)	1 975 (0 595)	2 507 (0 898)
	r_{M-Z}	2 057 (0 724)	2 068 (0 696)	2 052 (0 731)	2 042 (0 721)	2 004 (0 885)
	q_M / q_N	2 312 / -0 638	2 318 / -0 635	2 351 / -0 646	2 449 / -0 635	1 531 / -0 658
CO	$r_{M...N}$	2 426 (0 154)	2 408 (0 152)	2 400 (0 152)	2 522 (0 128)	2 420 (0 174)
	$\theta_M / \theta_N / \theta_E$	18 3 / 23 3 / 0 1	17 2 / 22 2 / 0 3	14 9 / 22 7 / 0 1	24 2 / 20 9	7 7 / 31 5
	r_{M-E}	2 060 (0 662)	2 070 (0 627)	2 079 (0 601)	1 967 (0 619)	2 495 (0 904)
	r_{M-Z}	2 231 (0 704)	2 231 (0 720)	2 228 (0 722)	2 211 (0 697)	2 215 (0 741)
	q_M / q_N	2 001 / -0 646	1 991 / -0 646	2 017 / -0 654	2 156 / -0 641	1 176 / -0 664
CN	$r_{M...N}$	2 441 (0 151)	2 386 (0 158)	2 443 (0 143)	2 578 (0 114)	2 475 (0 155)
	$\theta_M / \theta_N / \theta_E$	20 4 / 23 4 / 0 1	20 5 / 23 5 / 0 4	16 2 / 23 2 / 0 1	27 3 / 19 6	9 5 / 31 1
	r_{M-E}	2 046 (0 678)	2 059 (0 639)	2 061 (0 629)	1 947 (0 653)	2 479 (0 970)
	r_{M-Z}	2 266 (0 567)	2 286 (0 559)	2 262 (0 582)	2 238 (0 574)	2 203 (0 659)
	q_M / q_N	2 234 / -0 647	2 216 / -0 642	2 247 / -0 655	2 365 / -0 638	1 406 / -0 667
NH ₃	$r_{M...N}$	2 437 (0 169)	2 406 (0 170)	2 392 (0 171)	2 681 (0 094)	2 355 (0 217)
	$\theta_M / \theta_N / \theta_E$	20 3 / 24 0 / 0 1	19 4 / 22 7 / 0 9	16 0 / 22 6 / 0 1	31 0 / 15 9	3 4 / 30 1
	r_{M-E}	2 075 (0 605)	2 092 (0 565)	2 109 (0 531)	1 982 (0 572)	2 511 (0 844)
	r_{M-Z}	2 341 (0 267)	2 343 (0 267)	2 352 (0 255)	2 376 (0 204)	2 362 (0 265)
	q_M / q_N	1 803 / -0 647	1 813 / -0 645	1 913 / -0 650	1 884 / -0 629	1 154 / -0 656
CH ₃	$r_{M...N}$	2 508 (0 132)	2 440 (0 144)	2 506 (0 131)	2 649 (0 094)	2 548 (0 144)
	$\theta_M / \theta_N / \theta_E$	22 4 / 21 5 / 0 3	21 4 / 21 7 / 0 4	18 0 / 21 1 / 0 1	28 7 / 16 8	10 7 / 29 1
	r_{M-E}	2 061 (0 640)	2 073 (0 603)	2 077 (0 583)	1 961 (0 614)	2 496 (0 932)
	r_{M-Z}	2 253 (0 573)	2 269 (0 548)	2 249 (0 577)	2 233 (0 601)	2 186 (0 687)
	q_M / q_N	2 354 / -0 634	2 351 / -0 631	2 390 / -0 640	2 464 / -0 626	1 546 / -0 647
OH	$r_{M...N}$	2 444 (0 152)	2 386 (0 161)	2 418 (0 154)	2 558 (0 121)	2 460 (0 167)
	$\theta_M / \theta_N / \theta_E$	20 9 / 23 7 / 0 4	19 1 / 23 2 / 0 3	16 1 / 23 3 / 0 1	25 7 / 20 3	8 8 / 31 3
	r_{M-E}	2 072 (0 624)	2 083 (0 591)	2 090 (0 569)	1 978 (0 589)	2 511 (0 884)
	r_{M-Z}	1 935 (0 728)	1 943 (0 712)	1 927 (0 736)	1 926 (0 694)	1 889 (0 870)
	q_M / q_N	2 342 / -0 644	2 332 / -0 642	2 383 / -0 653	2 486 / -0 642	1 602 / -0 667
H ₂ O	$r_{M...N}$	2 435 (0 175)	2 364 (0 183)	2 440 (0 156)	2 658 (0 105)	2 371 (0 211)
	$\theta_M / \theta_N / \theta_E$	21 3 / 24 3 / 0 6	20 4 / 23 6 / 0 3	17 5 / 23 9 / 0 4	29 9 / 17 0	5 3 / 30 8
	r_{M-E}	2 064 (0 625)	2 082 (0 587)	2 091 (0 555)	1 979 (0 573)	2 511 (0 848)
	r_{M-Z}	2 198 (0 299)	2 204 (0 297)	2 223 (0 268)	2 243 (0 224)	2 231 (0 273)
	q_M / q_N	1 874 / -0 646	1 893 / -0 642	1 933 / -0 650	1 911 / -0 632	0 150 / -0 330

decreasing hardness of the metal. As expected, the structure of thiahafnatranes is slightly deformed than the rest of hafnatranes.

One interesting structural variation of these Group 4 metallatranes is that with $Z = \text{NH}_3$ and H_2O , these metallatranes do not maintain the local C_3 axis as revealed by the $\angle Z - M - N$ angle which are much less than 180° . This structural variation is more pronounced with oxygen as the equatorial substituent.

[3.3.1.2] Group 6 Metallatranes

The important geometrical parameters for chromatranes are found to be reasonably close to the experimentally observed ones (Table 3.5).^{6a, 6b, 6e} For example, the computed Cr - N, Cr - N_{eq} and Cr - C bond distances of 2.263 Å, 1.873 Å and 2.063 Å with CH_3^- and NSiH_3 as the respective apical and equatorial substituents are in excellent agreement with the corresponding experimental values of 2.250 Å, 1.878 Å and 2.078 Å.^{6b} The average lengthening of the calculated transannular Cr - N distances are found to be only 5% than the sum of the covalent radii (2.03Å) of Cr and N. Depending on the nature of the ligands (neutral or anionic) at the apical position, the metal atom of these metallatranes, viz., Cr, Mo and W can exist in either +3 or +4 oxidation states. Since, two spin states are possible ($S = 1/2$, doublet or $S = 3/2$, quartet) for metal ions in +3 state, therefore we have considered both the spin states in our study (Table 3.6). The relative stability of a particular spin state can be explained by invoking the spectrochemical series. As expected, the strong field ligand CO results in stabilization of the doublet state for all the chromatranes except thiachromatranes. For thiachromatranes, quartet state is more favorable than the doublet state by 4.2 kcal/mol (Table 3.6). Even with oxygen at the equatorial position, the energy difference between these two spin states is not significant implying that the spin state of this class of organometallic compounds can be tuned by putting suitable substituents at the apical and equatorial positions. In other words, the reactivity of these compounds can be tuned by changing the spin state as changes in spin states are found to have dramatic effect on chemical reactivity.²³ For the weak field ligands NH_3 and H_2O , high spin quartet state is the most stable state. In general, shorter and longer Cr - N distances are computed for neutral and anionic ligands respectively which can be correlated to their relative *trans* directing ability. While the weakly *trans* directing ligands (Cl^- , NH_3 , H_2O etc.) strengthens the Cr - N bond, the stronger ones (CO , CN^- , CH_3^-) weakens the same. For a given equatorial substituent, the longest Cr - N bonds are computed for CH_3^- as the apical ligand which is in tune with experimental

Table 3.5. B3LYP/LANL2DZ computed transannular distance (r_{M-Nax}), average metal – equatorial atom (r_{M-E}) and metal – apical (r_{M-Z}) bond distances (Å), pyramidalization angles (in degrees) around metal (θ_M), axial nitrogen (θ_N) and equatorial atom (θ_E), and natural charges at metal (q_M) and axial nitrogen (q_N) for Z-Cr[-ER(CH₂)₂]₃N]. The respective Wiberg Bond Index (WBI) values are given within parenthesis.

Z		E=NH	NCH ₃	NSiH ₃	O	S
Cl	$r_{M...N}$	2 119 (0 324)	2 119 (0 326)	2 124 (0 329)	2 197 (0 287)	2 165 (0 294)
	$\theta_M / \theta_N / \theta_E$	4 2 /23 4 /0 8	3 9 /22 8 /0 9	2 6 /22 7 /0 3	5 8 /20 8	0 9 /30 2
	r_{M-E}	1 843 (0 856)	1 868 (0 809)	1 861 (0 827)	1 792 (0 826)	2 290 (0 851)
	r_{M-Z}	2 309 (0 604)	2 367 (0 543)	2 352 (0 524)	2 262 (0 738)	2 261 (0 692)
	q_M / q_N	0 916 / -0 522	0 957 / -0 516	0 991 / -0 520	1 097 / -0 538	0 482 / -0 555
NH ₂	$r_{M...N}$	2 197 (0 245)	2 184 (0 244)	2 191 (0 254)	2 287 (0 210)	2 214 (0 245)
	$\theta_M / \theta_N / \theta_E$	6 0 /21 3 /0 9	4 9 /21 1 /1 0	4 1 /21 4 /0 1	8 0 /18 8	1 8 /30 3
	r_{M-E}	1 851 (0 837)	1 875 (0 800)	1 870 (0 809)	1 817 (0 758)	2 321 (0 796)
	r_{M-Z}	1 887 (0 751)	1 907 (0 706)	1 904 (0 687)	1 825 (0 958)	1 833 (0 920)
	q_M / q_N	0 956 / -0 545	0 972 / -0 543	1 013 / -0 544	1 169 / -0 566	0 604 / -0 573
CO	$r_{M...N}$	2 136 (0 272)	2 126 (0 273)	2 158 (0 267)	2 130 (0 292)	2 144 (0 282)
	$\theta_M / \theta_N / \theta_E$	4 0 /22 0 /0 5	3 4 /21 9 /1 2	3 3 /22 9 /0 1	2 6 /20 4	0 3 /30 1
	r_{M-E}	1 853 (0 848)	1 873 (0 812)	1 887 (0 805)	1 818 (0 786)	2 270 (0 908)
	r_{M-Z}	1 895 (0 878)	1 899 (0 874)	1 912 (0 838)	1 956 (0 719)	1 932 (0 764)
	q_M / q_N	0 503 / -0 530	0 508 / -0 526	0 600 / -0 535	0 782 / -0 541	0 115 / -0 552
CN	$r_{M...N}$	2 145 (0 257)	2 137 (0 259)	2 155 (0 256)	2 222 (0 221)	2 184 (0 228)
	$\theta_M / \theta_N / \theta_E$	4 1 /21 6 /0 9	3 5 /21 7 /0 6	2 7 /21 7 /0 3	5 6 /19 2	0 4 /29 4
	r_{M-E}	1 835 (0 855)	1 863 (0 808)	1 859 (0 826)	1 782 (0 838)	2 280 (0 858)
	r_{M-Z}	2 024 (0 610)	2 037 (0 586)	2 037 (0 563)	1 983 (0 692)	1 984 (0 656)
	q_M / q_N	0 889 / -0 546	0 906 / -0 542	0 946 / -0 547	1 085 / -0 565	0 467 / -0 586
NH ₃	$r_{M...N}$	2 118 (0 325)	2 119 (0 321)	2 133 (0 322)	2 107 (0 333)	2 143 (0 316)
	$\theta_M / \theta_N / \theta_E$	2 6 /21 9 /1 5	2 3 /22 0 /1 9	2 7 /22 8 /0 9	1 8 /20 3	0 1 /31 0
	r_{M-E}	1 957 (0 586)	1 968 (0 561)	1 975 (0 539)	1 898 (0 551)	2 394 (0 622)
	r_{M-Z}	2 134 (0 308)	2 136 (0 295)	2 129 (0 316)	2 093 (0 340)	2 099 (0 345)
	q_M / q_N	1 136 / -0 542	1 142 / -0 542	1 219 / -0 544	1 257 / -0 550	0 851 / -0 567
CH ₃	$r_{M...N}$	2 229 (0 175)	2 222 (0 177)	2 263 (0 170)	2 360 (0 123)	2 293 (0 157)
	$\theta_M / \theta_N / \theta_E$	5 3 /18 8 /1 1	4 6 /19 0 /1 5	4 6 /18 8 /0 3	8 1 /14 4	0 9 /28 2
	r_{M-E}	1 847 (0 834)	1 875 (0 788)	1 873 (0 798)	1 799 (0 789)	2 289 (0 844)
	r_{M-Z}	2 044 (0 709)	2 056 (0 689)	2 063 (0 683)	1 996 (0 812)	2 027 (0 727)
	q_M / q_N	0 967 / -0 571	0 990 / -0 568	1 039 / -0 574	1 168 / -0 592	0 585 / -0 602
OH	$r_{M...N}$	2 172 (0 278)	2 152 (0 281)	2 144 (0 299)	2 256 (0 245)	2 202 (0 274)
	$\theta_M / \theta_N / \theta_E$	5 3 /21 4 /0 8	4 2 /21 2 /0 7	3 0 /21 4 /0 2	7 1 /19 5	1 6 /29 7
	r_{M-E}	1 845 (0 846)	1 864 (0 808)	1 859 (0 821)	1 807 (0 784)	2 301 (0 847)
	r_{M-Z}	1 849 (0 667)	1 871 (0 618)	1 866 (0 579)	1 796 (0 816)	1 794 (0 765)
	q_M / q_N	1 005 / -0 538	1 010 / -0 534	1 046 / -0 533	1 239 / -0 558	0 619 / -0 565
H ₂ O	$r_{M...N}$	[a]	[a]	2 091 (0 370)	2 095 (0 368)	2 093 (0 371)
	$\theta_M / \theta_N / \theta_E$			2 3 /22 9 /0 1	1 9 /20 8	0 4 /28 5
	r_{M-E}			1 977 (0 536)	1 894 (0 556)	2 399 (0 621)
	r_{M-Z}			2 066 (0 239)	2 052 (0 246)	2 042 (0 248)
	q_M / q_N			1 260 / -0 527	1 296 / -0 543	0 884 / -0 548

[a] Broken structure

Table 3.6: Relative stability of the different spin states of Group 6 metallatranes at their +3 oxidation state computed at the B3LYP/LANL2DZ level of theory. The values for Cr, Mo and W are given in bold, normal and italics respectively.

Z	NH		NCH ₃		NSiH ₃		O		S	
	S = 1/2	S = 3/2	S = 1/2	S = 3/2	S = 1/2	S = 3/2	S = 1/2	S = 3/2	S = 1/2	S = 3/2
CO	0.0	15.1	0.0	14.6	0.0	6.3	0.0	2.8	0.0	-4.2
	0.0	34.6	0.0	35.6	0.0	34.5	0.0	24.0	0.0	25.2
	<i>0.0</i>	<i>43.3</i>	<i>0.0</i>	<i>43.0</i>	<i>0.0</i>	<i>40.5</i>	<i>0.0</i>	<i>27.3</i>	<i>0.0</i>	<i>36.4</i>
NH ₃	6.7	0.0	5.6	0.0	10.8	0.0	9.6	0.0	20.0	0.0
	0.0	15.3	0.0	15.4	0.0	11.5	0.0	7.3	0.0	4.0
	<i>0.0</i>	<i>15.5</i>	<i>0.0</i>	<i>19.4</i>	<i>0.0</i>	<i>17.1</i>	<i>0.0</i>	<i>8.6</i>	<i>0.0</i>	<i>12.6</i>
H ₂ O	27.8	0.0	28.1	0.0	7.6	0.0	8.5	0.0	15.6	0.0
	0.0	17.7	0.0	17.4	0.0	14.5	0.0	8.9	0.0	5.0
	<i>0.0</i>	<i>8.1</i>	<i>0.0</i>	<i>10.8</i>	<i>0.0</i>	<i>14.9</i>	<i>0.0</i>	<i>10.9</i>	<i>0.0</i>	<i>14.8</i>

observation.^{6b} On the other hand, longer Cr–N bonds are obtained when the highly electronegative oxygen atom occupies the equatorial position. As in the case with Group 4 analogs, replacement of the oxygen atom by the heavier sulphur atom results in deformation of the cage structure with the metal atom lying almost in the plane defined by the three equatorial sulphur atoms. The pyramidalization at the bridgehead nitrogen atom also increases by 8° - 13°. These geometrical changes at the metal and bridgehead nitrogen atom result in enhancement of the transannular interaction. Corresponding to the increase or decrease of Cr–N distance, the Cr–Z distances decrease or increase accordingly. This is also reflected in the values of the Wiberg Bond Indices (WBI) of respective bonds (Table 3.5). For example, between CH₃⁻ and NH₃ as the apical substituent, the Cr–N distances are more for the former whereas the Cr–Z distances are more for the later (low values of WBI). However, this correlation of simultaneous lengthening of transannular and strengthening of metal apical bond was not observed for CO as in this case, back donation from the filled metal orbital to the π* orbital of CO results in strengthening of the Cr–CO bond. For the azachromatranes, the Cr–N_{eq} bond strength decreases marginally from NH to NSiH₃.

The calculated transannular Mo–N and W–N distances are reasonably closer to the experimentally observed ones (Table 3.7 and Table 3.8).^{7, 3b, 8e} On an average, the calculated transannular Mo–N and W–N distances are found to be 7% and 9% longer than the sum of the covalent radii (2.15Å) of Mo and N and (2.05Å) of W and N atom respectively. Compared to chromatranes, doublet spin state is more stable for molybdenatranes and tungstenatranes, especially with CO as the apical ligand (Table 3.6). This is due to the

Table 3.7. B3LYP/LANL2DZ computed transannular distance ($r_{M-N_{ax}}$), average metal – equatorial atom (r_{M-E}) and metal – apical (r_{M-Z}) bond distances (Å), pyramidalization angles (in degrees) around metal (θ_M), axial nitrogen (θ_N) and equatorial atom (θ_E), and natural charges at metal (q_M) and axial nitrogen (q_N) for $Z-Mo[-ER(CH_2)_2-]_3N$. The respective Wiberg Bond Index (WBI) values are given within parenthesis.

Z		E=NH	NCH ₃	NSiH ₃	O	S
Cl	$r_{M...N}$	2 259 (0 307)	2 227 (0 318)	2 252 (0 309)	2 317 (0 280)	2 330 (0 280)
	$\theta_M / \theta_N / \theta_E$	9 1 / 24 3 / 0 5	8 1 / 23 5 / 0 3	6 7 / 23 6 / 0 3	10 8 / 22 7	3 8 / 31 9
	r_{M-E}	1 975 (0 837)	1 992 (0 810)	1 992 (0 811)	1 941 (0 754)	2 389 (0 942)
	r_{M-Z}	2 459 (0 654)	2 494 (0 602)	2 474 (0 614)	2 413 (0 731)	2 392 (0 772)
	q_M / q_N	1 288 / -0 559	1 277 / -0 548	1 328 / -0 560	1 514 / -0 577	0 479 / -0 569
NH ₂	$r_{M...N}$	2 331 (0 234)	2 307 (0 241)	2 321 (0 239)	2 415 (0 199)	2 405 (0 223)
	$\theta_M / \theta_N / \theta_E$	11 4 / 22 6 / 1 5	9 2 / 22 2 / 0 9	8 9 / 22 2 / 0 7	14 6 / 18 5	6 0 / 30 7
	r_{M-E}	1 992 (0 806)	2 003 (0 784)	2 009 (0 776)	1 968 (0 686)	2 416 (0 881)
	r_{M-Z}	2 028 (0 764)	2 043 (0 721)	2 031 (0 741)	1 968 (0 928)	1 969 (0 925)
	q_M / q_N	1 397 / -0 576	1 382 / -0 573	1 429 / -0 576	1 631 / -0 595	0 695 / -0 584
CO	$r_{M...N}$	2 316 (0 212)	2 300 (0 213)	2 309 (0 213)	2 299 (0 221)	2 330 (0 219)
	$\theta_M / \theta_N / \theta_E$	10 2 / 22 4 / 0 8	8 8 / 22 0 / 1 1	8 4 / 22 0 / 0 6	8 2 / 21 1	2 6 / 30 3
	r_{M-E}	1 980 (0 858)	1 993 (0 833)	2 004 (0 821)	1 954 (0 762)	2 379 (0 963)
	r_{M-Z}	1 958 (1 219)	1 959 (1 226)	1 964 (1 196)	1 981 (1 111)	1 986 (1 059)
	q_M / q_N	0 894 / -0 580	0 866 / -0 577	0 920 / -0 580	1 155 / -0 593	0 143 / -0 586
CN	$r_{M...N}$	2 307 (0 222)	2 268 (0 235)	2 305 (0 221)	2 362 (0 199)	2 376 (0 196)
	$\theta_M / \theta_N / \theta_E$	10 0 / 22 9 / 0 7	8 8 / 22 4 / 0 6	7 6 / 22 3 / 0 4	11 3 / 20 9	3 6 / 30 2
	r_{M-E}	1 973 (0 850)	1 989 (0 822)	1 990 (0 826)	1 933 (0 773)	2 381 (0 958)
	r_{M-Z}	2 099 (0 754)	2 119 (0 723)	2 109 (0 724)	2 082 (0 780)	2 061 (0 806)
	q_M / q_N	1 272 / -0 586	1 244 / -0 574	1 286 / -0 586	1 528 / -0 602	0 495 / -0 599
NH ₃	$r_{M...N}$	2 227 (0 325)	2 217 (0 330)	2 237 (0 318)	2 221 (0 317)	2 282 (0 319)
	$\theta_M / \theta_N / \theta_E$	6 0 / 23 4 / 1 7	5 3 / 23 3 / 1 5	5 9 / 23 6 / 0 5	5 0 / 21 9	2 0 / 31 8
	r_{M-E}	2 008 (0 783)	2 020 (0 754)	2 036 (0 732)	1 983 (0 690)	2 390 (0 934)
	r_{M-Z}	2 323 (0 291)	2 343 (0 276)	2 322 (0 302)	2 284 (0 306)	2 282 (0 341)
	q_M / q_N	1 046 / -0 546	1 033 / -0 542	1 110 / -0 547	1 268 / -0 565	0 378 / -0 551
CH ₃	$r_{M...N}$	2 375 (0 178)	2 350 (0 185)	2 378 (0 178)	2 466 (0 141)	2 474 (0 154)
	$\theta_M / \theta_N / \theta_E$	11 1 / 20 4 / 0 8	9 4 / 20 4 / 1 0	9 1 / 19 8 / 0 6	14 1 / 17 3	5 0 / 28 0
	r_{M-E}	1 985 (0 820)	1 999 (0 791)	2 004 (0 786)	1 948 (0 732)	2 395 (0 929)
	r_{M-Z}	2 176 (0 728)	2 187 (0 703)	2 183 (0 707)	2 131 (0 811)	2 128 (0 779)
	q_M / q_N	1 381 / -0 588	1 368 / -0 584	1 414 / -0 588	1 607 / -0 602	0 653 / -0 597
OH	$r_{M...N}$	2 302 (0 266)	2 275 (0 274)	2 285 (0 274)	2 372 (0 236)	2 379 (0 257)
	$\theta_M / \theta_N / \theta_E$	10 1 / 23 5 / 0 4	8 0 / 23 2 / 0 6	7 5 / 23 0 / 0 5	13 3 / 21 8	5 4 / 31 9
	r_{M-E}	1 986 (0 814)	1 994 (0 793)	2 001 (0 785)	1 959 (0 706)	2 407 (0 907)
	r_{M-Z}	1 996 (0 647)	2 015 (0 606)	1 993 (0 624)	1 941 (0 751)	1 930 (0 769)
	q_M / q_N	1 466 / -0 575	1 444 / -0 571	1 501 / -0 574	1 719 / -0 593	0 764 / -0 581
H ₂ O	$r_{M...N}$	2 212 (0 353)	2 202 (0 354)	2 216 (0 345)	2 210 (0 343)	2 265 (0 350)
	$\theta_M / \theta_N / \theta_E$	6 0 / 24 2 / 2 4	5 2 / 24 0 / 1 2	5 1 / 24 2 / 0 5	5 3 / 22 9	2 2 / 32 7
	r_{M-E}	2 008 (0 781)	2 010 (0 754)	2 030 (0 729)	1 982 (0 684)	2 391 (0 931)
	r_{M-Z}	2 269 (0 220)	2 284 (0 213)	2 246 (0 237)	2 219 (0 237)	2 218 (0 263)
	q_M / q_N	1 083 / -0 542	1 064 / -0 538	1 142 / -0 544	1 312 / -0 562	0 427 / -0 546

Table 3.8. B3LYP/LANL2DZ computed transannular distance (r_{M-Nax}), average metal – equatorial atom (r_{M-E}) and metal – apical (r_{M-Z}) bond distances (Å), pyramidalization angles (in degrees) around metal (θ_M), axial nitrogen (θ_N) and equatorial atom (θ_E), and natural charges at metal (q_M) and axial nitrogen (q_N) for $Z-W[-ER(CH_2)_2-]_3N$. The respective Wiberg Bond Index (WBI) values are given within parenthesis.

Z		E=NH	NCH ₃	NSiH ₃	O	S
Cl	$r_{M...N}$	2 215 (0 319)	2 203 (0 323)	2 207 (0 323)	2 244 (0 299)	2 263 (0 304)
	$\theta_M / \theta_N / \theta_E$	8 3 / 24 8 / 0 3	7 2 / 24 4 / 0 5	6 1 / 24 7 / 0 2	8 5 / 24 1	2 9 / 32 4
	r_{M-E}	1 973 (0 819)	1 986 (0 793)	1 990 (0 794)	1 940 (0 732)	2 382 (0 978)
	r_{M-Z}	2 468 (0 671)	2 497 (0 632)	2 480 (0 641)	2 428 (0 719)	2 407 (0 794)
	q_M / q_N	1 501 / -0 580	1 503 / -0 575	1 540 / -0 578	1 704 / - 600	0 581 / -0 585
NH ₂	$r_{M...N}$	2 267 (0 255)	2 252 (0 261)	2 260 (0 260)	2 309 (0 236)	2 335 (0 249)
	$\theta_M / \theta_N / \theta_E$	9 7 / 23 6 / 0 6	8 3 / 23 3 / 0 5	7 3 / 23 4 / 0 4	10 7 / 22 3	4 4 / 32 1
	r_{M-E}	1 987 (0 795)	1 998 (0 770)	2 002 (0 767)	1 964 (0 679)	2 407 (0 916)
	r_{M-Z}	2 035 (0 742)	2 049 (0 707)	2 040 (0 712)	1 974 (0 884)	1 978 (0 895)
	q_M / q_N	1 631 / -0 592	1 623 / -0 587	1 671 / -0 593	1 818 / -0 611	0 826 / -0 596
CO	$r_{M...N}$	2 287 (0 210)	2 272 (0 212)	2 281 (0 211)	2 290 (0 205)	2 297 (0 223)
	$\theta_M / \theta_N / \theta_E$	10 8 / 23 6 / 0 8	9 4 / 23 3 / 0 6	9 0 / 23 5 / 0 2	8 7 / 21 5	2 7 / 31 9
	r_{M-E}	1 978 (0 842)	1 989 (0 816)	1 988 (0 813)	1 948 (0 750)	2 374 (0 990)
	r_{M-Z}	1 933 (1 382)	1 935 (1 380)	1 938 (1 358)	1 939 (1 312)	1 959 (1 211)
	q_M / q_N	1 205 / -0 601	1 192 / -0 598	1 225 / -0 601	1 427 / -0 619	0 327 / -0 606
CN	$r_{M...N}$	2 271 (0 223)	2 256 (0 228)	2 271 (0 223)	2 304 (0 206)	2 324 (0 210)
	$\theta_M / \theta_N / \theta_E$	9 9 / 23 2 / 0 8	8 5 / 23 3 / 0 5	7 8 / 23 8 / 0 4	9 7 / 21 5	2 9 / 31 3
	r_{M-E}	1 971 (0 837)	1 983 (0 810)	1 989 (0 814)	1 933 (0 752)	2 374 (0 992)
	r_{M-Z}	2 057 (0 865)	2 071 (0 837)	2 066 (0 837)	2 055 (0 850)	2 038 (0 896)
	q_M / q_N	1 494 / -0 605	1 481 / -0 601	1 513 / -0 606	1 734 / -0 621	0 617 / -0 613
NH ₃	$r_{M...N}$	2 199 (0 334)	2 177 (0 348)	2 196 (0 335)	2 179 (0 337)	2 228 (0 347)
	$\theta_M / \theta_N / \theta_E$	6 9 / 24 9 / 1 2	5 7 / 25 0 / 0 7	6 0 / 25 6 / 0 2	4 4 / 23 4	1 6 / 34 2
	r_{M-E}	1 993 (0 790)	2 009 (0 751)	2 025 (0 731)	1 978 (0 681)	2 373 (0 974)
	r_{M-Z}	2 279 (0 346)	2 319 (0 305)	2 297 (0 330)	2 250 (0 332)	2 269 (0 364)
	q_M / q_N	1 219 / -0 567	1 199 / -0 556	1 266 / -0 562	1 414 / -0 587	0 456 / -0 564
CH ₃	$r_{M...N}$	2 310 (0 207)	2 291 (0 214)	2 311 (0 208)	2 363 (0 177)	2 385 (0 191)
	$\theta_M / \theta_N / \theta_E$	10 0 / 21 3 / 0 6	8 7 / 21 3 / 0 5	8 2 / 21 9 / 0 3	10 7 / 19 2	3 7 / 30 2
	r_{M-E}	1 981 (0 809)	1 993 (0 781)	1 999 (0 778)	1 947 (0 716)	1 384 (0 971)
	r_{M-Z}	2 179 (0 720)	2 191 (0 697)	2 186 (0 703)	2 141 (0 778)	2 136 (0 782)
	q_M / q_N	1 611 / -0 598	1 602 / -0 594	1 641 / -0 599	1 819 / -0 615	0 770 / -0 603
OH	$r_{M...N}$	2 243 (0 283)	2 224 (0 290)	2 230 (0 291)	2 272 (0 266)	2 299 (0 282)
	$\theta_M / \theta_N / \theta_E$	10 0 / 21 3 / 0 6	8 7 / 21 3 / 0 5	8 2 / 21 9 / 0 3	10 7 / 19 2	3 7 / 30 2
	r_{M-E}	1 982 (0 801)	1 991 (0 776)	1 996 (0 773)	1 957 (0 693)	2 396 (0 940)
	r_{M-Z}	2 005 (0 628)	2 019 (0 598)	1 998 (0 610)	1 957 (0 691)	1 938 (0 744)
	q_M / q_N	1 689 / -0 593	1 678 / -0 589	1 722 / -0 593	1 908 / -0 613	0 882 / -0 597
H ₂ O	$r_{M...N}$	2 185 (0 358)	2 162 (0 374)	2 162 (0 383)	2 168 (0 361)	2 212 (0 376)
	$\theta_M / \theta_N / \theta_E$	6 6 / 25 5 / 1 1	5 3 / 25 5 / 1 0	4 9 / 26 1 / 0 7	4 9 / 26 1 / 0 7	1 5 / 34 5
	r_{M-E}	1 990 (0 790)	2 006 (0 750)	2 014 (0 733)	1 976 (0 676)	2 374 (0 968)
	r_{M-Z}	2 213 (0 283)	2 264 (0 238)	2 333 (0 221)	2 179 (0 269)	2 209 (0 274)
	q_M / q_N	1 268 / -0 567	1 235 / -0 554	1 293 / -0 557	1 462 / -0 587	0 513 / -0 561

higher d-orbital splitting as we go down a group resulting in pairing of the electrons. In fact, all the doublet structures of molybdenatranes and tungstenatranes with neutral apical ligands are more stable than the quartet ones.

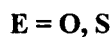
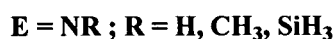
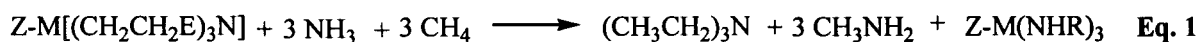
Barring few exceptions, the geometric variations obtained for these molecules are more or less similar to those found for their chromium analogs. For example, weaker *trans* directing groups like Cl^- , H_2O and NH_3 strengthens the $\text{M}-\text{N}$ ($\text{M} = \text{Mo}, \text{W}$) bonds while stronger groups like CO , CN^- and CH_3^- weakens the same. The $\text{M}-\text{N}$ distances decrease as the equatorial groups are changed from NH to NCH_3 and increase again with NSiH_3 . Surprisingly, oxygen at the equatorial position computes a relatively shorter $\text{M}-\text{N}$ bond than sulphur for these metallatranes. This strengthening of the transannular bond took place despite the fact that the values of θ_{M} and θ_{N} for the oxa isomers are considerably larger and smaller than those for the thia derivatives. However, such a geometric variation was not observed for their chromium and Group 4 analogs. Due to the soft character of Mo and W, $\text{M}-\text{S}$ bonds are consistently stronger than $\text{M}-\text{O}$ bonds.

Comparison of the geometrical parameters for Group 4 and Group 6 metallatranes reveals that the pyramidalization angles around the metal atoms are quite less for Group 6 metallatranes than for Group 4 ones. Natural charges computed using NBO¹⁸ routine reveal that there is a decrease in the positive and negative charge at metal centre and at bridgehead nitrogen atom respectively while going from Group 4 to Group 6 metallatranes. All these factors result in strengthening of the transannular interaction in Group 6 metallatranes.

[3.3.2] Stabilization Energy

In general, the stability of these metallatranes are largely governed by the degree of transannular $\text{M}-\text{N}$ interaction with significant contribution coming in from strengthening of the $\text{M}-\text{E}$ and $\text{M}-\text{Z}$ bonds. With few exceptions, the stabilization energy increases or decreases with decrease or increase in $\text{M}-\text{N}$ interactions. We have used two different sets of equations to compute the stabilization energies of these metallatranes – one for the azametallatranes (Eq 1), and the other for their chalcogen analogs (Eq 2).

The stabilization energies of Group 4 metallatranes increase with changes in equatorial substituents from NH to NCH_3 but decrease with NSiH_3 (Table 3.9) which can be correlated to increase or decrease in transannular distances (see Table 3.2 – 3.4). However, exceptions are there. For example, with CO as the apical ligand, azamethyl titanatranes compute higher value of stabilization energy than its silyl derivative even though the $\text{Ti}-\text{N}$ distance of the former is longer than that of the later. This can be explained by looking



at the relative strengths of the respective Ti – Z and Ti – E bonds of these two molecules. The Ti – CO and Ti – N bonds of azamethyl titanatranes are shorter and hence stronger (higher values of WBI) than that of azasilyl titanatranes. Thus, the strengthening of these two bonds apparently results in stabilization of the azamethyl derivative relative to its azasilyl isomer. Thiametallatranes are much more stable than oxa ones not only due to strong transannular interaction but also due to stronger M – E and M – Z bonds. Also, thiametallatranes compute the least positive charge at the metal centre which is due to extensive charge transfer from the three equatorial sulphur atoms to the central metal atom.

The stability of Group 6 metallatranes is higher than those of their Group 4 analogs owing to the presence of stronger transannular M – N bonds in the former. The stability trend obtained for aza derivative of these metallatranes is similar to those found for Group 4 analogs, i.e., the stability increases from NH to NCH₃ and decreases with NSiH₃. Like thiametallatranes of Group 4 elements, Group 6 ones are also strikingly more stable than oxametallatranes for the same reason as given for Group 4 analogs.

Table 3.9. B3LYP/LANL2DZ computed stabilization energies for Group 4 and 6 metallatranes. Ti and Cr values are given in bold, Zr and Mo values in normal and Hf and W values are in italics.

Z	E=NH		NCH ₃		NSiH ₃		O		S	
	Group 4	Group 6	Group 4	Group 6	Group 4	Group 6	Group 4	Group 6	Group 4	Group 6
Cl	21.6	66.1	27.6	62.3	16.6	61.3	15.8	66.7	27.5	67.8
	22.4	37.9	33.2	47.8	17.9	35.6	12.2	30.2	27.9	38.2
	22.5	53.6	34.1	47.5	19.2	40.0	9.5	43.9	29.8	48.6
NH ₂	19.1	46.9	23.3	46.7	16.1	45.7	14.5	53.1	24.4	51.9
	19.4	31.0	31.8	35.7	17.1	29.3	10.5	29.4	23.6	28.5
	19.7	35.0	32.2	39.5	16.9	34.1	7.9	29.4	25.7	34.7
CO	21.2	40.0	26.3	41.6	19.9	32.9	17.7	39.9	25.8	44.4
	20.9	34.0	27.1	37.8	20.1	32.1	13.5	26.6	28.4	38.1
	21.1	42.1	27.5	44.8	19.9	38.1	10.4	26.5	26.6	47.2
CN	20.0	44.1	22.9	44.9	16.4	36.1	15.1	34.8	26.8	42.7
	20.0	36.5	25.7	45.6	16.6	31.7	11.5	29.1	26.8	36.4
	20.2	44.4	31.8	49.8	18.0	40.3	8.5	32.7	28.5	46.0

NH ₃	19.0	25.5	27.7	33.4	20.4	26.4	16.0	26.8	28.6	32.8
	15.0	30.1	23.6	39.4	15.1	33.5	3.4	31.1	25.2	39.5
	16.7	24.7	22.6	33.8	14.3	30.4	2.8	20.1	25.5	48.6
CH ₃	15.3	32.3	18.8	35.0	11.7	24.4	10.8	28.3	20.8	31.3
	16.2	25.4	22.8	32.1	13.4	23.7	7.0	23.1	20.5	26.2
	16.7	33.8	29.2	40.8	14.6	30.9	4.6	25.1	22.6	35.9
OH	21.1	37.9	31.4	42.3	18.9	37.4	14.8	32.2	26.9	33.7
	22.1	33.1	29.1	39.7	19.9	32.5	11.1	32.1	27.0	29.7
	22.0	37.5	35.3	44.0	20.1	38.5	8.6	32.2	28.5	35.4
H ₂ O	19.9	[a]	29.1	[a]	23.3	24.5	11.8	22.2	26.7	28.7
	16.5	34.0	24.1	38.7	16.8	37.5	3.7	29.0	24.3	39.3
	19.1	22.8	30.6	29.4	13.4	20.8	2.1	18.2	23.6	46.4

[a] Broken structure.

[3.3.3] QTAIM Analysis

The topology of electron density in a molecule can be analyzed using Bader's atoms in molecules theory (AIM).²⁰ Generally, for covalent interactions (also referred to as "open-shell" or "shared" interactions), the electron density at the bond critical point (BCP), ρ_b is large (> 0.2 a.u.) while its laplacian $\nabla^2\rho$ is large and negative. On the other hand, for closed-shell interactions (e.g., ionic, van der Waals or hydrogen bonds), ρ_b is small (< 0.10 a.u.) and $\nabla^2\rho$ is positive. However, analysis of the bonding situation in transition metal compounds with QTAIM does not follow this usual notion since a covalent bond in transition metal compounds is characterized by small value of ρ_b and small and positive values of $\nabla^2\rho$ due to the diffuse character of the electron distribution.²⁴ Hence, the bonding situation in these compounds cannot be described with ρ_b and $\nabla^2\rho$ alone, rather a more specific descriptor should be applied and electronic energy density $H(r)$ at BCP best fits the purpose.

Cremer and Kraka²⁵ proposed that a value of $H(r) < 0$ at BCP indicates the presence of significant covalent character and accounts for the lowering of potential energy of electrons at BCPs. The magnitude of $H(r)$ reflects the "covalence" of interaction. We have adopted a similar approach to characterize the transannular M-N bonds in Group 4 and 6 metallatranes (Table 3.10 and 3.11).²⁴⁻²⁷ All these Group 4 metallatranes show a (3, -1) bond critical point at the M-N bond. The formation of (3, +1) ring critical points also support the presence of the transannular interaction which indicates the formation of five-member cycles in these molecules. As defined by Bader, the laplacian of electron density at BCP is given by $L(r) = \nabla^2\rho(r)$.^{20a} The accumulation of electron density, ρ_b and a larger value $L(r)$ along the bond path has an impact on the stability.^{28a} Larger values of $L(r)$ and ρ_b result in local stabilization of the structure due to increased shielding of the nuclei of the bonded pair.^{28b} Figure 3.2 shows a nice linear relationship between the transannular Ti-N distances with the electron density at the bond critical point, ρ_b , and its laplacian $\nabla^2\rho$. Hence, stronger bonds

Table 3.10. Topological parameters at the M...N bond critical points of Group 4 metallatranes. Electron density (ρ_b), its laplacian ($\nabla^2\rho$) and total electronic energy density $H(r)$ are all in a. u.

Z	M	E=NH			NCH ₃			NSiH ₃			O			S		
		ρ_b	$\nabla^2\rho$	$H(r)$	ρ_b	$\nabla^2\rho$	$H(r)$	ρ_b	$\nabla^2\rho$	$H(r)$	ρ_b	$\nabla^2\rho$	$H(r)$	ρ_b	$\nabla^2\rho$	$H(r)$
Cl	Ti	0.052	0.146	-0.010	0.062	0.173	-0.013	0.053	0.145	-0.010	0.034	0.101	-0.004	0.052	0.134	-0.010
	Zr	0.048	0.156	-0.003	0.054	0.176	-0.004	0.049	0.160	-0.002	0.037	0.124	-0.001	0.046	0.143	-0.006
	Hf	0.052	0.154	-0.005	0.058	0.174	-0.007	0.054	0.158	-0.006	0.039	0.120	-0.003	0.051	0.143	-0.006
NH ₂	Ti	0.042	0.134	-0.006	0.044	0.141	-0.006	0.047	0.145	-0.008	0.031	0.102	-0.003	0.047	0.136	-0.008
	Zr	0.042	0.144	-0.001	0.048	0.168	-0.002	0.044	0.153	-0.002	0.035	0.122	-0.001	0.043	0.141	-0.002
	Hf	0.045	0.143	-0.003	0.052	0.166	-0.006	0.049	0.152	-0.005	0.037	0.119	-0.002	0.046	0.140	-0.005
CO	Ti	0.054	0.186	-0.008	0.055	0.196	-0.008	0.057	0.200	-0.009	0.048	0.171	-0.006	0.062	0.208	-0.011
	Zr	0.047	0.166	-0.002	0.049	0.174	-0.002	0.049	0.173	-0.003	0.041	0.148	-0.001	0.051	0.176	-0.003
	Hf	0.050	0.160	-0.005	0.052	0.169	-0.005	0.053	0.170	-0.005	0.042	0.137	-0.003	0.052	0.164	-0.005
CN	Ti	0.049	0.143	-0.008	0.049	0.147	-0.008	0.049	0.140	-0.010	0.032	0.098	-0.004	0.051	0.134	-0.010
	Zr	0.045	0.149	-0.002	0.046	0.154	-0.002	0.045	0.147	-0.002	0.036	0.120	-0.001	0.043	0.135	-0.002
	Hf	0.050	0.148	-0.005	0.056	0.168	-0.007	0.050	0.148	-0.005	0.038	0.118	-0.003	0.048	0.137	-0.006
NH ₃	Ti	0.054	0.221	-0.006	0.055	0.228	-0.006	0.056	0.224	-0.007	0.052	0.208	-0.006	0.058	0.216	-0.008
	Zr	0.048	0.164	-0.002	0.050	0.178	-0.003	0.052	0.204	-0.002	0.041	0.135	-0.002	0.055	0.210	-0.003
	Hf	0.050	0.149	-0.005	0.053	0.162	-0.006	0.055	0.171	-0.006	0.033	0.086	-0.003	0.057	0.209	-0.006
CH ₃	Ti	0.041	0.118	-0.007	0.042	0.122	-0.007	0.042	0.118	-0.008	0.026	0.082	-0.002	0.045	0.115	-0.009
	Zr	0.040	0.130	-0.001	0.043	0.143	-0.003	0.041	0.131	-0.002	0.032	0.101	-0.001	0.040	0.119	-0.003
	Hf	0.044	0.130	-0.005	0.051	0.153	-0.005	0.045	0.131	-0.005	0.034	0.102	-0.003	0.043	0.118	-0.005
OH	Ti	0.049	0.162	-0.006	0.055	0.175	-0.009	0.051	0.157	-0.008	0.033	0.108	-0.003	0.048	0.143	-0.008
	Zr	0.045	0.157	-0.001	0.048	0.169	-0.002	0.048	0.168	-0.002	0.037	0.131	0.000	0.045	0.151	-0.001
	Hf	0.048	0.155	-0.006	0.055	0.177	-0.006	0.051	0.164	-0.005	0.039	0.127	-0.002	0.048	0.149	-0.005
H ₂ O	Ti	0.054	0.224	-0.005	0.056	0.232	-0.006	0.059	0.241	-0.008	0.053	0.197	-0.008	0.057	0.216	-0.007
	Zr	0.048	0.158	-0.002	0.052	0.174	-0.004	0.052	0.201	-0.002	0.040	0.126	-0.003	0.052	0.202	-0.002
	Hf	0.050	0.148	-0.005	0.058	0.176	-0.007	0.050	0.148	-0.005	0.034	0.091	-0.003	0.056	0.195	-0.006

Table 3.11. Topological parameters at the M...N bond critical points of Group 6 metallatranes. Electron density (ρ_b), its laplacian ($\nabla^2\rho$) and total electronic energy density $H(r)$ are all in a. u.

Z	M	E=NH			NCH ₃			NSiH ₃			O			S		
		ρ	$\nabla^2\rho$	$H(r)$	ρ	$\nabla^2\rho$	$H(r)$	ρ	$\nabla^2\rho$	$H(r)$	ρ	$\nabla^2\rho$	$H(r)$	ρ	$\nabla^2\rho$	$H(r)$
Cl	Cr	0.076	0.257	-0.021	0.076	0.258	-0.016	0.076	0.252	-0.017	0.065	0.219	-0.015	0.070	0.236	-0.017
	Mo	0.071	0.280	-0.019	0.077	0.301	-0.011	0.073	0.284	-0.010	0.065	0.244	-0.008	0.063	0.238	-0.007
	W	0.080	0.302	-0.016	0.082	0.310	-0.016	0.082	0.305	-0.016	0.077	0.285	-0.014	0.073	0.271	-0.014
NH ₂	Cr	0.062	0.249	-0.012	0.064	0.255	-0.013	0.063	0.248	-0.013	0.052	0.208	-0.008	0.061	0.235	-0.012
	Mo	0.060	0.254	-0.005	0.063	0.271	-0.006	0.061	0.260	-0.006	0.052	0.199	-0.005	0.052	0.212	-0.004
	W	0.070	0.289	-0.011	0.072	0.301	-0.011	0.072	0.293	-0.011	0.066	0.256	-0.010	0.062	0.243	-0.009
CO	Cr	0.069	0.300	-0.015	0.071	0.310	-0.016	0.066	0.286	-0.014	0.071	0.313	-0.016	0.069	0.293	-0.015
	Mo	0.062	0.266	-0.006	0.064	0.277	-0.007	0.063	0.271	-0.007	0.064	0.282	-0.007	0.060	0.261	-0.005
	W	0.068	0.267	-0.011	0.070	0.278	-0.012	0.069	0.271	-0.011	0.068	0.277	-0.011	0.067	0.269	-0.010
CN	Cr	0.071	0.254	-0.018	0.072	0.260	-0.018	0.070	0.249	-0.017	0.061	0.222	-0.012	0.066	0.239	-0.015
	Mo	0.065	0.256	-0.008	0.070	0.280	-0.009	0.065	0.257	-0.007	0.059	0.226	-0.007	0.057	0.220	-0.006
	W	0.072	0.268	-0.013	0.074	0.278	-0.013	0.072	0.268	-0.013	0.068	0.255	-0.012	0.065	0.242	-0.011
NH ₃	Cr	0.073	0.282	-0.018	0.073	0.284	-0.017	0.071	0.269	-0.017	0.076	0.286	-0.020	0.070	0.256	-0.017
	Mo	0.071	0.349	-0.008	0.073	0.367	-0.007	0.070	0.350	-0.006	0.074	0.344	-0.005	0.064	0.313	-0.006
	W	0.079	0.342	-0.014	0.081	0.397	-0.012	0.078	0.377	-0.012	0.082	0.389	-0.015	0.074	0.346	-0.010
CH ₃	Cr	0.060	0.231	-0.011	0.060	0.236	-0.011	0.056	0.215	-0.009	0.046	0.184	-0.005	0.053	0.209	-0.008
	Mo	0.057	0.223	-0.006	0.060	0.237	-0.007	0.057	0.221	-0.007	0.049	0.177	-0.005	0.048	0.176	-0.005
	W	0.067	0.253	-0.011	0.069	0.266	-0.012	0.067	0.252	-0.011	0.061	0.225	-0.011	0.059	0.213	-0.009
OH	Cr	0.065	0.257	-0.014	0.069	0.267	-0.016	0.070	0.267	-0.017	0.056	0.215	-0.010	0.062	0.239	-0.013
	Mo	0.064	0.271	-0.006	0.067	0.290	-0.008	0.066	0.280	-0.007	0.057	0.221	-0.006	0.055	0.224	-0.005
	W	0.074	0.304	-0.012	0.077	0.318	-0.013	0.076	0.308	-0.013	0.071	0.281	-0.011	0.066	0.267	-0.009
H ₂ O	Cr	[a]			[a]			0.078	0.290	-0.019	0.078	0.287	-0.020	0.079	0.276	-0.021
	Mo	0.073	0.363	-0.008	0.075	0.376	-0.008	0.073	0.365	-0.008	0.076	0.341	-0.010	0.066	0.323	-0.006
	W	0.081	0.353	-0.014	0.084	0.412	-0.013	0.084	0.390	-0.015	0.085	0.364	-0.017	0.076	0.358	-0.011

[a] Broken structure.

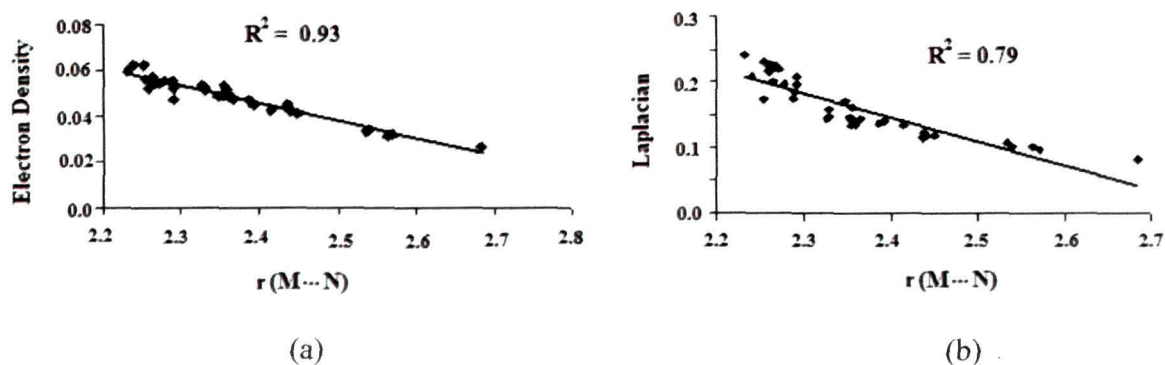


Figure 3.2. Variation of $r(\text{M}\cdots\text{N})$ (Å) with (a) electron density (ρ , a. u) and (b) laplacian [$\nabla^2\rho$ (bcp), a. u.] at the bond critical point of the transannular $\text{Ti}\cdots\text{N}$ bonds.

are associated with larger accumulation of ρ_b and a larger value of $L(r)$. The laplacian at the bond critical point, $\nabla^2\rho$, are all positive and increases with decrease in transannular $\text{M}\cdots\text{N}$ bonds. This is in tune with previous theoretical studies.²⁹⁻³¹

The contour plot of laplacian (Figure 3.3) in the $\text{N}\cdots\text{Ti} - \text{Z}$ plane clearly shows the effect of apical as well as equatorial ligands in titanatranes. A clear distinction between the

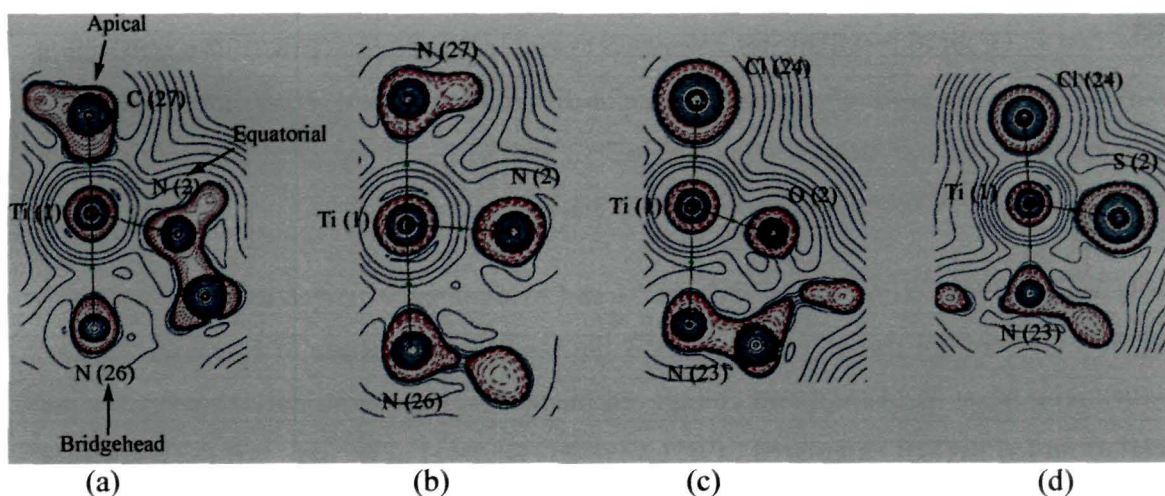


Figure 3.3. Contour plots of laplacian, $\nabla^2\rho$ (bcp), in $\text{N}\cdots\text{Ti} - \text{Z}$ plane (obtained with AIMALL program at B3LYP/6-31+G* level of theory) showing the effect of apical, (a) $\text{Z} = \text{CH}_3$ and (b) $\text{Z} = \text{NH}_3$ and equatorial substituents (c) $\text{E} = \text{O}$ and (d) $\text{E} = \text{S}$ on the bonding of titanatranes. Regions of charge depletion ($\nabla^2\rho > 0$) are denoted by solid blue lines while regions of charge concentration ($\nabla^2\rho < 0$) are denoted by dashed red lines. Green sphere denotes bond critical points (BCPs) and black solid line denotes bond paths.

transannular interaction involving the two apical ligands, viz, CH₃ and NH₃ can be seen in Figure 3.3a-b which reflects a stronger transannular Ti – N interaction with NH₃ than CH₃ as the VSCC (valence shell charge concentration) on the bridgehead nitrogen atom is more polarized towards the titanium atom in the former. Figure 3.3c-d shows the effect of equatorial substituents on the M – E bond strengths. Charge transfer from equatorial substituent to the titanium atom is stronger with sulphur than oxygen which accounts for the stronger Ti – S bond strengths compared to Ti – O bonds.

The topological descriptions of electron density at the M – N (M = Zr, Hf) bond critical point is almost similar to those observed for Ti – N bonds (Table 3.10). The values of local electron density $H(r)$ are least negative for Zr – N bonds compared to other Group 4 metallatranes.

The topological values of the electron density at the transannular M – N bonds for Group 6 metallatranes are almost similar to that of Group 4 metallatranes (Table 3.11). However, there are some major contrasts in the topological character of Group 4 and 6 metallatranes. For example, Group 6 metallatranes compute higher values of ρ_b and $L(r)$ and more negative values of $H(r)$ at the M – N bond critical point compared to Group 4 metallatranes. All these topological parameters point towards a stronger transannular interaction in Group 6 metallatranes compared to Group 4 analogs. This is also reflected in the WBI values, stabilization energies and delocalization index, $\delta(M, N)$ for the transannular M – N bonds of group 6 metallatranes (Table 3.12 and 3.13). Topological description of the M – N (M = Mo or W) bonds is quite similar to that of Cr – N bonds.

Table 3.12. Delocalization index between M and bridgehead nitrogen atom N [$\delta(M, N)$], magnitude of charge transfer from A to B [$|q(A \rightarrow B)|$], magnitude of Ehrenfest forces^a on the metal atom M [$|F(M)|$] and changes in nuclear – electron potential energy for the metal atom [$\Delta V_{ne}(M)$] calculated at B3LYP/6-31+G* level of theory. All the quantities are in atomic units.^b

Z	M		E = NH	NCH ₃	NSiH ₃	O	S
	Ti	$\delta(M, N)$	0.251	0.287	0.255	0.159	0.269
		$ q(N \rightarrow M) $	0.194	0.243	0.196	0.116	0.302
		$ q(Z \rightarrow M) $	0.657	0.378	0.639	0.618	0.537
		$ q(E \rightarrow M) $	0.400	0.482	0.403	0.469	0.325
		$ F(M) $	0.050	0.047	0.018	0.039	0.013
		$\Delta V_{ne}(M)$	-381.895	-458.902	-529.457	-386.869	-471.595
		$\Delta V_{ne}(M)$	14.616	14.995	14.462	14.514	12.480

Cl	Cr	$\delta(M, N)$	0.392	0.411	0.414	0.345	0.399
		$ q(N \rightarrow M) $	0.142	0.201	0.145	0.091	0.244
		$ q(Z \rightarrow M) $	0.656	0.309	0.632	0.563	0.559
		$ q(E \rightarrow M) $	0.327	0.412	0.326	0.411	0.212
		$ F(M) $	0.009	0.004	0.011	0.005	0.012
		$\Delta V^{ne}(M)$	-439.228	-523.679	-603.683	-445.858	-539.687
		$\Delta V^{ne}(M)$	18.499	18.351	18.440	19.990	14.651

^a The metal atom M is in the positive X axis and their respective Ehrenfest forces are negative – implying that the metal atom is attracted towards the bridgehead nitrogen atom which lies in the negative X axis with a positive Ehrenfest force. Only the magnitude of Ehrenfest forces for the metal atom $|F(M)|$ are tabulated.

^b The table shows the variation of these properties with respect to change in the equatorial substituents (E) for a particular apical ligand, Z = Cl.

Table 3.13. Delocalization index between M and bridgehead nitrogen atom N [$\delta(M, N)$], magnitude of charge transfer from A to B [$|q(A \rightarrow B)|$], magnitude of Ehrenfest forces on the metal atom M $|F(M)|$ and changes in nuclear – electron potential energy for the metal atom $[\Delta V^{ne}(M)]$ calculated at B3LYP/6-31+G* level of theory. All the quantities are in atomic units.^{a, b}

E	M		Z = Cl	NH ₂	CO	CN	NH ₃	CH ₃	OH	H ₂ O
	Ti	$\delta(M, N)$	0.251	0.190	0.258	0.234	0.393	0.174	0.223	0.288
		$ q(N \rightarrow M) $	0.194	0.231	0.245	0.184	0.468	0.225	0.226	0.307
		$ q(Z \rightarrow M) $	0.657	0.540	0.346	0.726	0.060	0.540	0.605	0.032
		$ q(E \rightarrow M) $	0.400	0.432	0.470	0.379	0.525	0.433	0.428	0.517
		$ F(M) $	0.050	0.006	0.017	0.022	0.020	0.015	0.005	0.023
		$\Delta V^{ne}(M)$	-381.895	-346.739	-364.402	-356.247	-355.327	-342.336	-350.305	-357.681
		$\Delta V^{ne}(M)$	14.616	14.857	13.151	14.712	11.262	14.520	15.486	11.379
NH	Cr	$\delta(M, N)$	0.392	0.326	0.376	0.368	0.393	0.283	0.346	
		$ q(N \rightarrow M) $	0.142	0.182	0.192	0.141	0.468	0.186	0.171	
		$ q(Z \rightarrow M) $	0.656	0.538	0.302	0.690	0.609	0.451	0.623	
		$ q(E \rightarrow M) $	0.327	0.369	0.380	0.324	0.255	0.373	0.344	[b]
		$ F(M) $	0.009	0.011	0.005	0.012	0.004	0.022	0.003	
		$\Delta V^{ne}(M)$	-439.228	-400.687	-423.983	-412.953	-402.828	-497.748	-404.169	
		$\Delta V^{ne}(M)$	18.499	18.980	16.75	18.762	15.808	18.057	19.466	

^a The table shows the variation of these properties with respect to change in the apical substituents (Z) for a particular equatorial group E = NH.

^b Broken structure.

The distribution of laplacian at the Cr–N bond critical points is shown in Figure 3.4 which illustrates the effect of apical as well as equatorial substituents on the Cr–N and Cr–E bond strengths. As seen for titanatranes, similar, but somewhat more, polarization of the VSCC on bridgehead nitrogen towards chromium is noticed here.

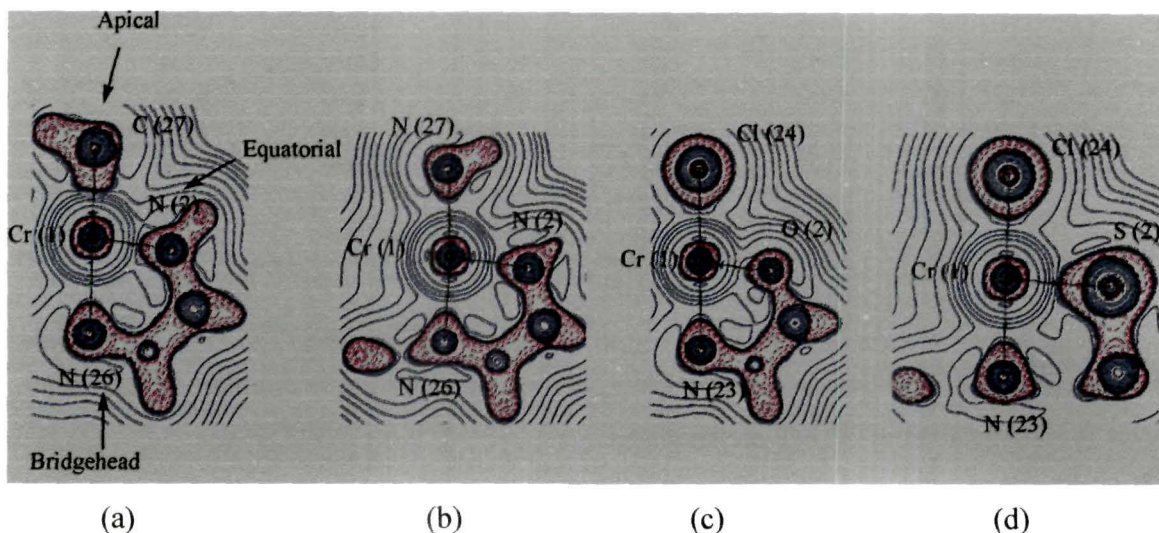


Figure 3.4. Contour plots of laplacian, $\nabla^2\rho$ (bcp), in $N\cdots Cr - Z$ plane (obtained with AIMALL program at B3LYP/6-31+G* level of theory) showing the effect of apical, (a) $Z = CH_3$ and (b) $Z = NH_3$ and equatorial substituents (c) $E = O$ and (d) $E = S$ on the bonding of chromatranes. Regions of charge depletion ($\nabla^2\rho > 0$) are denoted by solid blue lines while regions of charge concentration ($\nabla^2\rho < 0$) are denoted by dashed red lines. Green sphere denotes bond critical points (BCPs) and black solid line denotes bond paths.

Thus, the $M\cdots N$ bond critical point show low values of ρ_b , small and positive values of $\nabla^2\rho$ and negative values of $H(r)$. All these computed topological descriptors at the transannular $M\cdots N$ bond critical points of Group 4 and 6 metallatranes show considerable degree of covalency which increases from Group 4 to Group 6. Stronger transannular bonds have higher values of delocalization index $\delta(M, N)$, electron density, ρ_b and higher values of $L(r)$. The calculated Ehrenfest forces³² for the metal atom are attractive in every case drawing the metal atom towards bridgehead nitrogen atom. This attractive Ehrenfest force results in a stabilizing energy for the formation of $M|N_b$ (N_b is the bridgehead atom) surface. The external contribution to the nuclear – electron potential energy at the metal center $\Delta V^{e}_{ne}(M)$, dominates over the own contribution $\Delta V^0_{ne}(M)$, which accounts for the stability of these molecules.

[3.4] Conclusions

The nature of intramolecular transannular M–N bond, a key structural feature of Group 4 and 6 metallatranes, are found to be influenced not only by the substituents at apical and equatorial positions but also by the extent to which the metal and bridgehead nitrogen atoms are pyramidalized. Shorter and stronger M–N bonds are computed for molecules in which the metal atom is slightly pyramidalized whereas the bridgehead nitrogen atom is strongly pyramidalized. Weakly *trans* directing apical ligands such as Cl, NH₃, H₂O strengthens the transannular interaction while the stronger ones CO, CN, CH₃ weakens the same. The M–N bonds of Group 6 metallatranes are found to be stronger than their Group 4 analogs and accordingly, higher stabilization energies are computed for the former. The energetics of different spin states of Group 6 metallatranes are found to depend on the nature of apical as well as equatorial substituents. The nature of the transannular bond of these molecules was ascertained with the help of QTAIM analysis which reveal that they have - (i) small values of electron density (ρ_b), (ii) small and positive values of laplacian ($\nabla^2\rho$) and (iii) negative values of local electronic energy density [$H(r)$] at the bond critical points. Thus, the M–N bonds of these molecules have considerable amount of covalent character.²⁶ Ehrenfest forces for the metal atom are all attractive in nature and the atomic contribution for the stability of these molecules comes from large negative values of external contribution to nuclear – electron potential energy at the metal center, ΔV^e_{ne} . We feel that our study will further help the experimentalists in designing new and efficient metallatrane based catalytic systems.

[3.5] Bibliography

1. (a) Verkade, J. G. *Coord. Chem. Rev.* **137**, 233 – 295, 1994. (b) Chuit, C. et. al., *Chem. Rev.* **93** (4), 1371 – 1448, 1993. (c) Pestunovich, V. et. al., In *The Chemistry of Organic Silicon Compounds*; Rappoport, Z., Apeloig, Y., Eds.; John Wiley & Sons: New York, 1998; Vol. 2, Part 1, Chapter 24. (d) Schrock, R. R. *Acc. Chem. Res.* **30** (1), 9 – 16, 1997.
2. (a) Duan, Z., & Verkade, J. G. *Inorg. Chem.* **34** (17), 4311 – 4316, 1995. (b) MacMillan, S. et. al., *Chem. Commun.* 4172 – 4174, 2007. (c) Kim, Y. et. al., *Organometallics* **18** (1), 36 – 39, 1999.
3. (a) Schrock, R. R. et. al., *Angew. Chem., Int. Ed. Engl.* **34** (18), 2044 – 2046, 1995. (b) Scheer, M. et. al., *Angew. Chem., Int. Ed. Engl.* **35** (21), 2492 – 2496, 1996.
4. (a) Schubart, M. et. al., *Inorg. Chem.* **33** (18), 3893 – 3898, 1994. (b) Duan, Z. et. al., *Inorg. Chem.* **34** (22), 5477 – 5482, 1995.
5. (a) Morton, C. et. al., *Organometallics* **18** (22), 4608 – 4613, 1999. (b) Morton, C. et. al., *J. Organomet. Chem.* **606**, 141 – 146, 2000.
6. (a) Smythe, N. C. et. al., *Inorg. Chem.* **45** (18), 7111 – 7118, 2006. (b) Filippou, A. C., & Schneider, S. *Organometallics* **22** (15), 3010 – 3012, 2003. (c) Filippou, A. C. et. al., *Eur. J. Inorg. Chem.* 2928 – 2935, 2002.
7. Schrock, R. R. et. al., *J. Am. Chem. Soc.* **119** (49), 11876 – 11893, 1997.
8. (a) Scheer, M. et. al., *Chem. Commun.* 2505 – 2506, 1998. (b) Schrock, R. R. et. al., *Organometallics* **16** (24), 5195 – 5208, 1997. (c) Schrock, R. R. et. al., *Organometallics* **17** (6), 1058 – 1068, 1998.
9. (a) Hirose, et. al., U. S. Patent, 4, 420, 498. (b) Buhl, R. et. al., *Thin solid films.* **80** (1-3), 265 – 270, 1981.
10. (a) Ajjou, J. A. N. et. al., *J. Am. Chem. Soc.* **120** (2), 415 – 416, 1998. (b) Ajjou, J. A. N. et. al., *J. Am. Chem. Soc.* **120** (51), 13436 – 13443, 1998. (c) Monoi, T. et. al., Eur. Patent 1041085, 2000. (d) Ajjou, J. A. N., & Scott, S. L. *J. Am. Chem. Soc.* **122** (37), 8968 – 8976, 2000. (e) Schmid, R., & Ziegler, T. *Can. J. Chem.* **78**, 265 – 269, 2000. (f) Scott, S. L. et. al., *Chem. Eng. Sci.* **56** (13), 4155 – 4168, 2001.
11. Schmid, R., & Ziegler, T. *Organometallics* **19** (14), 2756 – 2765, 2000.
12. (a) Kol, M. et. al., *J. Am. Chem. Soc.* **116** (10), 4382 – 4390, 1994. (b) O'Donoghue, M. et. al., *J. Am. Chem. Soc.* **119** (11), 2753- 2754, 1997.

13. (a) Pinkas, J. et. al., *J. Am. Chem. Soc.* **115** (10), 3925 – 3931, 1993. (b) Pinkas, J. et. al., *Inorg. Chem.* **33** (23), 5244 – 5253, 1994. (c) Shutov, P. L. et. al., *Inorg. Chem.* **41** (23), 6147 – 6152, 2002. (d) Kim, Y., & Verkade, J. G. *Inorg. Chem.* **42** (16), 4804 – 4806, 2003.
14. (a) Windus, T. L. et. al., *J. Am. Chem. Soc.* **116**, 11449 – 11455, 1994. (b) Schmidt, M. W. et. al., *J. Am. Chem. Soc.* **117** (28), 7480 – 7486, 1995. (c) Korlyukov, A. A. et. al., *Inorg. Chem.* **41** (20), 5043 – 5051, 2002. (d) Soran, A. P. et. al., *Organometallics* **26** (5), 1196 – 1203, 2007.
15. (a) Rioux, F. et. al., *Organometallics* **16** (2), 158 – 162, 1997. (b) Filippou, A. C. et. al., *Inorg. Chem.* **42** (22), 6974 – 6976, 2003.
16. B3LYP is Becke's three-parameter hybrid method using the LYP correlation functional (a) Becke, A. D. *J. Chem. Phys.* **98** (7), 5648 – 5652, 1993. (b) Lee, C. et. al., *Phys. Rev. B.* **37** (2), 785 – 789, 1988. (c) Vosoko, S. H. et. al., *Can. J. Phys.* **58** (8), 1200 – 1211, 1980.
17. (a) Hay, P. J., & Wadt, W. R. *J. Chem. Phys.* **82** (1), 270 – 283, 1985. (b) Wadt, W. R., & Hay, P. J. *J. Chem. Phys.* **82** (1), 284 – 298, 1985. (c) Hay, P. J., & Wadt, W. R. *J. Chem. Phys.* **82** (1), 299 – 310, 1985.
18. (a) Glendening, E. D. et. al., *NBO Program 3.1*: Madison, W. T. 1988. (b) Reed, A. E. et. al., *Chem. Rev.* **88** (6), 899 – 926, 1988.
19. Frisch, M.C. et al., *Gaussian 03*, revision D.02; Gaussian, Inc.: Wallingford CT, 2004.
20. (a) Bader, R. F. W. *Atoms in Molecules: a Quantum Theory*; Oxford University Press: Oxford, U. K., 1990 (b) Bader, R. F. W. *J. Phys. Chem. A.* **102** (37), 7314 – 7323, 1998. (c) Bader, R. F. W. *Chem. Rev.* **91** (5), 893 – 928, 1991.
21. Bader, R. F. W. AIMPAC; <http://www.chemistry.mcmaster.ca/aimpac/>.
22. Keith, T. A.; AIMAll (Version 10.02.09), 2010 (<http://aim.tkgristmill.com>).
23. (a) Macedo, J. L. C., & Harvey, J. N. *J. Am. Chem. Soc.* **126** (18), 5789 – 5797, 2004. (b) Poli, R. *J. Organometal. Chem.* **689**, 4291 – 4304, 2004. (c) Wasbotten, I. H., & Ghosh, A. *Inorg. Chem.* **46** (19), 7890 – 7898, 2007.
24. Farrugia, L. J. et. al., *J. Phys. Chem. A.* **110** (25), 7952 – 7961, 2006.
25. Cremer, D., & Kraka, E. *Angew. Chem., Int. Ed. Engl.* **23** (8), 627 – 628, 1984.
26. Macchi, P., & Sironi, A. *Coord. Chem. Rev.* **238 – 239**, 383 – 412, 2003.
27. Nakanishi, W. et. al., *J. Phys. Chem. A.* **113** (37), 10050 – 10057, 2009.
28. (a) Gatti, C. Z. *Kristallogr.* **220**, 399 – 457, 2005. (b) Gibbs, G. V. et. al., *J. Phys. Chem. A.* **112** (16), 3693 – 3699, 2008.



CHAPTER - 4

**Structure, Stability and Reactivity of
Different Carbon Bases**

[4.0] ABSTRACT

Organic carbon compounds are mostly found in a formal oxidation state of IV. However, carbon compounds in a formal oxidation state of II, (e. g., carbene) which once thought to be a reactive intermediate, are now available in a bottleable form. Very recently, a unique bonding situation in carbon compounds has been proposed which predicts a formal oxidation state of carbon as low as zero.

The first part of this chapter deals with the study of the reactivity of heterocyclic carbenes which may help in realizing the existence of “hidden” carbon(0) character in them. Quantum chemical calculations reveals the presence of “hidden” carbon(0) character in 2,2' bipyridyl carbene which is supported by very high values of second proton affinity as well as significant values of the bond dissociation energies for gem-dimetallation. Even Arduengo type carbene also shows significant values of BDE for gem-dimetallation. All the dimetallated derivatives show metallophilic interactions.

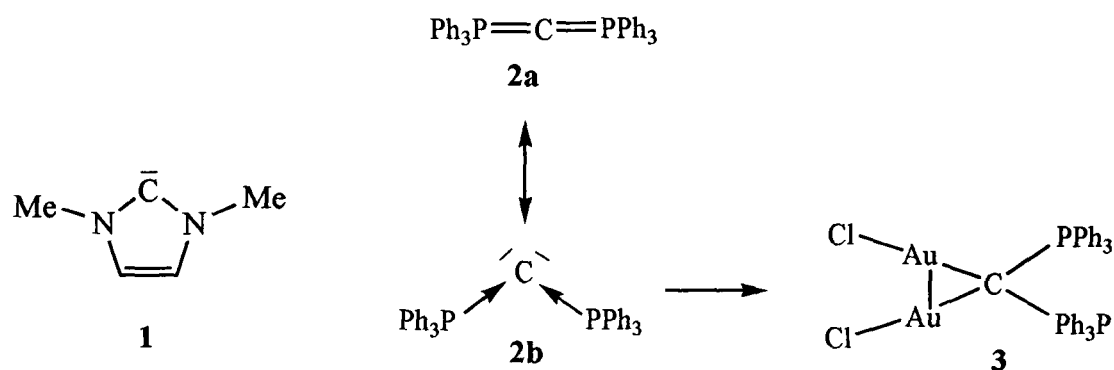
In the next part of this chapter, some new cyclic and acyclic carbon(0) compounds stabilized by differential coordination modes (such as abnormal, remote and a mixture of both) of *N*-heterocyclic carbenes are studied theoretically. The cyclic carbon (0) compounds proposed in this study are unusual in the sense that they contain a five membered ring consisting of *only* carbon atoms with a central carbon atom in the formal oxidation state of zero. All these compounds are found to be very strong nucleophiles which might have wide implications in catalysis. Calculation of first proton affinities of these molecules reveal that they are better σ donors than the carbon(0) compound supported by normal *N*-heterocyclic carbenes. Quantum chemical calculations indicate that these molecules possess very high donor-acceptor L \rightarrow C bond strengths and are thermodynamically stable. Calculation of the bond dissociation energies for the complexation of one and two molecules of AuCl indicates the possible isolation of their gem dimetalated derivatives.

The last part of the chapter deals with the quantum chemical calculations on different carbon bases to understand the origin of their reactivity. Both carbon(0) and carbon(II) bases may show very high values of second proton affinity as well as bond dissociation energies for gem-dimetallation. Thus, their distinction becomes blurred when subjected to electrophilic attack. However, unlike carbon(0) bases, carbon(II) bases are ambiphilic in nature owing to the presence of a σ symmetric lone pair and a vacant π orbital concentrated on the central carbon atom. Thus, they show different reactivity when subjected to nucleophilic attack. This reactivity difference may be considered for the unequivocal distinction between these two classes of compounds.

[4.1] Revisiting the Reactivity of Heterocyclic Carbenes

[4.1.1] Introduction

The element carbon can have different formal oxidation states other than IV as observed in usual organic compounds. For example, divalent C(II) species (carbenes) and divalent C(0) species (carbones) are now known. One such experimentally known divalent C(II) specie is the Arduengo's *N*-heterocyclic carbene, **1** (Scheme 4.1.1).^{1a} On the other extreme, divalent carbon in a formal oxidation state of zero are now identified and explored.² The first of such a C(0) specie was carbodiphosphorane, C(PPh₃)₂ (**2**), synthesized by Ramirez *et al.* in 1961³ and structurally characterized by X-ray analysis in 1978.⁴

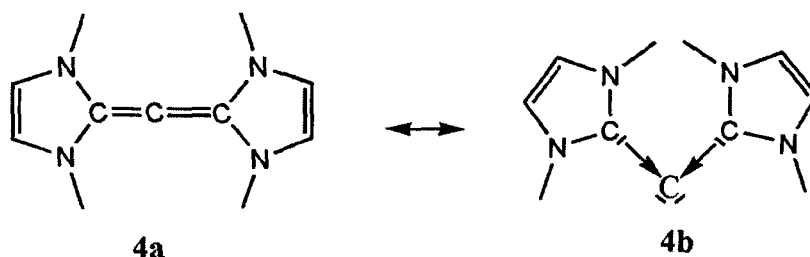


Scheme 4.1.1. Schematic representation of Arduengo carbene **1** and carbodiphosphorane **2**. Resonance form **2b** which represents the C(0) character of **2** are also shown.

The resonance extreme **2b** which suggests the presence of two lone pairs at the central carbon atom was also proposed,^{2b,2c,3,4} but unsuccessful isolation of any geminal dimetallated derivative of **2a** posed a question on the existence of the resonance extreme **2b**. However, in 2002, Vicente *et al.* in a carefully designed experimental work, reported the isolation and characterization of the first geminal dimetallated derivative of **2**.⁵ The successful isolation of **3**, the dimetallated derivative of **2** clearly demonstrated the dominant contribution of the resonance extreme **2b** (Scheme 4.1.1) in describing the reactivity of **2**.

In an effort to understand the actual nature of bonding in **2** and related compounds, Frenking *et al.* and others carried out a series of systematic study and concluded that the bond between the central carbon atom and the two donor ligands, L is of donor-acceptor type, L→C←L (where L can be any donor moiety).⁶ This bonding situation results in the retention of two lone pairs, one having σ symmetry and the other having π symmetry at the central carbon atom. In another report, Frenking *et al.* theoretically predicted that the compound

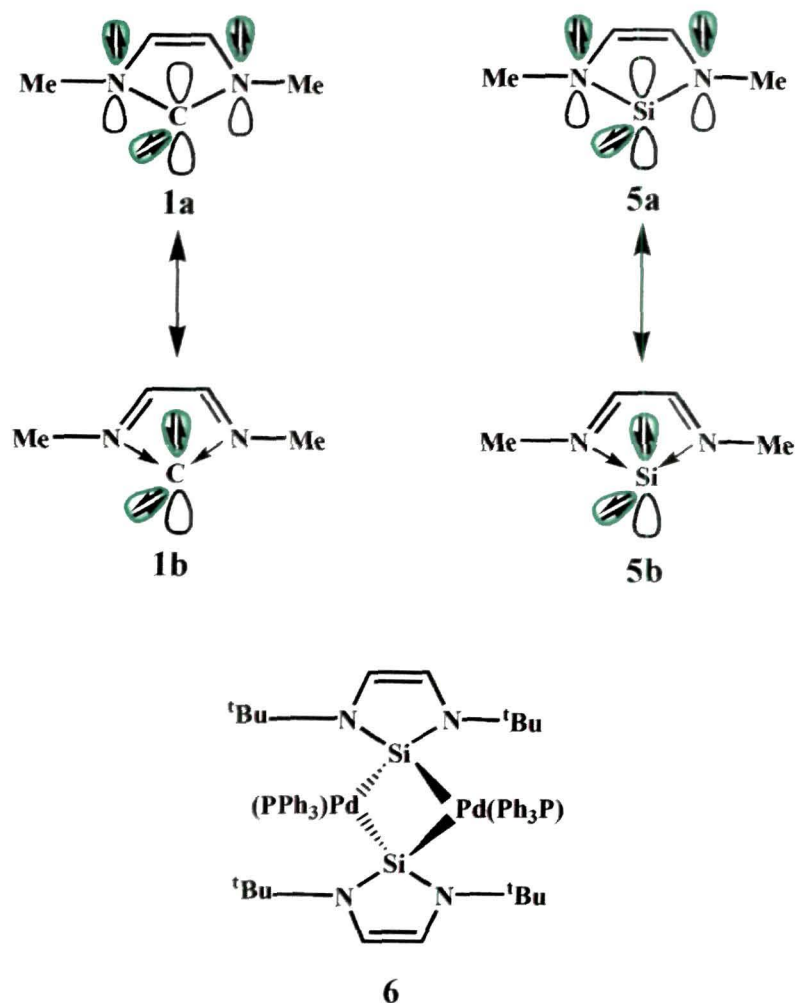
$C(NHC)_2$ (**4**) (NHC=*N*-heterocyclic carbene) exhibits the characteristics of divalent $C(0)$ compounds and could be isolable.⁷ Experimental verification of this theoretical prediction came soon after when the group of Bertrand^{2a} synthesized a benzannulated derivative of **4** (Scheme 4.1.2).



Scheme 4.1.2. Carbodicarbene, $C(NHC)_2$ (**4**) and its resonance form **4b** indicating its $C(0)$ character.

Although the bonding in $C(0)$ compounds are described in terms of donor-acceptor interactions, this may not be always realized when the bonding situation in their equilibrium geometry is considered.⁸ Thus, various reactivity parameters need to be considered for an unambiguous description of the bonding. One such reactivity parameter is the first and second proton affinity of these compounds. Since $C(0)$ compounds have two lone pairs centred on the central carbon atom, they should have high first as well as second proton affinities.^{8,9} The second proton affinity, more precisely, is a decisive indicator to distinguish a divalent $C(II)$ specie (carbenes) from a divalent $C(0)$ specie (carbones).^{8,9} Both carbene and carbone have very high values of first proton affinities, however, the former has a much lower second proton affinity than the later. Various other reactivity parameters such as complexation with main group as well as transition metal fragments are also suggested for distinguishing carbenes from carbones.⁶⁻⁹

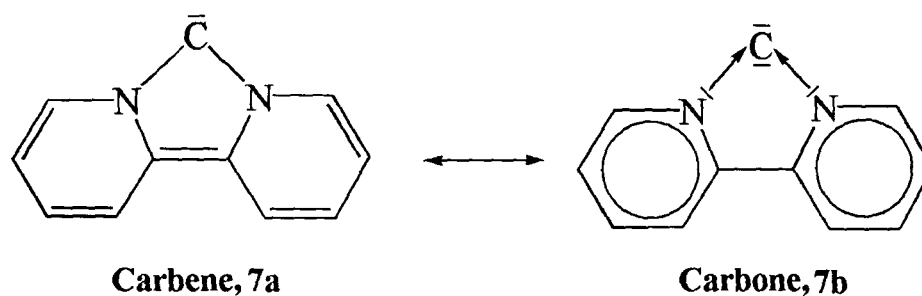
In principle, classical *N*-heterocyclic carbene **1a** (Scheme 4.1.3) can be thought to have a resonance form **1b** in which the central carbon atom will have two lone pairs and thus, may show the characteristics of a $C(0)$ compound. Nevertheless, resonance form **1b** may be ignored in practice because the π type lone pair will be delocalized resulting in the loss of the aromatic sextet. Reduction of aromaticity destabilises the resonance form **1b**.^{2b} On the contrary, the resonance form **5b** for *N*-heterocyclic silylene **5a** can be realized as less favourable orbital overlap between the π type lone pair and the adjacent $N-C \pi^*$ orbitals results in more electron density at the central silicon atom and thus, gives **5b** a larger



Scheme 4.1.3. Possible resonance forms of *N*-heterocyclic carbene and silylene showing its divalent element (II) character **1a**, **5a** and divalent element (0) character **1b**, **5b**.

importance.^{2b} This assertion has already been verified by the experimental characterization of a dinuclear Pd(0) complex (**6**) with bridging silylene ligands¹⁰ proving the existence of some degree of hidden silicon (0) character in **6**.

In 1998, Weiss *et al.*¹¹ have synthesized a formal 1:1 complex of 2, 2'-bipyridine and a singlet carbon (2,2'-bipyridyl carbene) **7**, which was assigned as a carbene (form **7a**, Scheme 4.1.4) based on *ab initio* calculations. Based on their *ab initio* calculations, the



Scheme 4.1.4. Possible resonance forms of 2, 2'-bipyridyl carbene **7** showing carbene (**7a**) and carbone (**7b**) character.

resonance extreme **7b** which resembles a C(0) compound (carbone) was suggested to be less likely.¹¹ However, they also reported a geminal diprotonated salt of **7**, although its crystal structure was not available. The formation of a geminal diprotonated derivative of **7** suggests the existence of the resonance extreme **7b**. This has prompted us to reinvestigate the bonding scenario and probe the importance of the resonance form **7b** in demonstrating its reactivity.

[4.1.2] Computational Details

Geometry optimizations of all the molecules were carried out without any symmetry constraints at BP86 level of theory.¹² Triple zeta valence polarization basis set TZVP¹³ was used for all the main group elements while the relativistic small-core ECP of Stuttgart/Dresden (SDD)¹⁴ was used for the transition metals. Frequency calculations were performed at the same level of theory to characterize the nature of the stationary point. All the structures were verified as minimum by confirming that their respective hessian (matrix of analytically determined second order energy derivative) is all real. Nucleus independent chemical shift (NICS) values are calculated at the BP86/6-31+G* and BP86/cc-pVTZ¹⁵ level of theory. All the calculations were performed using Gaussian 03 suite of program.¹⁶ The bonding nature was analyzed using the natural bond orbital (NBO)¹⁷ method available within Gaussian 03. Unless otherwise stated, we have used the same computational procedure for the other two sections of this chapter.

[4.1.3] Results and Discussion

Figure 4.1.1 shows the optimized geometries of **1**, **4**, and **7**. The C-N bond lengths involving the central carbon atom are slightly shorter in the *N*-heterocyclic carbene **1** than in

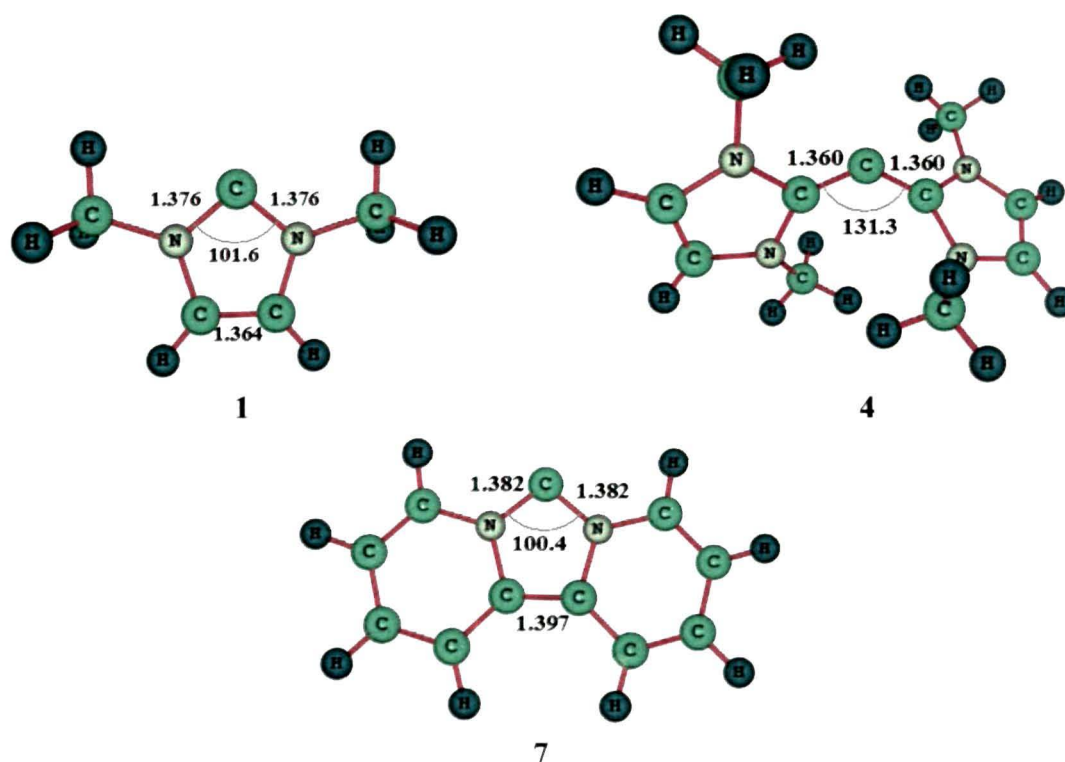


Figure 4.1.1. Optimized geometries of **1**, **4**, and **7** at BP86/TZVP level of theory. Bond lengths are in Å and angles are in degrees.

7. However, the C-C backbone of the central five membered ring (N-C-N-C-C) in **7** is elongated upto ~ 0.03 Å than that in **1**. This might be due to the presence of the exocyclic ring in **7** which elongates the C-C backbone due to conjugation. The angles around the central carbon atom of both these two compounds are similar. Carbodicyclic **4**, on the other hand, has a wider central $\angle C_c - C_0 - C_c$ angle (C_c is the carbenic carbon and C_0 is the central C(0) atom). NBO analysis of **4** suggests that the bonding situation in its equilibrium geometry should be best described as $C_c=C_0=C_c$ rather than $L \rightarrow C \leftarrow L$. This is in tune with previous observation by Frenking *et al.*^{6c}

Figure 4.1.2 shows the frontier orbitals obtained using NBO¹⁷ method at BP86/TZVP level of theory. The HOMO of **1** represents the σ symmetric lone pair orbital centered on carbenic carbon while HOMO-1 is the π symmetric orbital delocalized on the N-C-N moiety. On the other hand, the HOMO and HOMO-1 of **4** and **7** are of π and σ symmetry respectively. It is interesting to note that the frontier orbitals of **4** and **7** are similar in nature. Like **4**, the π symmetric HOMO of **7** is delocalized into the neighboring nitrogen atoms although the central carbon atom has the largest contribution. This posed a dilemma in assigning the true nature of **7** - carbene or carbene? To resolve this dilemma, we have

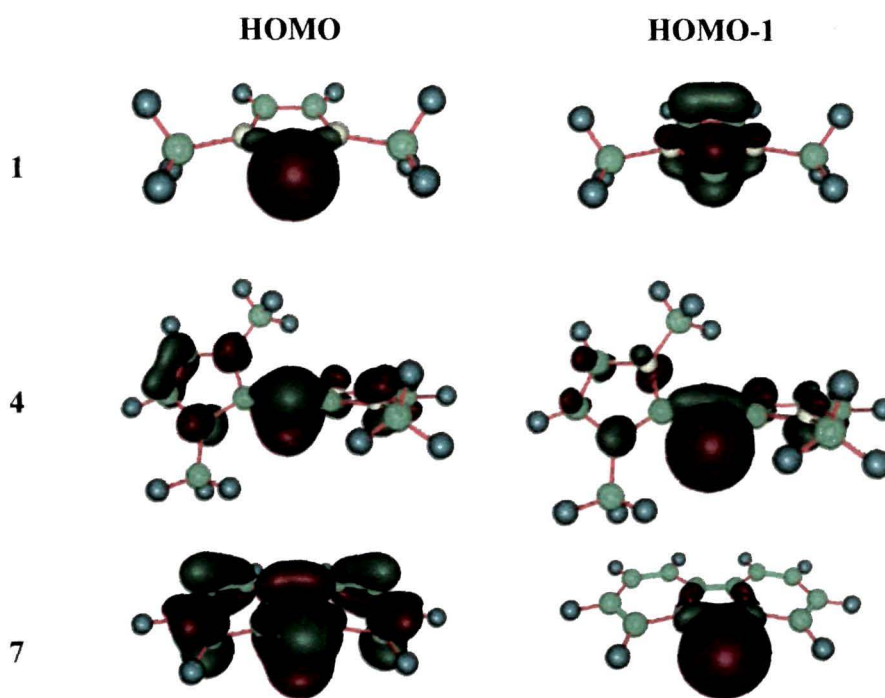


Figure 4.1.2. Shapes of the HOMO and HOMO-1 of **1**, **4**, and **7** obtained at BP86/TZVP level of theory.

calculated the first and second proton affinities of **1**, **4**, and **7** (Table 4.1.1) which were used previously for an unambiguous distinction between a carbene and a carbene.^{8,9}

The values of the first proton affinities of all these compounds are very high. Surprisingly, the value of the second proton affinity of **7** is closer to that calculated for **4**, and is much higher than that of **1**. This higher value of second proton affinity suggests that carbene **7** may have some “hidden” C(0) character thereby highlighting the importance of resonance form **7b**. It should be noted that a geminal diprotonated salt of **7** was synthesized but not characterized by X ray analysis.¹¹ The optimized geometries of the singly and doubly protonated derivatives (Figure 4.1.3) of **1** and **7** clearly demonstrates the contribution of the resonance forms **1b** and **7b**. Both the first protonated derivatives **1-H¹⁺** and **7-H¹⁺** do not show any significant structural variation compared to their parent ones, **1** and **7**. This might be due to the fact that the first protonation takes place at the in plane σ symmetric lone pair orbital. This orbital is not involved in any delocalization and thus protonation at this orbital does not change the structure. However, second protonation dramatically changes the structure. The C-C back bone of the central five membered ring elongates while the N-C bonds involving the carbon atom of the C-C backbone and the heteroatom strengthens. The

N-C bonds involving the central carbon atom also elongates dramatically. This structural variation clearly resembles the resonance form **1b** and **7b**. The structural change brought in

Table 4.1.1. Energies of the highest occupied π and σ symmetric orbitals (E_π and E_σ in eV) and their occupancies^[a], first (E_{PA-1}) and second (E_{PA-2}) proton affinities^[b] in kcalmol⁻¹ calculated at BP86/TZVP level of theory.

Entry	E_π	E_σ	Occupancy		E_{PA-1}	E_{PA-2}
			σ	π		
1	-5.6	-4.8	1.268	0.685	258.7	76.0
4	-3.2	-3.6	1.347	1.146	287.4	169.8
7	-4.6	-5.2	1.246	0.733	261.0	133.8

[a] Occupancies of the NBO enforced lone pairs at the central carbon atom. [b] The first proton affinity, E_{PA-1} refers to the energy difference between the optimized geometries of the first protonated species and the parent molecule, while, the second proton affinity, E_{PA-2} refers to the energy difference between the optimized geometries of the second and the first protonated species. The calculations were performed including zero point energy corrections.

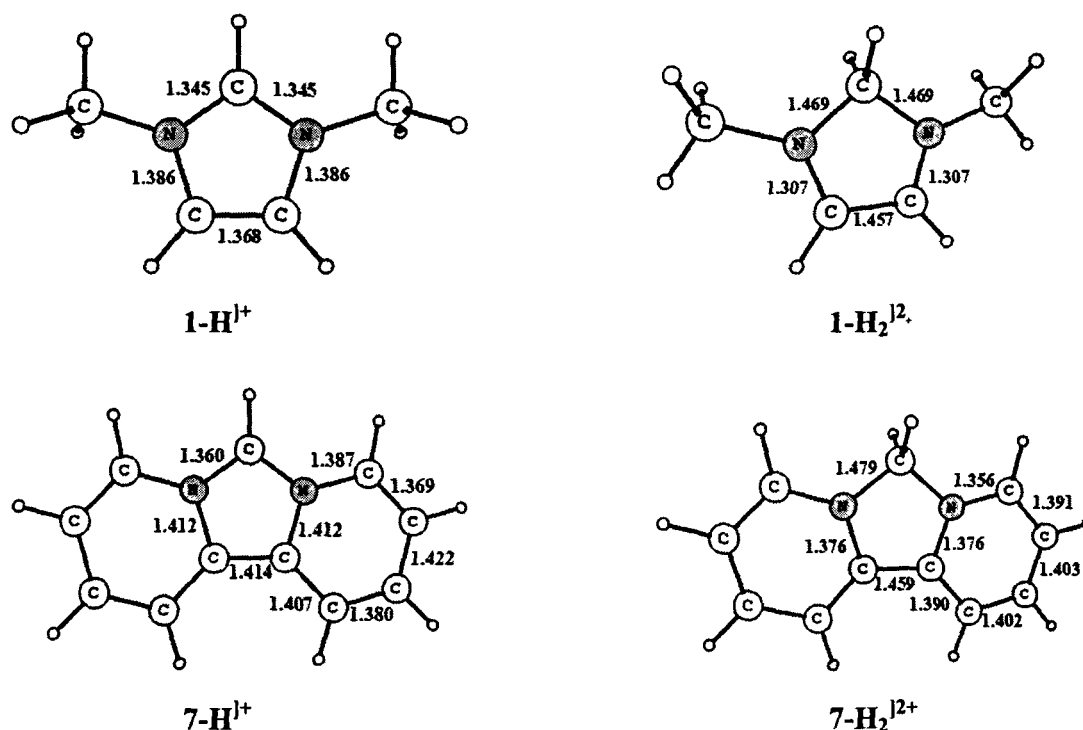


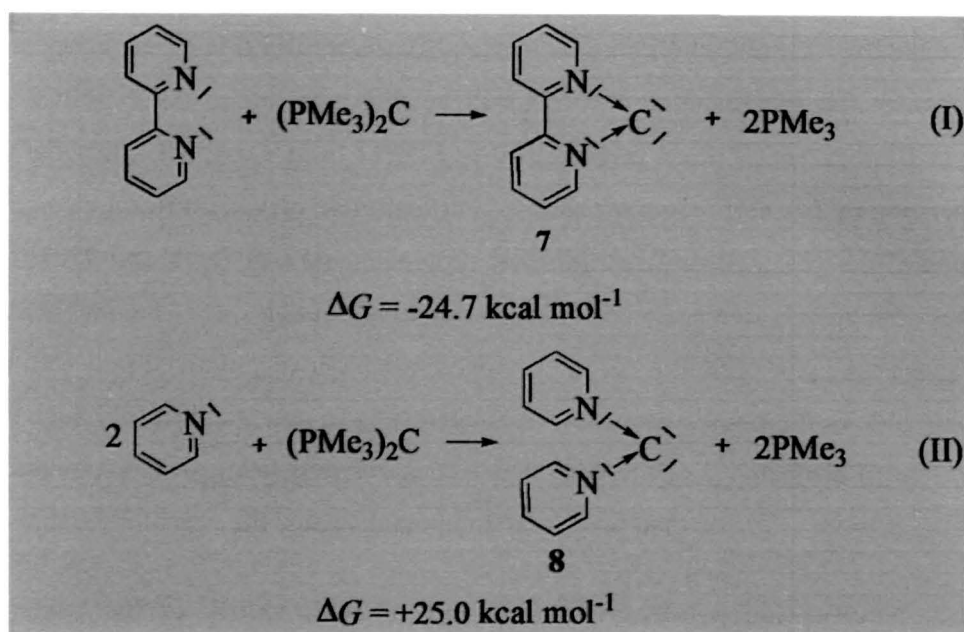
Figure 4.1.3. Optimized geometries of the first and second protonated species of **1** and **7**. Bond lengths are in Å.

by second protonation may be traced to the loss of aromaticity of the central five membered ring as the second protonation takes place at the out of plane π symmetric orbital which were involved in aromatic delocalization. To verify the loss of aromaticity on protonation, we have carried out nucleus independent chemical shift (NICS) calculations at BP86/6-31+G* and BP86/cc-pVTZ level of theory (Table 4.1.2) by placing a ghost atom (Bq) at the geometric centre of the ring (NICS-0) and at 1 Å above the plane of the ring (NICS-1) as suggested by Scheleyer *et al.*¹⁸ More negative value of NICS indicates more cyclic delocalization or larger aromatic character. It is evident from Table 4.1.2 that the NICS values calculated for **1** and **7** at BP86/6-31+G* and BP86/cc-pVTZ level of theory are very close and hence, the remainder of the text will be discussed based on the NICS values calculated at BP86/6-31+G* level of theory. It is evident from Table 4.1.2 that the central five member ring of **7** is more aromatic than **1**. Further, there is no significant change in the NICS values of the parent ligand and the first protonated species for **1** and **7**. However, NICS values dramatically decreases on further protonation. This is due to the involvement of the out of plane lone pair orbital in second protonation which was involved in delocalization thus resulting in loss of aromatic character. It is interesting to note that in **7**, although there is a dramatic loss of aromaticity of the central five member ring (R_{central}) on protonation, the exocyclic ring is more aromatic than the parent compound. Thus, the loss of aromatic

Table 4.1.2. Nucleus independent chemical shift (NICS) values of the central five member ring (R_{central}) and the exocyclic six member ring (R_{exo}) calculated at the BP86/6-31+G* level of theory. Values within parenthesis refer to the NICS calculations at BP86/cc-pVTZ level of theory.

Entry	R_{central}		R_{exo}	
	NICS-0	NICS-1	NICS-0	NICS-1
1	-11.6(-11.6)	-9.4(-9.5)	-	-
1-H ¹⁺	-13.4	-9.7	-	-
1-H ₂ ²⁺	-3.9	-5.4	-	-
7	-17.8(-17.7)	-15.5(-15.7)	-5.3(-5.0)	-6.4(-5.0)
7-H ¹⁺	-16.8	-12.8	-7.6	-8.7
7-H ₂ ²⁺	-1.8	-1.6	-6.6	-8.7

character of the central ring of **7** due to protonation is partly compensated by the gain in aromaticity of the exocyclic six member ring, and this accounts for the high value of second proton affinity obtained for **7**. The fact that cyclic electron delocalization plays a major role in enhancing the stability of **7** can be ascertained by comparing the energetic of reaction I and II. The formation of cyclic compound **7** is exergonic by $24.7 \text{ kcal mol}^{-1}$ while the formation of its acyclic derivative, **8** is endergonic by similar amount. Thus, **8** is thermodynamically less stable than **7**.



Recently, on the basis of experimental studies, Fürstner *et al.* suggested that divalent carbon compounds of the type CR_1R_2 should be considered as carbenes if they form stable complexes as $[\text{R}_1\text{R}_2\text{C}(\text{AuCl})_2]$.¹⁸ Such an observation is substantiated theoretically by Frenking *et al.*²⁰ Hence, we also checked the possibility of complexation of **1**, **4**, and **7** with one and two molecules of AuCl and $\text{Ni}(\text{CO})_2$ respectively. Table 4.1.3 contains the bond dissociation energies (BDE) and Figure 4.1.4 shows the optimized geometries of all the complexes. The calculated BDE for the dissociation of one molecule of AuCl and $\text{Ni}(\text{CO})_2$ from E-AuCl and $\text{E-Ni}(\text{CO})_2$ are almost same for all the ligands **E**, indicating that binding of first AuCl and $\text{Ni}(\text{CO})_2$ to **E** take place with equal strength. The BDE for the dissociation of one molecule of AuCl and $\text{Ni}(\text{CO})_2$ from E-(AuCl)_2 and $\text{E-}\{\text{Ni}(\text{CO})_2\}_2$ are comparable for **1** and **7**. However, these values are smaller than that for **4**. This indicates that binding of second molecule of AuCl and $\text{Ni}(\text{CO})_2$ to 1-AuCl and $\text{7-Ni}(\text{CO})_2$ take place with equal strengths but with a greater strength to 4-AuCl and $\text{4-Ni}(\text{CO})_2$. However, calculated BDE

suggest that synthesis of both mono and geminal dimetallated derivatives of **1**, **4**, and **7** are feasible. The significant values of BDE obtained for **1** and **7** is a clear manifestation of the dominant role played by resonance forms **1b** and **7b**.

The optimized geometries of the monoaurated complexes of **1**, **4**, and **7** show similar structures. The computed Au-C distances are almost similar for all the monoaurated complexes. The angle around the central carbon atom for **1** and **7** widens slightly in their

Table 4.1.3. Calculated bond dissociation energies in kcal mol⁻¹ (including zero-point vibrational correction) for the dissociation of one molecule of AuCl and Ni(CO)₂ from E-M and E-(M)₂ respectively [E = **1, **4**, and **7**; M = AuCl and Ni(CO)₂].**

Entry (E)	E-AuCl → E + AuCl	E-(AuCl) ₂ → E-AuCl + AuCl
1	76.4	35.0
4	72.2	50.8
7	74.9	37.1
	E-Ni(CO) ₂ → E + Ni(CO) ₂	E-{Ni(CO) ₂ } ₂ → E-Ni(CO) ₂ + Ni(CO) ₂
1	42.0	31.3
4	36.4	37.6
7	40.6	33.1

monoaurated complexes while narrows by $\sim 10^0$ for **4**. Diaurated complexes of these ligands show elongation of the C-N bonds (involving the central carbon atom). The most interesting geometrical observation of these diaurated complexes is the presence of an aurophilic interaction.²¹ The Au-Au distance in **1**-(AuCl)₂ and **7**-(AuCl)₂ are 2.729 Å and 2.764 Å respectively. These Au-Au distances are nearly ~ 0.3 Å shorter than that in **4**-(AuCl)₂. This might be due to the fact that the angle at the central carbon atom of **4** is much larger than that of **1** and **7**. The \angle C – Au – Cl angle for **1**-(AuCl)₂ and **7**-(AuCl)₂ are 159.5° and 163.0° while it is 177.7° for **4**-(AuCl)₂. It is interesting to note that both the geminal diaurated complexes of **1** and **7** are stable despite the fact that resonance form **1b** and **7b** are less favourable due to loss of aromaticity.^{2b} This loss of aromaticity is partly compensated by strong aurophilic interactions present in these complexes. Such aurophilic interaction is known to stabilize higher coordinated complexes, E(AuR)_n with coordination number 'n' may be higher than normally observed.²²

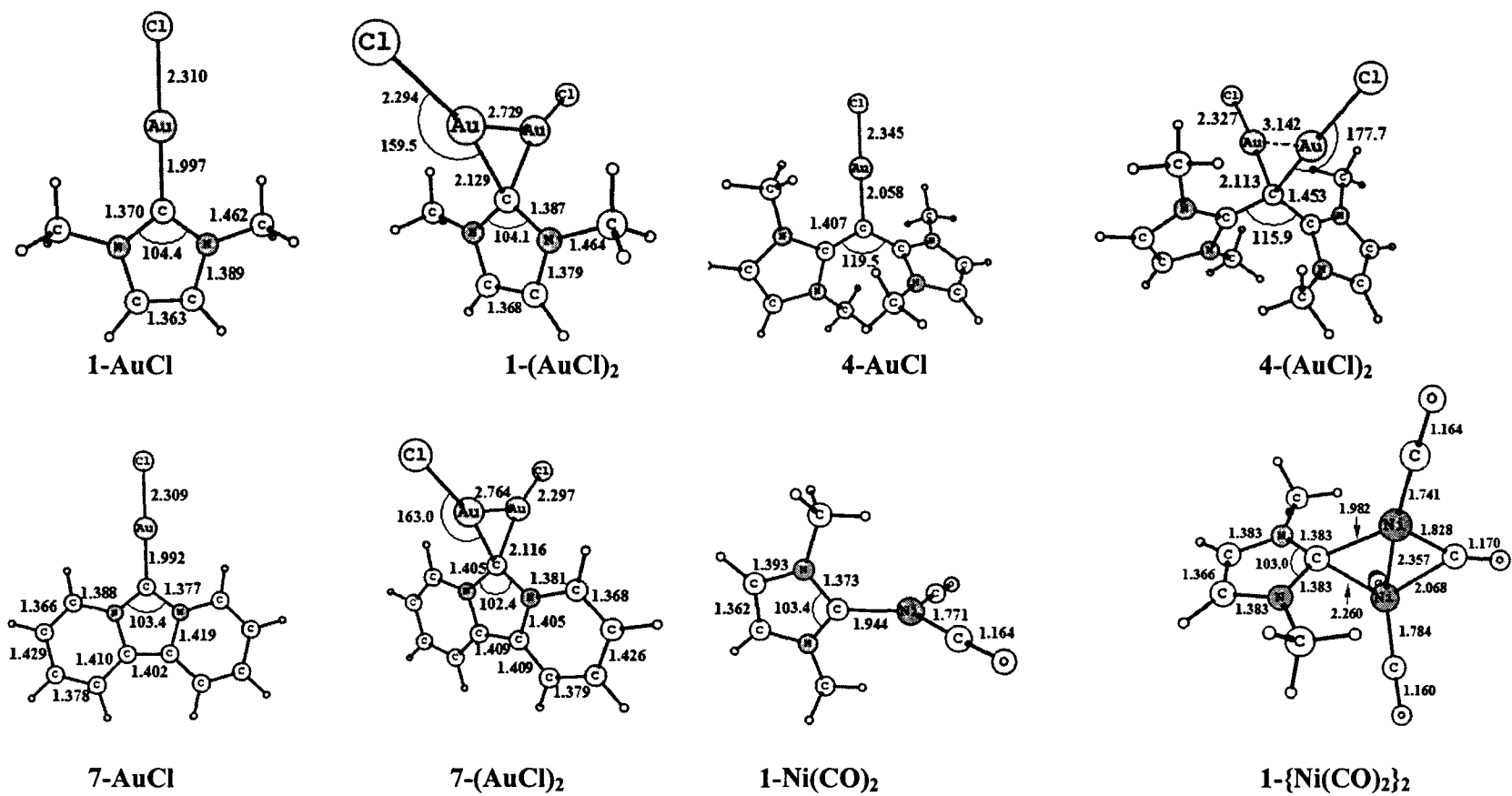


Figure 4.1.4. Lowest energy structures of E-AuCl, E-(AuCl)₂, E-Ni(CO)₂ and E{Ni(CO)₂}₂ (E = 1, 4, and 7) computed at BP86 level of theory. Bond lengths are in Å and angles are in degrees.

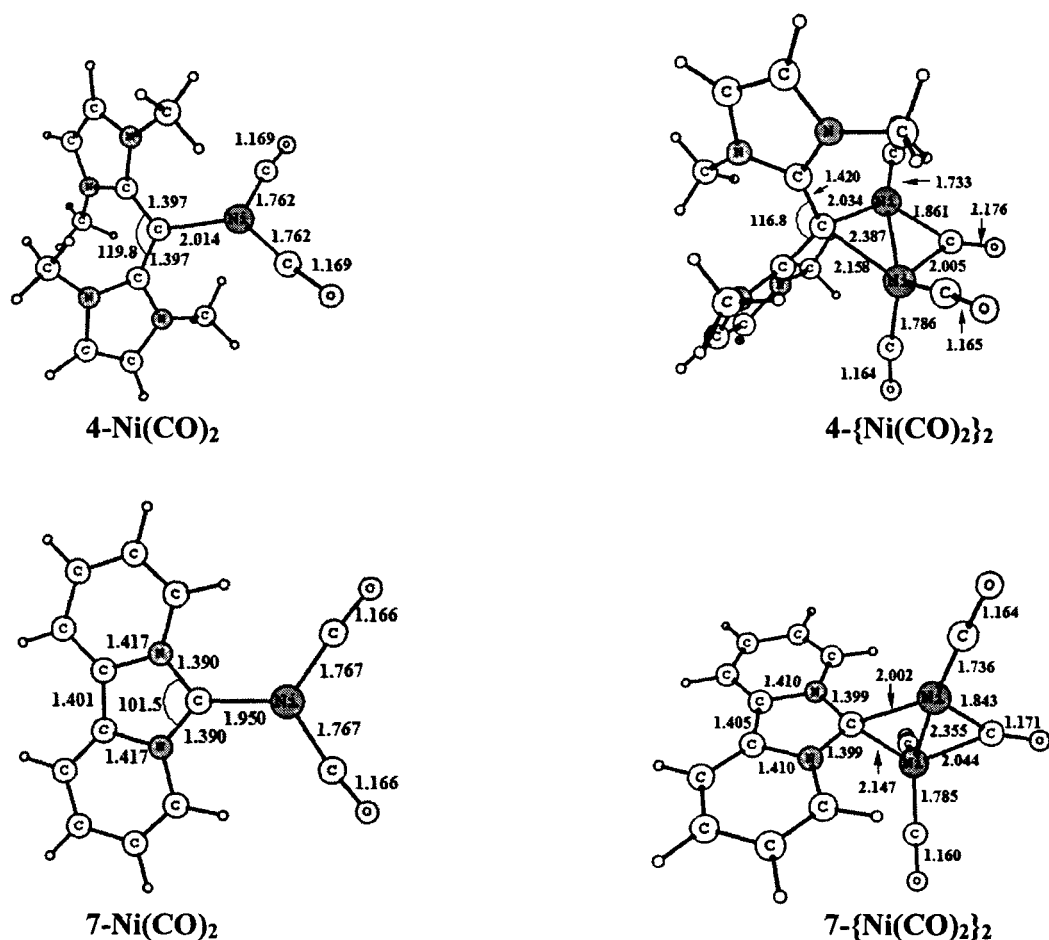


Figure 4.1.4. (Continued).

The lowest energy optimized geometries of the mono metallic derivatives $E\text{-Ni(CO)}_2$ ($E = 1, 4,$ and 7) are trigonal planar with angles around the Ni atom close to 360° . The computed Ni-C distances nicely correlates with BDE for the dissociation of one molecule of Ni(CO)_2 from E . For example, Ni-C distances for 1-Ni(CO)_2 and 7-Ni(CO)_2 are 1.944 \AA and 1.950 \AA with a BDE of 42.0 and $40.6 \text{ kcal mol}^{-1}$ respectively while the Ni-C distance for 4-Ni(CO)_2 is 2.014 \AA with a BDE of $36.4 \text{ kcal mol}^{-1}$. The dimetalled Ni complexes show some interesting structural features. Firstly, the range of calculated Ni-Ni distances for these complexes is 2.355 \AA to 2.387 \AA which is well within the typical range of some reported Ni-Ni distance of $2.512 - 2.649 \text{ \AA}$.²³ Secondly, the dimetalled $E\text{-Ni(CO)}_2$ derivatives show a semibridged carbonyl structures with two different Ni-CO distances.²⁴

[4.1.4] Conclusions

In conclusion, theoretical calculations predict that 2, 2'-bipyridyl carbene **7** has “hidden” C(0) character as evidenced from the very high value of second proton affinity as well as significant values of BDE obtained for gem-dimetalation of **1** and **7**. This higher value of second proton affinity of **7** can be attributed to the higher degree of delocalization in the exocyclic rings. The second proton affinity can be described by invoking the resonance form **7b**. The mono and dimetallated derivatives of **1** and **7** show similar structural features as that of a C(0) compound, **4** although the BDE values for the dissociation of one molecule of AuCl and Ni(CO)₂ from E-(AuCl)₂ and E-{Ni(CO)₂}₂ are somewhat lower. Further support for resonance forms such as **1b** and **7b** came from recent isolation of some bridged *N*-heterocyclic carbene (NHC) complexes (Figure 4.1.5, **9** – **11**)²⁵ thereby highlighting the possible existence of “hidden” C(0) character even in Arduengo type *N*-heterocyclic carbenes.

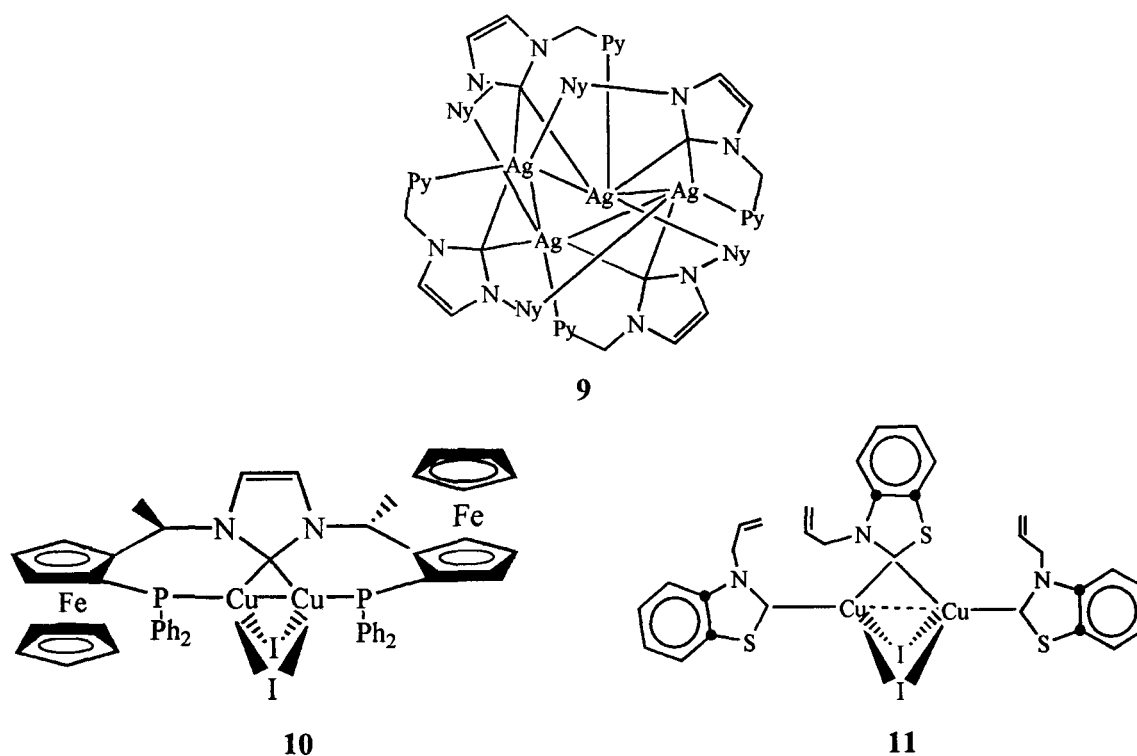
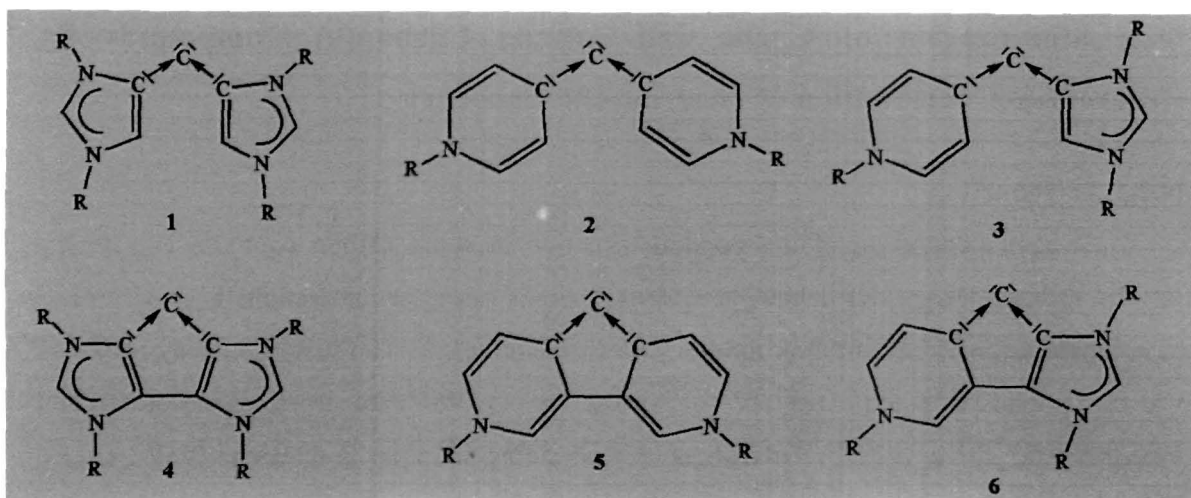


Figure 4.1.5. Experimentally characterized bridging complexes of NHC.

[4.2] Stabilization of Cyclic and Acyclic Carbon(0) Compounds By Differential Coordination of Heterocyclic Carbenes

[4.2.1] Introduction

Recent recognition of the bonding situation in some carbon compounds with the general formula CL_2 which takes place through donor-acceptor interactions $L \rightarrow C \leftarrow L$ ⁶⁻⁹ has prompted researchers to look for many new derivatives.²⁻⁵ The first of such a compound was carbodiphosphorane (CDP) $C(PPh_3)_2$ synthesized in 1961³ and structurally characterized by X-ray analysis in 1978.⁴ The realization of bonding situation in CDPs as $Ph_3P \rightarrow C \leftarrow PPh_3$ ⁶ led Frenking and coworkers to predict a hitherto unknown compound, carbodicarbene $C(NHC)_2$ (NHC = *N*-heterocyclic carbene), as a stable carbon(0) compound on the basis of quantum-chemical calculations.^{6b} Experimental characterization of $C(NHC)_2$ came soon after when the group of Bertrand and coworkers synthesized a benzannulated derivative of $C(NHC)_2$.^{2a} The choice of NHC as L group in stabilizing CL_2 species was prompted because NHCs have strong σ donation abilities as well as they are often compared with classical two electron donors such as phosphines.^{1a} Recent studies also show that NHCs can have π donating as well as π accepting abilities.²⁶ The exciting features of NHC ligands are their ability to activate small molecules²⁷ and stabilize main group elements, especially in their formal zero oxidation states.^{2a,28} Also, identification of different coordination modes (such as abnormal and remote) of NHC ligands²⁹ may provide diversity in the domain of element(0) compounds. Recently, Frenking *et. al.* predicted that carbodiphosphorane can highly activate olefin-metathesis catalysts.³⁰ Hence, it may be rewarding to study the stability and reactivity of carbodicarbenes stabilized by abnormal (*a*NHC) and remote (*r*NHC) *N*-heterocyclic carbenes (Scheme 4.2.1). Moreover, cyclization of these derivatives through coupling of the β -carbon atoms of these NHCs may also become interesting examples of cyclic carbon(0) compounds or cyclic carbodicarbenes.



Scheme 4.2.1. Schematic representation of acyclic carbodicarbenes (**1 – 3**) with both the L groups as abnormal carbene (**1**), remote carbene (**2**) and one of the L groups is abnormal and the other one is remote carbene (**3**) and their cyclic derivatives **4 – 6**.

While the structure, stability and reactivity of heterocyclic carbenes has been thoroughly studied, that of carbon(0) compounds is still at its infancy and needs attention. Herein we report the first theoretical investigation of both acyclic (**1 – 3**) and cyclic carbodicarbenes (**4 – 6**) stabilized by two abnormal, remote and a mixture of both abnormal and remote NHCs respectively (Scheme 4.2.1). Cyclic carbodicarbenes **4 – 6** are of particular interest as the central five membered rings of these compounds consist of all carbon atoms with a central carbon atom in the formal oxidation state of zero. It may be noted that the known examples of five membered ring compounds with a central C(0) atom contains heteroatom as the ring constituents.^{31b, 32} Recently, with the help of quantum chemical calculations, we have demonstrated the existence of hidden C(0) character even in 2,2'-bipyridyl carbene, a type of *N*-heterocyclic carbene.³³ We feel that our study may contribute to the growing library of carbon(0) compounds.

[4.2.2] Results and Discussion

[4.2.2.1] Molecular Geometry

Figure 4.2.1 shows the optimized geometries of the acyclic and cyclic carbodicarbenes **1-6**. The acyclic derivative **1** formed by two abnormal NHCs are almost planar at the central carbon atom with the two abnormal NHCs lying in the same plane. The central carbon atom (C_0) of **2** is in a linear arrangement with the two carbenic carbon (C_c)

atoms ($\angle C_c-C_0-C_c = 179.3^\circ$) and the two remote NHCs are orthogonal to each other. The remote NHC in **3** makes an angle of $\approx 56^\circ$ with the plane containing the remote NHC and the central carbon atom resulting in a slightly twisted geometry of **3**. The C_c-C_0 distance is

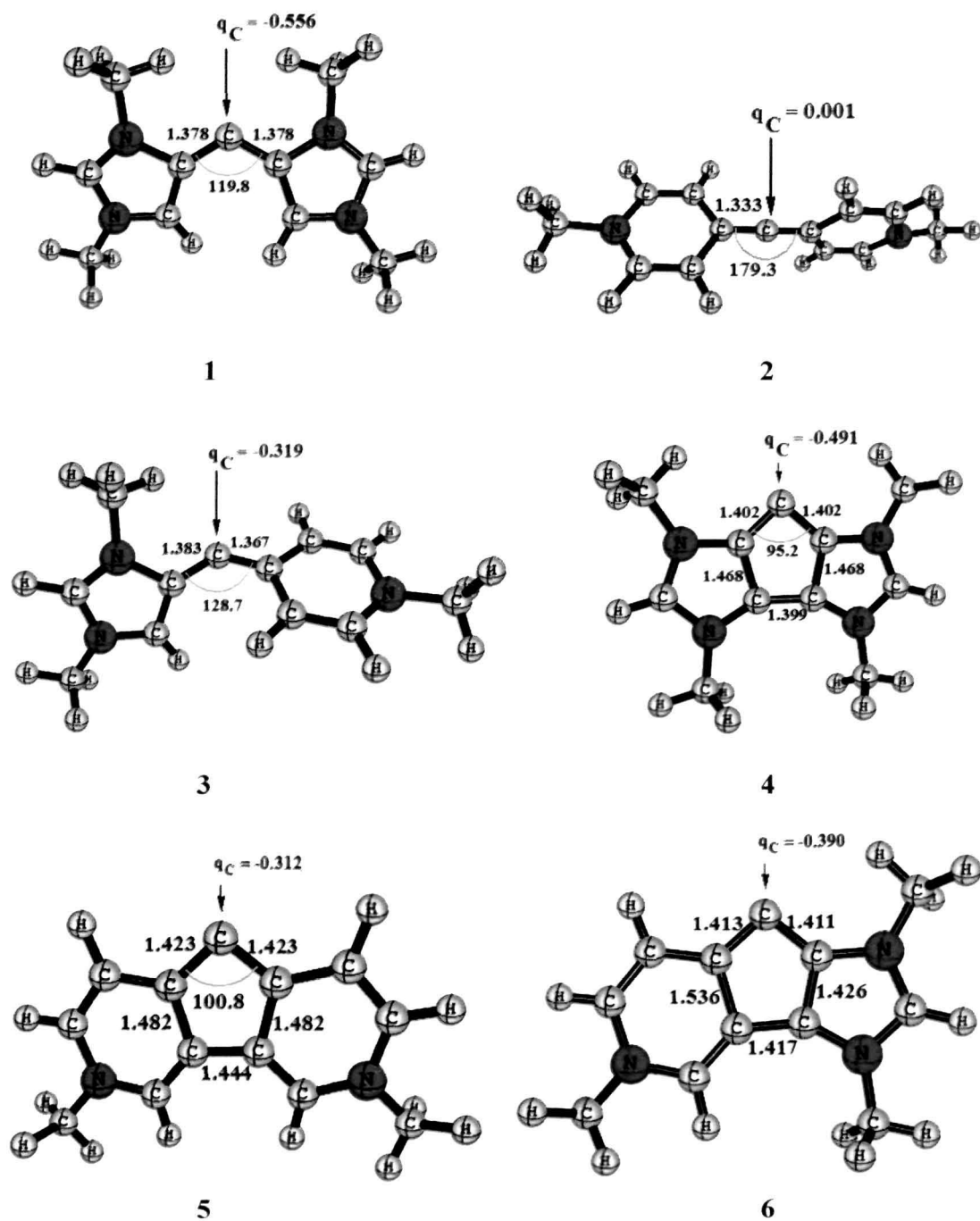


Figure 4.2.1. Lowest energy optimized geometries of **1-6**. Bond lengths are in Å and angles are in degrees. q_C represents the natural charge at the central carbon atom.

found to be ≈ 0.05 Å shorter in **2** than those in **1** and **3**. The cyclic derivatives **4** – **6** are perfectly planar. The C-C backbone of the central five member ring shortens for **4** while it is significantly elongated for **5**. Except **2**, which has a quasi linear geometry at the central carbon atom, the $\angle C_c-C_0-C_c$ angle is more obtuse for the acyclic ones than their cyclic derivatives. It may be noted that although the bonding situation in these compounds are described as donor-acceptor type, natural bond orbital (NBO) analysis do not show any donor-acceptor interactions $L \rightarrow C \leftarrow L$ in the equilibrium geometries of **1** – **6**. However, the computed natural charges q_C at the central carbon atom are negative for all the compounds except for **2** which reveals that the bonding situation can be described as $L \rightarrow C \leftarrow L$, indicating the possible C(0) character of these compounds. These negative charges at the central carbon atoms are manifestation of the strong σ donation of the two NHCs towards the central carbon atom. Although the quasi linear geometry of **2** suggests that it should be considered as an allene, calculated proton affinities (*vide infra*) shows that it should be better described as a carbon(0) compound. The slight positive charge at the central carbon atom of **2** arises from high degree of electron delocalization from the central carbon atom to the vacant p_π orbital of the adjacent carbenic carbon atoms.

[4.2.2.2] Molecular Orbital (MO) Analysis

Although the bonding in C(0) compounds are described in terms of donor-acceptor interactions, this may not be always realized when the bonding situation in their equilibrium geometry is considered.⁸ Thus, various chemical properties need to be considered for an unambiguous description of the bonding. The most important chemical property of these compounds is their ability to serve as double Lewis base owing to the presence of two lone pairs. Figure 4.2.2 shows the highest lying occupied frontier orbital centered at the central carbon atom of **1** – **6**. The HOMO and HOMO-1 of **1** are π and σ symmetry respectively.

The π symmetric HOMO of **1** is mostly centred on the central carbon and is delocalized on to the adjacent carbenic carbons. The two highest occupied orbitals of **2** represent the out of plane and in plane π orbitals when viewed along the local $C_c-C_0-C_c$ axis and both are energetically degenerate owing to its quasi linear geometry. On the other hand, the HOMO and HOMO-1 of **3** are of σ and π symmetry respectively.

The HOMO and HOMO-1 of **4** – **6** are of σ and π symmetry respectively. The HOMO-1 orbital is mainly localized at the C_0 atom and is partially delocalized on to the neighbouring C_c atoms. This is because the formally vacant p_π orbital of the C_c atoms are in conjugation with the π type lone pair orbital centred on the C_0 atom. Both the two carbenic

p_π orbitals have equal contribution to this MO except in **6** where the remote carbenic p_π orbital has slightly higher contribution than that of the abnormal one. Nevertheless, the HOMO-1 orbitals of these molecules are largely concentrated on the C_0 atom.

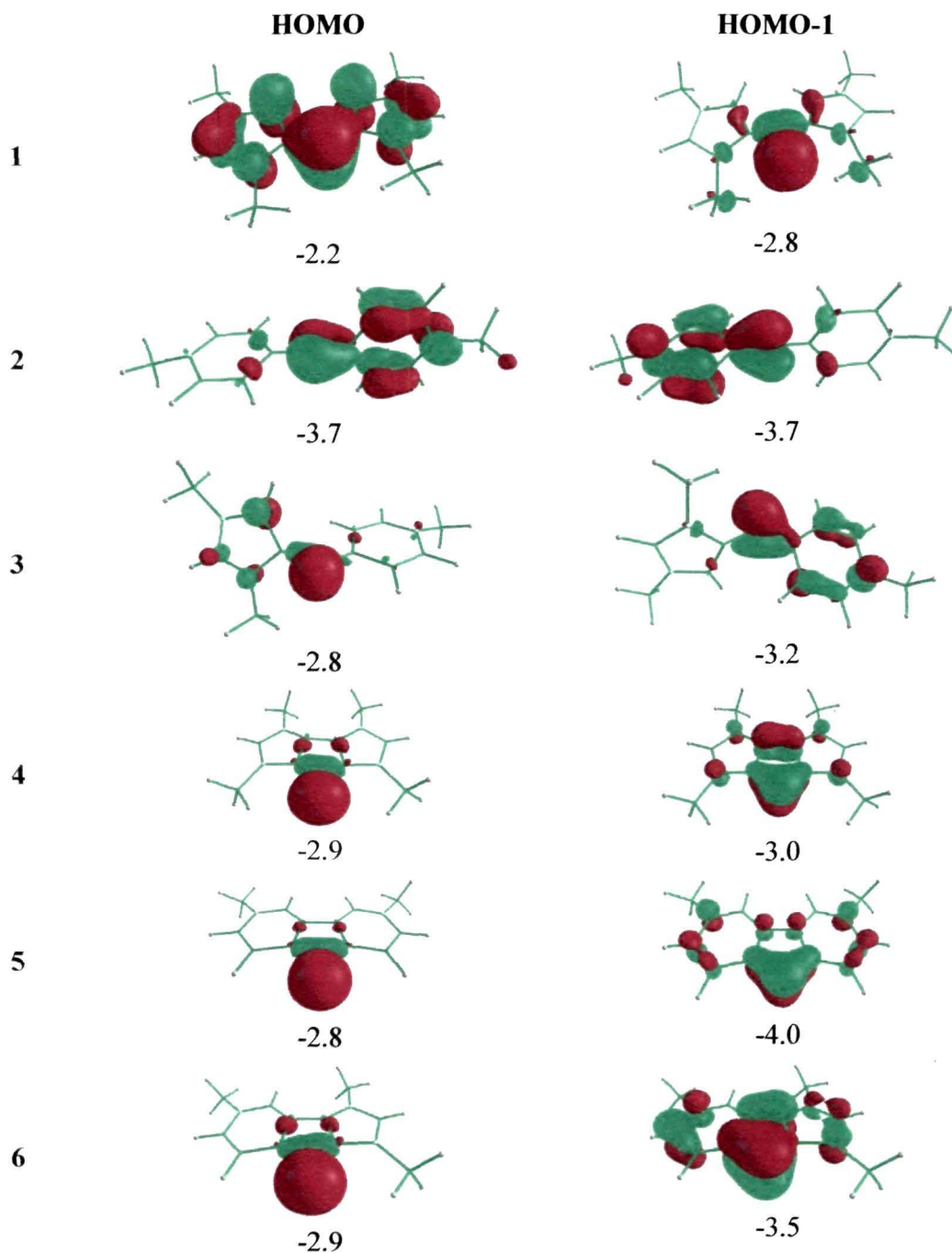


Figure 4.2.2. Energies (eV) and shapes of the highest occupied molecular orbitals for **1 – 6** at BP86/TZVP level of theory.

[4.2.2.3] Proton Affinities

It is evident from Figure 4.2.2 that all these carbodicarbenes are highly basic and hence, we have also calculated the first and second proton affinity of these molecules (Table 4.2.1). The values of the first proton affinity for **1** – **6** which refers to the protonation at the σ

Table 4.2.1. First (E_{PA-1}) and second (E_{PA-2}) proton affinities in kcal mol⁻¹ calculated at BP86/TZVP level of theory.

Entry	E_{PA-1}	E_{PA-2}
1	311.9	183.6
2	290.6	162.9
3	306.7	170.6
4	313.4	168.3
5	312.0	150.3
6	311.5	158.7
C(PMe₃)₂	279.5	160.4
NHC_{Me}	258.7	76.0

symmetric lone pair orbitals are very high, and in fact higher than that of C(PMe₃)₂. The C₀ atoms of all the first protonated derivatives are in the same plane with the two carbenic carbon atoms and the proton indicating that first protonation takes place at the σ symmetric lone pair orbital (Fig 4.2.3). Thus, carbodicarbenes **1** – **6** are predicted to be very basic and the basicity of acyclic ones are comparable to that of the cyclic derivatives. Interestingly, the C₀ atom of **1** – **6** has significant negative charge even after first protonation, thus supporting the description of donor-acceptor interaction L → C ← L. The second proton affinity values for **1** – **6** are also very high and close to that obtained for C(PMe₃)₂. A nice correlation between the orbital energies and proton affinities of **1** – **6** is obtained (Figure 4.2.4). However, the second proton affinity values for **1** – **3** are slightly larger than those obtained for their cyclic derivatives **4** – **6**. This can be traced to the lower energies of the π symmetric lone pair orbital (HOMO) of the first protonated derivatives of **4** – **6**. Interestingly, second proton affinity values for **1** – **6** are nearly double than that of *N*-methylated NHC, NHC_{Me}. It should be noted that the second proton affinity values, more precisely, has been used to distinguish a divalent C(II) specie (carbene) from divalent C(0) specie (carbones).⁸ As these carbodicarbenes **1** – **6** have very high values of second proton affinity, hence, they may safely be considered as carbon(0) compounds. Moreover, the calculated first proton affinity values of **1** – **6** reveal that they are better σ donors than the carbon(0) compounds supported by normal NHCs.³⁹

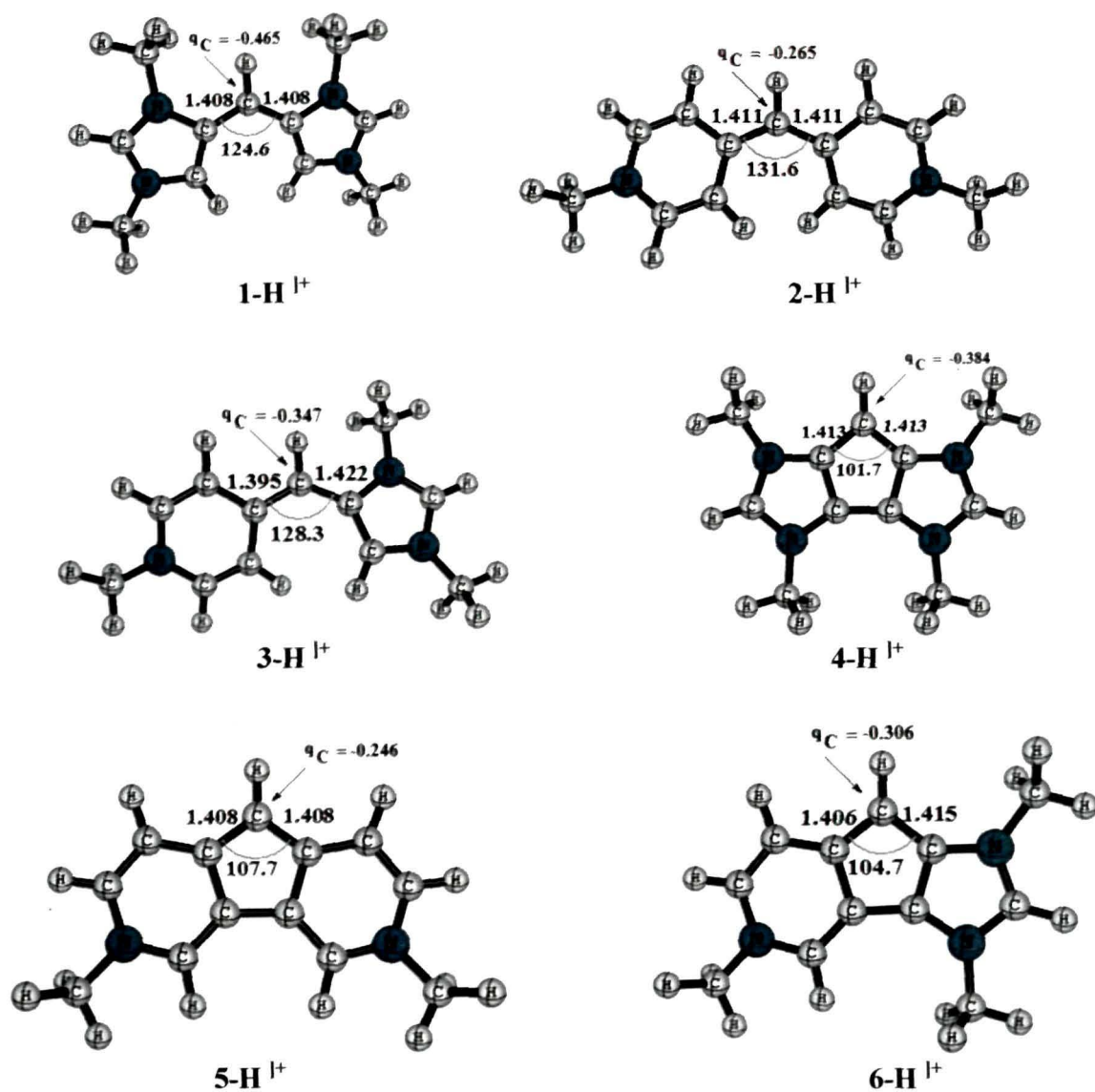


Figure 4.2.3. Optimized geometries of the first protonated derivatives of the molecules 1 – 6 at BP86/TZVP level of theory. Bond lengths are in Å and angles are in degrees. q_C represents the natural charge at the central carbon atom.

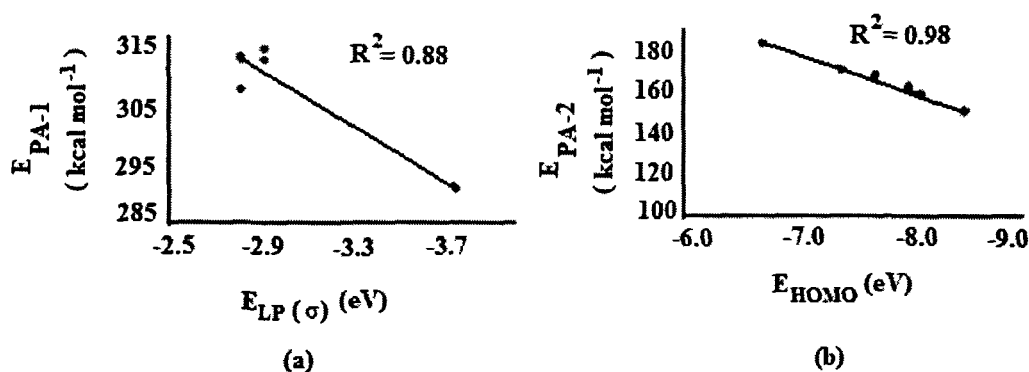


Figure 4.2.4. Correlation plot between (a) first proton affinity and energy of the σ symmetric lone pair orbital, and (b) second proton affinities and energies of the π symmetric HOMO of the first protonated derivatives of **1** – **6**.

[4.2.2.4] Donor-Acceptor Bond Strengths and Thermodynamic Stabilities

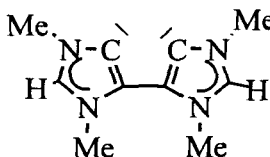
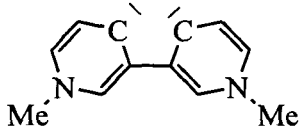
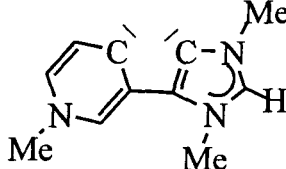
The strength of the carbon-ligand bond is an important aspect for these compounds.^{6c} Thus, we have calculated the bond dissociation energies (BDE) of the carbon-ligand bonds of **1** – **6** using the reaction (1). It should be noted that the L^1 and L^2 groups are identical except for **3** and **6**. Since, reaction (1) is spin-forbidden as the ligands L have singlet ground states



while the carbon atom has a triplet ground state, we added the triplet-singlet $C(^3P) \rightarrow C(^1D)$ excitation energy (42.1 kcal mol⁻¹ calculated at BP86/TZVP level of theory) with the reaction energies to minimize the error. Table 4.2.2 contains the BDEs for **1** – **6** including this correction.

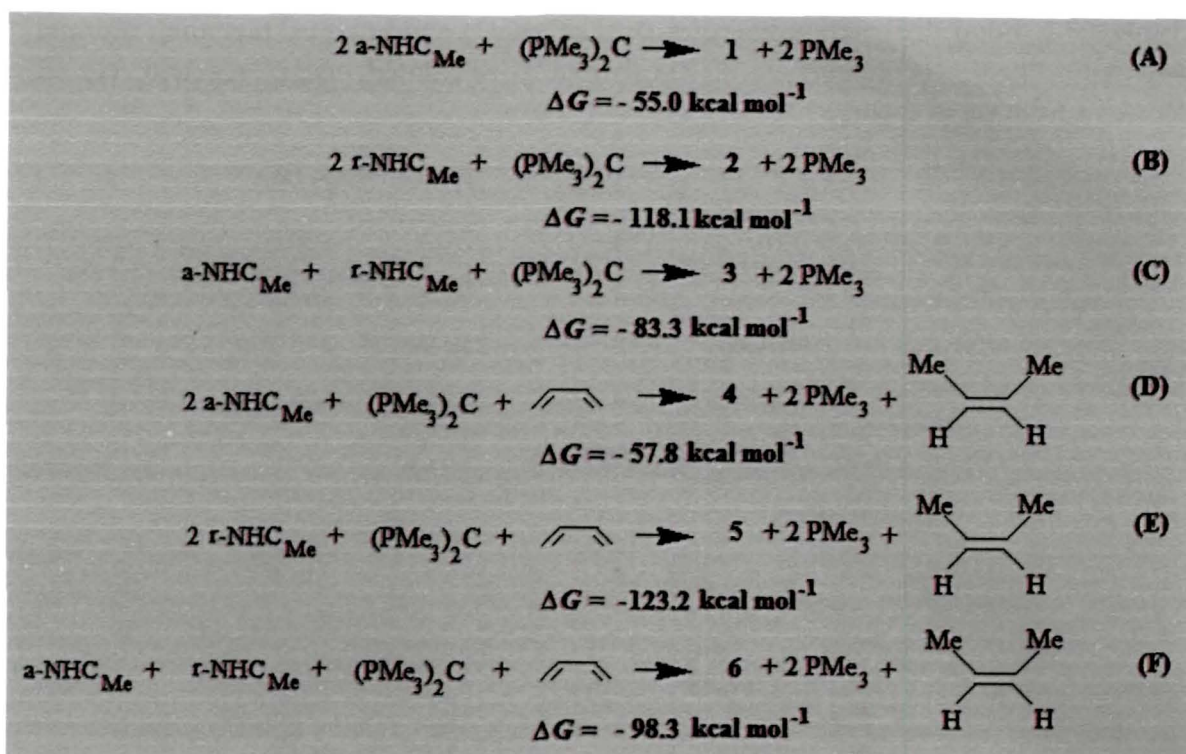
It is evident from Table 4.2.2 that the calculated BDEs are quite large. The calculated BDEs of **1** – **3** indicate that carbodicarbene **2** formed by the two remote NHCs ($rNHC_{Me}$) have the strongest bonds while the weakest is found in **1** which is formed by two abnormal NHCs ($aNHC_{Me}$). The bonds formed between the C_0 atom and the C_c atom of $rNHC_{Me}$ is so strong that it results in a linear geometry for **2** (Fig 4.2.1). The BDE of **3** lies in between that of **1** and **2**. The BDEs of the cyclic derivatives **4** – **6** follow the same trend as their acyclic counterparts. However, the calculated BDE values for the cyclic derivatives are somewhat smaller than that of their acyclic counterparts. This might be due to the fact that the calculation of BDEs for **4** – **6** were carried out by considering the more stable *trans* geometry

Table 4.2.2. Bond dissociation energies D_e (kcal mol⁻¹) and energies including thermal and vibrational corrections D_0^{298} (kcal mol⁻¹) calculated using reaction (1) at BP86/TZVP level of theory.

L^1	L^2	Entry	D_e	D_0^{298}
a-NHC _{Me}	a-NHC _{Me}	1	221.2	220.6
r-NHC _{Me}	r-NHC _{Me}	2	285.9	284.2
a-NHC _{Me}	r-NHC _{Me}	3	250.9	248.7
		4	193.6	186.4
		5	255.4	246.5
		6	228.7	220.2

(with respect to the two lone pairs centered on the carbenic carbon) of the L group. Formation of **4** – **6** requires rotation of the central C-C bond of the L groups which lowers the BDEs.

The thermodynamic stabilities of **1** – **3** are ascertained by using the reactions **A-C**, while the thermodynamic stabilities of **4** – **6** are ascertained using reactions **D-F** (at BP86/TZVP level). The energetic of these reactions reveal that the formations of **1** – **6** are highly exergonic implying their high thermodynamic stability.



[4.2.2.5] Complexation Energies

Since dimetallation was used as a criteria to ascertain the presence of C(0) character in a given ligand,^{19,20} therefore, we checked the possibility of complexation of **1** - **6** with one and two molecules of AuCl. Table 4.2.3 contains the bond dissociation energies of mono and diaurated complexes of **1** - **6**. It is evident from Table 4.2.3 that the BDE for the dissociation

Table 4.2.3. Calculated bond dissociation energies in kcal mol⁻¹ (including zero-point vibrational correction) for the dissociation of one molecule of AuCl from N-AuCl and N-(AuCl)₂ respectively [N = 1 - 6].

N	N-AuCl → N + AuCl	N-(AuCl) ₂ → N-AuCl + AuCl
1	81.8	59.9
2	67.8	46.5
3	83.2	48.1
4	93.7	53.4
5	93.5	46.1
6	93.4	48.5

of one molecule of AuCl from N-AuCl (N = **1** - **3**) are almost equal for **1**-AuCl and **3**-AuCl while it is slightly lower for **2**-AuCl. The BDE for the dissociation of one molecule of AuCl from N-AuCl (N = **4** - **6**) suggest that the binding of AuCl to the cyclic derivatives **4** - **6**

takes place with slightly greater strength than their acyclic counterparts **1** – **3**. The binding of AuCl to **1**-AuCl and **4**-AuCl takes place with slightly greater strength while it takes place with almost equal strengths to other mono aurated complexes. However, the BDEs for the dissociation of AuCl from N-(AuCl)₂ are significant enough for the possible isolation of the gem dimetalated derivatives of **1** – **6**. The optimized geometries (Fig 4.2.5) of all the monoaurated complexes show almost similar structural behaviour. The computed Au-C distances in these monoaurated complexes do not vary significantly (2.0 – 2.05 Å). The most interesting structural feature shown by the gem diaurated complexes is the presence of an aurophilic interaction in all the complexes.²¹ The computed Au-Au distance is found to be shortest for **5**-(AuCl)₂ (2.756 Å) while the longest is found for **1**-(AuCl)₂ (3.369 Å). The computed Au-Au distances of the cyclic carbodicarbenes are shorter than those obtained for acyclic ones. However, no correlation has been obtained between BDEs and Au-Au distances in these diaurated complexes which is in agreement with recent theoretical calculations.³³

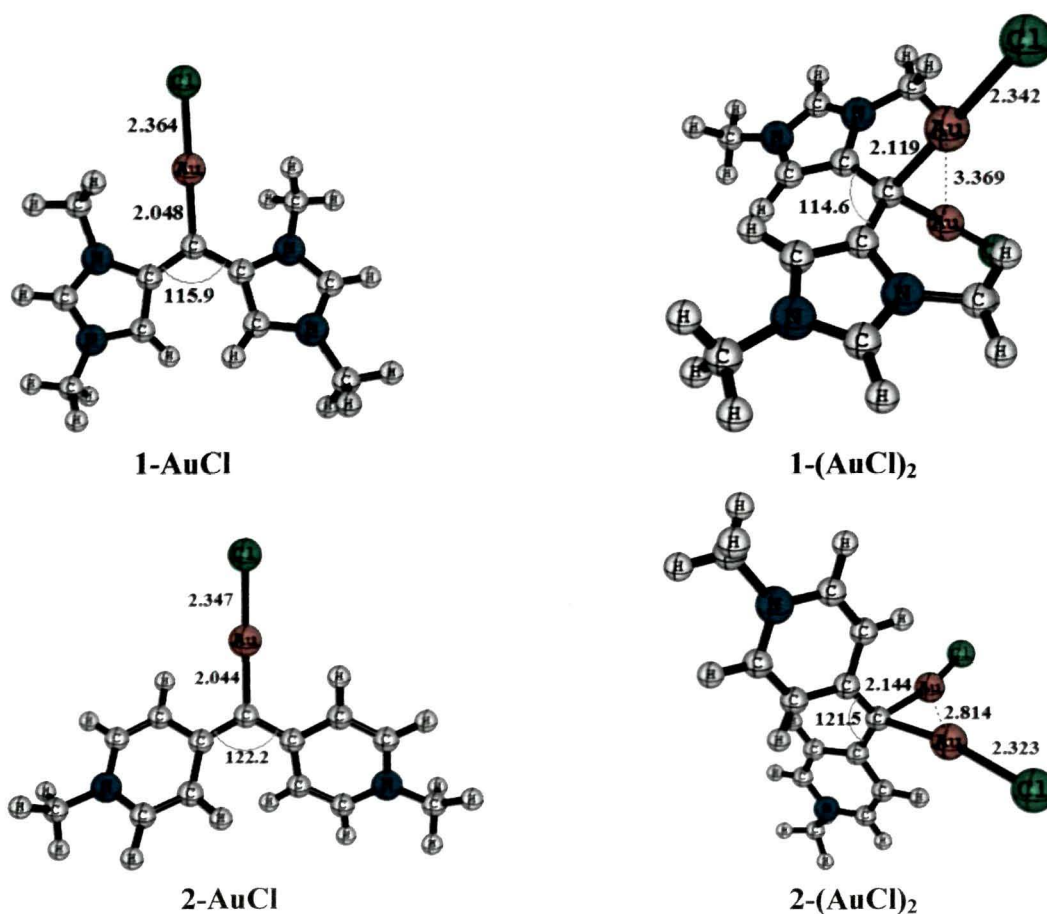
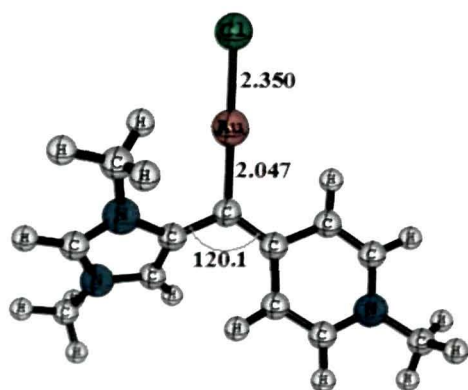
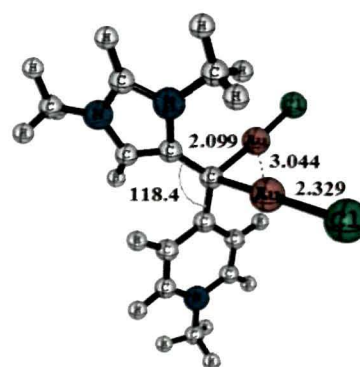


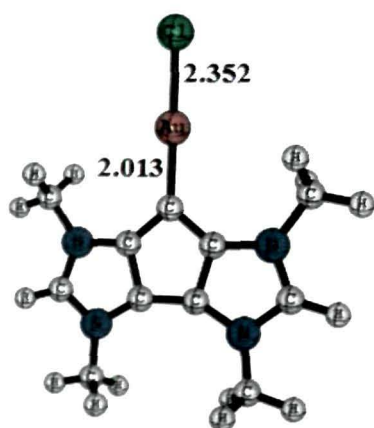
Figure 4.2.5. Lowest energy optimized geometries of N-AuCl and N-(AuCl)₂ (N = 1 – 6) calculated at BP86/TZVP level of theory. Bond lengths are in Å and angles are in degrees.



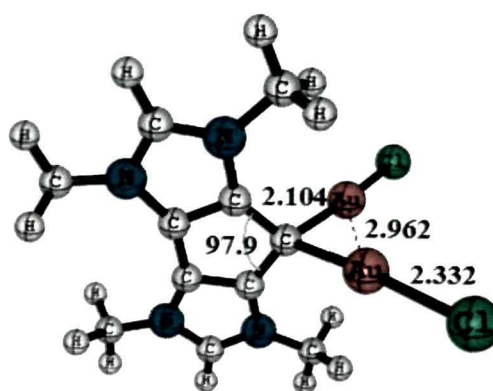
3-AuCl



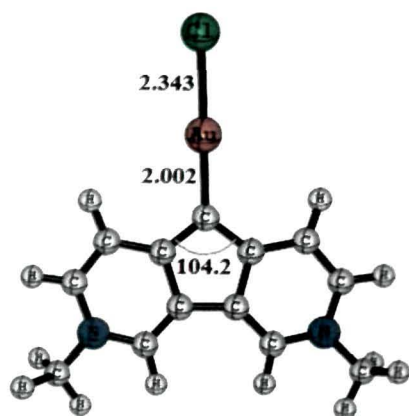
3-(AuCl)₂



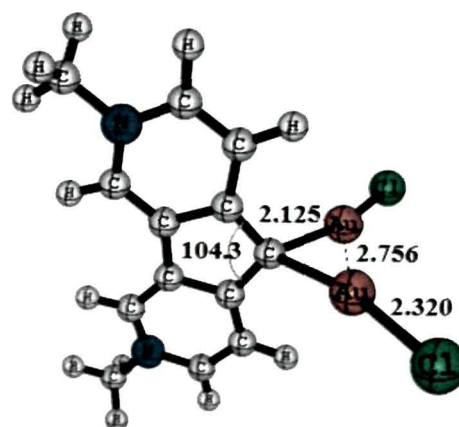
4-AuCl



4-(AuCl)₂



5-AuCl



5-(AuCl)₂

Figure 4.2.5. (Continued).

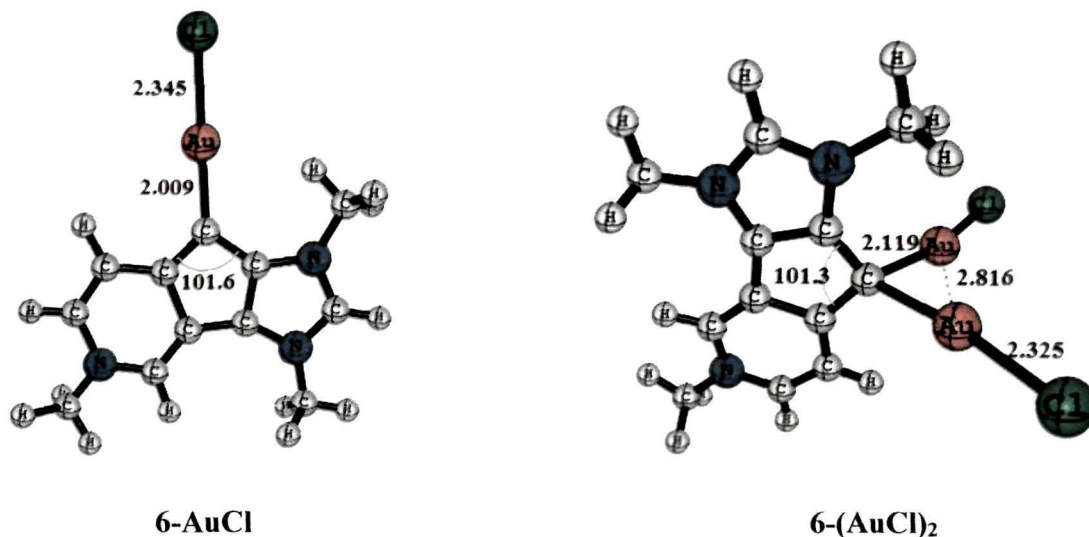


Figure 4.2.5. (Continued).

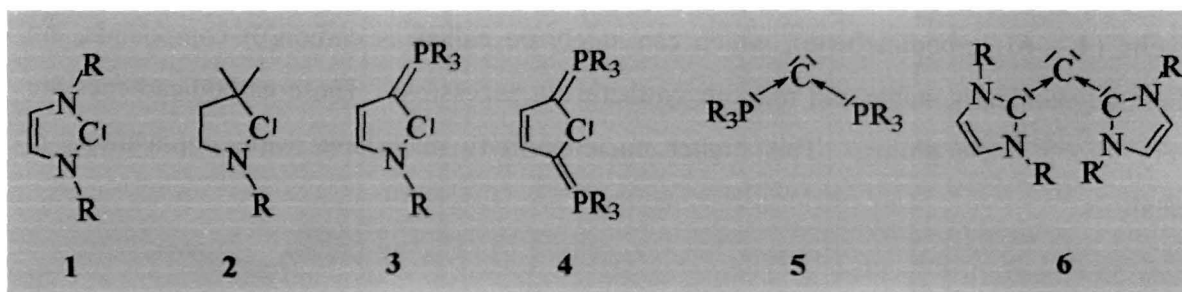
[4.2.3] Conclusions

Differential coordination modes of *N*-heterocyclic carbenes such as abnormal, remote etc. are one of the unique features of this ligand. In this report, we emphasized the role of these differential coordination modes in stabilizing a central carbon atom in a formal oxidation state of zero. Quantum chemical calculations predict that both acyclic (**1 – 3**) and cyclic (**4 – 6**) carbodicarbenes, which can safely be called as carbon(0) compounds, are thermodynamically stable and may be synthetically accessible. These carbodicarbenes are very strong nucleophiles. This higher nucleophilicity may have wide implications in catalysis.³⁴

[4.3] Reactivity of Different Carbon Bases

[4.3.1] Introduction

Usual organic compounds are composed of carbon atoms where all the four valence electrons of it are involved in bonding. A rather unusual situation where only two of its valence electrons are involved in bonding as in carbenes, CR_2 , is now known.¹ This bonding situation in carbenes results in retention of the remaining two electrons in the same orbital to form a lone pair (singlet carbenes), they may occupy different orbitals with opposite spins to form excited singlet states (open-shell singlet) or they may occupy different orbitals with same spin (triplet carbenes). Although the parent carbene CH_2 has a triplet ground state,³⁵ stable singlet carbenes containing a lone pair of electrons are also known.¹ One such classic example of a stable singlet neutral carbene is *N*-heterocyclic carbene (NHC), **1** (Scheme 4.3.1).^{1a} NHCs are excellent σ donor owing to which it can substitute some of the classical two electron donor ligands such as amines and phosphanes. Although the σ donation ability of NHCs are well explored,³⁶ recent theoretical^{26a} and experimental^{27b-d} studies suggest that NHCs have π donating and accepting abilities too. Thus, NHCs can be considered as both σ and π donor as well as π acceptor.



Scheme 4.3.1. *N*-heterocyclic carbene **1**, cyclic(alkyl)(amino)carbene **2**, (amino)-(ylide) carbene **3**, carbocyclic carbene stabilized by two ylides **4**, carbodiphosphorane **5** and carbodicarbene **6**. R = Me.

Both steric and electronic factors have been used to stabilize carbenes. Among them, the most common mode of stabilization is the use of π donating as well as σ withdrawing substituents attached to the carbenic centre. One such substituent is the amino group which has good π donating as well as σ withdrawing ability owing to the presence of a lone pair of electrons and high electronegativity respectively. However, the presence of electronegative nitrogen atoms somehow render the carbenic centre slightly electron poor due to the larger

negative inductive (-I) effect of nitrogen. This results in a lower basicity of NHCs. Thus, it is expected that replacement of nitrogen atom by more electropositive atom (such as carbon) may increase the basicity of these NHCs. One such example where one of the amino nitrogen atom has been replaced by a carbon atom is cyclic(alkyl)(amino)carbene **2**, commonly known as CAAC,^{37,38} which is found to be more basic than **1**.³⁹ Another way to enhance the basicity of carbenes is to introduce ylide centres adjacent to the carbenic carbon atom.⁴⁰ The larger π donating ability and smaller -I effect of the phosphorous ylide than that of amino nitrogen result in more electron density at the carbenic carbon. This results in an enhanced basicity of carbenes. Several (amino)-(ylide) carbenes (AYC), **3** are now been reported which contain single ylide centre.⁴⁰ Hence, it is expected that introduction of two ylides (as in **4**) may further enhance the basicity of carbenes.

On the other extreme, a recent electronic structure study further revealed that it is also possible for carbon atoms within stable molecules to use none of its valence electrons, thereby forming stable divalent carbon(0) compounds, carbones (CL₂).⁶⁻⁸ The bonding situation in these carbon(0) compounds, CL₂ is described as donor-acceptor type, L→C←L,⁶⁻⁸ which results in the retention of two lone pairs of electrons unlike carbon(II) compounds (carbenes) which possess only a single lone pair. Thus, carbones can bind two Lewis acids due to the presence of two lone pairs,⁶⁻⁸ whereas carbenes usually bind to only one. Moreover, carbones possess a very high value of first and, more precisely, second proton affinity which has been used as a decisive indicator to distinguish carbones from carbenes.⁸ Very recently, Frenking *et. al.* has suggested the use of other reactivity parameter such as complexation with one and two molecules of AuCl to distinguish a carbon(0) from a carbon(II) compound.²⁰ However, in the same study, they have also shown that the diaurated derivative of NHC [NHC-(AuCl)₂] has two η^1 bonded Au atoms with moderate bond strength that might be large enough for their possible isolation.²⁰ This has raised some intriguing questions: (i) Does a high value of second proton affinity really distinguish a carbene from a carbene? (ii) Does complexation with Lewis acids provides clue to the carbon(0) or carbon(II) character of these Lewis bases? (iii) If not then, what other criterion should be used to distinguish a carbene from carbene? To address these questions, quantum mechanical calculations have been carried out on the following closed-shell singlet carbenes (**1-4**) and carbones (**5-6**) as shown in Scheme 4.3.1.

[4.3.2] Results and Discussion

Figure 4.3.1 shows the frontier molecular orbitals of 1-6. It is evident from Figure 4.3.1 that the occupied π molecular orbital of all these molecules are delocalized to the neighbouring atoms, and thus appears quite similar. The trend in energies of the σ and π donating orbitals of 1-6 can be explained by invoking the -I effect and π donating abilities of the groups attached to carbenic centre. Decrease in the -I effect of the substituents attached to the carbenic carbon increases the σ donation abilities of these carbenes. On the other hand, increase in the π donating abilities of the groups attached to the carbenic centre increases the π donating abilities of these carbenes. Thus, replacement of an electronegative nitrogen atom of 1 by a more electropositive carbon atom as in 2 increases the σ donation ability. However, the lack of π donating ability of one substituent ($-\text{CR}_2$) in 2 results in lower π donating ability of the molecule (2) itself. As a consequence, the π accepting ability of 2 increases. Due to the smaller -I effect and larger π donating abilities, introduction of ylide centres increases both the σ and π donation abilities of carbenes. Thus, compound 3 is more basic than 1 and 2. Introduction of two ylides as in 4, further increases such abilities of carbenes. However, their π acceptance abilities are comparable to that of 1.

As expected, compound 5 and 6 are very good σ and π donors. Remarkably, 3 and 4 have almost equal (or higher) σ and π donation abilities as that of 5 and 6 (Figure 4.3.1). Thus, introduction of ylide centres adjacent to the carbenic carbon renders the basicities of these carbenes comparable to that of known carbon(0) compounds, 5 and 6. However, these carbenes 1-4 have moderate to strong π accepting abilities unlike 5 and 6 which are poor π acceptors owing to the very high energy of the π^* orbital (Figure 4.3.1). As the basicity of 3 and 4 are comparable to that of 5 and 6, it is also expected that they will show similar reactivities. Hence, we also calculated their first and second proton affinities as well as the complexation energies with one and two molecules of AuCl (Table 4.3.1).

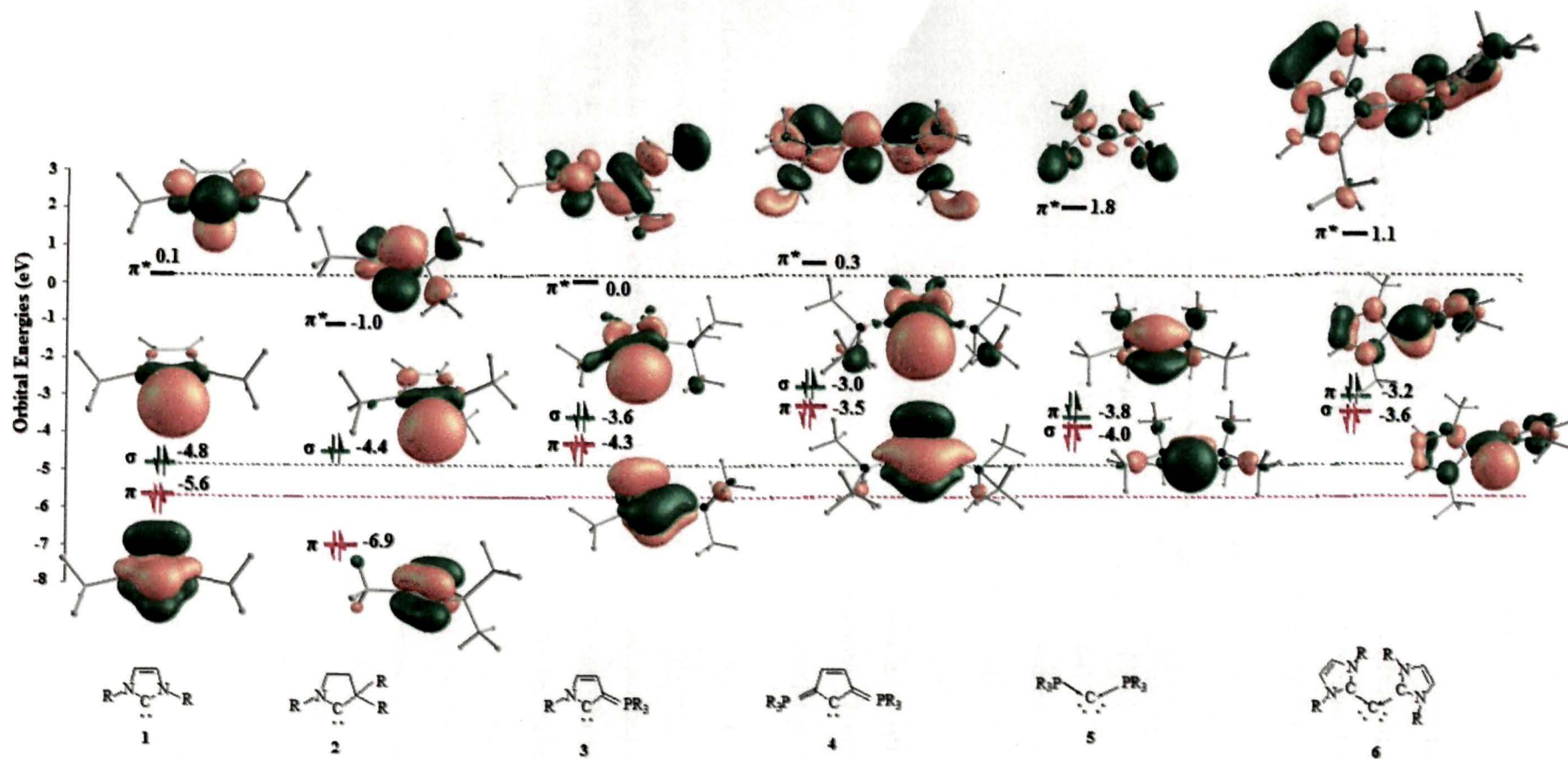


Figure 4.3.1. Important frontier molecular orbitals of 1-6. Energies are in eV. R = Me.

Table 4.3.1 contains the computed natural charge at the central carbon atom, proton affinity values and bond dissociation energies (BDE) for the dissociation of one molecule of

Table 4.3.1. Computed natural charge at the central carbon atom (q_C), first and second proton affinities (PA, in kcal mol⁻¹) and bond dissociation energies (BDE in kcal mol⁻¹) for the dissociation of one molecule of AuCl from L-AuCl and L-(AuCl)₂. All the energies include zero point vibrational correction.

L	q_C	PA-1	PA-2	BDE-1	BDE-2
1	0.042	258.7 ^[a]	76.0	76.4	35.0
2	0.090	262.4	^[b]	80.3	35.7
3	-0.160	290.2	124.9	89.5	41.8
4	-0.368	310.5	161.8	98.5	48.4
5	-1.419	279.5	160.4	72.0	62.3
6	-0.499	287.4	169.8	72.2	50.8

[a] Literature value of PA-1 for **1**(R = Me) is 258.3 kcal mol⁻¹ using CBS-QB3 method.^{35c} [b] Optimization of the second protonated specie leads to a broken geometry where ring opening of the five membered ring takes place.

AuCl from L-AuCl and L-(AuCl)₂, (L = 1-6). It is evident from Table 4.3.1 that introduction of ylide increases the nucleophilicity of the carbenic carbon as revealed by the increase in negative charges. The highest and lowest first proton affinity values are calculated for **4** and **1** respectively, which can be traced to their respective σ donation abilities (Figure 4.3.1). The first protonated derivatives of all these molecules are perfectly planar at the central carbon atom (Figure 4.3.2) indicating that protonation takes place at the σ symmetric orbital.

Thus, the energy of the σ symmetric lone pair orbital dictates the value of first proton affinity and in fact, a nice correlation has been obtained between the energies of the σ symmetric lone pair orbital and first proton affinity (Figure 4.3.3).

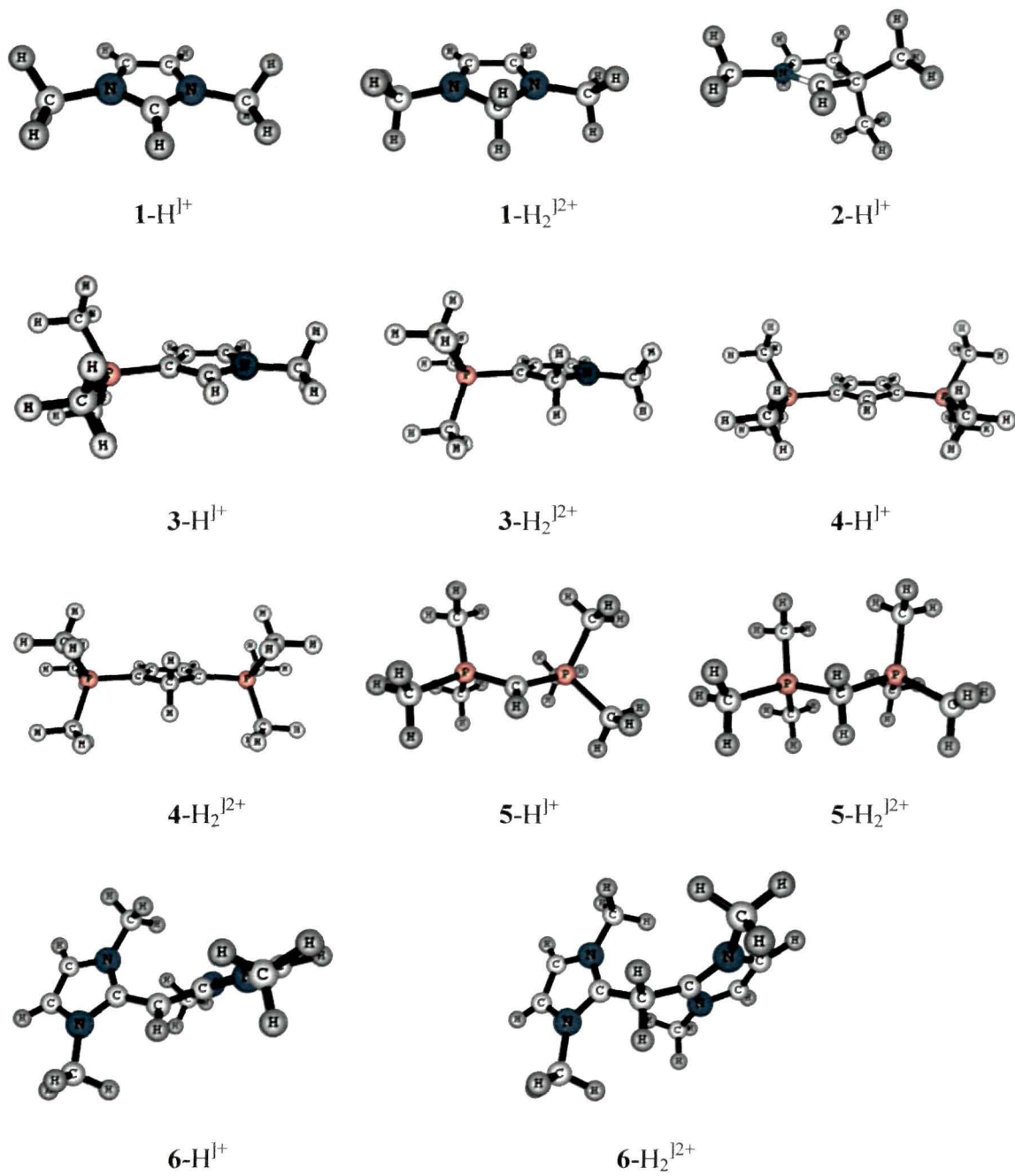


Figure 4.3.2. Optimized geometries of the first and second protonated species of 1-6. The optimized geometry of the second protonated species of 2 is not shown as optimization leads to a broken geometry.

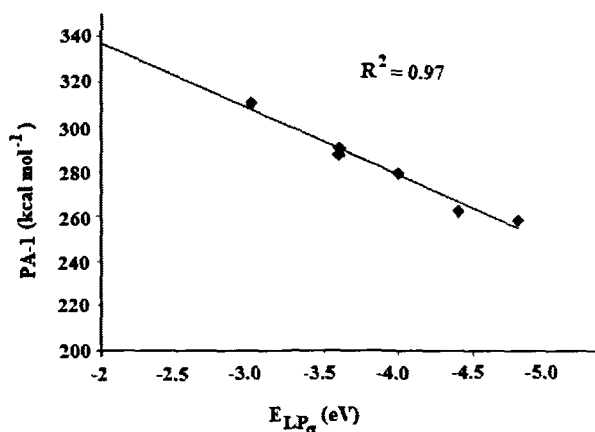


Figure 4.3.3. Correlation plot between the energy of the σ symmetric lone pair orbital and first proton affinity.

We reason that more attention should be given to the second proton affinity values as a higher value of second proton affinity was proposed to distinguish a carbene from carbene.⁸ As expected, the calculated value of second proton affinity for **1** is quite low. Interestingly, the second proton affinity values increase dramatically as ylide centres are introduced adjacent to the carbenic centre. In fact, the second proton affinity value of **4** is very close to that obtained for **5** and **6**. A nice correlation has been obtained between the energies of the lone pair orbital of the first protonated species and second proton affinity values (Figure 4.3.4). Thus, it is apparent that while it is easy to distinguish a normal heterocyclic

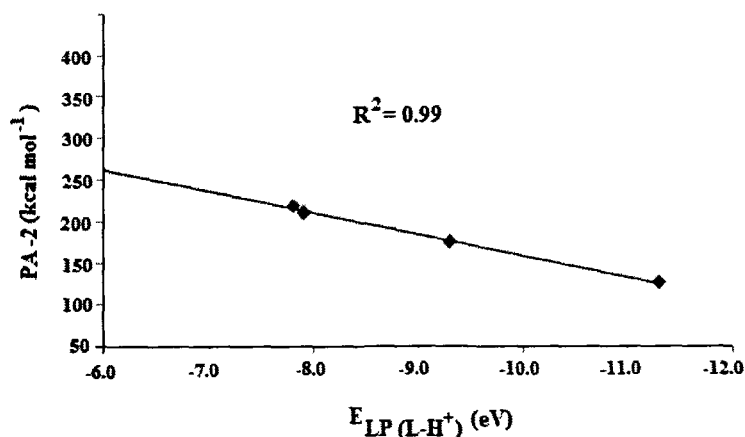


Figure 4.3.4. Correlation plot between the energy of the lone pair orbital of the first protonated species and second proton affinity.

carbene (e. g., **1** and **2**) from a carbene, the distinction becomes blurred with the increase in basicity of carbenes. While the high basicity associated with carbon(0) compounds can be traced to the presence of two high energy lone pair orbitals, the same for carbon(II) compounds are related to the presence of a high energy lone pair orbital at the carbenic centre as well as a $3c-2e$ π donor orbital.

A recent experimental study conducted by Fürstner *et. al.* suggested that divalent carbon compounds of the type CR_1R_2 should be considered as carbenes if they form stable complexes as $[R_1R_2C(AuCl)_2]$.¹⁹ This has been substantiated further by recent theoretical calculations.²⁰ Optimized geometries of all the monoaurated complexes (Figure 4.3.5) are found to be in η^1 form. Although the optimized geometry of the second protonated species of

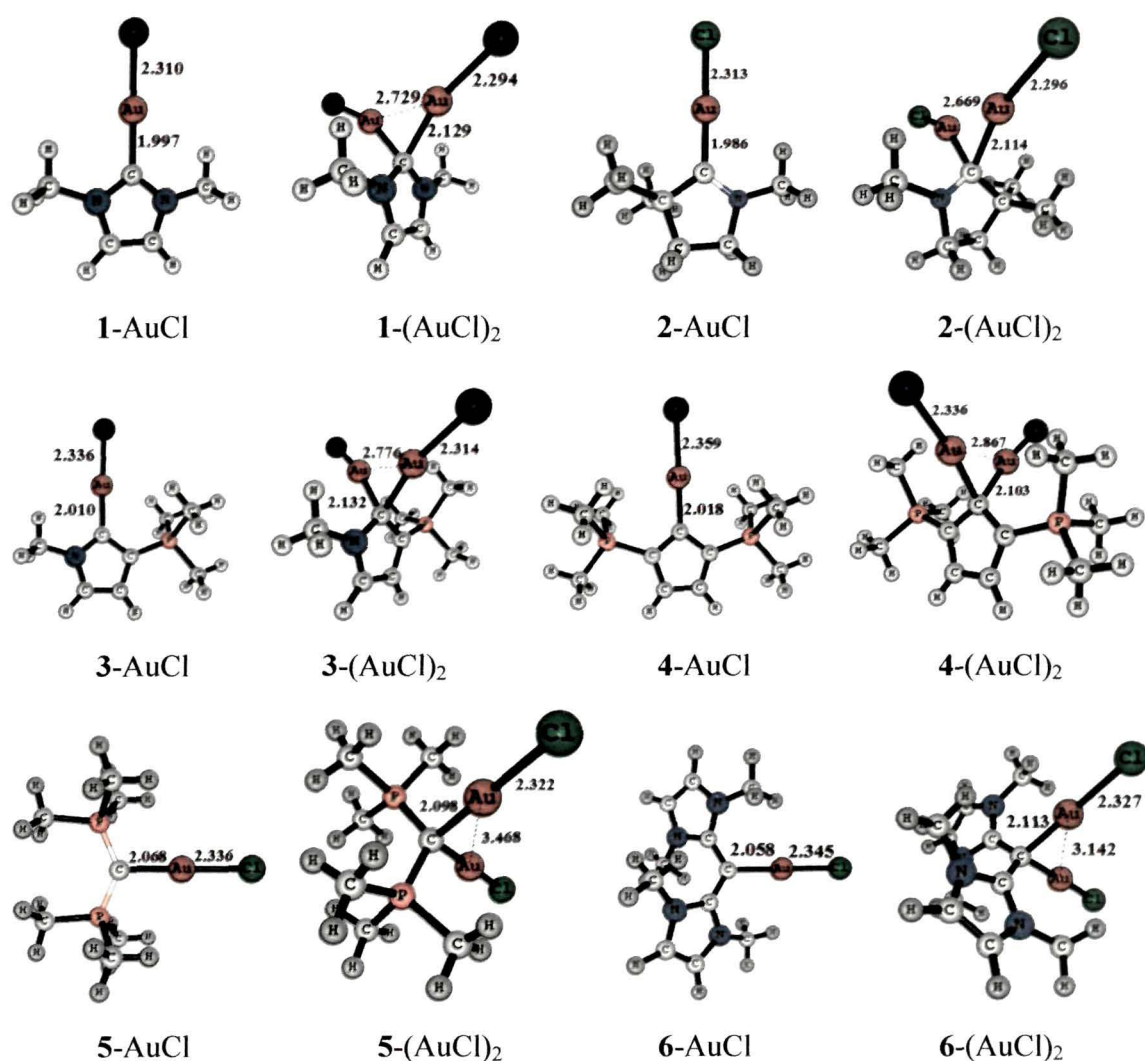
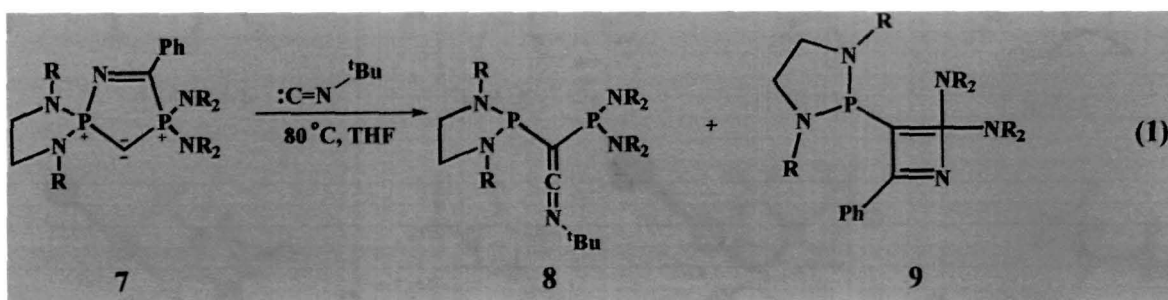


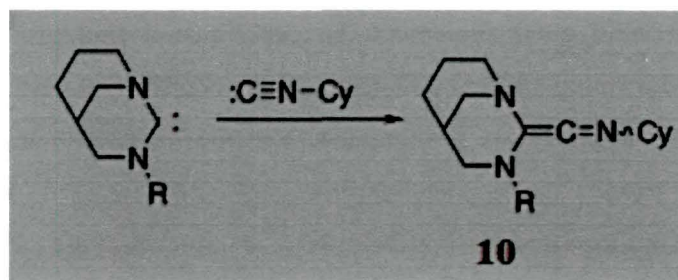
Figure 4.3.5. Optimized geometries of mono and diaurated complexes of **1-6**. Bond lengths are in Å.

2 is found to have a broken geometry, the same for the diaurated species of **2** is found to be intact. This might be due to the presence of aurophilic interaction²² (Au-Au distance in **2**-(AuCl)₂ is found to be 2.668 Å, Figure 4.2.5) which is believed to stabilize higher coordination numbers.²² The calculated bond dissociation energy (BDE-1) for the dissociation of one molecule of AuCl is found to be the highest for **4** and lowest for **6**. All these diaurated complexes are found to be in η^1 form stabilized by aurophilic interactions.²¹ The calculated value of BDE-2 for the dissociation of one molecule of AuCl from **4**-(AuCl)₂ is very close to that calculated for **5** and **6**. Thus, introduction of ylide groups not only increases the value of the second proton affinity but also increases the possibility of dimetallation.

Thus, it is apparent from the above considerations that both carbenes and carbenes may show similar reactivity towards electrophiles such as H⁺ and AuCl. This is expected because of the basic nature of both these class of compounds. However, unlike carbenes, carbenes are ambiphilic in nature due to the presence of a lone pair and a suitable low energy π^* orbital. Accordingly, carbenes are more prone to nucleophilic attack than carbenes. In fact, it has been demonstrated that carbenes react with various electrophiles (CO₂, SO₂, etc).^{41,6a,2c} However, carbenes may not form stable complex with nucleophiles. For example, Baceiredo and coworkers⁴² reported a reaction (1) between cyclic carbodiphosphorane **7** with a nucleophile (*tert*-butyl isocyanide) where **7** decomposes to produce the rearranged products **8** and **9**. This reaction further reveals that the nucleophile prefers to bind to the diphosphinocarbene resulting in the formation of a carbene adduct **8**. On the other hand,

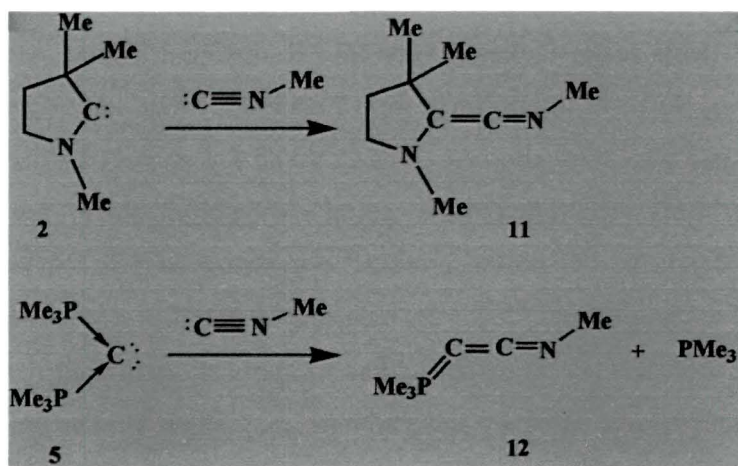


electrophilic carbenes readily undergoes nucleophilic attack as evidenced by the formation of keteneimine **10** (Scheme 4.3.2).³⁹ In view of these experimental reports, we set out to check how the molecules considered in this study will behave when subjected to attack by a nucleophile. We have chosen CAAC **2** and carbodiphosphorane **5** as the representative



Scheme 4.3.2. Nucleophilic addition reaction of electrophilic carbene.³⁹

carbene and carbene molecules respectively, and considered their reaction with methyl isocyanide. On full geometry optimization, **2** yields the expected adduct **11** while **5** undergoes P-C bond cleavage giving rise to a phosphinocarbene adduct **12** and a free PMe_3 molecule (Scheme 4.3.3, optimized geometries of **11** and **12** are shown in Figure 4.3.6).



Scheme 4.3.3. Theoretically calculated nucleophilic addition reactions of **2** and **5** yielding **11** and **12** respectively.



Figure 4.3.6. Optimized geometries of the adducts **11** and **12**.

Thus, our calculation is in good agreement the experimental findings and confirms the inability of carbones in forming adducts with nucleophiles. Further support for the absence of π accepting ability of carbones may be obtained from the metal-carbon distances in their transition metal complexes.^{2f, 42} The metal-carbon bonds (Pd-C: 2.12 Å; Rh-C: 2.11 Å) are significantly longer than those reported for metal-NHC complexes (Pd-C: 2.00 Å; Rh-C: 2.06 Å).^{2f} Despite being slightly weaker donor, metal-NHC distances are significantly stronger and are due to π donation from the metal to the formally vacant carbenic p_{π} orbital.

[4.3.3] Conclusions

To summarize, the increase in the energy of σ and π symmetric frontier occupied molecular orbitals of ylide stabilized carbenes and their consequent reactivities, e. g., very high value of second proton affinity as well as complexation energy, places them at par with known carbon(0) species such as carbodiphosphorane (**5**) and carbodicarbene (**6**). Such similar reactivity patterns really makes it very hard to distinguish these carbon(II) species from carbon(0) ones. However, it is evident from Figure 4.3.1 that, unlike carbones **5** and **6**, carbenes also possess π accepting abilities. Indeed, while **1-4** possess a suitable low lying π symmetric vacant orbital concentrated at the central carbon atom, such a low energy orbital was not found for **5** and **6**. Thus, the presence or absence of a low lying π symmetric molecular orbital is a *key* electronic feature which may distinguish a carbene from carbone. The presence or absence of π accepting ability has an implication on their reactivity towards nucleophiles. Although both carbenes and carbones may show similar reactivity towards electrophiles, they behave differently when subjected to nucleophilic attack.

[4.4] Bibliography

1. (a) Arduengo, A. J. et. al., *J. Am. Chem. Soc.*, **113** (1), 361-363, 1991. (b) Baceiredo, A. et. al., *J. Am. Chem. Soc.* **107** (16), 4781-4783, 1985. (c) Bertrand, G. et. al., *J. Am. Chem. Soc.* **110** (19), 6463-6466, 1988.
2. (a) Bertrand, G. et. al., *Angew. Chem. Int. Ed.* **47** (17), 3206-3209, 2008. (b) Fürstner, A. et. al., *Nat. Chem.* **1**, 295-301, 2009. (c) Alcarazo, M. *Dalton Trans* **40**, 1839-1845, 2011. (d) Kaufhold, O., & Hahn, F. E. *Angew. Chem. Int. Ed.* **47** (22), 4057-4061, 2008. (e) Dyker, C. A., & Bertrand, G. *Science* **321**, 1050-1051, 2008. (f) Bertrand, G. et. al., *Angew. Chem. Int. Ed.* **49** (47), 8810-8849, 2010.
3. Ramirez, F. et. al., *J. Am. Chem. Soc.* **83** (16), 3539-3540, 1961.
4. Hardy, G. E. et. al., *J. Am. Chem. Soc.* **100** (25), 8001-8002, 1978.
5. (a) Vicente, J. et. al., *Organometallics* **21** (26), 5887-5900, 2002. (b) For the first synthesis of a *gem*-dimetallated carbodiphosphorane see: Schmidbaur, H., & Gasser, O. *Angew. Chem. Int. Ed.* **15** (8), 501-502, 1976.
6. (a) Frenking, G. et. al., *Inorg Chem.* **44** (5), 1263-1274, 2005. (b) Tonner, R., & Frenking, G. *Chem—Eur J.* **14** (11), 3260-3272, 2008. (c) Tonner, R., & Frenking, G. *Chem—Eur J.* **14** (11), 3273-3289, 2008. (d) Tonner, R., & Frenking, G. *Organometallics* **28** (13), 3901-3905, 2009. (e) Tonner, R., & Frenking, G. *Pure Appl. Chem.* **81** (4), 597-614, 2009. (f) Patil, D. S., & Bharatam, P. V. *Chem. Commun.* 1064-1066, 2009. (g) Kaufhold, O., & Hahn, F. E. *Angew. Chem. Int. Ed.* **47** (22), 4057-4061, 2008.
7. Tonner, R., & Frenking, G. *Angew. Chem. Int. Ed.* **46** (45), 8695-8698, 2007.
8. Frenking, G. et. al., *ChemPhysChem* **9** (10), 1474-1481, 2008.
9. Frenking, G., & Tonner, R. *WIREs Comput Mol Sci* 2011, DOI: 10.1002/wcms.53.
10. Fürstner, A. et. al., *Chem. Commun.* 2372-2373, 2001.
11. Weiss, R. et. al., *Angew. Chem. Int. Ed.* **37** (3), 344-347, 1998.
12. (a) Becke, A. D. *Phys Rev A.* **38** (6), 3098-3100, 1988. (b) Perdew, J. P. *Phys Rev B.* **33** (12), 8822-8824, 1986.
13. (a) Ahlrichs, R. et. al., *J. Chem. Phys.* **97** (4), 2571-2577, 1992. (b) Ahlrichs, R. et. al., *J. Chem. Phys.* **100** (8), 5829-5835, 1994.
14. Dolg, M. et. al., *J. Chem. Phys.* **86** (2), 866-872, 1987.
15. Kendall, R. A. et. al., *J. Chem. Phys.* **96** (9), 6796-6807, 1992.
16. Pople, J. A. et. al., Gaussian 03, revision D.01, Gaussian, Inc.: Pittsburgh, PA, 2004.

17. (a) Reed, A. E., & Weinhold, F. *J. Chem. Phys.* **78** (6), 4066-4072, 1983. (b) Reed, A. E. et. al., *J. Chem. Phys.* **83** (2), 735-747, 1985. (c) Reed, A. E. et. al., *Chem. Rev.* **88** (6), 899-926, 1988.
18. Schleyer, P. v. R. et. al., *J. Am. Chem. Soc.* **118** (26), 6317 – 6318, 1996.
19. (a) Fürstner, A. et. al., *Angew. Chem. Int. Ed.* **47** (17), 3210-3214, 2008. (b) Fürstner, A. et. al., *Chem-Eur. J.* **16** (32), 9746-9749, 2010.
20. Esterhuysen, C., & Frenking, G. *Chem-Eur. J.* **17** (36), 9944-9956, 2011.
21. Schmidbaur, H. *Gold Bull.* **33**, 3-10, 2000.
22. (a) Schmidbaur, H. et. al., *Angew. Chem. Int. Ed.* **27** (11), 1544-1546, 1988. (b) Schmidbaur, H. et. al., *Angew. Chem. Int. Ed.* **28** (4), 463-465, 1989.
23. (a) Sinclair, R. A., & Burg, A. B. *Inorg. Chem.* **7** (10), 2160-2162, 1968. (b) Zhang, Z. -Z. et. al., *J. Organomet. Chem.* **347**, 269-275, 1988. (c) Me'zailles, N. et. al., *J. Organomet. Chem.* **541**, 277-283, 1997. (d) Kamiński, R. et. al., *Phys. Chem. Chem. Phys.* **13** (26), 10280-10284, 2011.
24. Cotton, F. A., & Wilkinson, G. *Advanced Inorganic Chemistry*, 5th Ed.; Wiley: New York, 1988.
25. (a) Garrison, J. C. et. al., *Chem. Commun.* 1780-1781, 2001. (b) Catalano, V. J., & Malwitz, M. A. *Inorg. Chem.* **42** (18), 5483-5485, 2003. (c) Gischig, S., & Togni, A. *Organometallics* **24** (2), 203-205, 2005. (d) Zhang, X. et. al., *Organometallics* **27** (17), 4401-4406, 2008. (e) Han, X. et. al., *Organometallics* **29** (11), 2403-2405, 2010.
26. (a) Jacobsen, H. et. al., *J. Organomet. Chem.* **690**, 5407-5413, 2005. (b) Meyer, K. et. al., *Organometallics* **22** (4), 612-614, 2003. (c) Meyer, K. et. al., *Organometallics* **23** (4), 755-764, 2004. (d) Fürstner, A. et. al., *Angew. Chem. Int. Ed.* **49** (14), 2542-2546, 2010.
27. Bertrand, G. et. al., *Angew. Chem. Int. Ed.* **45** (21), 3484-3488, 2006.
28. (a) Bertrand, G. et. al., *Angew. Chem. Int. Ed.* **49** (34), 5930-5933, 2010. (b) Robinson, G. H. et. al., *Science* **321**, 1069-1071, 2008. (c) Robinson, G. H. et. al., *J. Am. Chem. Soc.* **130** (45), 14970-14971, 2008. (e) Robinson, G. H. et. al., *Chem-Eur. J.* **16** (2), 432-435, 2010.
29. For a review of “abnormal” mode of binding of NHCs see: (a) Arnold, P. L. & Pearson, S. *Coord. Chem. Rev.* **251**, 596-609, 2007. (b) Albrecht, M. *Chem. Commun.* 3601-3610, 2008. (c) Crabtree, R. H. et. al., *Chem. Commun.* 2274-2275, 2001. (d) Bertrand, G. et. al., *Science* **326**, 556-559, 2009; For “remote” mode of binding of NHCs see: (e) Meyer, W. H. et. al., *Dalton Trans.* 413-420, 2004. (f) Schuster, O., & Raubenheimer, H. G. et. al.,

- Inorg. Chem.* **45** (20), 7997-7999, 2006. (g) Albrecht, M. et. al., *Chem. Rev.* **109** (8), 3445-3478, 2009 and references therein.
30. Tonner, R., & Frenking, G. *Chem. Commun.* 1584-1592, 2008.
31. (a) Baceiredo, A. et. al., *Angew. Chem. Int. Ed.* **45** (44), 7447-7450, 2006. (b) Baceiredo, A. et. al., *Angew. Chem. Int. Ed.* **45** (16), 2598-2601, 2006.
32. Schmidbaur, H. et. al., *Angew. Chem. Int. Ed.* **19** (7), 555-556, 1980.
33. Guha, A. K. & Phukan, A. K. *Chem-Eur. J.* **18** (14), 4419-4425, 2012.
34. Herrmann, W. A. *Angew. Chem. Int. Ed.* **41** (8), 1290-1309, 2002.
35. (a) Balasubramanian, K., & McLean, A. D. *J. Chem. Phys.* **85** (9), 5117-5119, 1986. (b) Allen, W. D., & Schaefer, H. F. *Chem Phys* **108** (2), 243-274, 1986. (c) Magill, A. M. et. al., *J. Am. Chem. Soc.* **126** (28), 8717-8724, 2004.
36. (a) Bertrand, G. et. al., *Organometallics* **30** (20), 5304-5313, 2011. (b) Bertrand, G. et. al., *Angew. Chem. Int. Ed.* **49** (47), 8810-8849, 2010.
37. Bertrand, G. et. al., *Angew. Chem. Int. Ed.* **44** (35), 5705-5709, 2005.
38. Bertrand, G. et. al., *Angew. Chem. Int. Ed.* **45** (21), 3484-3488, 2006.
29. Bertrand, G. et. al., *Angew. Chem. Int. Ed.* doi: 10.1002/anie.201202137.
40. (a) Nakafuji, S. Y. et. al., *Angew. Chem. Int. Ed.* **47** (6), 1141-1144, 2008. (b) Bertrand, G. et. al., *Inorg. Chem.* **47** (10), 3949-3951, 2008. (c) Fürstner, A. et. al., *Angew. Chem. Int. Ed.* **47** (43), 8302-8306, 2008. (d) Kobayashi, J. et. al., *Chem. Commun.* 6233-6235, 2008.
41. Schmidbaur, H. et. al., *Angew. Chem.* **94** (4), 321-322, 1982.
42. (a) Baceiredo, A. et. al., *Angew. Chem. Int. Ed.* **45** (44), 7447-7450, 2006. (b) Baceiredo, A. et. al., *Angew. Chem. Int. Ed.* **45** (16), 2598-2601, 2006.



CHAPTER - 5

Mechanistic Study of Dinitrogen Reduction

[5.0] ABSTRACT

Mechanistic detail of dinitrogen reduction is still a fascinating area of research. Reduced forms of dinitrogen are very important for the sustainment of life on earth. Although industrial process of dinitrogen reduction (Haber-Bosch) is available, but it involves high temperature as well as pressure. Therefore, current research is focused towards transition metal catalyzed dinitrogen reduction at ambient condition.

The first part of this chapter deals with the mechanistic detail and energy profile for the conversion of hydrazine to ammonia mediated by vanadium(III) thiolate complexes at B3LYP/LANL2DZ//TZVP level of theory. The calculated energy profile revealed that all the reduction steps were exergonic while the protonation steps were endergonic. The generation of first equivalent of ammonia and the reduction of the cationic complex $[V-NH_3]^+$ to the neutral V-NH₃ species were found to be the most exergonic of all the steps. Based on the calculated energy profile, both *VPS3* and *VNS3* were found to be catalytically active for the reduction of hydrazine to ammonia, although some quantitative differences in free energy profile had been observed.

The next part of this chapter deals with the complete reduction of dinitrogen to ammonia mediated by vanadium triamidoamine complex. For most of the cases, protonation at the amido nitrogen atom is more favorable compared to the terminal one. Further, the most important steps of the mechanism were compared with the well established chemistry of nitrogen fixation mediated by molybdenum. Such a comparison helps in understanding why vanadium triamidoamine complex performs poorly compared to molybdenum. The main factors responsible for the poor performance of the vanadium complex towards NH₃ production are identified as low exergonic cleavage of the N-N bond and limitation of the ligand exchange step via dissociative mechanism at the end of the cycle to only one possible pathway. A major aspect of the failure of the vanadium complex to mediate the reduction of N₂ to ammonia is the fact that the protonation steps involve major barriers, which cannot be surmounted thermally. Moreover, unlike molybdenum, associative mechanism with vanadium triamidoamine complex is not likely to operate during the NH₃/N₂ exchange step.

[5.1] Mechanistic Details for the Conversion of Hydrazine to Ammonia Mediated by Vanadium(III) Thiolate Complexes

[5.1.1] Introduction

Hydrazine is supposed to be a substrate and an intermediate of nitrogenase,^{1,2} the enzyme responsible for biological nitrogen fixation.³⁻⁵ Like Mo – Fe nitrogenase,^{4,6-8} V – Fe nitrogenase⁵ is now known. In vanadium nitrogenase, the vanadium atom is thought to reside in a similar environment as the molybdenum atom in the cofactor FeMoco of Fe – Mo nitrogenase [5]. Moreover, the catalytic efficiency of V – Fe nitrogenase in the selective formation of ammonia comes next to Mo – Fe nitrogenase. Thus, to understand the mode of action of this enzyme, the chemistry of vanadium centre containing three sulfur donor sites which mimic the sulfido environment of the V site in vanadium nitrogenase, is of great importance. So far, limited synthetic models are known that catalyze the conversion of N₂H₄ to NH₃, the late stage of ammonia synthesis.⁹⁻¹⁵ Davies and coworkers reported vanadium complexes of the N(CH₂CH₂S)₃³⁻ and O(CH₂CH₂S)₂²⁻ ligands.¹⁶ They successfully isolated the V(NS₃)N₂H₄ adduct but none of these complexes catalyze the reduction of N₂H₄ to NH₃. However, after six years, Hsu and coworkers have reported the synthesis of vanadium thiolate complexes [V(PS₃)(Cl)]⁻ [1, PS = P(C₆H₃ – 3 – Me₃Si – 2 – S)₃³⁻] and [V(PS'₃)(Cl)]⁻ [2, PS'₃ = P(C₆H₃ – 5 Me – 2 – S)₃³⁻] and successfully carried out the reduction of N₂H₄ to NH₃ with 1.¹⁷ However, they have not characterized any intermediate which may form during the catalytic reduction of N₂H₄ to NH₃. Herein, we present density functional theory (DFT) calculation for the conversion of N₂H₄ to NH₃ mediated by vanadium (III) thiolate complexes. On the basis of the free energy profile obtained by calculation, a probable mechanism is proposed.

[5.1.2] Computational Details

All the structures were completely optimized using the hybrid HF-DFT method, labelled as B3LYP.¹⁸⁻²¹ This is based on Becke's three-parameter functional including Hartree-Fock exchange contribution with an exchange potential proposed by Becke together with gradient corrected correlation energy suggested by Lee et al. We have used the LANL2DZ basis set with the effective core potentials (ECP) of Hay and Wadt²²⁻²⁴ as implemented in the Gaussian 03 suite of programs.²⁵ The structures were further confirmed as real minima by running analytical vibrational frequency calculations at the same level of theory. In order to get reliable energetic, we have further performed single point calculations

on the B3LYP/LANL2DZ optimized geometries employing the same functional but with a triple-zeta basis set TZVP.²⁶ For simplification of computation, the tetradentate ligand is considered as *PS3* [*S3* = (SCH₂CH₂)₃³⁻]. Protonation and reduction steps were considered relative to the processes LutH⁺ → Lut and [Cp*₂Cr] → [Cp*₂Cr]⁺ respectively and their respective energies were calculated without any simplification of the molecules involved. Zero-point energy (ZPE), thermal, as well as solvent (Acetonitrile) corrections were employed in computing the standard free enthalpies.

[5.1.3] Results and Discussion

Optimized geometries of all the intermediates involved in the catalytic cycle are shown on the right side of Figure 5.1.1 and 5.1.2 for *VPS3* and *VNS3* systems, respectively. Natural charges computed at B3LYP/LANL2DZ level of theory, V-N_α and N_α-N_β stretching frequencies are collected in Table 5.1.1.

Table 5.1.1. Natural charges and vibrational stretching frequencies (cm⁻¹) calculated at the B3LYP/LANL2DZ level of theory.

Molecule	V	X ^a	N _α	N _β	ν(V-N _α)	ν(N _α -N _β)
1	0.759	0.883				
2	0.485	0.897	-0.742	-0.740	435.3	1058.5
3	0.424	0.912	-0.722	-0.607	387.0	970.6
4	0.302	0.886	-0.925		716.5	
5	0.318	0.946	-1.115		482.6	
6	0.489	0.896	-1.128		449.5	
7	0.908	-0.569				
8	0.646	-0.571	-0.717	-0.737	424.2	1066.4
9	0.600	-0.564	-0.698	-0.607	379.9	969.2
10	0.463	-0.585	-0.865		710.6	
11	0.494	-0.561	-1.076		463.6	
12	0.650	-0.572	-1.101		423.9	

^a X is the bridgehead atom

The starting complex **1** is a trigonal monopyramidal vanadium (III) thiolate complex with triplet ground state. Addition of hydrazine to **1** gives a hydrazine bound vanadium (III)

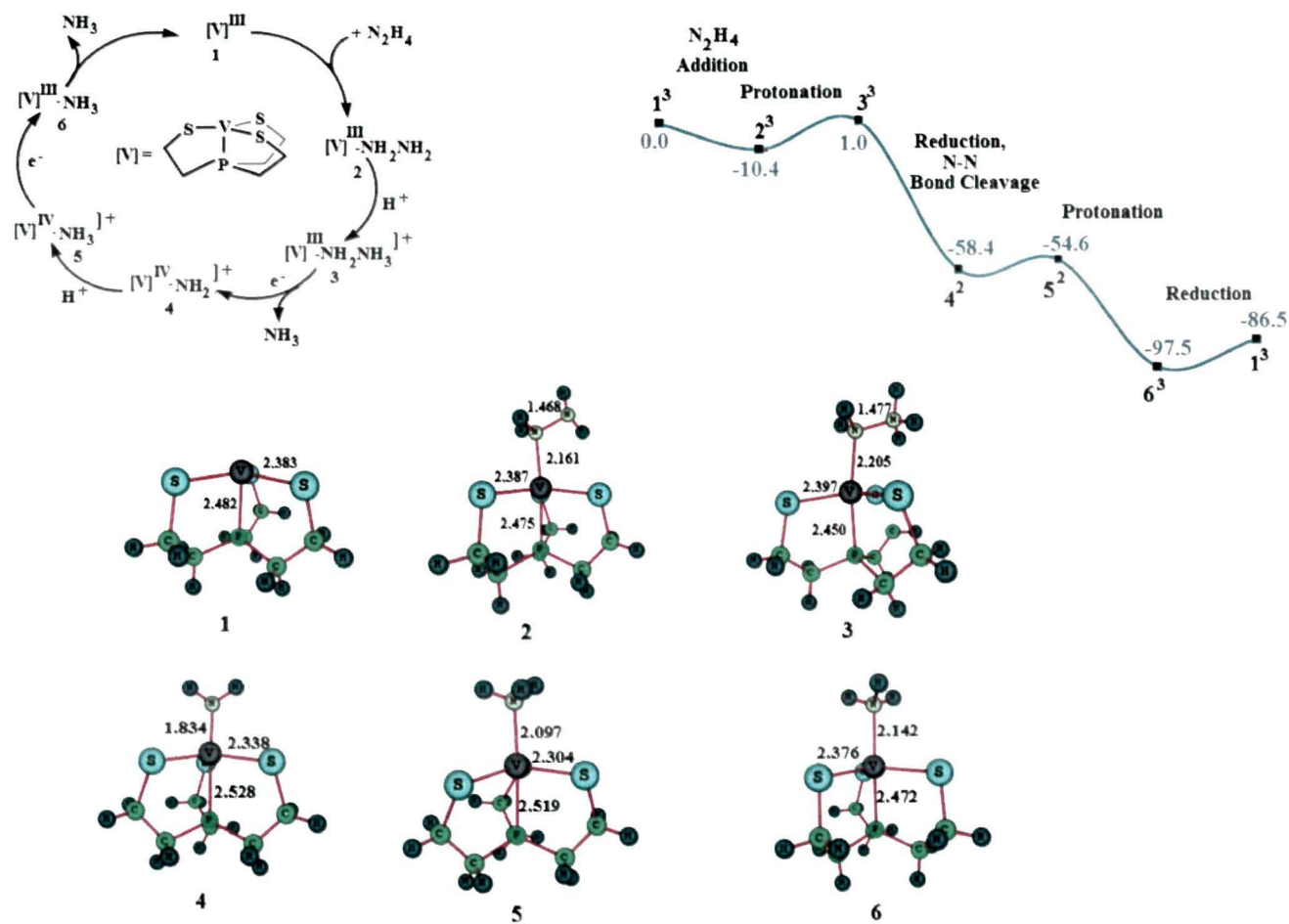


Figure 5.1.1. Catalytic cycle and energy profile (in kcal/mol) for the reduction of hydrazine to ammonia mediated by vanadium (III) thiolate [VPS3] complex computed at the B3LYP/LANL2DZ//B3LYP/TZVP level of theory.

thiolate complex **2**, $[V(N_2H_4)] [V = V\{P(SCH_2CH_2)_3\}]$ with no change in multiplicity. The process is exergonic by an amount -10.4 kcal/mol. The computed natural charges show equal probability of protonation at N_α and N_β (Table 5.1.1). However, Eldik and Tuzcek have shown that protonation at N_α does not lead to the cleavage of N–N bond at ambient condition.²⁸ Hence, the possibility of protonation at N_α is ruled out. Protonation of **2** at N_β relative to the process $LutH^+ \rightarrow Lut$ leads to **3** with no change in multiplicity. This process is endergonic by an amount +11.4 kcal/mol. Protonation of **2** leads to a lengthening of N – N bond length and decrease in the transannular V – P distance in **3** (Figure 5.1.1). The lengthening of N-N bond in **3** is also reflected in the calculated stretching frequency of **3** which drops from 1058.5 cm^{-1} in **2** to 970.6 cm^{-1} in **3** (Table 5.1.1). The next step involving the cleavage of the N – N bond is the most crucial step. Reduction of **3** to **4** relative to the process $[Cp^*_2Cr] \rightarrow [Cp^*_2Cr]^+$ leads to change in multiplicity from triplet to doublet and is calculated to be highly exergonic by an amount -57.5 kcal/mol (with Cp^*_2Co , the process is found to be exergonic by -51.9 kcal/mol). Thus, addition of one electron to **3** spontaneously cleaves the N – N bond along with significant lengthening of the transannular V – P bond (2.450 Å in **3** and 2.528 Å in **4**). This step is responsible for the formation of the first equivalent of ammonia. Tuzcek and Studt²⁹ have carried out theoretical study on the catalytic reduction of dinitrogen to ammonia mediated by molybdenum triamidoamine complex (Schrock Cycle).³⁰⁻³¹ They have found that the step corresponding to N – N bond cleavage is the most exergonic one. Further, in a combined experimental and theoretical study, Eldik and Tuzcek observed an activationless exothermic N-N bond cleavage in Mo/W hydrazidium complexes.²⁸ Our observation is in good agreement with Tuzcek and coworkers.^{28,29}

Protonation of **4** leading to **5** is slightly endergonic by an amount +3.9 kcal/mol with slight decrease in transannular V – P distance from 2.528Å to 2.519Å. This also results in weakening of the V- N_α bond which is reflected in the V- N_α stretching frequency which drops from 716.5 cm^{-1} in **4** to 482.6 cm^{-1} in **5**. The next step is the reduction of **5** to generate **6**. This process with Cp^*_2Cr is calculated to be highly exergonic (-42.9 kcal/mol) and leads to a neutral V – NH₃ complex **6** with further decrease in transannular V – P and V- N_α distance. With Cp^*_2Co as the reductant, this process is calculated to be exergonic by -37.3 kcal/mol. The final step in the catalytic cycle is the regeneration of the starting complex **1** and production of second equivalent of ammonia. This step is found to be endergonic by an amount of +11.0 kcal/mol. Removal of NH₃ from the neutral complex $[V – NH_3]$ **6**, leading to the formation of the starting complex **1**, is accompanied by slight increase in transannular distance and is calculated to be an energy demanding process along with all the protonation

steps. However, steps corresponding to the generation of first equivalent of ammonia and reduction of the cationic $[V - NH_3]^+$ complex **5** with both the reducing agents (Cp^*_2Cr and Cp^*_2Co) to the neutral complex **6** are calculated to be highly exergonic.

Thus, the catalytic cycle consists of subsequent protonation and reduction steps and leads to the generation of two equivalent of ammonia according to the following equation,



The total free reaction enthalpy ΔG_R^0 for the above reaction (1) is -94.8 kcal/mol – signifying that one turnover in the catalytic cycle is strongly spontaneous favouring the formation of two equivalents of ammonia. This total free reaction enthalpy is consistent with the calculated free energy profile.

In view of the reported inability of the $VNS3$ [$S3 = (SCH_2CH_2)_3^{3-}$] complex to convert hydrazine to ammonia,¹⁶ we have decided to carry out similar calculation for this system as well. The geometrical parameters obtained for both the vanadium systems mediated intermediates follow almost a similar trend (Figure 5.1.1 and 5.1.2). Replacement of the bridgehead phosphorus atom of the $VPS3$ system by nitrogen in the $VNS3$ system does not lead to any appreciable changes in the $V - N_\alpha$ and $N_\alpha - N_\beta$ distances. The computed natural charges at N_α and N_β as well as the $V - N_\alpha$ and $N_\alpha - N_\beta$ stretching frequencies follow similar trend as observed for $VPS3$ system (Table 5.1.1). A comparison of the energy profiles given in Figure 5.1.1 and 5.1.2 reveals that the standard free energy of formation of almost all the steps with $VPS3$ and $VNS3$ are remarkably similar.

[5.1.4] Conclusions

The energy profile for the reduction of hydrazine to ammonia mediated by vanadium (III) thiolate complexes has been studied theoretically and based on the computed energy profile, a probable mechanism has been proposed. Our calculation reveals that both $VPS3$ and $VNS3$ complexes are capable of mediating this catalytic reduction.

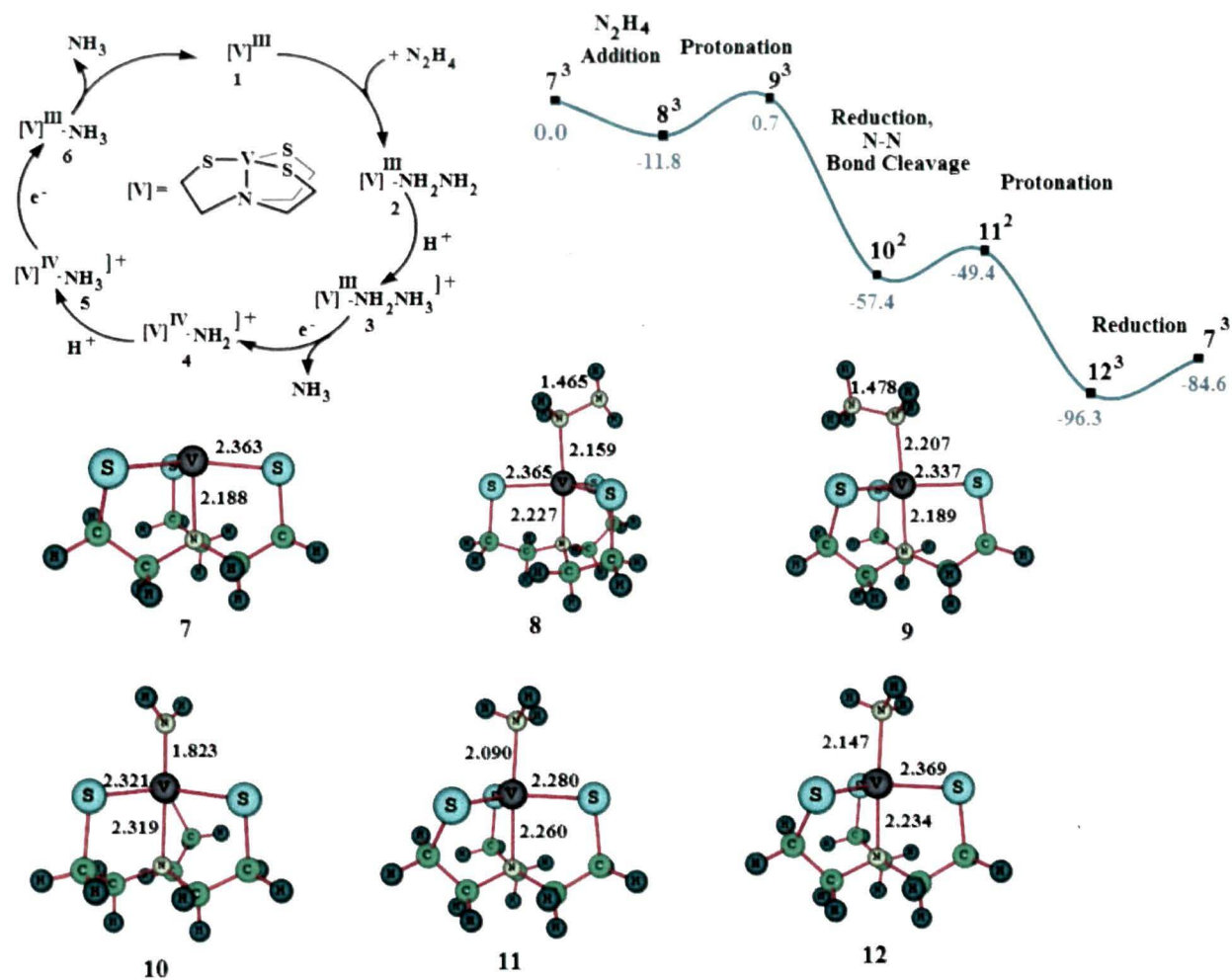


Figure 5.1.2. Catalytic cycle and energy profile (in kcal/mol) for the reduction of hydrazine to ammonia mediated by vanadium (III) thiolate [VNS3] complex computed at the B3LYP/LANL2DZ//B3LYP/TZVP level of theory.

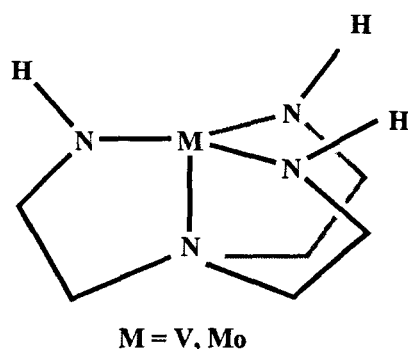
[5.2] Mechanistic Study for the Complete Conversion of Dinitrogen to Ammonia Mediated by Vanadium Triamidoamine Complex

[5.2.1] Introduction

The actual mechanism for the conversion of dinitrogen to ammonia by nitrogen fixing organisms is one of the unsolved problems of biology and chemistry.^{4,6} The current face of interest in chemical nitrogen fixation started in the early 1960's with the discovery of the first transition metal dinitrogen complex, $[\text{Ru}(\text{NH}_3)_5\text{N}_2]^{2+}$, by Allen and Senoff³² and extraction of the bacterial nitrogenase in the active form.³³ Also, with the revelation of the basic structure of the active site of the molybdenum nitrogenase,³⁴ much of the research was devoted to the synthetic development of transition metal homogeneous catalysts for dinitrogen reduction.³⁵ One such truly catalytic system for ammonia synthesis working under ambient condition is the molybdenum complex of a triamidoamine ligand, $[(\text{RNCH}_2\text{CH}_2)_3\text{N}]^{3-}$ where R = hexa-*iso*-propyl terphenyl (HIPT), synthesized by the research group of Schrock.^{30,31,36} Based on the isolated and characterized intermediates, a probable mechanism has been proposed by them which was the subject of various theoretical investigations.^{28,29,37,38} Tucek et al.²⁹ have carried out density functional calculations on the various intermediates that may appear in the catalytic cycle proposed by Schrock et al.^{30,31,36} and obtained a free energy profile for the reduction of dinitrogen to ammonia. Based on the energy profile so obtained which included different possible spin states of the intermediates, they concluded that the first step in the catalytic cycle is the protonation of the catalyst rather than its reduction. Reiher et al.^{38a} also carried out density functional calculations on some of the key steps of Schrock's catalytic cycle. Among them are the protonation of the $[\text{Mo}]\text{-N}_2$ ($[\text{Mo}] = [(\text{RNCH}_2\text{CH}_2)_3\text{N}]\text{Mo}$) intermediate, dissociation of NH_3 , and addition of N_2 . Three different possibilities were considered for transfer of the first proton and electron to the coordinated N_2 intermediate. This study showed that protonation of the equatorial nitrogen followed by reduction and protonation to generate the neutral $[\text{Mo}]\text{-N}=\text{NH}$ molecule was thermodynamically more favorable than direct protonation of the terminal nitrogen followed by reduction. Thus, all these theoretical studies were conducted mainly on Schrock's molybdenum catalyst.

Alternative vanadium nitrogenases are now known⁵ but structurally not well characterized. In vanadium nitrogenase, the vanadium atom is thought to reside in a similar environment as the molybdenum atom in the cofactor FeMoco of Fe – Mo nitrogenase.⁵ Moreover, the catalytic efficiency of V nitrogenase in the selective formation of ammonia comes next to Mo – Fe nitrogenase. In 2006, Schrock et al.^{35h} have prepared a vanadium

triamidoamine complex, analogous to the molybdenum complex, and attempted the reduction of dinitrogen with this vanadium complex. They also proposed a plausible mechanism for the same. However, no ammonia was formed using this catalyst under the same condition that was successful with the analogous molybdenum catalyst. Hence, it could be rewarding to carry out a thorough theoretical investigation on the mechanism of dinitrogen fixation mediated by vanadium and to compare them with the well established chemistry of molybdenum (Scheme 5.2.1).^{30,31,36-38} To the best of our knowledge, till date, there exists no systematic study in the literature about nitrogen fixation catalyzed by vanadium complexes except the one by us where mechanistic details for the conversion of hydrazine to ammonia mediated by vanadium thiolate complex were studied.³⁹ We report here, for the first time, a systematic theoretical study on the thermodynamics of dinitrogen fixation mediated by vanadium triamidoamine complex and compared them with the energetics obtained for similar molybdenum complex. The key question we would like to address in this report is why vanadium complexes are not active towards NH₃ production in comparison to similar molybdenum complexes.



Scheme 5.2.1. Model vanadium and molybdenum complexes of triamidoamine ligand.

[5.2.2] Computational Details

We have used density functional theory (DFT), a practical and effective computational tool, especially for transition metal compounds⁴⁰ for the present study. We have used PBE1PBE⁴¹ functional, since it performs exceedingly well for the evaluation of energetic of a reaction^{42a} as well as many other properties.^{42b} The relativistic small-core ECP of Stuttgart/Dresden (SDD)^{43a} for the transition metals with the corresponding valence basis set of D95V^{43b} for the main group elements were used. As stated by Neese et al, the combination of PBE1PBE and SDD can safely be used for studying transition metal complexes.^{42b} Frequency calculations were performed at the same level of theory to

characterize the nature of the stationary points. All the ground state structures were verified as minimum by confirming that their respective Hessian (matrix of analytically determined second order derivative of energy) is all real while the transition states were characterized as stationary points with one imaginary frequency. In our calculations, the experimentally reported ^{35h} hexa-*iso*-propyl terphenyl (HIPT) substituents at the equatorial nitrogen were modeled with hydrogen atoms so as to save computational time. In spite of this simplification, we observed an excellent agreement with the available X-ray data^{35h} (Table 5.2.1) which justifies this simplification and the level of theory used. Moreover, replacement of the bulky HIPT group by hydrogen does not change the nature of the reaction, although quantitative differences are observed (Table 5.2.2). Energies corresponding to the reduction and protonation steps were calculated relative to the process $[\text{Cp}^*_2\text{Cr}] \rightarrow [\text{Cp}^*_2\text{Cr}]^+ + \text{e}^-$ and $\text{LutH}^+ \rightarrow \text{Lut} + \text{H}^+$ (Lut = 2,6-dimethylpyridine) respectively, without making any simplifications of the molecules involved. Zero-point energy (ZPE), thermal, as well as solvent (heptane) corrections was employed in computing the standard free energies of formation. The bonding nature of all the compounds were analyzed by natural bond orbital (NBO) analysis.²⁷ All the computations were performed using the Gaussian 03 program,²⁵ while the charge decomposition analysis (CDA)⁴⁴ were performed using the QMForge 2.1 program.⁴⁵

Table 5.2.1. Comparison with the available X-ray data of [V]-NH₃ complex^{35h}

Geometrical parameters	Experimental value (X-ray data ^{35h})	Theoretical value at PBE1PBE/SDD	Difference
$r_{V\dots N_{ax}}$ (Å)	2.148	2.138	0.010
$r_{V-N_{eq}}$ (Å)	1.955	1.923	0.032
	1.957	1.922	0.035
	1.952	1.924	0.028
r_{V-NH_3} (Å)	2.162	2.186	0.024
$\langle N_{eq}-V-N_{eq} \rangle$ (°)	118.19	118.41	0.22
$\langle N_{ax}-V-NH_3 \rangle$ (°)	179.43	179.46	0.03

Table 5.2.2. Comparison of the energetic with previous reported studies.

Reaction	Reiher et al ^{38a}	Cao et al ^{38d}	This work
$[\text{Mo}]-\text{NH}_3 \rightarrow [\text{Mo}] + \text{NH}_3$	+27.7	+18.4	+6.6
$[\text{Mo}]-\text{NH}_3^{\ddagger} \rightarrow [\text{Mo}]-\text{NH}_3$	-111.4	-106.1	-64.1
$[\text{Mo}] + \text{N}_2 \rightarrow [\text{Mo}]-\text{N}_2$	-37.4	-16.1	-28.5

[5.2.3] Results and Discussion

[5.2.3.1] Mechanistic Details of [V] ([V] = (N₃N)V)

Dinitrogen binding to a transition metal centre is crucial as it activates the strong N≡N bond. The interaction involves donation of electron density from the filled orbital of the Lewis base N₂ into the empty metal d (d_z^2) orbital resulting in the formation of σ -bond. The filled metal (d_{xy} and d_{xz}) orbital on the other hand, back donates electron density to the lowest unoccupied orbital of N₂ resulting in the formation of a π back bond. The extent of back donation from the metal centre is responsible for the activation of the N≡N bond as electron density from the filled metal orbital enters into the antibonding orbital of N₂ of appropriate symmetry. Charge decomposition analysis (CDA) of Frenking et al.⁴⁴ helps in analyzing such a situation (Table 5.2.3). Since the residue terms (Δ) are nearly zero, the metal-N₂ interaction can be discussed within the framework of the familiar Dewar-Chatt- Duncanson donor-acceptor model.⁴⁶ The values of back donation (b) from the metal center to the π^*

Table 5.2.3. Charge decomposition (CDA) analysis of [V]-N₂ and [Mo]-N₂ complexes calculated at PBE1PBE/SDD level of theory along with NBO occupancies of the two orthogonal π^* orbitals of N≡N in their respective complexes. ν_{NN} (cm⁻¹) is the infrared N₂ stretching frequencies (without scaling).

Complex	N ₂ → M donation (d)	M → N ₂ back-donation (b)	b/d	repulsion (r)	residue (Δ)	Occupancy of $\pi^*_{N\equiv N}$	ν_{NN}
[Mo]-N ₂	0.217	0.339	1.562	-0.325	-0.033	0.169/0.184	1894.8
[V]-N ₂	0.234	0.264	1.128	-0.164	-0.066	0.136/0.125	2090.4

orbital of N₂ and the ratio b/d are found to be higher for [Mo] catalyst compared to [V]. Hence, [Mo] is more efficient in activating the N≡N bond compared to [V] ($r_{N\equiv N} = 1.200$ Å and 1.141 Å in [Mo]-N₂ and [V]-N₂ respectively). Infrared N₂ stretching frequencies (without scaling) as well as the occupancies of the two orthogonal π^* orbitals of N≡N also show the same trend, i.e., [Mo]-N₂ has higher occupancies of the two π^* orbitals of N≡N and has lower N₂ stretching frequency. Hence, CDA and Natural Bond Orbital (NBO) results show that the degree of dinitrogen activation is higher with [Mo] compared to [V]. However, several controlled studies have revealed that the degree of dinitrogen activation and the extent of reactivity may not always correlate.⁴⁷

The most crucial steps in the initial stage of the mechanism are the addition of dinitrogen followed by its successive protonation and reduction. Figure 5.2.1 shows three possible pathways of dinitrogen addition, protonation, and reduction. According to the

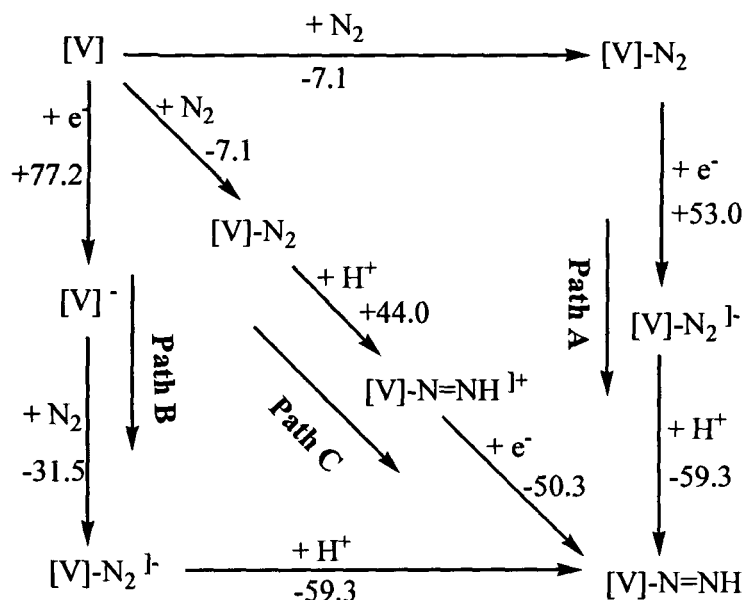


Figure 5.2.1. Three possible pathways of dinitrogen addition, protonation and reduction of $[V]$ ($[V] = (N_3N)V$) to yield $[V]-N=NH$. Energies are in kcal/mol.

energy profile obtained at PBE1PBE/SDD level of theory, path C, which is the addition of dinitrogen to the neutral $[V]$ catalyst followed by subsequent protonation and reduction to yield $[V]-N=NH$, is the most preferred pathways of the three possibilities shown in Figure 5.2.1. The high energetic barrier of path B, which involves reduction of $[V]$ prior to the addition of dinitrogen makes it least likely. This is in tune with Tucek's mechanism where protonation of the coordinated dinitrogen takes place prior to reduction.²⁹ Slightly more endergonic character of path A compared to C also makes this path less likely. Further, the proton may attach either to the terminal nitrogen, N_β of the dinitrogen ligand or it can attach to the amido nitrogen atom (N_{eq}) of the ligand. Therefore, we have also checked this possibility as shown in Figure 5.2.2. The computed energy profile shows that protonation at N_{eq} resulting in the formation of $[V-N_{eq}H]-N_2^{1+}$, is nearly 60 kcal/mol more favorable compared to protonation at N_β . More negative charge at N_{eq} (-0.97) compared to N_β (0.05) favors protonation at N_{eq} . Similar energetics were obtained by Reiher et al.^{38a} for protonation at amido and terminal nitrogen atoms of the related $[Mo]$ complex. Using a

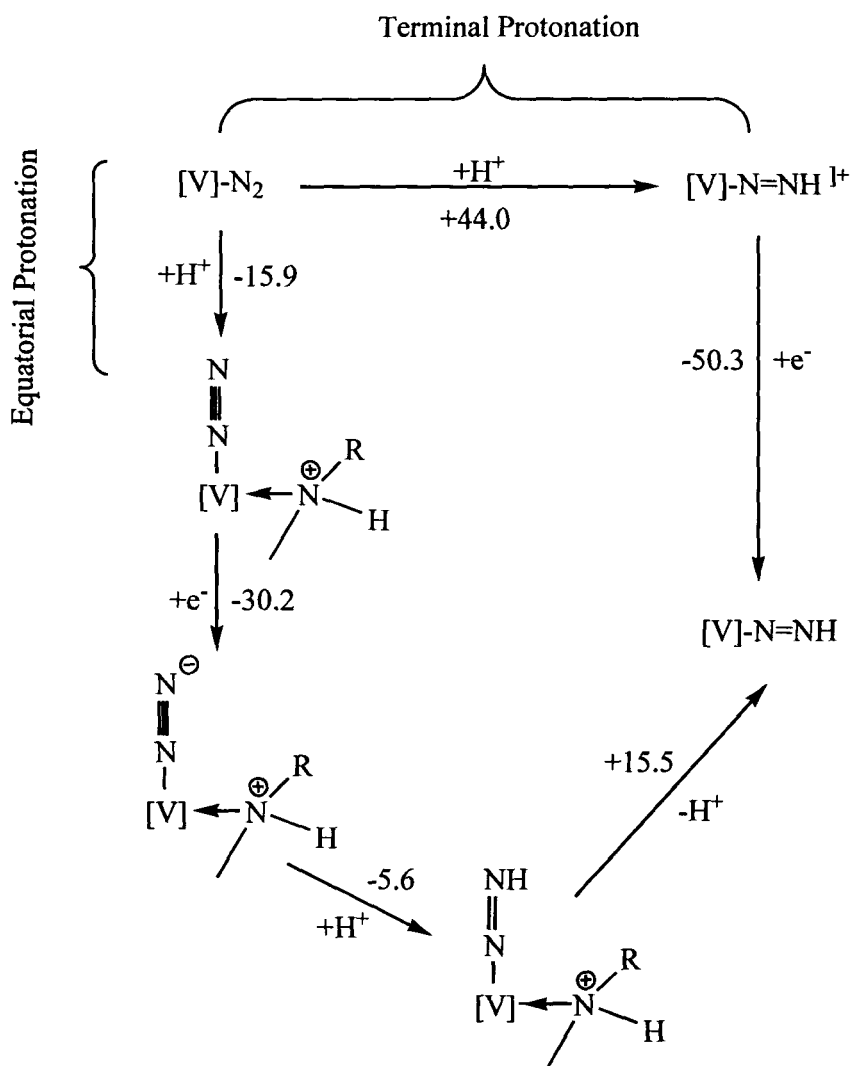


Figure 5.2.2. Two possibilities (ligand derived amido and terminal) for the initial protonation of $[\text{V}]\text{-N}_2$ ($\text{R} = \text{H}$). Energies are in kcal/mol.

combination of EPR/ENDOR spectroscopy and DFT computations, Schrock and coworkers have recently shown that the incoming proton preferentially binds to the amido ligand (i.e., one of the equatorial nitrogen atoms) prior to its eventual migration to the N_β of N_2 .⁴⁸ The protonated molecule $[\text{V}\text{-N}_{\text{eq}}\text{H}]\text{-N}_2^{\text{H}+}$ then undergoes reduction to produce $[\text{V}\text{-N}_{\text{eq}}\text{H}^+]\text{-N}\equiv\text{N}^-$ which is exergonic by 30.2 kcal/mol. The resulting complex then undergoes protonation at the N_β position to produce $[\text{V}\text{-N}_{\text{eq}}\text{H}^+]\text{-N}=\text{NH}$ which on further deprotonation, produces $[\text{V}]\text{-N}=\text{NH}$. Thus, it is evident from Figure 5.2.2 that protonation at amido position is much more favorable than the terminal one to produce $[\text{V}]\text{-N}=\text{NH}$ and is “proton catalyzed”. This is in tune with previous theoretical and experimental results for the analogous $[\text{Mo}]$ complexes.^{36c,38a-38b,48} Based on the above observations, a mechanism has been proposed and

its corresponding standard free energies have been calculated and plotted in Figure 5.2.3 against the reaction coordinate ρ .

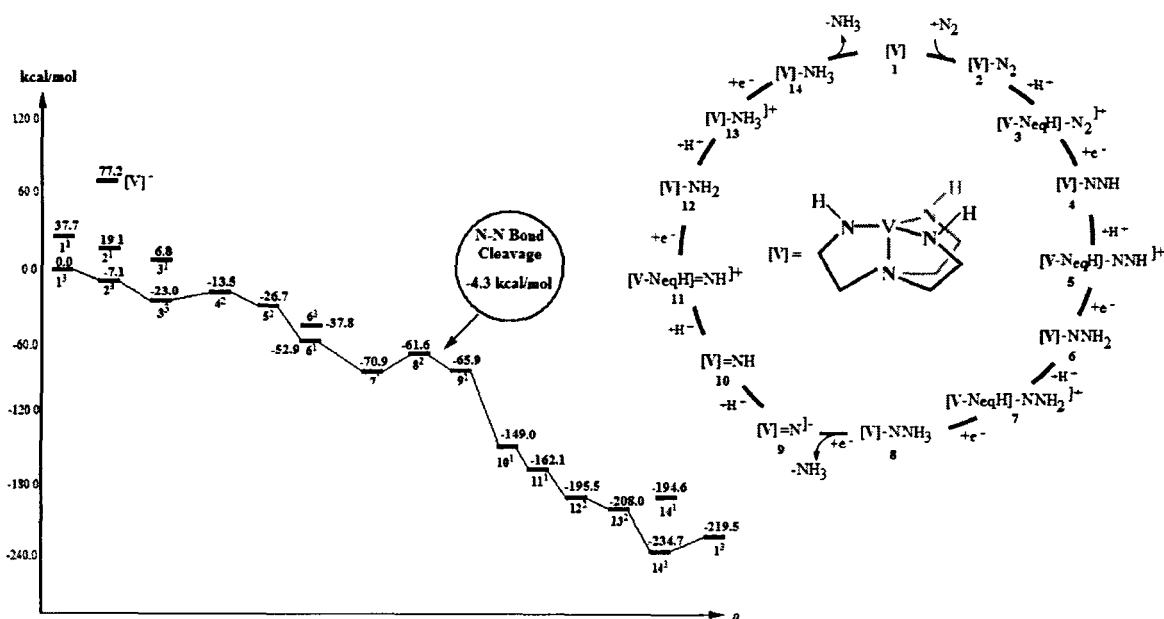


Figure 5.2.3. Catalytic cycle (top right) and free energy profile for the reduction of N₂ to ammonia mediated by [V] ([V] = (N₃N)V) systems. Energies correspond to standard free energies of formation (ΔG^0) and are in kcal/mol. Energies shown are not to scale.

The starting complex 1, [V] ([V] = (N₃N)V), is a trigonal monopyramidal complex which gives rise to $S = 0$ and $S = 1$ states. The singlet - triplet energy separation of 1 is 37.8 kcal/mol, with the triplet state being more stable. Addition of neutral N₂ results in an end on bound dinitrogen complex [V]-N₂ (2) with triplet ground state (the singlet state lies 26.2 kcal/mol higher in energy than the triplet state). This addition is found to be exergonic by an amount of 7.1 kcal/mol. The next step is a crucial one which involves protonation of the dinitrogen complex. As evident from Figure 5.2.2, protonation of the coordinated dinitrogen complex is more favorable at the amido position rather than at N _{β} , to form [V^{III}-N_{eq}H]-N₂¹⁺ (3) with triplet ground state (the singlet state is 29.8 kcal/mol higher in energy than the triplet state). This protonation process is exergonic by 15.9 kcal/mol. The resulting protonated dinitrogen complex then undergoes reductive proton migration to N _{β} via a “proton catalyzed” pathway (Figure 5.2.2) resulting in the formation of [V^{IV}-N=NH] (4) with doublet ground state. This process is endergonic by 9.5 kcal/mol. Interestingly, the reductive proton migration step for the related molybdenum complex is exergonic by 22.4 kcal/mol. Since the conversion of 3 to 4 involves a barrier of 9.5 kcal/mol, hence, we decided to look for any

possible intermediate or transition state for this conversion (Figure 5.2.4). We could obtain an intermediate **3I** which is formed via 1, 2 proton shift from the amido nitrogen to the

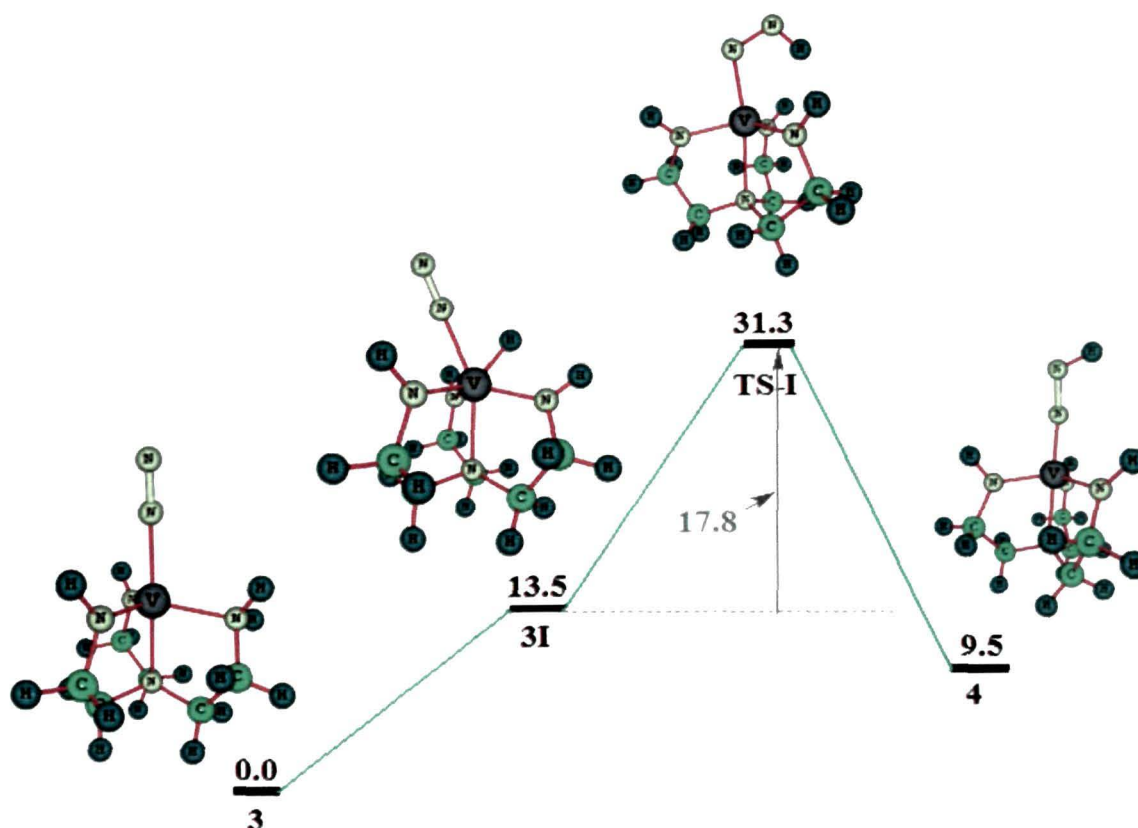


Figure 5.2.4. Possible intermediate and transition state for the conversion of **3** to **4**. Energies correspond to standard free energies of formation (ΔG^0) and are in kcal/mol.

vanadium atom during the reduction of **3**. The N_2 moiety in **3I** is tilted away from the axis defined by the $N_b - V - N_a$ (N_b is the bridgehead nitrogen atom) atoms making an angle of 155.3° at the vanadium center. The formation of this intermediate is calculated to be endergonic by 13.5 kcal/mol. The intermediate **3I** then rearranges to **4** via a transition state **TS-I** in which the proton migrates from the vanadium center to the terminal nitrogen atom. This transition state lies +17.8 kcal/mol higher in energy than the intermediate **3I**. Thus, transformation of **3** to **4** may involve one probable intermediate **3I** and a transition state **TS-I**.

As in the case of first protonation, complex **4** then undergoes further protonation at the equatorial position (for a comparison of equatorial versus terminal protonation, see Table 5.2.4) to form $[V^{IV}-N_{eq}H]-N=NH^{1+}$ (**5**) with no change in multiplicity. This process is exergonic by 13.2 kcal/mol. The next step is the reductive proton migration of the cationic complex **5** to form the neutral complex $[V]^V=N-NH_2$ (**6**) with singlet ground state (the triplet

state is 15.1 kcal/mol higher in energy than the singlet state) and may proceed via a “proton catalyzed” pathway as observed in the case of **2** → **4** conversion (Figure 5.2.2). Such proton catalyzed pathways are not considered for other protonation steps but instead, only the equatorial protonation and its reductive proton migration to terminal N_β position are considered. The conversion of **5** to **6** is exergonic by 26.2 kcal/mol. Protonation of **6** at the equatorial position is favorable by 28.1 kcal/mol compared to terminal protonation (Table 5.2.4) and results in the formation of the cationic complex [V^V-E_{eq}H]-NNH₂¹⁺ (**7**) with no change in multiplicity and is exergonic by 18.0 kcal/mol. The reductive proton migration of **7** results in the formation of the neutral complex [V]^{IV}-NNH₃ (**8**) with doublet ground state. Since the conversion of **7** to **8** also involves an energetic barrier of 9.4 kcal/mol as in the conversion of **3** → **4**, we decided to look for the presence of possible intermediate or transition state that may form during this transformation (Figure 5.2.5). We could obtain an

Table 5.2.4. Energetic (kcal/mol) of the equatorial and terminal protonation of various steps involved in the catalytic reduction of N₂ to NH₃ by vanadium triamidoamine complex. For numbering of the molecules, see Figure 5.2.3 of the main text.

Reaction	Equatorial	Terminal
2 + H ⁺ → 3	-15.9	+44.0
4 + H ⁺ → 5	-13.2	+0.4
6 + H ⁺ → 7	-18.0	+9.8
9 + H ⁺ → 10	-69.1	-83.2
10 + H ⁺ → 11	-27.2	-5.9
12 + H ⁺ → 13	-14.9	-12.6

intermediate **7I** which is formed via 1, 3 proton shift from the amido nitrogen to the N_α atom. The formation of this intermediate is found to be exergonic by 13.7 kcal/mol. It then rearranges via 1, 2 shift to produce **8** via a transition state **TS-II** which lies 42.5 kcal/mol higher in energy than **7I**. However, as proton transfer reactions are very fast due to high tunneling ability of proton, these intermediates as well as the transition state may not be observed experimentally.

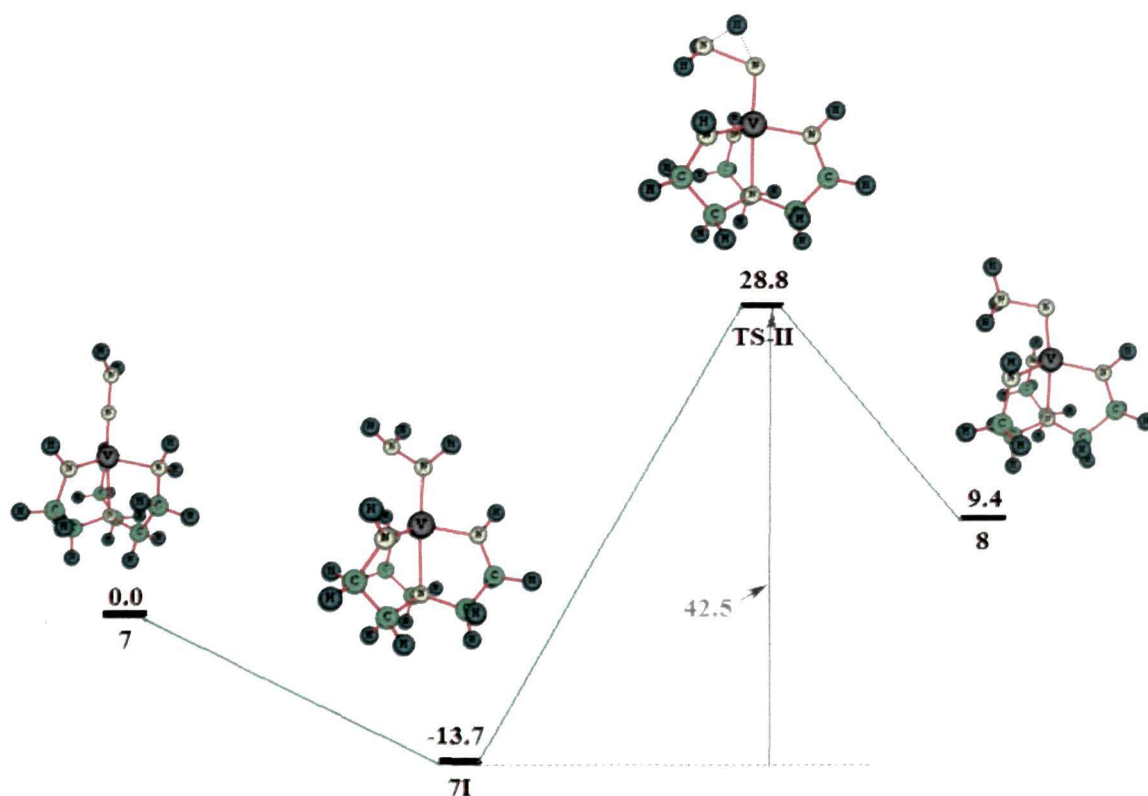


Figure 5.2.5. Possible intermediate and transition state for the conversion of **7** to **8**. Energies correspond to standard free energies of formation (ΔG^0) and are in kcal/mol.

The next step is a key one which involves the generation of the first equivalent of ammonia. It involves reduction of the neutral complex **8** to yield the anionic complex $[V]^V=N^-$ (**9**) with subsequent generation of the first equivalent of ammonia. The N-N bond in **8** is highly activated as is evident from the large N-N distance of 1.535 Å compared to 1.098 Å in free N_2 .⁴⁹ This activation of the N-N bond in **8** facilitates its exergonic cleavage which is calculated to be 4.3 kcal/mol. In principle, such activated N-N bond should have resulted in a highly exergonic cleavage of the N-N bond and facile release of NH_3 . The fact that release of NH_3 is not so facile (exergonic by only 4.3 kcal/mol), further lends support to the observation that the degree of nitrogen activation and the extent of reactivity may not always correlate.⁴⁷

The next two steps are the protonation of **9** to produce the neutral complex $[V]^V=NH$ (**10**) with subsequent protonation of **10** to produce the cationic complex $[V^V-N_{eq}H]=NH^{1+}$ (**11**) with no change in multiplicity. For simple electrostatic reason, protonation of **9** is more favorable at the terminal nitrogen atom rather than the amido one. However, protonation of **10** is more favorable at the amido nitrogen atom. These two protonation steps are found to be

exergonic (Figure 5.2.3) with the first one, i.e., **9** → **10** being highly exergonic by 83.1 kcal/mol. Reduction of **11** yields the neutral complex $[V]^{IV}\text{-NH}_2$ (**12**) with doublet ground state. This reduction process was calculated to be exergonic by 33.3 kcal/mol. The next step is the protonation of the neutral complex **12** to yield $[V]^{IV}\text{-NH}_3^{1+}$ (**13**) with no change in multiplicity. The protonation of **12** at the terminal and amido nitrogen atoms proceeds with almost equal probability (Table 5.2.4) and hence, the terminal protonated molecule **13** is retained in the mechanism. This protonation is found to be exergonic by 12.6 kcal/mol. The next step is the reduction of the cationic complex **13** to the neutral $[V]^{III}\text{-NH}_3$ complex (**14**) with triplet ground state (the singlet state is 40.1 kcal/mol higher in energy than the triplet state), and is calculated to be exergonic by 26.7 kcal/mol. The last step is an important one where regeneration of the catalyst and production of second equivalent of ammonia takes place. This process is found to be endergonic by an amount of 15.2 kcal/mol.

It can be seen from Figure 5.2.3 that whenever there is a possibility for more than one spin states, the high spin geometry lies lower in energy than the low spin one except in case of $[V]=N\text{-NH}_2$ (**6**) where the high spin (triplet) state lies 15.1 kcal/mol higher in energy than the low spin (singlet) state. Also, in agreement with experimental findings by the group of Schrock^{35h}, we find that the conversion of $[V]=NH$ (**10**) to $[V]\text{-NH}_3$ (**14**) via $[V]\text{-NH}_2$ (**12**) is quite facile.

[5.2.3.2] Comparison between [V] and [Mo] catalyst

Since no ammonia was generated using the [V] catalyst under the same condition that was successful for the analogous [Mo] catalyst,^{35h} we, therefore, decided to investigate the factors which might be responsible for the lower activity of the [V] catalyst. It is clear from Figure 5.2.3 that the key steps for the generation of ammonia are – (i) N – N bond cleavage along with the generation of the first equivalent of NH_3 (process **8** → **9**) and (ii) release of the second molecule of NH_3 and regeneration of the catalyst (process **14** → **1**).

The N-N bond cleavage step is found to be exergonic by only 4.3 kcal/mol. However, the N-N bond cleavage step with [Mo] is found to be exergonic by 75.9 kcal/mol at the same level of theory. In order to understand the origin of such a large difference in energetics, one has to look at the energies of the σ antibonding orbital of the $N_\alpha\text{-}N_\beta$ bond of the isoelectronic d^1 species $[V]\text{-NNH}_3$ and $[\text{Mo}]\text{-NNH}_3^{1+}$ respectively as NH_3 will be released from these molecules upon reduction. It is found that the $\sigma_{N_\alpha\text{-}N_\beta}^*$ orbital of $[V]\text{-NNH}_3$ lies 2.4 eV higher in energy than that for $[\text{Mo}]\text{-NNH}_3^{1+}$ (energies of $\sigma_{N_\alpha\text{-}N_\beta}^*$ for $[V]\text{-NNH}_3$ and $[\text{Mo}]\text{-NNH}_3^{1+}$ are 4.1 eV and 1.7 eV respectively, Figure 5.2.6). Thus, the molybdenum complex readily

undergoes reduction than the vanadium one and hence, N-N bond cleavage and subsequent release of NH₃ is highly exergonic in this case. However, due to the much higher energy of the $\sigma^*_{N\alpha-N\beta}$ orbital of the vanadium complex, it is quite difficult to reduce the N _{α} -N _{β} bond. It is this difficulty in reducing the N _{α} -N _{β} bond which is responsible for the significantly less exergonic cleavage of the N _{α} -N _{β} bond, and this account for the inefficient release of NH₃ from the vanadium complex than in the related molybdenum complex. Also, natural charge at the vanadium atom of [V]-N-NH₃¹⁺ is 0.90e while that of molybdenum in [Mo]-N-NH₃¹⁺ is 1.31e, further probing lower electrophilicity of the vanadium complex. This lower exergonic cleavage of the N-N bond with [V] may account for one of the major drawbacks of the [V] catalyst towards NH₃ production.

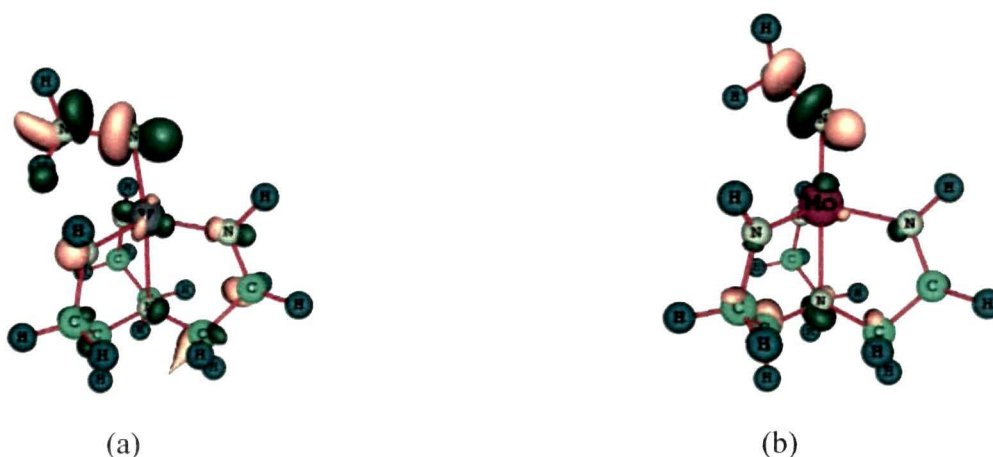


Figure 5.2.6. $\sigma^*_{N\alpha-N\beta}$ orbitals of (a) [V]-N-NH₃ (**8**) (Energy = 4.1 eV) and (b) [Mo]-N-NH₃¹⁺ (Energy = 1.7 eV).

Three possibilities (Figure 5.2.7) exist for the generation of the second equivalent of ammonia and regeneration of the catalyst (the start over of a new cycle). Both experimental^{36c} and theoretical^{38a} reports suggest that different routes for the catalytic cycle are possible. Hence, we have checked three possible pathways of ligand exchange at the end of the cycle, i.e., dissociation of NH₃ and addition of N₂. Similar mechanistic possibilities were studied previously by Reiher et al^{38a} for the [Mo] catalyst with the full HIPT ligand. They concluded that dissociation of the NH₃ ligand may proceed via the neutral pathway or via the anionic one, the later being the most favorable. As evident from Figure 5.2.7, dissociation of NH₃ is favorable via neutral and anionic pathway; the cationic pathway is least likely, while addition of N₂ is most favorable via the anionic pathway. It is also clear from Figure 5.2.7 that the reduction of [V]-NH₃¹⁺ to the neutral complex [V]-NH₃ is quite exergonic (-26.7 kcal/mol) with Cp₂Cr* as the reductant, while the subsequent reduction of

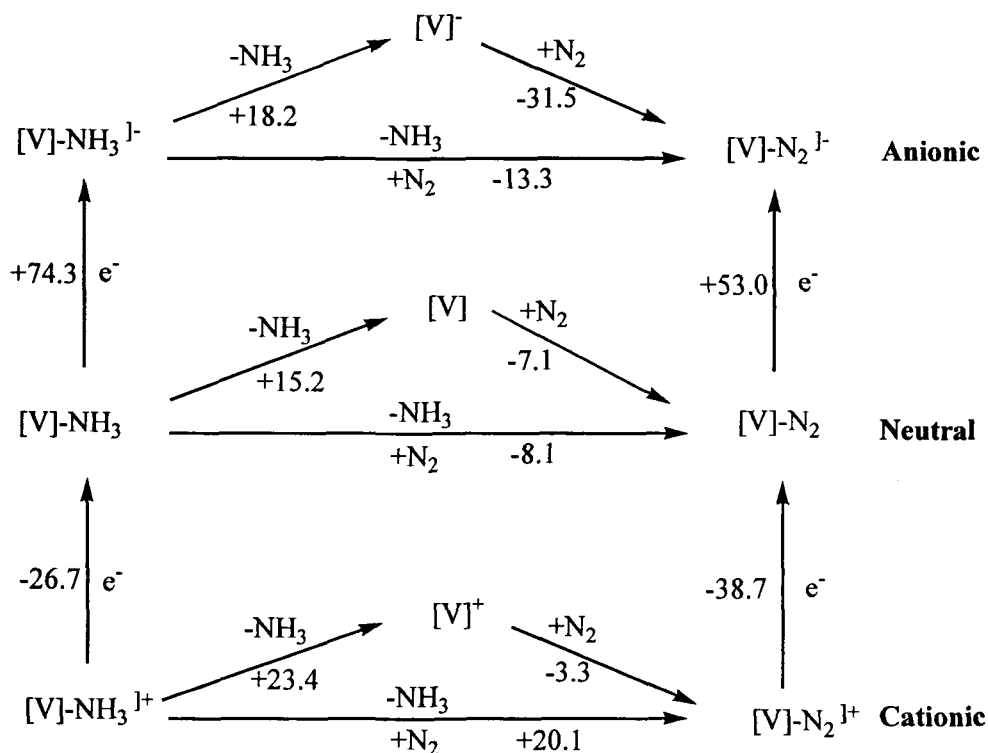
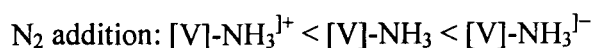
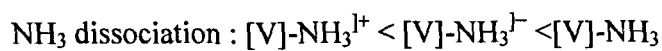


Figure 5.2.7. Different possibilities of initial NH_3/N_2 exchange. Energies are in kcal/mol.

the neutral complex $[\text{V}]\text{-NH}_3$ to the anionic one $[\text{V}]\text{-NH}_3^{1-}$ is very unlikely owing to the high endergonic (+74.3 kcal/mol) character of the reaction. Figure 5.2.7 reveals that the reduction of $[\text{V}]\text{-N}_2$ to $[\text{V}]\text{-N}_2^{1-}$ is thermodynamically difficult (the reaction is endergonic by 53.0 kcal/mol). Thus, the reverse of the above reaction, i.e., the oxidation of $[\text{V}]\text{-N}_2^{1-}$ is thermodynamically favorable. This theoretical finding corroborates experimental finding that $\{[\text{V}]\text{-N}_2\}\text{K}$ readily undergoes oxidation.^{35h} Further, conversion of $[\text{V}]\text{-NH}_3$ to $[\text{V}]\text{-N}_2^{1-}$ is thermodynamically unfavorable owing to the high endergonicity associated with the reduction of $[\text{V}]\text{-NH}_3$ to $[\text{V}]\text{-NH}_3^{1-}$. This may be the cause for the failure in converting $[\text{V}]\text{-NH}_3$ into $[\text{V}]\text{-N}_2^{1-}$ by the group of Schrock.^{35h}

A closer look at Figure 5.2.7 also reveals that the relative ease of dissociation of ammonia and addition of dinitrogen to the cationic, neutral and anionic systems follow the order



Thus, the only possible pathway of ligand exchange with $[\text{V}]$ catalyst is the neutral one since generation of $[\text{V}]\text{-NH}_3^{1-}$ from $[\text{V}]\text{-NH}_3$ is thermodynamically quite unfavorable,

while both neutral and anionic pathways are viable for [Mo].^{38a} This restriction may also account for the difficult regeneration of the catalyst or start over of a new cycle.

Reiher et al reported that the NH_3/N_2 exchange may involve associative (addition-elimination) mechanism via the formation of a stable six-coordinate complex $[\text{Mo}](\text{NH}_3)(\text{N}_2)$.^{38c} They could also optimize the six-coordinate complex using BP86/TZVP-SVP level of theory and proposed that the course of the reaction could be followed by vibrational frequency analysis (provided that the six-coordinated complex has sufficient life time). Hence, we also tried to optimize the six coordinate $[\text{V}](\text{NH}_3)(\text{N}_2)$ complex that may form during the associative mechanism. We tried to attach N_2 from both the top and side entrance, and fully optimized both the complexes. However, the optimized geometries obtained from both the approaches are same. We also characterized them to be minimum in the potential energy surface by calculating the frequencies which were found to be all real. However, during optimization, we observed that the N_2 ligand moved away from the $[\text{V}]-\text{NH}_3$ complex and ultimately attained a distance of 3.572 Å from the vanadium center (Figure 5.2.8). Interestingly, this distance is larger than the sum of the van der Waals' radii of

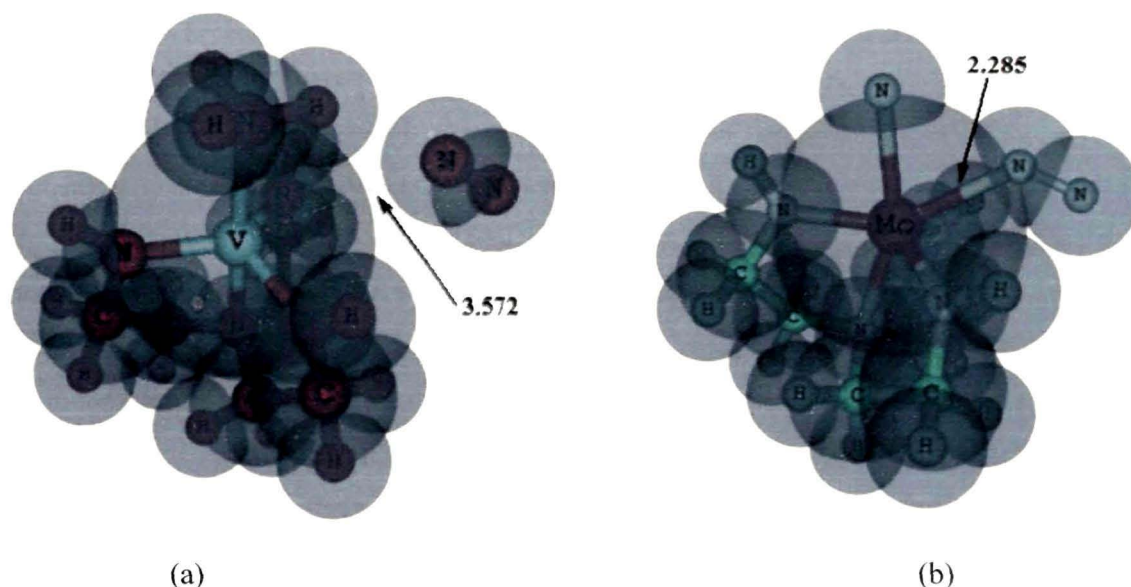


Figure 5.2.8. Optimized geometries of the (a) $[\text{V}](\text{NH}_3)(\text{N}_2)$ and (b) $[\text{Mo}](\text{NH}_3)(\text{N}_2)$ complex. The spheres represent the van der Waals' spheres of the atoms. Hydrogen atoms are omitted for clarity.

vanadium and nitrogen (3.34 Å). However, the analogous six-coordinate molybdenum complex has a distance of only 2.285 Å between molybdenum and N_2 which is well within

their sum of van der Waals' radii (3.64 Å). It suggests that the formation of the six coordinate intermediate $[V](NH_3)(N_2)$ may not be possible while it is possible for the analogous molybdenum complex as reported by Reiher et al.^{38c} Moreover, the standard free energy of addition of N_2 to $[V]-NH_3$ is endergonic by 7.8 kcal/mol which is 14.9 kcal/mol higher than the addition of N_2 to the naked "[V]" complex. Thus, the formation of the six coordinate $[V](NH_3)(N_2)$ complex via the addition of N_2 to $[V]-NH_3$ is thermodynamically unfavorable. Hence, while the associative mechanism may be operative in case of molybdenum complex,^{38c} it is less likely to occur with the vanadium catalyst. This might also be a possible reason of the inferiority of the vanadium complex in comparison to the molybdenum complex.

[5.2.4] Conclusions

Energy profile for the conversion of N_2 to NH_3 mediated by vanadium triamidoamine has been obtained. This theoretical study corroborates with most of the experimental^{35h} findings and is in tune with previous theoretical studies.³⁷⁻³⁸ The most important steps for the catalytic conversion of N_2 to NH_3 are examined with all the mechanistic possibilities. Our calculation shows that for most of the cases, protonation is more favourable at the equatorial position than the terminal one except for the protonation of $[V]=N^-$ and $[V]-NH_2$ where terminal protonation is more favorable for the former and equally favorable for the later. This is in agreement with previous theoretical and experimental studies.^{38a,48} Some of the key steps of the mechanism were further compared with the well established chemistry of molybdenum.^{30,31,36-38} These key steps include N-N bond breaking step and the ligand exchange step at the end of the cycle. The N-N bond breaking step with [V] is very less exergonic (- 4.3 kcal/mol) compared to [Mo] which is highly exergonic (-75.9 kcal/mol). This can be traced to the presence of higher lying $\sigma^*_{N\alpha-N\beta}$ orbital and lower positive charge at the vanadium center compared to molybdenum of the respective complexes prior to reduction. This lower exergonic character of the N-N bond cleavage step with [V] may account for the lower efficiency of [V] towards NH_3 production.^{35h} The other important step i. e., the ligand exchange step at the end of the cycle reveals that reduction of $[V]-NH_3$ to $[V]-NH_3^{1-}$ is very unlikely which corroborates experimental findings.^{35h} Further, the only possible pathway of ligand exchange with [V] is the neutral one, while both anionic and neutral pathways are possible with [Mo]. This restriction provides another clue to the possible limitations of the [V] catalyst. Moreover, associative (addition-elimination) mechanism of NH_3/N_2 exchange with vanadium is less likely compared to the analogous

molybdenum complex which might be another possible reason of the inferiority of the vanadium complex in comparison to the molybdenum complex. Thus, we feel that this theoretical finding may help in understanding the possible reasons for the poor performance of vanadium triamidoamine complex towards NH_3 production.

[5.3] Bibliography

1. Eady, R. E. et. al., *Nature* **272**, 557-557, 1978.
2. Barney, B. M. et. al., *J. Am. Chem. Soc.* **127** (43), 14960-14961, 2005.
3. Howard, J. B., & Rees, D. C. *Chem. Rev.* **96** (7), 2965-2982, 1996.
4. Burgess, B. K., & Lowe, D. J. *Chem. Rev.* **96** (7), 2983-3012, 1996.
5. Eady, R. R. *Chem. Rev.* **96** (7), 3013-3030, 1996.
6. Hardy, R. W. F. et. al., *A Treatise on Dinitrogen Fixation*; Willey – Interscience: New York. (1979).
7. Veeger, C., & Newton, W. E. *Advances in Nitrogen Fixation Research*, Dr. W. Junk/Martinus Nijhoff: Boston, 1984.
8. Coughlan, M. P. Ed. *Molybdenum and Molybdenum – containing Enzymes*, Pergamon: New York, 1980.
9. Schrock, R. R. et. al., *J. Am. Chem. Soc.* **113** (2), 725-726, 1991.
10. Schrock, R. R. et. al., *J. Am. Chem. Soc.* **115** (5), 1760-1772, 1992.
11. Block, E. et. al., *J. Am. Chem. Soc.* **114** (2), 758-759, 1992.
12. Hitchcock, P. B. et. al., *J. Chem. Soc., Dalton Trans.* 4747, 1997.
13. Coucouvanis, D. et. al., *J. Am. Chem. Soc.* **115** (25), 12193-12194, 1993.
14. Demadis, K. D. et. al., *Inorg. Chem.* **35** (13), 4038-4046, 1996.
15. Malinak, S. M. et. al., *J. Am. Chem. Soc.* **117** (11), 3126-3133, 1995.
16. Davies, S. C. et. al., *Inorg. Chem.* **39** (16), 3485-3498, 2000.
17. Hsu, H. –F. et. al., *Inorg. Chem.* **45** (8), 3164-3166, 2006.
18. B3LYP is Becke's three-parameter hybrid method using the LYP correlation functional.
19. Becke, A. D. *J. Chem. Phys.* **98** (7), 5648 – 5652, 1993.
20. Lee, C. et. al., *Phys. Rev. B.* **37** (2), 785 – 789, 1988.
21. Vosko, S. H. et. al., *Can. J. Phys.* **58** (8), 1200 – 1211, 1980.
22. Hay, P. J., & Wadt, W. R. *J. Chem. Phys.* **82** (1), 270-283, 1985.
23. Wadt, W. R., & Hay, P. J. *J. Chem. Phys.* **82** (1), 284-298, 1985.
24. Hay, P. J., & Wadt, W. R. *J. Chem. Phys.* **82** (1), 299-310, 1985.
25. Pople, J. A. et. al., *Gaussian 03, Revision D.01*, Gaussian, Inc., Wallingford CT, 2004.
26. (a) Ahlrichs, R. et. al., *J. Chem. Phys.* **97** (4), 2571-2577, 1992. (b) Ahlrichs, R. et. al., *J. Chem. Phys.* **100** (8), 5829-5835, 1994.

27. (a) Glendening, E. D. et. al., *NBO Program 3.1*: Madison, W. T. 1988. (b) Reed, A. E., Weinhold, F. & Curtiss, L. A. *Chem. Rev.* **88** (6), 899 – 926, 1988.
28. Tuzcek, F. et. al., *Inorg. Chem.* **44** (9), 3031-3045, 2005.
29. Studt, F., & Tuzcek, F. *Angew. Chem. Int. Ed.* **44** (35), 5639-5642, 2005.
30. Yandulov, D. V., & Schrock, R. R. *Science.* **301**, 76-78, 2003.
31. Schrock, R. R. et. al., *Inorg. Chem.* **42** (3), 796-813, 2003.
32. Allen, A. D., & Senoff, C. V. *J. Chem. Soc. Chem. Commun.* 621-622, 1965.
33. Carnahan, J. E. et. al., *Biochem. Biophys. Acta*, **38**, 188-189, 1960.
34. (a) Kim, J., & Rees, D. C. *Science* **257**, 1677-1682, 1992. (b) Kim, J., & Rees, D. C. *Nature* **360**, 553-560, 1992.
35. Chatt, J. & Leigh, G. J. *Chem. Soc. Rev.* **1**, 121-144, 1972. (b) Chatt, J. et. al., *Chem. Rev.* **78** (6), 589-625, 1978. (c) Hidai, M., & Mizobe, Y. *Chem. Rev.* **95** (4), 1115-1133, 1995. (d) Pickett, C. J., & Talarmin, J. *Nature* **317**, 652-653, 1985. (e) George, T. A., & Kovar, R. A. *Inorg. Chem.* **20** (1), 285-287, 1981. (f) Fryzuk, M. D. et. al., *J. Am. Chem. Soc.* **124** (28), 8389-8397, 2002. (g) Peters, J. C. et. al., *Angew. Chem., Int. Ed.* **46** (30), 5768-5771, 2007. (h) Schrock, R. R. et. al., *Inorg. Chem.* **45** (23), 9197-9205, 2006.
36. (a) Yandulov, D. V. & Schrock, R. R. *J. Am. Chem. Soc.* **124** (22), 6252-6253, 2002. (b) Schrock, R. R. et. al., *J. Am. Chem. Soc.* **126** (19), 6150-6163, 2004. (c) Schrock, R. R. *Angew. Chem. Int. Ed.* **47** (30), 5512-5522, 2008.
37. (a) Studt, F. & Tuzcek, F. *J. Comput. Chem.* **27** (12), 1278-1291, 2006. (b) Tuzcek, F. et. al., *Chem. Eur. J.* **14** (2), 644-652, 2008.
38. (a) Reiher, M. et. al., *Inorg. Chem.* **44** (26), 9640-9642, 2005. (b) Reiher, M. et. al., *Inorg. Chem.* **47** (9), 3634-3650, 2008. (c) Reiher, M. et. al., *Chem. Eur. J.* **15** (20), 5073-5082, 2009. (d) Cao, Z. et. al., *Int. J. Quantum Chem.* **103** (3), 344-353, 2005. (e) Neese, F. *Angew. Chem. Int. Ed.* **44** (19), 2908-2912, 2005. (f) Hölscher, M., & Leitner, W. *Eur. J. Inorg. Chem.* 4407, 2006. (g) Morokuma, K. et. al., *Mol. Phys.* **100** (4), 523-532, 2002.
39. Guha, A. K. & Phukan, A. K. *Inorg. Chim. Acta*, **363** (13), 3270-3273, 2010.
40. (a) Ehlers, A. W., & Frenking, G. *J. Am. Chem. Soc.* **116** (4), 1514-1520, 1994. (b) Delley, B. et. al., *J. Chem. Phys.* **100** (8), 5785-5791, 1994. (c) Barckholtz, T. A., & Bursten, B. E. *J. Am. Chem. Soc.* **120** (8), 1926-1927, 1998. (d) Niu, S., & Hall, M. B. *Chem. Rev.* **100** (2), 353-406, 2000. (e) Ziegler, T., & Autschbach, J. *Chem. Rev.* **105** (6), 2695-2722, 2005.
41. Perdew, J. P. et. al., *Phys. Rev. Lett.* **77** (18), 3865-3868, 1996.
42. (a) Grimme, S. *J. Phys. Chem. A* **109** (13), 3067-3077, 2005. (b) Neese, F. et. al., *J. Chem. Theory Comput.* **4** (9), 1449-1459, 2008.

43. (a) Dolg, M. et. al., *J. Chem. Phys.* **86** (2), 866-872, 1987. (b) Dunning Jr. et. al., in *Modern Theoretical Chemistry*; Ed. H. F. Schaefer III, Vol. 3 (Plenum, New York, 1976) 1-28.
44. Dapprich, S., & Frenking, G. *J. Phys. Chem.*, **99** (23), 9352-9362, 1995.
45. (a) Tenderholt, A. L. *QMForge*, Version 2.1, <http://qmforge.sourceforge.net>. (b) Tenderholt, A. L. et. al., *J. Comput. Chem.* **29** (5), 839-845, 2008.
46. (a) Dewar, M. J. S. *Bull. Soc. Chim. Fr.* **18**, C71-79, 1951. (b) Chatt, J., & Duncanson, L. A. *J. Chem. Soc.* 2939-2947, 1953.
47. (a) Fryzuk, M. D. & Johnson, S. A. *Coord. Chem. Rev.* **200-202** (1-2), 379-409, 2000. (b) Hazari, N. *Chem. Soc. Rev.* **39** (11), 4044-4056, 2010.
48. Schrock, R. R. et. al., *Inorg. Chem.* **50** (2), 418-420, 2011.
49. Huheey, J. E. et. al., *Inorganic Chemistry: Principles of Structure and Reactivity*; Fourth Edition, Pearson Education (Singapore) Pte. Ltd., 2004.

[5.4] List of Publications

1. A. K. Phukan; A. K. Guha, B. Silvi, "Is Delocalization a Prerequisite for Stability of Ring Systems? A Case Study of Some Inorganic Rings" *Dalton Trans*, 2010, 39, 4126-4137.
2. A. K. Guha, S. Sarmah, A. K. Phukan "Effect of Substituents at the Heteroatom on the Structure and ligating Properties of Heterocyclic Carbene, Silylene, Germylene and Abnormal Carbene: A Theoretical Study" *Dalton Trans*, 2010, 39, 7374-7383.
3. A. K. Guha, A. K. Phukan, "Theoretical Study on the Mechanism of Catalytic Reduction of Hydrazine to Ammonia Mediated by Vanadium (III) Thiolate Complexes" *Inorg. Chim. Acta*, 2010, 363, 3270-3273.
4. A. K. Phukan, A. K. Guha, "Nature of Transannular Intramolecular Interactions in Group 4 and 6 Metallatranes: A Combined Density Functional Theory and Atoms in Molecules Theory Study" *Inorg. Chem*, 2010, 49, 9884-9890.
5. A. K. Guha, C. Das, A. K. Phukan, "Heterocyclic carbenes of diverse flexibility: A theoretical insight" *J. Organomet. Chem*, 2011, 696, 586.
6. A. K. Phukan, A. K. Guha, "Nature of Intramolecular Transannular Interaction in Group 13 Atranes: A Theoretical Study" *Inorg. Chem*, 2011, 50, 1361-1367.
7. A. K. Guha, A. K. Phukan, "Why Vanadium Complexes Perform Poorly in Comparison to Related Molybdenum Complexes in the Catalytic Reduction of Dinitrogen to Ammonia (Schrock Cycle): A Theoretical Study" *Inorg. Chem*, 2011, 50, 8826.
8. A. K. Guha, B. Konwar, S. Sarmah, "Effect of Substituents at the Heteroatoms on the Structure and Ligating Properties of Carbodicarbenes and Its Silicon Analog: A Theoretical Study" *Theor. Chem. Acc*, 2011, 131, 1134.
9. U. Gogoi, A. K. Guha, A. K. Phukan, "Nature of Intramolecular Metal-Metal Interactions in Supported Group 4- Group 9 and Group 6- Group 9 Heterobimetallic Complexes: A Combined Density Functional and Topological Study" *Organometallics*, 2011, 30, 5991.
10. A. K. Guha, A. K. Phukan, "Do Carbenes have "Hidden" Carbon (0) Character? Revisiting the Electronic Structure of 2,2'-Bipyridyl Carbene" *Chem. Eur. J.* 2012, 18, 4419.
11. A. K. Phukan, A. K. Guha, "Stabilization of cyclic and acyclic carbon(0) compounds by differential coordination of heterocyclic carbenes: A theoretical study" *Dalton. Trans.* 2012, 41, 8973.

12. **A. K. Guha**, A. K. Phukan, "*Revisiting the Reactivity of Different Carbon Bases-A Theoretical Study*" (Communicated).

[5.5] List of School/Workshop/Summer School Attended

- 1. “14th National Workshop on Catalysis, catalysis for Clean Environment and Sustainable Future”** Dec 21-23, 2009 held at Tezpur University, Assam, India.
- 2. “DST Sponsored Summer School on Green Chemistry, June 2-22, 2009”** held at Tezpur University, Assam, India.
- 3. “Frontier Lecture Series in Chemistry, Nov 20-22, 2009”** sponsored by JNCASR held at Tezpur University, Assam, India.
- 4. “Frontiers in Chemical Sciences, Dec 3-4, 2010”** organized by Indian Institute of Technology (IIT), Guwahati, Assam, India.
- 5. International Seminar on “Applied Theory on Molecular Systems, Nov 2-5, 2011”** organized by Indian Institute of Chemical Technology (IICT), Hyderabad, India.